THE DEVELOPMENT AND EVALUATION OF A SHADOW-PHOTOGRAMMETRIC METHOD FOR DETERMINING THE TOPOGRAPHY OF AN OPAQUE SURFACE

By

JOHN LOVE, JR.

Bachelor of Arts
University of Missouri
Columbia, Missouri
1939

Bachelor of Science in
Mechanical Engineering
University of Missouri
Columbia, Missouri
1951

Master of Science in
Mechanical Engineering
University of Missouri
Columbia, Missouri
1953

Submitted to the Faculty of the Graduate School
of the Oklahoma State University
in partial fulfillment of the requirements
for the degree of
DOCTOR OF PHILOSOPHY
May, 1966

THE DEVELOPMENT AND EVALUATION OF A SHADOW-PHOTOGRAMMETRIC METHOD FOR DETERMINING THE TOPOGRAPHY OF AN OPAQUE SURFACE

Thesis Approved:

Glen W. Zamvatt
Thesis Adviser

Ladislaus J. Fila

Jerald W. Parker

Dale D. Groveman

J. H. Boggs
Dean of the Graduate School

PREFACE

A large group of important problems requires the study of the topography of a surface. The determination of the surface contours becomes extremely difficult if the field to be studied is a transient or liquid surface. This dissertation describes a new photographic method, using a single lens camera, for finding the topography of any opaque surface with relatively inexpensive equipment. It may be used by unskilled personnel. The accuracy is as good or better than other methods that are now available. The practical use of the method has been shown by an application to surface of flowing water. Quantitative data can now be obtained from water table analogies with much less effort. This should increase the usefulness of this important tool.

The experimental phases of the study were done at Oklahoma State University in the Mechanical Engineering Laboratory. The computations were done at the University of Missouri Computing Center.

It is impossible to acknowledge all those who made this work possible. I am indeed grateful to all my former teachers. Dean H. O. Croft, Dr. J. H. Boggs, and the National Science Foundation made it possible for me to initiate the studies that lead to this dissertation by granting me a sabbatical leave from the University of Missouri, accepting me as a student at Oklahoma State University's Summer Institute, and granting me a National Science Teachers Fellowship. Also, I want to express my appreciation to the members of my Doctor of Phil-

osophy Committee, Dr. J. D. Parker, Professor L. J. Fila, and Dr. O. H. Hamilton for their help and advice.

A special expression of appreciation and acknowledgement is given to my major advisor, Dr. G. W. Zumwalt, Associate Professor at Oklahoma State University, for his help, advice, and patience during our association over the past four years. Without his thorough understanding of the complex student-teacher relationship during the trials and tribulations pertaining to a work of this type, it would have never been brought to a close.

I also wish to thank Mrs. Kenneth Buchert, Computer Operation Supervisor and Programmer, for her assistance in developing the computer programs.

Finally, I wish to dedicate this dissertation to my wife, Marjorie O. (Vicki), who not only typed the final draft, assisted in the experimental work, did much of the preliminary calculations, but also offered encouragement, and confidence at every turn.

TABLE OF CONTENTS

Chapter		Page
I.	INTRODUCTION.	1
II.	REVIEW OF THE LITERATURE.	4
	Hydraulic Analogy.	4
	Flow Visualization	6
	Depth Determination.	7
III.	THE DEVELOPMENT OF A PHOTOGRAPHIC METHOD FOR DETERMINING THE CONTOURS OF AN OPAQUE SURFACE	11
	Foreshortening Corrections and Depth Determinations. .	14
	Print Distortion Corrections	20
	Calibration and Procedure.	28
	Discussion of Problems Encountered	34
	Data Reduction Methods	36
	Mark I Method	36
	Mark II Method.	42
	Mark III Method	44
IV.	APPLICATION OF THE SHADOW-PHOTOGRAMMETRIC METHOD TO A HYDRAULIC ANALOGY PROBLEM	50
	Description of Apparatus	55
	Set-up and Procedure	57
V.	RESULTS AND DISCUSSION OF THE INVESTIGATION	71
	Shadow-photogrammetric Method.	71
	Discussion of the Field Plots.	86
	Critique of the Shadow-photogrammetric Method.	139
	Hydraulic Analogy Check.	141
	Critique of the Water Analogy Application.	147
VI.	CONCLUSIONS AND RECOMMENDATIONS	148
SELECTED BIBLIOGRAPHY.		150

Chapter Page

APPENDICES 154

A. Computation of Expected Errors in Results Due to Errors of Measurements 154
B. Computer Programs 162
C. Figure-Film Reference 176

LIST OF TABLES

Table | Page

I. Comparison of Actual With Computed Values by the Different Methods for Calibration Run 1802 74

II. Comparison of Values Computed by Different Methods for Run 1904 81

LIST OF FIGURES

Figure		Page
1.	Section at Principal Plane.	16
2.	Projection Plane.	18
3.	Calibrated Focal Length	25
4.	Overall Correction Factor	26
5.	Principal Distance.	33
6.	Graphical Method.	45
6a.	Principal Plane	47
7.	Aluminum Particles Being Recirculated by Pump	60
8.	Calibration of Grid by Water Method	61
9.	Typical Streak Lines for Open Slot; No Secondary Flow	62
10.	Typical Streak Lines for Particles Issuing From Slot; Secondary to Main Stream Head Approximately 1.00.	63
11.	Typical Shadow Pattern With Aluminum Powder for Plugged Slot.	65
12.	Typical Weak Shadow Pattern With Aluminum Powder for Plugged Slot.	66
13.	Shadow Pattern for Zero Depth Calibration Positions; White Painted Bottom.	67
14.	Shadow Pattern for .090 Inch Depth Calibration Position; Glass Plate	68
15.	Shadow Pattern for .369 Inch Depth Calibration Position; Glass Plate	69
16.	Isogrametric Depth Lines for Plugged Slot; No Secondary Flow.	83

Figure Page

17. Shadow Pattern for Plugged Slot; No Secondary Flow; Slot at Geometric Throat. 84

18. Typical Streak Lines for Plugged Slot; Slot at Geometric Throat. 85

19. Isogrametric Depth Lines for Open Slot; No Secondary Flow; Slot at Geometric Throat. 87

20. Shadow Pattern for Open Slot; No Secondary Flow; Slot at Geometric Throat. 88

21. Typical Streak Lines for Open Slot; Slot at Geometric Throat. 89

22. Isogrametric Depth Lines for Secondary to Main Stream Head Ratio of 1.00; Injection at Geometric Throat. 91

23. Shadow Pattern for Secondary to Main Stream Head Ratio of 1.00; Injection at Geometric Throat 92

24. Typical Streak Lines for Secondary to Main Stream Head Ratio of 1.00; Injection at Geometric Throat. 93

25. Typical Streak Lines for Secondary to Main Stream Head Ratio of 1.00; Injection at Geometric Throat. 94

26. Isogrametric Depth Lines for Secondary to Main Stream Head Ratio of 1.50; Injection at Geometric Throat. 95

27. Shadow Pattern for Secondary to Main Stream Head Ratio of 1.50; Injection at Geometric Throat 96

28. Typical Streak Lines for Secondary to Main Stream Head Ratio of 1.50; Injection at Geometric Throat. 97

29. Typical Streak Lines for Secondary to Main Stream Head Ratio of 1.50; Injection at Geometric Throat. 98

30. Isogrametric Depth Lines for Secondary to Main Stream Head Ratio of 1.75; Injection at Geometric Throat. 99

31. Shadow Pattern for Secondary to Main Stream Head Ratio of 1.75; Injection at Geometric Throat 100

32. Typical Streak Lines for Secondary to Main Stream Head Ratio of 1.75; Injection at Geometric Throat. 101

33. Typical Streak Lines for Secondary to Main Stream Head Ratio of 1.75; Injection at Geometric Throat. 102

Figure Page

34. Isogrametric Depth Lines for Secondary to Main Stream Head Ratio of 2.00; Injection at Geometric Throat. 103

35. Shadow Pattern for Secondary to Main Stream Head Ratio of 2.00; Injection at Geometric Throat 104

36. Typical Streak Lines for Secondary to Main Stream Head Ratio of 2.00; Injection at Geometric Throat. 105

37. Typical Streak Lines for Secondary to Main Stream Head Ratio of 2.00; Injection at Geometric Throat. 106

38. Isogrametric Depth Lines for Secondary to Main Stream Head Ratio of 1.00; Injection at 4° Upstream of Geometric Throat. 107

39. Shadow Pattern for Secondary to Main Stream Head Ratio of 1.00; Injection at 4° Upstream of Geometric Throat. 108

40. Typical Streak Lines for Secondary to Main Stream Head Ratio of 1.00; Injection at 4° Upstream of Geometric Throat. 109

41. Typical Streak Lines for Secondary to Main Stream Head Ratio of 1.00; Injection at 4° Upstream of Geometric Throat. 110

42. Isogrametric Depth Lines for Secondary to Main Stream Head Ratio of 1.50; Injection at 4° Upstream of Geometric Throat. 111

43. Shadow Pattern for Secondary to Main Stream Head Ratio of 1.50; Injection at 4° Upstream of Geometric Throat. 112

44. Typical Streak Lines for Secondary to Main Stream Head Ratio of 1.50; Injection at 4° Upstream of Geometric Throat. 113

45. Typical Streak Lines for Secondary to Main Stream Head Ratio of 1.50; Injection at 4° Upstream of Geometric Throat. 114

46. Isogrametric Depth Lines for Secondary to Main Stream Head Ratio of 1.75; Injection at 4° Upstream of Geometric Throat. 115

47. Shadow Pattern for Secondary to Main Stream Head Ratio of 1.75; Injection at 4° Upstream of Geometric Throat. 116

Figure Page

48. Typical Streak Lines for Secondary to Main Stream Head Ratio of 1.75; Injection at 4° Upstream of Geometric Throat. 117

49. Typical Streak Lines for Secondary to Main Stream Head Ratio of 1.75; Injection at 4° Upstream of Geometric Throat. 118

50. Isogrametric Depth Lines for Secondary to Main Stream Head Ratio of 2.00; Injection at 4° Upstream of Geometric Throat. 119

51. Shadow Pattern for Secondary to Main Stream Head Ratio of 2.00; Injection at 4° Upstream of Geometric Throat. 120

52. Typical Streak Lines for Secondary to Main Stream Head Ratio of 2.00; Injection at 4° Upstream of Geometric Throat. 121

53. Typical Streak Lines for Secondary to Main Stream Head Ratio of 2.00; Injection at 4° Upstream of Geometric Throat. 122

54. Isogrametric Depth Lines for Secondary to Main Stream Head Ratio of 1.00; Injection at 8° Upstream of Geometric Throat. 123

55. Shadow Pattern for Secondary to Main Stream Head Ratio of 1.00; Injection at 8° Upstream of Geometric Throat. 124

56. Typical Streak Lines for Secondary to Main Stream Head Ratio of 1.00; Injection at 8° Upstream of Geometric Throat. 125

57. Typical Streak Lines for Secondary to Main Stream Head Ratio of 1.00; Injection at 8° Upstream of Geometric Throat. 126

58. Isogrametric Depth Lines for Secondary to Main Stream Head Ratio of 2.00; Injection at 8° Upstream of Geometric Throat. 127

59. Shadow Pattern for Secondary to Main Stream Head Ratio of 2.00; Injection at 8° Upstream of Geometric Throat. 128

60. Typical Streak Lines for Secondary to Main Stream Head Ratio of 2.00; Injection at 8° Upstream of Geometric Throat. 129

Figure Page

61. Typical Streak Lines for Secondary to Main Stream Head Ratio of 2.00; Injection at 8° Upstream of Geometric Throat. 130

62. Isogrametric Depth Lines for Secondary to Main Stream Head Ratio of 1.00; Injection at 4° Downstream of Geometric Throat. 131

63. Shadow Pattern for Secondary to Main Stream Head Ratio of 1.00; Injection at 4° Downstream of Geometric Throat. . . . 132

64. Typical Streak Lines for Secondary to Main Stream Head Ratio of 1.00; Injection at 4° Downstream of Geometric Throat. 133

65. Typical Streak Lines for Secondary to Main Stream Head Ratio of 1.00; Injection at 4° Downstream of Geometric Throat. 134

66. Isogrametric Depth Lines for Secondary to Main Stream Head Ratio of 2.00; Injection at 4° Downstream of Geometric Throat. 135

67. Shadow Pattern for Secondary to Main Stream Head Ratio of 2.00; Injection at 4° Downstream of Geometric Throat. . . . 136

68. Typical Streak Lines for Secondary to Main Stream Head Ratio of 2.00; Injection at 4° Downstream of Geometric Throat. 137

69. Typical Streak Lines for Secondary to Main Stream Head Ratio of 2.00; Injection at 4° Downstream of Geometric Throat. 138

70. Characteristic Particle Flow Pattern. 142

71. Characteristic Particle Flow Pattern. 142

72. Shadow Pattern for Secondary to Main Stream Head Ratio of 1.00; 3/4 Inch Main Stream Head 144

73. Comparison of Blockage for Injection at Geometric Throat. . . 146

LIST OF SYMBOLS

B = true distance of projection plane from zero datum plane

d = true distance from the optical axis to wire

h' = principal distance of photograph

h = true depth of water at unknown point

r = true distance from wire to shadow

S = true distance of the shadow from perspective axis

θ = effective illumination angle

S_a = apparent distance of shadow from the optical axis

S'_a = apparent distance of shadow from the optical axis corrected for paper shrinkage

$[S'_a]$ = true apparent distance from the optical axis

S''_a = true apparent shadow location projected on zero datum plane

S_l = true distance of a datum point from the principal axis

S_{la} = true apparent distance of a datum point from the principal axis

Subscripts o and c refer to zero datum plane and calibration values respectively.

CHAPTER I

INTRODUCTION

Many experimental techniques make use of a quantitative study of surfaces to provide the data needed for the final analysis. Such studies include panel flutter, thermally induced displacements of plates, and the application of the hydraulic analogy to fluid amplifiers, jet and stream interactions, and blast waves interactions with solid bodies. Quantitative studies of surfaces require a method of accurately determining the topography of the surfaces with as little interference to the induced shape as possible. Stationary solid surfaces can be mapped relatively easily with a depth micrometer, but liquid surfaces are more difficult. Deformation studies under quasi-steady and unsteady conditions require a rapid method of obtaining the contours. Strain gages have been used extensively for solid surfaces, however, large collections of these with the connecting wires tend to modify the character of the surface, and, of course, this method is not available for the study of liquid surfaces. A photographic method seems to offer the best solution; it is almost instantaneous, obtains the data for the whole field at the given instant, and does not alter the quantity to be measured.

This study began as an extension to an experimental study of injection of a gas into a two-dimensional transonic flow region which was carried on at Oklahoma State University beginning in 1962. It was

prompted by problems of controlling the thrust of a solid fuel rocket engine. It was desired to apply the hydraulic analogy (in which the depth is analogous to the density and temperature, and related to the pressure of a perfect gas) to the gas flow fields in an attempt to gain further knowledge of the phenomena. Another study of blast waves was undertaken at about the same time in which the hydraulic analogy was to be used. The need for a rapid method for determining the topography of the water surface soon became evident.

The usefulness of the hydraulic analogy is shown by the many hundreds of papers occurring in the literature, however, the measurement of the depths is a difficult problem and has bothered investigators since its inception. The utility of the water table and the applications of the water analogy could be increased manyfold if a relatively simple, inexpensive, reliable technique could be found to obtain the depths of the water for both steady and unsteady state problems, with as little dependence on the observer's judgment as possible.

The two most recent attempts to obtain the topography of a water surface under transient conditions were reported by Mann (1, 2)*. In the first, a capacitive probe was inserted into the flow. This disturbed the flow pattern and required many corrections to be made. In the second, a stereophotogrammetric method was developed along the lines used for aerial mapping. The surface was made visible by dusting sawdust on the water. Mann used glass plate negatives in his cameras which, while stopping the transient phenomena for observation, precluded the possibility of rapid-sequence photographs so that the sur-

---

*Numbers in parentheses refer to references in Bibliography.

face variations with time could be determined. The stereophotogrammetric method requires a highly skilled observer to reduce the data.

A new relatively simple method using a single lens camera, and inexpensive equipment and supplies, which can be used by unskilled observers has been developed and evaluated by the author. As an illustration of a practical use, it was applied to the study of gas injection into a nozzle throat using the hydraulic analogy.

CHAPTER II

REVIEW OF LITERATURE

Hydraulic Analogy

The hydraulic analogy for a gas flow is well known, and stems from the similarity of the basic flow equations. For two-dimensional steady flow, many authors have shown the equations of continuity, momentum, and energy to be identical in mathematical form for the flow of an irrotational isentropic perfect gas with a specific heat ratio of 2, and for an incompressible frictionless flow of liquid in an open channel of rectangular cross-section (3, 4, 5, 6). Loh (7) presents the results for one-dimensional unsteady flow, and shows that the above equations together with the wave, and wave propagation equations for an isentropic perfect gas, with any specific heat ratio, are identical to those for an incompressible frictionless water flow in a horizontal open channel if the cross-section is described by $W = Ch^n$, where W is the width, h the depth, C the velocity of propagation of long gravity waves in water, and n is the exponent depending on the specific heat ratio desired.

In his dissertation of 1962, Hoyt (6) surveyed some 112 papers in his review of the hydraulic analogy literature; his review is an excellent discussion of the development of the analogy and its applications and is recommended as a starting point for those who wish to apply the

analogy. The analogy has been widely used in the study of nozzle flow (the first application), combustion, shock wave interactions, atmospheric flow problems, flow in turbines and reciprocating engines, radar wave propagation, transonic flow and blast wave effects. In two extensive papers Preiswerk (3, 8) discusses the hydraulic analogy in its application, first, to supersonic gas flow without shocks, and, second, to nozzle flow and supersonic flow over wedges. In general, one can conclude from his results that he was able to match well the theoretical gas values and the analog results for the nozzle when water stagnation heads were less than 1 inch. Steep gradients must be avoided if the analogy is to hold well. Preiswerk lowered the out flow end of the table bottom to account for boundary layer.

Laitone (9) discusses the importance of using shallow depths if the analogy is to be valid; he concluded that the model must be large compared to the depth, the shock waves (hydraulic jumps) must be small, and the depth of about 1/4 inch used. He used a model mounted on a moving framework carrying the camera to obtain photographs of the wave patterns. Gupta (10) has derived an analytical method of evaluating the optimum depth for the analogy; he gives it as $(3T/gP)^{1/2}$ where T is the surface tension, g the gravitational constant, and P the density.

In reviewing the many papers applying the hydraulic analogy to various flow fields the predominate problem that seemed to plague the investigators was measuring the depths of the water in the active field, also certain flow visualization problems were troublesome, e.g., determining separation and reattachment points accurately.

Flow Visualization

Many methods have been devised to visualize gas flow fields such as smoke, dust, China clay, oil streaks, schlieren, shadowgraph and interferometer. The permanent record is usually made by photographing the field with a single lens camera; measurements made on such photographs, i.e. angles and etc., are very doubtful unless the field is exactly two-dimensional and/or the field has very limited depth and the photographs are rectified to eliminate the foreshortening. Investigators using the water analogy have devised several analogs to the above methods of flow visualization. The usual methods of dusting the surface of the water with sawdust, ground cork, and aluminum powder are well known and have been used extensively.

Werlé (11) of the Hydraulic Analogy Laboratory in France has devised several unique flow visualization techniques for use with the water table. In addition to the effective use of air bubbles and streams of colored fluids, he devised an optical scheme which resembles the shadowgraph and interferential methods of gas flow observations. In the first, he projected light on to a translucent screen placed in contact, and below the glass bottom of the table; the photographs show the waves as shadows. In the second, he placed an opaque screen, painted with red, green, and white bands about 1/2 inch in width, about 8 inches below the bottom and illuminated it from the side with photoflood lamps; the refractions caused by the water waves gave the appearance of an interferometer photograph. His photographs were made with a single lens camera.

Johnson, Nial, and Witbeck (12) developed a shadowgraph technique

in which shadows produced by the water waves were collected on a ground glass screen placed a short distance above the water; the water table was illuminated from underneath with parallel light. Hoyt (6) also used this method to obtain angles of waves present in his fields; he, however, did not use parallel light (a 750 watt slide projector was used) and preliminary tests at the beginning of this study showed that the shadows could easily be displaced by simply moving the light source. It should also be noticed that refraction through the waves will give a displacement of the shadows and must be taken into account.

Clutter and Smith (13) have devised a relatively inexpensive technique of flow visualization in water which used hydrogen bubbles produced by electrolysis of the water. The application discussed was its use in a towing tank with the camera mounted over the model on the model carriage. They made no attempt to gain any quantitative data from their photographs; it would be very difficult as the bubbles rise in the water so thay they do not remain in a given known plane and foreshortening problems occur.

Depth Determination

Apparently one of the major obstacles in the application of the water analogy to a large variety of problems, where quantitative data are necessary, is the determination of the depth which is analogous to the density and related to the pressure of a gas. The standard method of using a micrometer probe supported from a framework above the table is at best tedious and laborious, and of course is useless for non-steady state problems.

Heen and Mann (1) in their study of the partial admission turbine applied the water analogy to this non-steady flow problem; they devised a capacitive water-depth probe in which the water was used as part of the diaelectric, thus changes in depth changes the capacitance of the circuit to produce a signal. It was necessary to mount permanently the probe and thus it remained in the flow path during the tests. This scheme disturbs the flow pattern and corrections must be made for the probes' effect on the flow. Apparently they were not satisfied with the probe as a depth measuring device as they suggest a stereophotogrammetric method would be used in a subsequent paper.

In a second paper, Mann (2) discusses the advantages of using the hydraulic analogy, with all its problems, in which the depths are measured by an optical method over the opticals techniques, such as schlieren and interferometry, used to determine the density gradients and density in gas flows; and describes in some detail the equipment and techniques of applying stereophotogrammetry to measurements of depths on the water table; he concludes that even with the difficulties of data reduction of the photogrammetric method it is probably faster and less difficult than schlieren and interferometric data reduction.

The topography of an undulating surface can be determined by photogrammetry in much the same manner as in topographical mapping, however, the photographs are close-ups compared to those used in mapping and lens and camera alinement errors become more difficult to handle. Mann (2) used two Wild T-2 phototheodolite cameras modified to accomodate a nominal object distance of about 3 feet. Glass plate negatives were used to eliminate as far as possible the dimensional changes in the emulsion (this is more important for close work than in

aerial photography). The surface of the water was made visible by the use of sawdust particles, and it was illuminated from directly above which gave glare problems. His photographs were exposed at 1/500 second which stopped the motion of his non-steady field; however, the use of glass negatives prevented rapid-sequenced exposures. The stereo-pair photographic plates were analyzed with a Wild ST-3 folding mirror stereoscope. A specially trained operator "with fairly good stereo acuity" could estimate the required parallex measurements to $\pm$0.040 inch, which gave depth measurements to $\pm$0.006 inch (2). The problems of alinement and orientation of the stereo-pair and the warpage and misalinement of the optical components of the system "--sometimes contributed errors as large as 4 % --" near the extremes of the overlap regions. He obtained an overall accuracy for the system of $\pm$5 % which in his specific application gave depths to $\pm$0.02 inch.

Mann apparently was not completely satisfied with the accuracy of his results, as he mentions that new cameras are being designed around two war-surplus Metragon lenses to improve the system, because no commercially available cameras were suitable for short object distance. Reading the data from a stereoscope field is very tedious and he suggests that the human fatigue and resulting errors can be reduced by use of an automatic plotter such as the Kelsh plotter. This also will eliminate the individual observer error, i.e., some always read high others always read low. Three points stand out: the equipment required for the system is expensive, the method requires highly trained personnel, and data reduction is laborious.

Poetzschke and Menne (14) credit themselves with the development of the stereophotogrammetric method of determining the topography of a

water surface without giving a single reference to Mann's work which preceded them by two years. Their system was essentially the same as Mann's except they projected a random dot pattern straight down onto the surface of the water which was made somewhat opaque by adding cutting oil. The resulting change in density probably alters the analogy considerably (9). Glass plates were used as negatives so rapid-sequenced photographs were excluded. Their data were reduced on a Wild A-7 Autograph. They applied their system to the study of a fluid amplifier.

Moore (15) describes a photographic method of obtaining the contours of a soap film in which he projected a concentric circle pattern down from directly above the film model and photographed the reflections with a single lens camera. He made an approximate analysis of the positions of the reflections and from it he deduced the contours of the soap film. He stated that if an exact analysis with complete theory of optical geometry had been used, that "the analysis would be so complicated it was not worth doing". This paper was the only one that could be found that might suggest the shadow-photogrammetric method developed here.

CHAPTER III

THE DEVELOPMENT OF A PHOTOGRAPHIC METHOD FOR DETERMINING THE CONTOURS OF AN OPAQUE SURFACE

A method, using shadow-displacements, has been developed for finding the constant depth contours on a water table for use in the hydraulic analogy to gas flow. These lines of equal surface heights with respect to a reference surface are termed "isogrametric lines". The method is applicable to contour determinations of opaque surfaces of any type and, since the reaction of a shadow is instantaneous, quasi-steady and transient problems can be handled with as much ease as the steady state. The time required to obtain the initial data for a large field is determined by the available film and camera speed.

The concept leading to this method is as old as trigonometry and its use in measurement of heights of structures by sun angle and shadow lengths. The essential feature of the method is to photograph, with a single lens camera, the shadow pattern produced by a wire grid, illuminated at a small angle by a fixed high-intensity source, on the surface of the water rendered opaque by the addition of a water soluble paint. The true location and height of a particular shadow are calculated from measurements made on the photograph of the displacement of the shadow from the zero height location.

As with any other optical method, considerable care is required in setting up the equipment to insure good results with a minimum of

data reduction. The camera, grid, and light source must be absolutely rigid so no relative movement is allowed. Minute errors in camera and enlarger or projector alinement are unimportant so long as they remain constant for all photographs pertaining to a given calibration set-up. High quality miniature cameras (16 or 35mm) are suitable. Interpretation of the final prints presents many problems which are in common with aerophotography, however, since better control can be exerted over the placement of the camera in the experimental set-up, vertical rather than tilted photographs may be obtained as a rule.

A photograph is a perspective, generally distorted, representation of the field of view of the camera, and therefore can only be metric in one given plane perpendicular to the line of sight. Even with a perfect optical and photographic system, the apparent distance of the shadow from the axis of perspective of the photograph must be corrected for foreshortening to find the true location relative to the flow field if the shadow is below or above the projection plane. Calibration data then allow the depth and location to be found for the required datum points.

The apparent shadow location, measured directly on the final print or projection, is subject to errors of the optical system of the camera and enlarger or projector, film and paper shrinkage, film carrier offset and distortion introduced by nonparallelism of the film plane with the water surface and datum planes. Correction for the latter--tilt--are very laborious, but can be eliminated by careful alinement of the camera and projector for the application discussed here (16, 17). These various errors will be discussed in detail below.

The following precise definitions are analogous to those used in

aerophotogrammetry. However, the primary concern is with vertical or near vertical photographs and therefore the nomenclature has been modified to more aptly apply to the shadow-photogrammetry developed herein.

Fiducial marks--Reference marks in the photograph necessary for identifying the optical center of the photograph.

Optical center--The point where the optical axis of the lens strikes the photograph.

Vertical or nadir point--That point where a plumb line through the optical center of the lens would have pierced the negative or print, as the case may be. It is identical with the optical axis for a vertical print.

Equivalent focal length--The distance measured along the optical axis from the rear nodal point of the lens to the plane of best definition over the entire field. This term is often properly applied to a photograph, however, "principal distance" shall be used (see below).

Calibrated focal length--An adjusted value of the equivalent focal length so computed as to eliminate the effect of lens distortion at a selected annular zone of the photograph. Depending upon the accuracy required, it may be selected so that the maximum negative and positive linear distortion is equalized to distribute the effect of distortion over the entire field.

Perspective center--The point of origin or termination of the bundles of perspective rays. It is located on the perpendicular to the photograph erected, in this case, at the optical center. There are two such points associated with a photograph, the interior and exterior perspective centers corresponding to the front and rear nodal points of the lens. The angles subtended by a given object and its image from

the two perspective centers are equal only in a perfect lens system, and the perspective of the negative and thus the print is determined at exposure by the image angle from the interior perspective center.

Principal distance--The perpendicular distance from the projection or reference plane to the internal perspective center of the print. It is equal to the equivalent focal length of the camera at the time of exposure, times the enlargement or reduction factor.

Principal plane--The plane containing the perspective center, the vertical point, and the "point source" of illumination. The principal plane cuts the projection plane at the principal axis of the photograph.

Perspective plane--The plane containing the perspective center, and the vertical point which is orthogonal to the principal plane. It cuts the projection plane at the perspective axis of the photograph.

Apparent location--The location of a point on the print relative to a given reference line. It is subject to many errors.

True apparent location--The location of a point on a theoretical print obtained by perfect optics and non-distorting photographic materials. It is subject only to perspective displacement from its true position.

Foreshortening Corrections and Depth Determinations

It is assumed in the discussion immediately following that the true apparent shadow location is known, the camera alinement is perfect, and the perspective center is known and constant for all zones, i.e., the optical system is perfect. The foreshortening correction is a radial displacement in the photograph toward, or away from, the

optical center for points which are below, or above the projection plane; however, it is shown below that it may be assumed to be a translation parallel and perpendicular to the principal axis of the photograph.

The foreshortening and depth calculations can be based on either the plane of the wire grid or the zero reference plane. Figure 1 represents both, but since minor variations in wire locations (straightness, etc.) and the deviation of the grid from a true plane (sag and misalinement) are at best difficult to determine and maintain for different set-ups, the analysis given is based on the use of the zero datum plane. The analysis is general and the discussion assumes a "point source" illumination for the grid. Obviously, if a line source of parallel light is used the number of calibration constants would be reduced, that is, the effective light angle for each wire would be constant and the data reduction less laborious. However, the shadow definition would be somewhat impaired with the use of parallel light.

The following sign convention has been followed: distances from the perspective axis toward the illumination source are plus, away negative, and longitudinal reference line locations are considered plus on either side of the principal axis. For vertical measurements, B, h, and a are positive upward from the zero plane or wire, i.e., in the directions shown in figure 1.

Referring to figure 1, one notes that the true location of a point in the principal plane, but not on the plane of projection is

$$S = S_a + (B-h) \tan \beta = S_a + S_a [(B-h)/h'],$$

or

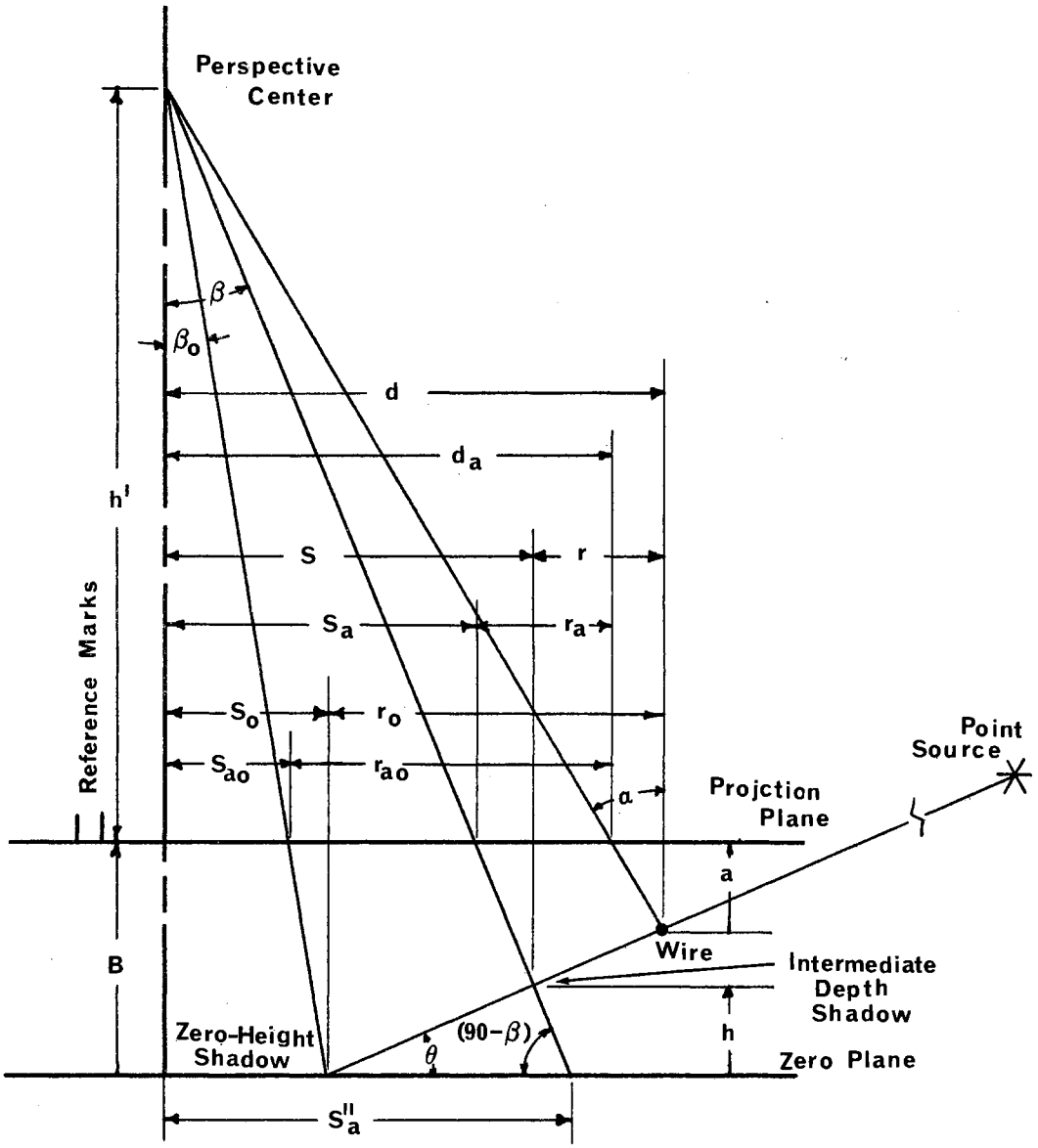

Figure 1. Section at Principal Plane.

$$S = S_a\,[1 + (B-h)/h'\,]. \tag{1}$$

The depth, h, is given by the trigonometric relation,

$$h = \frac{S''_a - S_o}{\cot\theta + \cot(90-\beta)} = \frac{S''_a - S_o}{\cot\theta + \tan\beta}, \tag{2}$$

however, note that,

$$S''_a = (h' + B) \tan\beta = (h' + B)(S_a/h'),$$

and

$$\cot\theta = (S_c - S_o)/h_c.$$

Note that S_c is simply S for a calibration point at $h = h_c$. Therefore,

$$h = \frac{[(h' + B)(S_a/h')] - S_o}{[(S_c - S_o)/h_c] + (S_a/h')}. \qquad (3)$$

Equation 3 gives the depth of a datum point with one measurement, S_a, from the photograph and the calibration constants for the point in question. The true location is then computed by equation 1. If the sign convention suggested above is followed, equation 3 will automatically account for displacements to the left of the perspective axis (as seen in figure 1). Since all wires are illuminated by the same "point source", the illumination angle, θ, will vary from wire to wire and also along each wire. Thus, several calibration constants are needed for each wire.

Since a photograph has only one point of perspective, figure 1 represents the foreshortening in any plane containing the perspective center and the nadir point that is perpendicular to the projection plane. However, the illumination angle will appear as true size only in the principal plane. Equation 1 therefore applies along any radial line in the projection plane through the nadir point. The displacement of a point due to perspective is then radially toward the nadir point. But, by use of figure 2, an axis of perspective can be assumed and the displacements computed by the components parallel and perpendicular to the principal axis. (Note that figure 2 is the projection plane as

seen from the camera.)

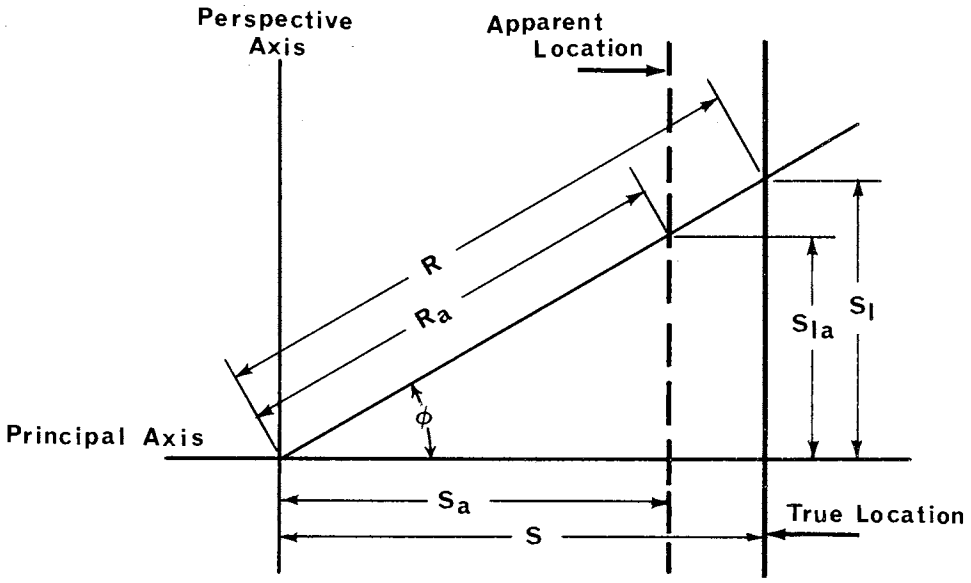

Figure 2. Projection Plane.

Recalling figure 1, and writing equation 1 in terms of the radial distance, R, we have

$$R = R_a\,[1 + (B-h)/h'],$$

or,

$$R = (S_a/\cos\phi)\,[1 + (B-h)/h'],$$

and

$$S = R\cos\phi = S_a\,[1 + (B-h)/h']. \qquad (1)$$

Thus, measurements made from the perspective axis parallel to the principal axis, rather than radially, may be used in computing the true longitudinal location of a point.

From the projection plane, figure 2, one sees that the lateral location, S_l, of a point is

$$S_l = S_{la} + (R - R_a)\sin\phi,$$

or,

$$S_l = S_{la} + (S - S_a) \tan \phi,$$

from which,

$$S_l = S_{la} [1 + (S - S_a)/S_a] = S_{la} (S/S_a).$$

But from equation 1,

$$S/S_a = 1 + (B-h)/h',$$

and therefore,

$$S_l = S_{la} [1 + (B-h)/h']. \qquad (4)$$

The principal axis of figure 1, then becomes the lateral perspective axis for points not located in the principal plane, and those not in the projection plane are foreshortened as before. The radial displacement is now resolved into the two components as stated above.

The true lateral location, given by equation 4, is a linear function of the distance below the projection plane, (B-h), for a constant S_{la}, and therefore the points representing the true positions of an object point on a lateral wire and its shadow all lie in a straight line through the "point source". However, note that, in this case, it is not parallel to the principal axis and the cotangent θ computed by $\cot\theta = (S_c - S_o)/h_c$ is the effective cotangent instead of a true value. This presents no additional complications in the interpretation of the photographs since the illumination angle, θ, varies along each lateral wire for a "point source". It may now be seen that equations 3, 1, and 4 can be solved in that order to give h, S, and S_l.

In view of the preceding paragraph and the fact that the greatest shadow displacement due to depth changes is longitudinal, the interpretation of the final photographs is facilitated by establishing ref-

erence lines, drawn on the print, parallel to the principal axis along which measurements are made. When a rather small mesh of points is required the bookkeeping is also simplified. Since the effective illumination angle changes slowly laterally, the depth of points near a reference line may be found with little error without recalibration of the illumination angle between the reference lines. Of course the mesh may be made finer in important areas where the depths are changing rapidly. Also note that no regular mesh is required since each calculation is independent of all others.

The simplified analysis given above assumes that the true apparent shadow location is known; however, the determination of this value is the most difficult one to be made from the final photographs. This is particularly true when one must use the commonly available equipment and photographic supplies, so that specially corrected lenses, film carriers, and "stable" film and print supplies are not at hand. The residual distortions of the print may be conveniently classified as material errors, optical errors, and set-up errors. It may be very laborious or, in fact, well nigh impossible, with the equipment at hand to determine the absolute values of the errors in the first two classifications, but the effective overall error for the film image at a given time is rather easily found.

Print Distortion Corrections

The residual distortions classified as "material errors" are those due to film and print shrinkage. Glass plates coated with emulsions are the ultimate in stability for photographic products; their use for the application discussed here is out of the question since rapid-

sequenced and motion pictures must be used for quasi-steady and transient phenomena (18). Also, glass and film based prints are expensive compared to paper based prints. The apparent shadow location corrected for print shrinkage will be designated "the corrected apparent location", S'_a, which is still subject to errors.

It is characteristic of all photographic films to undergo dimensional changes which may be either permanent or temporary. Permanent shrinkage results from processing and aging due to loss of residual solvent from the base, plastic flow of the base under the compressive forces of the emulsion, and the recovery of stretch introduced during manufacture. Reversible or temporary changes are the result of thermal and humidity expansion and contraction. Humidity effects are also subject to some hysteresis (19). The newer high stability films such as "Kodak Estar Base" are also subject to most of these dimensional changes, however, they are only about one-half as great as for acetate base films, and may be considered stable for many applications. Processing shrinkage for acetate base films at 50 % relative humidity may be as high as 0.12 % (19). Applying this to a point at the edge of a 20 inch print made from a 35mm negative results in a 0.014 inch error on the print, which would be increased by up to 8 % when corrected for foreshortening. Under ordinary conditions of use, these dimensional changes are at best difficult to determine, and can be handled most expeditiously by including these errors in an "optical error correction factor". Manufacturing processing gives wide variations in film characteristics within a given lot of film and therefore each roll of film must be calibrated (20). It is suggested that calibration photographs be taken at the beginning and end of a roll for comparison to determine

the average film characteristics. Of course, careful handling will reduce the possibility of introducing mechanical damage while processing the exposed film. The effect of dimensional instability of the film will be included in the optical errors given below.

For this application, ordinary enlarging paper is useless for making prints because of differential shrinkage. However, the results with a water resistant paper, such as "Kodak Resisto Rapid", were satisfactory. It was found that the shrinkage of the latter was less than that of other available papers; it was in the "with the grain" direction, and not dependent on lateral position for a particular sheet if processed as recommended by the manufacturer (21). The print shrinkage, of course, occurs during processing and if each print is not to be completely calibrated for shrinkage, all prints for a given depth calibration should be made at the same time under identical conditions. If it is inconvenient to print all the prints pertaining to a given depth calibration at the same time, so that all are made with the film in identical atmospheric conditions, then a new set of calibration prints is required for each lot of "run" photographs. The paper shrinkage factor is determined by comparing the image of the grid on the print at the time of measuring the print with that projected by the enlarger at the time of printing.

Interpretation of the photographs may be made anytime subsequent to stabilization of a lot at room conditions, however, each print must have associated with it the shrinkage factor, dependent upon room conditions, the zonal perspective center or optical error correction factor, and the depth calibration factors. These are unique for a given print or a lot and may be properly called properties of the

print. Note that the print shrinkage error is determined absolutely.

The residual distortions classified as optical errors are those due to manufacturing defects in the camera and enlarger lenses, which at present can not be entirely removed, and in the glass negative carrier in the enlarger which can not be eliminated because of the necessity of holding the film perfectly flat for printing. Although not an optical error, the film shrinkage will be included in the correction factor for optical errors because of the difficulty of isolating it. An overall correction factor will be developed.

Lenses are subject to many aberrations. Designers strive for an acceptable balance between over and under correction of the several aberrations to give the best average performance over the entire field of view; this is true even in lenses especially designed for a specific use. Kingslake (22) presents an excellent elementary discussion of lens corrections. Let it suffice to say, that even high quality lenses, while giving average to good definition over the entire field, are subject to residual zonal aberrations that cause a displacement in the image of an object point from its true relative position. That is, two points in the same plane of the object, one of which is twice as far from the perspective axis as the other, will not have this same relationship on the film. The net shift, resulting from the camera and enlarger lenses, was toward the optical center in the outer zones for the lenses used in this study.

It was found necessary to use a negative carrier equipped with glass pressure plates to hold the film flat for printing. Several other schemes were tried, but only the glass carrier proved to give acceptable results. The bottom glass is in the optical path of the

image formed by the enlarger, and according to Ask (23) "--the radial distortion introduced by the insertion of a glass plate into an optical system results in a radial displacement of the image point toward or away from the center of the field, depending on whether the plate is inserted between lens and image or between lens and object respectively". A simple ray analysis will confirm this statement (see figure 4). Thus in the lens systems used in this study the glass plate tends to compensate for the inward shift due to the zonal aberrations of the lenses. In aerial photography, compensating plates are often specially ground to compensate for the lens errors; they are undoubtedly useful with glass plate negatives, but their usefulness with unstable film is questioned.

Bench-testing of the optical components will give the desired characteristics of the lenses, however, it is more expeditious to calibrate the whole optical system with a given camera and enlarger combination for a specific roll of film in a given atmospheric condition. Note that the projected image is affected by the film condition and the optical errors of the camera, the glass plate, and the enlarger. Thus, if the dimensions of, say, the zero shadow positions of the original field are known and compared with those computed from the projected field, an overall calibration factor, including the film shrinkage, may be found for each zone. A well-made grid provides an excellent reference for calibration of the optics.

The proceeding analysis for foreshortening assumed that the point of perspective was known, but, for real lenses with distortion, this value is elusive and can not be found by physical measurements of the camera and enlarger. The approaches to this problem are discussed

below; the second was concluded to be more appropriate, and was used for this study.

In aerial photogrammetry the "calibrated focal length" is often used to recover the effective perspective center for a point. The concept and use of the calibrated focal length is shown in figure 3, where the interior and exterior nodal points, P_1, are shown coincident for simplicity and OO' is the optical axis (23). Due to zonal distortions the perspective ray AP_1 emerges from the internal nodal point as a slightly deflected ray striking the image point at a'; the radial distortion is aa'. If no distortion were present the ray would have struck at a, giving the true angular field β . Considering the projected image, we wish to recover the internal perspective center for

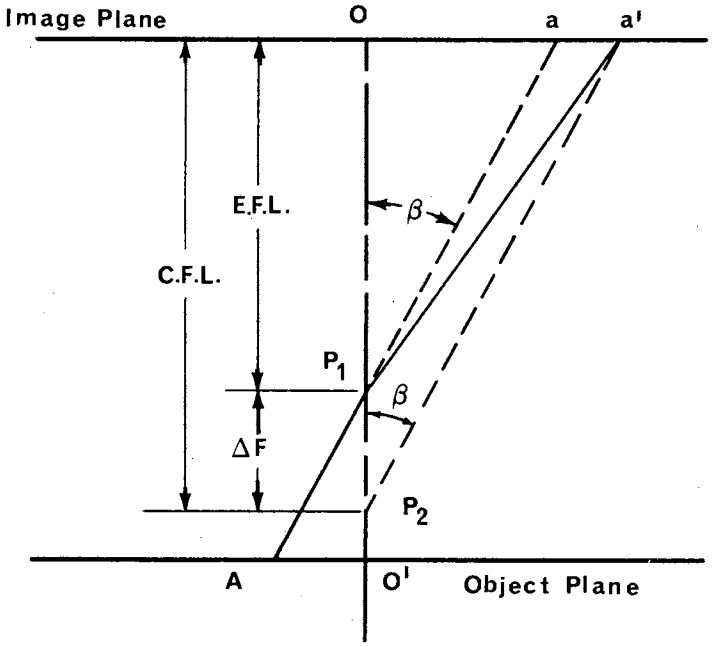

Figure 3. Calibrated Focal Length.

the ray in question, i.e., to find the true angle β . Note that the perspective center of a point at a' is found by drawing a parallel to

AP_1 through a' and extending it until it cuts the center line at P_2. The calibrated focal length is E.F.L. $\pm$ ΔF (figure 3), which varies for each annular zone of the lens with residual aberrations, and may be found, as stated above, if the object and image distances and the magnification or reduction factor are known, i.e., $\Delta F = (aa')/\tan\beta$. The calibrated focal length is especially useful with the Kelsh Plotter, and the Wild Autograph in connection with interpreting aerial photographs (23).

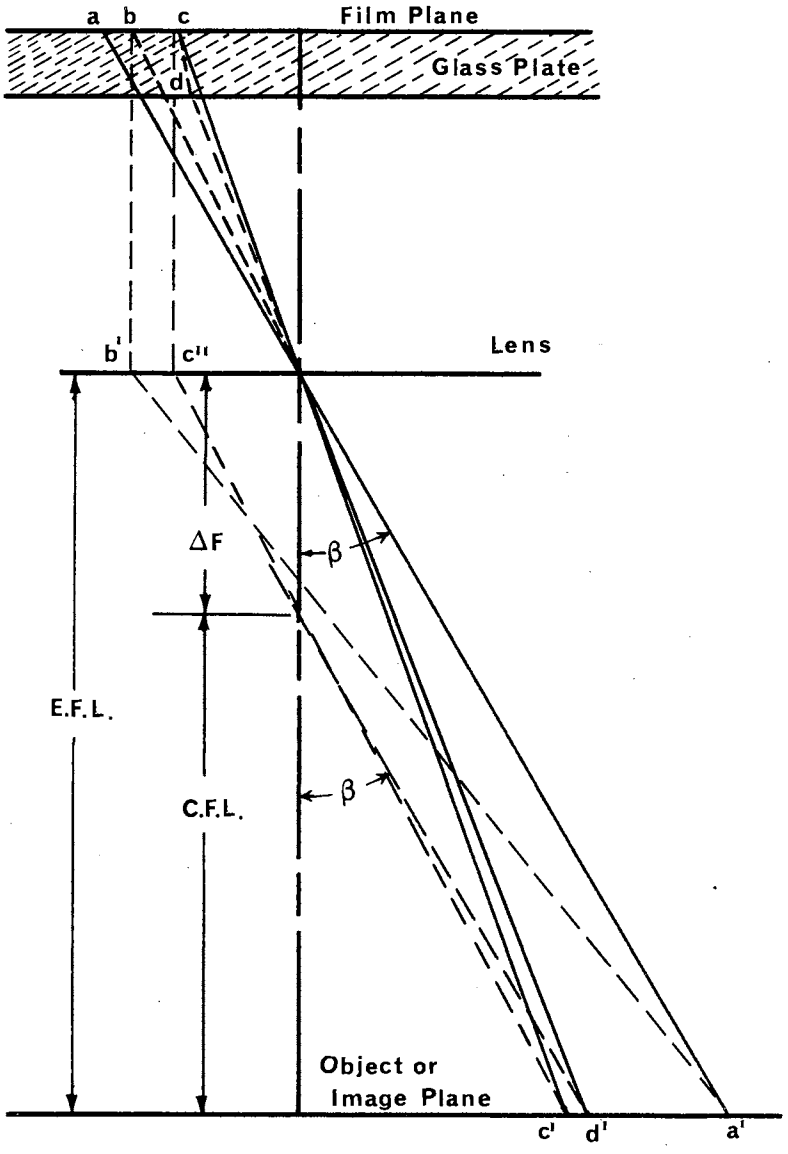

Figure 4. Overall Correction Factor.

Figure 4 illustrates graphically (errors greatly exaggerated) a calibrated focal length, or properly, since it is applied to a print, a "calibrated principal distance" developed to account for all the optical errors and the film shrinkage at the same time. This figure is a composite of the perspective rays of both the camera and the enlarger, and for simplicity shows the same lens used for exposure and projection. In the interpretation of figure 4, it should be pointed out that the glass plate was used only in the enlarger (line cdd') and that ray cc' was shown to confirm Ask's (23) statement relative to glass plate displacement errors (compare with cdd'). Line a'a is the undeflected principal ray of point a' while a'b and a'b'b are the deflected rays due to the residual aberrations, resulting in displacement ab. Point c represents the position of b after film processing shrinkage has occurred; and cdd' is the path of the principal printing ray. Note that the lens is irreversible in distortion, because the film shrinkage displaces a point so that its projected parallel ray does not pass through the same zone of the lens as it did during exposure (compare bb' with cc").

Although the true angle, β , and the perspective center is recovered for the point in question, and the relative displacements for points above or below the image plane may be found by use of the calibrated focal length, the true location of a point such as a' on the object plane is not regained. Since, of course, the true location of a point in the field, or object plane, is as important as the perspective displacement, it becomes necessary to compute the true apparent location in the projection or image plane, $[S'_a]$, which may then be used with the principal distance of the photograph (E.F.L. in figure 4) to

correct for perspective displacements of points above or below the projection plane. Note that the true view angle, β , is regained also. In other words, actual field measurements of a point made in a plane not to be used as the projection plane (say below the projection plane so that the point is to the right and below a' in figure 4) are compared to those of the photograph (corrected for foreshortening by equation 1) to develop an expression for an overall correction factor to be applied to the photograph measurements to recover the true location of the point.

Most of the set-up errors may be eliminated by careful alinement of the camera and the enlarger so that vertical photographs are obtained. Errors due to tilt of either camera or enlarger will not be discussed here, and nonparallelism of the film plane with the water surface is not important, because the effective instead of the actual illumination angle was obtained by the calibration procedure. It is important, however, that all prints are made with the optical center of the film coincident with the optical center of the enlarger lens system. Failure to properly aline the film in the enlarger will give erroneous true locations since the overall correction factor varies from zone to zone of the lens, and it is found from a calibration print.

Calibration and Procedure

It is necessary to obtain vertical photographs to eliminate the laborious tilt corrections and therefore the camera and enlarger alinement are extremely important. They may be adjusted by a precision level applied to the film holder of the camera and the film carrier of the enlarger. The alinement can be checked by photographing a centered

rectangle (in this study the grid was used) and making a print; if the rectangle is recovered in the print, alinement is correct; incorrect alinement will show the rectangle as a trapezoid (17). It may be noted in the above test that the sides of the rectangle may appear slightly bowed either in or out as a result of lens aberrations, but the corners will form a rectangle (24). When the camera alinement was considered satisfactory, reference marks were scribed on the top surface of the nozzle, which was chosen as the projection plane (it may be any well-defined plane above the flow field), and the vertical projections of the optical center, the perspective axis, and the principal axis were scribed on the zero datum plane (bottom of table). The latter lines will appear, if visible, in their true angular position in the final prints.

The shadow producing grid was affixed at a convenient height above the highest water surface that was expected in the flow field, and the illumination source (a 750 watt slide projector was used in this study) was adjusted to give the desired multiplication factor, i.e., at 20°, a shadow displacement from the zero position of 0.01 inch is equivalent to 0.0036 inch of depth. Defraction around the wires dictates that the grid must not be a great distance from the zero datum plane for sharp shadows. The grid was positioned laterally and longitudinally so that one wire was directly over the perspective axis and another over the principal axis, so that these axes could be identified on the prints. Optical errors and sag in the grid will not displace these lines from their true positions if the ends of the two wires are all in a plane parallel to the film plane; the optical center is thus also identified. When all adjustments were completed, the positions of the center line

of all shadows on the zero datum plane were measured, relative to the perspective axis at each reference line position, as accurately as possible and recorded for use in computing the correction factor of the final prints. It was found that the most convenient method of obtaining the other calibration photographs was to place a painted glass plate supported by gage blocks in the field of view above the zero datum plane.

The final prints were made full size at the plane of the top of the nozzle blocks, that is, the projection plane was about three inches above the water table. This allowed true measurements on the photograph to be made with an accuracy of $\pm$0.005 inch with an engineers scale, which gave the depth to within approximately $\pm$0.002 inch; this was considered adequate for the hydraulic analogy. Special micrometer scales and optical comparators are available with which accuracies up to $\pm$0.001 inch can be obtained in aerial-photogrammetry (25). All measurements were made along longitudinal reference lines drawn directly on the print parallel to the principal axis with the perspective axis as zero. It proved expeditious to separate the two judgments required for each measurement, i.e., first the estimation of the center of the shadow, and second, the interpolation between the scale marks. To accomplish this the photographs were Brailized (indented with a fine needle) at the center of each shadow where it crossed a reference line, and the measurements were then made on the back of the print where only the indentations were visible. It was found that after a little practice and with the use of a magnifier the location of the center line of a shadow could be estimated without change in several repeated determinations, however, different observers did not agree, therefore,

calibration and "run" prints were all read by the same individual. This method was used on all subsequent prints to obtain the "raw" data.

To aline the film properly in the enlarger the first calibration frame was carefully adjusted so that the optical center of the print and the enlarger lens coincided as nearly as practicable, and the perspective and principal axis were traced on the enlarger easel, so that all other frames could be alined in the same way. Any errors in alinement were then constant for a given roll of film and were accounted for as an optical error. When the proper alinement was obtained, the projections of the positions of the zero shadows and the wires of the grid were found by direct measurement and recorded for use in determining the shrinkage factor.

The shrinkage factor was determined at the time of measuring the prints, which may, as it was in this case, be a considerable time after processing the prints. It was found as stated above by comparing the value found from the print measurement with the actual projected value. The shrinkage factor was determined for the shadows of the zero position calibration print since the zero datum plane was perfectly flat and these values were to be used subsequently in determining the optical corrections. The shrinkages of the "run" photographs were determined by the wire positions which, of course, appeared in all the data photographs. Shrinkage may be of the order of 2 or 3 % for "Kodak Rapid Resisto" paper, but it was very uniform for a given set of prints. All data were corrected for print shrinkage before other calculations were made.

With the projected shadow position, S'_a, known, the overall optical error correction factor (correction for foreshortening and film shrink-

age) could be found for each zone of the photograph. This factor should be constant for any radial line through a circular zone, but the combination of optical components used in this study gave an unsymmetrically warped field. The latter problem proved to be the most time consuming, laborious, and difficult one of this entire study. Correction factors were therefore found for each field position along each reference line; this lent itself to the read-out procedure which eliminated the difficulties inherent in the use of polar coordinates for field plotting. The correction factors were found by comparing the true location of the shadow at zero depth with the value computed by equation 1 using the equivalent focal length, h', and the corrected apparent location, S'_a. The differences of these values were plotted versus the corrected apparent location for each reference line, and the curve approximated by straight line segments. Equations for the true apparent location were of the form

$$[S'_a] = S'_a + C_1 + C_2 S'_a. \tag{5}$$

Where C_1 and C_2 are constants found from the plots above.

Equations 1, 3 and 4 must be slightly modified to account for the errors discussed above. The true apparent location is used, and the equations become

$$S = ([S'_a])\ (1 + (B-h)/h'), \tag{1a}$$

$$h = \frac{[(h' + B)\ ([S'_a]/h')] - S_o}{[(S_c - S_o)/h_c] + ([S'_a]/h')}, \tag{3a}$$

and,

$$S_1 = S_{1a}\ [1 + (B-h)/h']. \tag{4a}$$

Note that since the reference lines are drawn directly on the print

their true locations are known without corrections.

According to Bagley (17), the effective principal distance of a photograph corresponds closely to the focal length of the camera with which it was taken, for one to one prints, but differs from the latter according to the shrinkage of the negative and the print. As stated in the definition on page 14, this would be increased for enlargements of the negative. Two methods were used to obtain the principal distance, P. First, from the data and position of the camera lens when focused on a point at "infinity" the location of the rear nodal point relative to the front lens ring can be found; this together with the distance of

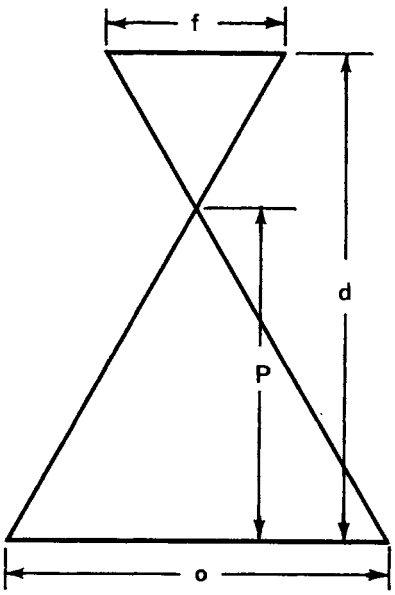

Figure 5. Principal Distance.

the lens ring from the projection plane at time of exposure gives the effective principal distance of a photograph showing the projection plane full size. Second, as shown in figure 5, the dimensions d, f, and o can be measured by observing the object field after the camera has been properly focused without film in the camera. By simple

proportion: $P = od/(f+o)$. The values obtained by the two methods agreed quite closely at 1989.35 units (all dimensions are given in units of 1/50 inch throughout this paper, unless otherwise stated). Since all photographs relative to the problem at hand were taken without moving the camera, the effective principal distance was constant. Note that the film shrinkage was not considered here, but that the method of using the true apparent location instead of the calibrated focal length is compatible with the above.

Each flow field was covered by approximately 200 discrete points. The results for each reference line were plotted on a depth versus true location graph with the depth exaggerated. Smooth curves were drawn through the points giving a longitudinal cross-section of the flow field. Interpolation for the location of a given depth was made from the above curves, which in turn was plotted on a drawing of the field. This graphical interpolation proved to be extremely useful in helping to visualize the warped surface and in determining the shape of the curve between the isogrametric points in the field plot.

Discussion of Problems Encountered

The shadow-photogrammetric method described above is disastrously, deceptively simple in concept and holds many pitfalls for one who is not versed in the usual problems associated with aerial-photogrammetry. The problem here is even more difficult in some ways, because a miniature camera was used at close range. In fact, it is so simple at first sight, the writer believes that some data commonly obtained photographically may be in error because of failure to account for the foreshortening effects and optical errors, in addition to parallax error.

Even in simple streak pictures, the foreshortening effect will lead to erroneous estimations of the velocities if the surface is warped and the picture is not properly rectified.

The photographs used for this study were exposed using the water table in the Mechanical Engineering Laboratory at Oklahoma State University during the summers of 1963 and 1964. Some 400 photographs were made for the first run, showing the streak patterns for various conditions of flow at various shutter speeds from 1/50 to 1/2 second, and the corresponding shadow patterns. A series of calibration pictures was made on one roll of film. Aluminum powder was used to give an opaque surface for the shadows. Because of the temporary nature of the experiments and the limitation of funds, the writer's camera (thought to be high quality) was used in a jerry rigged set-up, which was judged to be entirely adequate at the time, but proved to be too crude to give acceptable results in the depth calculation for the calibration prints. The results for the depth of intermediate points were 15 to 20 % from the true values, leaving the practical usefulness of the method in doubt. However, it was felt that it still held promise of producing results with improved techniques.

Under Dr. Zumwalt's guidance a special steel framework to support rigidly the camera and illumination source was built over the water table during the winter semesters of 1963-64 to obtain some motion pictures of a blast wave flow field (26). The new support was used by the writer to obtain a final run of some 200 photographs of the shadow patterns corresponding to the flow conditions of the first run. The precision of measurements was improved, and data were obtained to allow more errors to be evaluated. Calibration photographs were made for

each roll of film in addition to a complete calibration run made by the use of the glass plate to obtain the intermediate shadow positions. Many of the precautions given in the procedure section are the result of problems encountered in the data reduction process. The first confirmation of the practicality of the method was found from the calibration run in which the raw data were corrected only for foreshortening (all other errors were constant for the group). The computed intermediate depths all fell, as they must, on a straight line between the two extreme points. Errors of 1 % or less were found. Note that although the true depth may be found without correcting for shrinkage and optical errors, the true location of the point in the object field is not determined. Encouraged by this result, the remainder of the flow field pictures were taken, using water soluble show card paint to give an opaque surface of the water. This gave a more uniform and continuous field of view so the shadow positions were easier to determine. The same camera and enlarger were used for both groups of experiments.

Data Reduction Methods

Mark I Method

The difficulty of reducing the data is mainly concerned with the determination of the position of the point in question; it results from the unsymmetrically warped and non-linear field projected by the optical system. Three different methods, two analytical and one graphical, were investigated with several variations of each. All the preliminary calculations were made on a desk calculator, but the final results were run on a digital computer at the University of Missouri.

The programs are included in the Appendix.

In order to obtain the desired accuracy in the measurements of the photographs, the projection plane was printed full size on two 8 by 10 inches pieces of "Rapid Resisto" paper (not available in larger sizes) so that the perspective axis appeared in both with considerable overlap, showing at least two identical shadows in each print. A comparison of the measurements for identical shadows was used to orient properly the pairs of prints so that the other measurements from the two would be compatible. The shadow of a given wire was always on the same print as the wire. All prints for a given run were seasoned and then processed as rapidly as possible so that the moisture content was constant. The prints were prepared by first accurately locating the perspective (wire nine as shown in the figures) and the principal axes on each; the reference lines were then drawn parallel to the principal axis at suitable locations, taking care that they coincided on all prints associated with a given set of calibration photographs. After preparation, the prints were Brailized as stated above and the measurements were recorded for further processing. It required approximately three hours to prepare and measure 200 points for each pair of prints.

The print shrinkage was accounted for by correcting the raw data, as stated above, for the two analytical methods, designated as Mark I and Mark II, by a series of three simple proportional equations for each group of prints. The same corrected data were used for both computations. No corrections for shrinkage were made for the graphical method, Mark III.

The first, Mark I, computations followed the method given above on page 32, that is, the effective illumination angle, θ, was found

from the true positions, as computed by equation 1a, of the two calibration shadows corresponding to a given lateral wire at a given reference line. The correction equations for the optical errors were found by comparing the true location of a shadow for zero depth to that computed by equation 1, using the apparent location, S'_a, and the principal distance, h', of 1989.35 units; the differences divided by the foreshortening constant, $1 + B/h'$ for zero depth, were then plotted to a large scale versus the apparent location. Note that the correction applies to the apparent values, not to the true apparent values. The curves were approximated by two straight lines and equations of the form

$$|[S'_a]| = |S'_a| + A + BS'_a \qquad E \geq S'_a,$$

and

$$|[S'_a]| = |S'_a| + C + DS'_a \qquad S'_a < E,$$

fitted to them, where E is a constant. A set of equations was required for each reference line, for each series. Some preliminary checking in the middle of the field seemed to give the results that were expected, so a computer program was developed to compute the depth, the depth ratio, the depth ratio squared (corresponding to pressure for the gas analogy), and the Froude number based on the main stream stagnation head, and the complete series was computed. The results were of a discrete nature revealing little information as to the shape of the surface so an additional computer program was developed to interpolate (only longitudinal interpolation permitted) the field for the positions of isogrametric depths. When the results of a known field were plotted on a diagram of the flow field the points appeared as random collec-

tions on different reference lines, i.e., points that should have been more or less equally spaced along a reference line were not, and the "bunching" was not the same on adjacent reference lines. It became apparent during the checking and cross checking of this computation that values numerically interpolated by the computer shed little light on the true shape of the surface between the points. Thus, machine interpolation is not recommended.

The cause of the "bunching" of the points could not be discovered by carefully checking the data and the computations. However, it was noted that values of the cotangent θ across the field varied by 3 % or more and that the cotangent θ did not monotonically increase, as it should, as one proceeded away from the light source (a reversal of up to 4 % was found). In an effort to "smooth" the results, a Mark Ia computation was run using the average value of the illumination angle, θ, laterally across the field. This "smoothed" some of the results but, all in all, it was no better than the Mark I computation. Similar results were obtained by using the illumination angle computed along only the principal axis. Further checking along this line seemed to be fruitless. At this point it was evident that the method of the Mark I calculations had to be modified considerably if better results were to be had, and a series of investigations was launched to discover where the method was in error.

The calculation of the expected error due to errors in measurements from the photographs and the set-up showed that, if the true apparent location could be found, an error of $\pm$1.3 % could be expected in the depth. It was also found that the depth equation was very sensitive to errors in the value of the cotangent θ. Thus accuracies of

this magnitude were to be sought.

As an extremely sensitive cross check of the Mark I results, the location of the illumination source above the zero datum plane was computed by use of the angles of adjacent points. More or less random values were found ranging from 5202 to 837 units. No pattern was found in the results to indicate a general error in computations, but apparently the angles computed by the true apparent shadow locations, as given by the first set of optical error equations, were inexact. Several minor investigations were conducted such as taking the average of the above heights to compute the angles; computing the calibrated principal distance from actual and computed values of S_o; and finding a new set of optical error correction equations from the known and observed values of S_o which included the shrinkage. The latter proved promising down to the center of the field, at which point it failed.

It was concluded that the angles for the illumination source were not accurate enough to give results within the expected error, or to "smooth" the results for the entire field. Any further attempts to use only the true values of S_o and the photographs were discarded. It had been thought that only the photographs and the camera location were required. Note that the above does not invalidate the optical error correction equations, however, they were in doubt.

Better values of the illumination source angles, of course, could be found from the measurements of the set-up, however, these dimensions were not known with a high degree of accuracy, i.e., the dimensions from the perspective axis and the zero datum plane to the bottom of the lens ring of the projector were known accurately, but this was not the apparent light source. The calibration run in which several interme-

diate depths were known with good precision by the use of the glass plate was used to find the mean location of the source. All calculations were made along the principal axis with a new and more accurate set of optical error correction equations, developed as above, and adjustments were made in the measured values until the depth of a known intermediate point could be predicted to within less than 1 %, which was better than the expected error. The position of the illumination source was found to be 1026.25 units above the zero datum plane and 1775 units upstream from the principal axis. This placed the effective light source 3 inches in front, and 3/4 inch above, the light lens ring to which the measurements mentioned above were made.

With the effective location of the illumination source known, the effective illumination angle for each reference point could be computed from two different sources of data, the true location and the computed true location of the zero depth shadow. The latter was used in subsequent calculations; although it is less accurate than the former, it is compatible with the intermediate points because any distortion induced by the optical error correction equations would be in both values. The second ($h_c > o$) calibration point could now be used as a known depth that must be predicted from its apparent location on the print (this was known for each series).

A new program for the IBM 1620 computer was developed to compute the second calibration point, as suggested above, from the known position of the illumination source using the first set of optical error correction equations. It was found that the error in the predicted calibration depth was less than 1 % from wire 1 (farthest upstream) to wire 6, from 1 to 2 % from wire 6 to 12, and 4 % or greater from

wire 12 to 18. The shadow of wire 7, and wire 9 were in the center of the field. These errors were found for the whole series. Any attempt to improve the optical correction equations with two straight line approximations intersecting near the center of the field, as they should for symmetrical lenses, proved futile. It was here that the unsymmetrical warpage of the projected image was discovered. Thus, if the true apparent location of a shadow was to be predicted accurately, an optical error correction factor would have to be determined for each shadow in each of its possible positions from zero to the maximum depth. This, of course, was out of the question, since it would have to be done for each roll of film and would require hundreds of photographs.

The computed true position of a point in question is the major problem, since the depths can be found, as stated above, without finding the true location. However, the depths were not correctly predicted using the computed true locations. Both are required.

Mark II Method

Since the results of the above examination of the errors in the predictions of the calibration depths showed definite breaks in the accuracy of the prediction between wires 6 and 7 and wires 11 and 12, a second set of optical error correction equations was determined for each series, by trial and error, so that at the beginning and end of each interval the error of the prediction was less than 1 %. Straight lines were assumed between the end points. The trial and error method was used because the accuracy required in the equations did not lend itself to graphical determination. Note that this gave some overlap

in the corrections because each shadow was displaced by the correction equation according to which wire it belonged rather than its location in the field. The sign change for the data of S_o for wire 7 made the equations extremely difficult to determine. Therefore the equations for the whole field were tied to the known position of the wire 9 shadow at zero depth which was near the center line of the field. As one progressed from the center line toward the ends of the field the values of the computed zero position shadow locations were allowed to float away from the true values while the separation between S_o and S_c would give the proper calibration depth prediction at the end points. The maximum error between the computed and true locations of S_o was 4 % which gave the true depth and location within the expected error. Film shrinkage made it necessary to develop a set of equations for each roll.

Encouraged by the above results, which have little to support them except that they gave better results in the prediction of the second calibration point's depth for the whole series (errors were less than 2 %), a new Mark II program, given in the Appendix, was developed to use the known light source location and the equations developed above. Preliminary results seemed promising so the method was applied to a flow field photograph. The simplest flow field was used, namely, the one having the secondary-injection slot plugged. This could be compared with the measurements of Preiswerk (8). Some random grouping of the points, while less than given by the Mark I calculations, still occurred in the machine interpolated values for the rather flat flow field used for checking the results.

As a further check on the Mark II results, depth versus longitudinal location curves were plotted for the check field. It was found

that the unavoidable original measurement errors on the prints accounted for about half of the difference in the depth on adjacent reference lines, i.e., when the depths were plotted with tolerance the ends of the tolerance marks overlapped. Thus, the method was being pushed to its limits of accuracy. However, if the depth versus length curves were plotted along a reference line with an extremely magnified scale for the depth and smooth curves drawn through the points not obviously in error, a field plot could be developed from the Mark II computations that compared well with that expected (8). Graphical interpolation was used on all subsequent field plots.

Mark III Method

The results of the Mark II computations were better than those of the Mark I computations for the check field, however, there was no good logical argument that the optical error correction equations, as developed for the Mark II computations, would give the true location of a given data point. So, as a final check of the foregoing results, a graphical method was developed that eliminated the determination of the illumination source location, camera errors, shrinkage and projection errors. The graphical method, illustrated in figure 6, requires a set of calibration prints (several depths), in addition to the field prints, and the true location of the shadows for zero depth and <u>one</u> other calibration point as measured from the set-up.

The left side figure 6 was constructed as follows: [1] The observed values of S_o were plotted versus the true location of S_o and the points approximated by a straight line. Thus if an observed point was entered on the ordinate, the intersection with the S_o line gave its

true location projected to the zero datum plane, S''_a, on the abscissa below (see figure 6a). [2] The depth curve, h, was determined by plotting the various calibration depths on the auxiliary ordinate (depth) versus the projected location. [3] The known true position of a second calibration, S_c, point was plotted using the abscissa for true location and the auxiliary scale for depth, and was connected by a straight

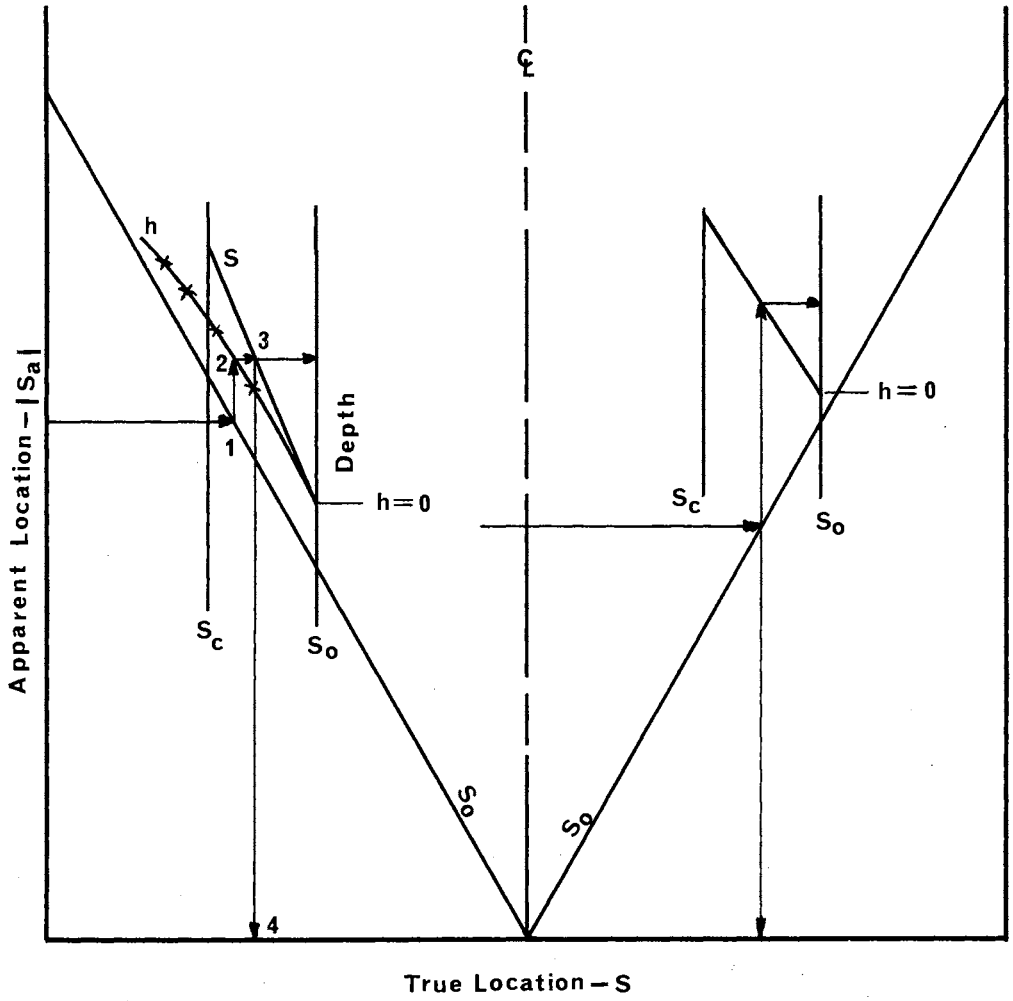

Figure 6. Graphical Method.

line, S, to the zero depth point. Figure 6 illustrates the construction for only one wire and one reference line, and many such graphs would be needed for a large field. Note that no scales are given and

the curves are exaggerated for clarity; in general all scales would be different.

Figure 6 is used as follows: One enters the observed distance of the shadow from the perspective axis on the ordinate. The intersection with the S_o line, 1, gives the projected location of the point directly below on the abscissa. The depth is given at the intersection with the h line, 2, read from the auxiliary scale to the right of 2. The intersection with the S line, 3, gives the true location on the abscissa at 4. Note: The depth is linear with the true location, but not with the projected location (see figure 6a).

Curves for the graphical method were drawn for each series for each reference line to determine the slope of the S_o location line. It was found, within the accuracy of a large scale plot, to be practically constant at 0.90 for all runs if the corrections were linearized. Thus to eliminate the time required to draw the graphical method curves, a computer program was developed to compute the results rather than reading the graphs (program in the Appendix). Note: The same data from the photographs are required for all methods except Mark III which requires several calibration prints rather than two.

From figure 6a (figure 1 simplified) it is seen that

$$h/h_c \doteq (S''_a - S_o)/(S''_{ac} - S_o),$$

or

$$h \doteq [h_c/(S''_{ac} - S_o)]\,(S''_a - S_o) = K_1\,(S''_a - S_o), \qquad (6)$$

where K_1 is the proportionality constant for a given wire position. The approximation made in equation 6 is quite good, introducing only an error due to β angle differences at h and h_c, where h_c is the maximum

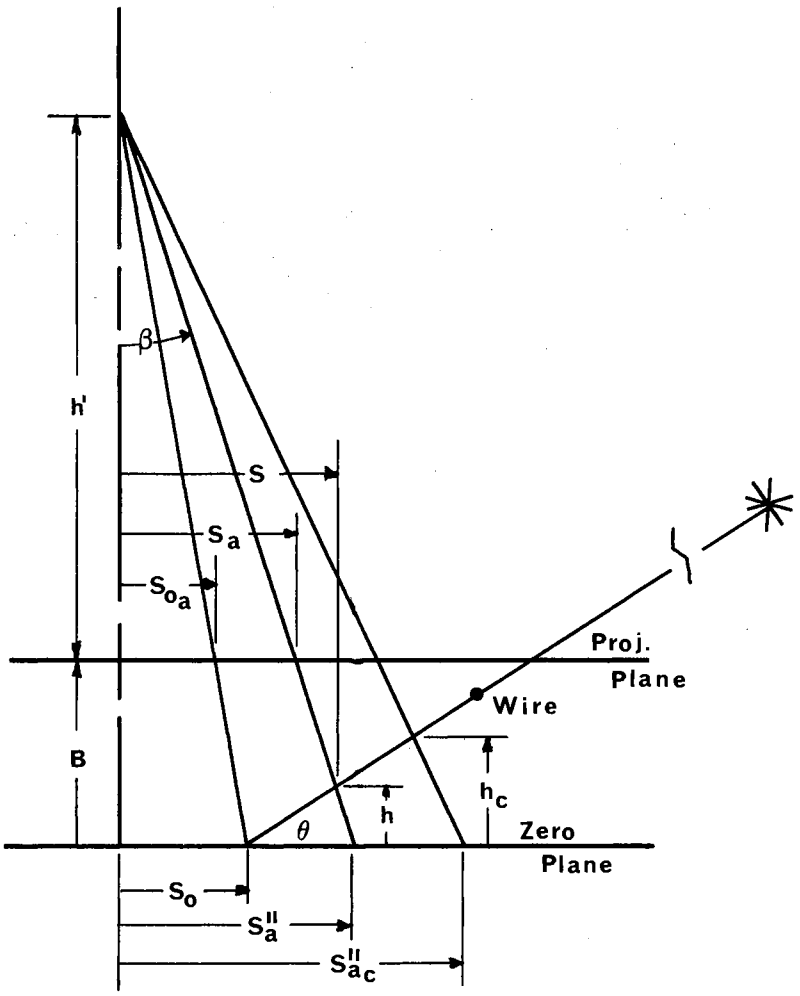

Figure 6a. Principal Plane.

calibration point. For the combination of conditions for maximum error in the test set-up, the error in h is less than 2.8 % or 0.0093 inch, which is about the same as the errors introduced from the measurements of the photographs. It is also seen that the true location is given by,

$$S = S''_a - h \tan \beta ,$$

or

$$S = S''_a - h \, [S''_a/(B+h')],$$

whence

$$S = S''_a \, [1 - h/(B+h')]. \qquad (7)$$

The simple equations used for the computer program were:

$$S''_a = S_a/0.90,$$

$$K_1 = h_c/(S''_{ac} - S_o),$$

$$h = K_1 \, (S''_a - S_o),$$

$$S = S''_a \, [1 - h/(B+h')],$$

and the lateral correction given, as before, by,

$$S_1 = S_{1a} \, [1 + (B-h)/h'].$$

The location corrections are small, because h compared to B+h' is small, and the reference line location was known exactly. In this study the maximum value of h was 28 units and the minimum value of B+h' was 2167 units, thus the true longitudinal location of a point is 98.7 %, or more, of the projected value. The last two equations require the principal distance and the location of the projection plane which were not needed for the pure graphical method.

The right side of figure 6 represents the computer program without the correction for location discussed above. For work in which the location and depth are required only to the accuracy given above, they can be read directly from a plot similar to the right side of figure 6 without further corrections. Note that the depth curve has been linearized, plotted with only two calibration points, as in equation 6. This approximate method offers a considerable saving in time as only two calibration prints are to be read and the true locations of the shadows for a calibration depth are not needed. The latter were difficult to obtain unless the glass plate was used.

A check of the calibration series showed that an intermediate depth between the two calibration depths could in general be predicted within an accuracy of 2 % or less. However, several points were in error by 4 to 6 %. The larger errors were random throughout the field and were probably due to inaccurate data.

A tabulation of the results for each of the three methods is given in the next section for a comparison of the values.

CHAPTER IV

APPLICATION OF THE SHADOW-PHOTOGRAMMETRIC METHOD TO A HYDRAULIC ANALOGY PROBLEM

The shadow-photogrammetric method described above was developed because of the application given here rather than the other way around. The desire to learn more about a transonic flow field with a second fluid injected transversely into the stream at various conditions required quantitative data of the pressures, mass flows, direction, and speed of the flow. The water table analogy to gas flow seemed to offer another approach to obtaining required experimental data. It became immediately apparent that finding the depths of the water at representative points throughout the field presented a major obstacle in using the water table. It was fortunate that during the preliminary work in setting up the experiment to develop the technique of obtaining the photographs of the streak lines that the shadows of the reference probes (needles) were noted on the surface of the aluminum particles, this led to the shadow-photogrammetric method. Obtaining the data for the whole field simultaneously is, of course, attractive.

The problem of secondary injection into a nozzle throat arose from an attempt to provide a practical thrust-control for solid-propellant rockets. Rocket motors must be designed for given specific operating conditions of a rather narrow range and operation at off design condi-

tions is at best difficult to achieve mechanically. Fuel flow control has been successfully used to throttle liquid-fuel rocket motors but no really successful mechanical means, such as differential covering of the propellant and acoustical energy sources, have been devised to control the burning rate in a solid-propellant rocket motor (27, 28). Control of the throat area seems to offer the best method of controlling the burning rate of a solid-propellant rocket (28).

The current interest in the problem of throat area control is shown by the patent activity, and the attention it is receiving in the literature and by the Air Force. At least fifteen patents have been granted to inventors of nozzle modifications intended to control the thrust of turbo-jet and rocket engines. Some thirteen or so papers dealing directly with aerodynamic control of nozzles have appeared since 1957, and the Air Force let a sizable contract in the summer of 1963 for the study of throat injection and the attendant hardware necessary for the control of hot gas injection.

The feasibility of controlling the thrust of an air nozzle with secondary injection at the throat was demonstrated by Jackomis (28) in an M.S. Thesis at Oklahoma State University. His cold air test indicated that an effective throat area change was about twice as large as the percent of injection-to-primary flow. This led Dr. G. W. Zumwalt to plan a long range experimental program of investigation into the injection of a gas into a two-dimensional transonic flow region. At the outset it was planned to make pressure field measurements of an air nozzle with secondary injection of the same gas at various locations near the throat, and use flow visualization techniques to determine the physical characteristics of the interaction between the two

streams so that a possible analytical analysis could be made of the whole problem.

The experimental phase of this work was undertaken in the Mechanical Engineering Laboratory at Oklahoma State University in three steps by Messers. R. O. Warloe, W. I. Maegley, and R. D. Stutzman under the immediate direction of the writer and under the general supervision of the faculty advisor, Dr. G. W. Zumwalt. Messers. Warloe (29) and Maegley (30) reported the results of their work in their Master of Science Reports presented to the Graduate School in August of 1963. Mr. Stutzman's (31) work was reported in a special unpublished report to Dr. Zumwalt in June 1963. As the first step, Mr. Warloe designed and set up an experimental nozzle with a rotating throat block that provided for cold gas secondary injection into the throat region of a converging-diverging nozzle. He mounted the nozzle in the supersonic wind tunnel facility of the laboratory, studied the aerodynamic blockage, and made pressure field measurements. Mr. Warloe was hampered in any attempt to analyze the flow field, because the separation between the main and secondary streams was not known. In the second step, Mr. Stutzman set up a hydraulic analogy of Warloe's nozzle using a geometrically similar nozzle on the laboratory water table. He carried on some preliminary flow field studies which were not complete enough to determine the interface between the two streams, or to allow a check on the validity of the water analogy for the problem at hand. In the third step, Mr. Maegley modified Warloe's equipment and procedures so that shadowgraph and schlieren photographs of the flow field with secondary injection of cold air and sulfur hexafluoride could be obtained. Due to diffusion no sharp interface between the two streams

was found by Maegley (30) and attempts to estimate the percent of area reduction of the throat did not compare with that found by Warloe.

Additional experimental work was done by the writer, in the summers of 1963 and 1964, with improved equipment and techniques to determine the velocity and pressure fields, the interface between the two streams, and check the validity of the hydraulic analogy for secondary injection into a transonic flow field. It became apparent at the outset, that determining the isogrametric depth lines was to be a major problem due to the inability to maintain steady state conditions for the long period of time required for the usual method of measuring depths with a micrometer probe from a fixed height X-Y plotter frame. A photographic method seemed to offer the best means of obtaining the raw data.

The importance and the difficulty of analyzing the transonic flow field began with DeLaval's discovery that a gas could be accelerated to supersonic velocities by use of a constriction. It is still with us. The difficulty arises from the fact the fundamental non-linear differential equation for the flow field changes from the elliptic type in the subsonic region to the hyperbolic in the supersonic region. The first attempt to construct the streamlines and the lines of constant velocity in the neighborhood of the throat of a converging-diverging nozzle was made by Th. Meyer in his dissertation in 1908. Many, many papers have followed, and several writers have found "exact" and approximate solutions to certain particular cases that shed considerable light on the complicated character of transonic flow, however, one must still conclude that a general solution to the problem is not at hand; more study is certainly necessary.

The problem considered here, a transonic flow field with a sonic inflow at right angles to the main stream, for the application of the shadow-photogrammetric method is far more complicated than that of a simple nozzle. An extensive literature survey revealed several papers concerning the aerodynamic control of a converging nozzle in which the authors postulated completely mixed and unmixed flow of the streams; high injection pressures through narrow slots seemed to favor the latter. The first report, in the open literature of an experimental investigation of the aerodynamic throat control of a converging-diverging nozzle was made by McAulay (32) of Lewis Research Center, in September 1959. This was a cold gas flow experiment in which the stagnation pressures for the two streams were equal and the secondary flow controlled by slot width; the injection was upstream of the throat at approximately Mach = 0.3; the principal result was the demonstration of the feasibility of aerodynamic throat control. In a second paper Rodriquez (33) used throat injection for thrust vector control; the injection was slightly upstream of the geometric throat; he too found the main stream flow and the thrust were modulated, but he found no thrust vector control. The last significant paper on throat injection preceding the work on this problem at Oklahoma State University was a Russian paper by Nesterov (34) in 1962. The main part of this paper is concerned with converging nozzles, however, he discusses a cylindrical throat Laval nozzle with injection; he assumes complete mixing of the two streams, and that the separated region, just below injection, has the isentropically determined main stream pressure at the end of the cylindrical section, and develops a one-dimensional analysis resulting in seven equations which require successive approximations

for solution; he presents some results of his calculations. His separated region pressure assumption seems doubtful.

The latest references in the open literature are those of Zumwalt and Jackomis (35), Jackomis (28), Warloe (29), Maegley (30), and Stutzman (31) describing the work done at Oklahoma State University which was reviewed briefly earlier. It was hoped that the application of the new found technique of shadow-photogrammetry to the water analogy together with streak pictures would shed enough light on the problem that perhaps another solution could be presented. However, the water analogy failed to do so.

Description of Apparatus

The water table used in these studies was built by the writer in the fall semester 1962, with the help of the laboratory technicians, from modified plans developed by John Samos (36) in his Masters Report 1960. The table is essentially a flat glass plate, with 4 inch sides, mounted on an angle iron framework with a catch tank and reservoir. A centrifugal pump was used to circulate the water and the flow control to the reservoir was through a globe valve after the pump so that the secondary flow could be tapped off without disturbing the delivery to the reservoir. It was provided with a sluice gate and a hinged weir so the speed and depth of the water on the table could be controlled (these were not used in this work). An X-Y plotting frame was mounted above the table so heights along the glass plate could be measured with a micrometer probe at a known location.

The half nozzle (side of the table provided the center line) was geometrically similar to the gas flow nozzle used by Warloe and Maegley

in their studies; it was 16 times as large, i.e., nozzle radius 30.00 inches, throat width 5.39 inches, injection slot width 0.124 inch and approximately 4 inches high. It was built of 3/4 inch plywood with the working face covered with black 3/16 inch formica mounted in such a way that this face formed a near perfect circular arc; the facing was glued on with water proof glue so that no fasteners were exposed to disturb the flow. A water box was built in the center of the frame to serve as the reservoir for the secondary flow, and the secondary flow converging nozzle was fashioned from wood blocks. The secondary flow slot was cut after the nozzle was stabilized and the secondary nozzle finished by sanding through the slot so that it was very smooth. All the important center lines and angle reference lines were scribed on the completed nozzle after painting.

The shadow producing wire grid was made of 0.040 inch diameter annealled steel wire which was twisted with a hand drill until it became cold worked, hard, and straight (about 75 feet were twisted at one time). The wires were cut to the approximate lengths and selected for straightness. The pattern for the grid was laid out accurately in half inch squares on heavy (3/16 inch) poster board and the wires were held in alinement by pinning them to the board. They were soldered at each point where they crossed and finished by filing and sanding off the surplus solder except at one joint for each transverse wire; these joints were used as identifying marks in the photographs. The grid was cut to fit the nozzle throat after painting dull black (to prevent reflections on the water surface). The grid was supported on balsa wood strips and blocks carefully placed and glued on the nozzle face and the side of the water table. Slight changes in the dimensions of

the nozzle frame required the blocks on the nozzle to be replaced for each series of runs.

The camera used for this study was a Tower (Sears and Roebuck) high quality 35mm through-the-lens reflex which belonged to the writers wife; it was used with a 58mm f2.4 Takumar lens, stopped down to f16-f22, reported to be of excellent quality. The camera was mounted at approximately 36 inches above the table on a heavy duty tripod with a universal mount. In the first series of photographs the tripod was mounted on a weighted step ladder to prevent movement for the desired position; in the second series the steel frame work mentioned above was used. A plumb bob and an accurate machinist level was used to obtain the preliminary alinement which was checked by photographing the grid.

The illumination source was a standard 750 watt slide projector obtained from the Audio-Visual Center of Oklahoma State University. In the first series, it was hung from the ceiling of the laboratory by wires; in the second series it was rigidly clamped to the steel frame on which the camera was mounted. The projector had a 3 inch lens.

Set-up and Procedure

The water table bottom was prepared by spray painting the surface with dull white paint (black for the first series) to prevent light transmission up through the glass and to provide a screen for the shadow projections; when dry it was lightly sanded to a smooth surface. The bottom was then laid out geometrically with a steel rule and an awl so that the perspective and principal axes, the center lines of the angles of injection (0, 4, and 8 degrees upstream and 4 degrees down-

stream of the geometric throat) and the circular contour of the nozzle were located. The latter gave a check on the accuracy of the arc of the face of the nozzle and provided a means of rotating it around its center of arc.

The nozzle was mounted in the center, near the edge, of the water table with an adjustable head piece to close off completely the reservoir out-flow so that all the water coursed through the nozzle; no tail piece was necessary as the nozzle exit was out of the field of interest. The nozzle was carefully alined with the proper reference marks and weighted down to prevent movement while it was being sealed to the table. Masking tape was used to seal and hold the head piece in place. Glazing compound was then forced in the joint between the nozzle and the bottom and the excess trimmed off so that the face of the nozzle and the compound were smooth and at right angles to the bottom (the compound shows as a thin white line in the figures). The secondary water box and injection nozzle were also sealed with glazing compound. Considerable attention was given to these joints to prevent a disturbance of the water flow. The whole set-up was checked for water leaks before any data were taken.

For the first series of tests it was desired to obtain streak photographs at various shutter speeds so the stream lines could be determined and possibly the speed could be estimated from the lengths of the streaks. Two problems developed in recirculating the water by the pump; first, it was found that the flow could not be held steady for the 15 minutes or so required for a complete set of photographs, and second, the aluminum particles which recirculated appeared in the stream on or near the bottom moving at a slower speed than those float-

ing, making interpretation of the prints difficult. No efficient filter could be devised for the aluminum powder with a capacity compatible with the flow rate (see figure 7). As it was also desired to measure the mass flows, of each stream, the water supply system was modified to a flow-through system. The main stream was metered by a calibrated rotary water meter and the secondary stream by a calibrated rotometer. Cloth bags of detergent were placed in the reservoir to reduce the capillary attraction of the water with little or no noticeable result.

A series of calibration photographs was taken using aluminum powder on the surface of still water retained at the desired depth by damming up the nozzle exit (see figure 8). Depths at 0.05 inch intervals were used. As discussed elsewhere, this proved to be of no use in determining the depths of subsequent runs due to film shrinkage.

The procedure for the first series of experiments, after the calibration run, was as follows: The water flow was adjusted to the desired heads--secondary to main stream head ratios of 0, 1.50, 1.75, and 2--corresponding to the pressure heads used by Warloe and was allowed to stabilize; a series of photographs of the main stream was taken with aluminum powder dusted on the surface at 1/4 inch intervals by a special device, also a corresponding view was made with the aluminum powder issuing from the slot with the secondary flow (see figures 9 and 10); five photographs were taken at each flow condition at shutter speeds of 1/2, 1/5, 1/10, 1/25, and 1/50 of a second; the wire grid was then positioned and photographed at 1/10 second shutter speed, with a large dusting of the aluminum powder covering the whole field. The streak photographs were illuminated by two 150 watt incandescent bulbs in reflectors, placed at each end of the field. The grid photographs

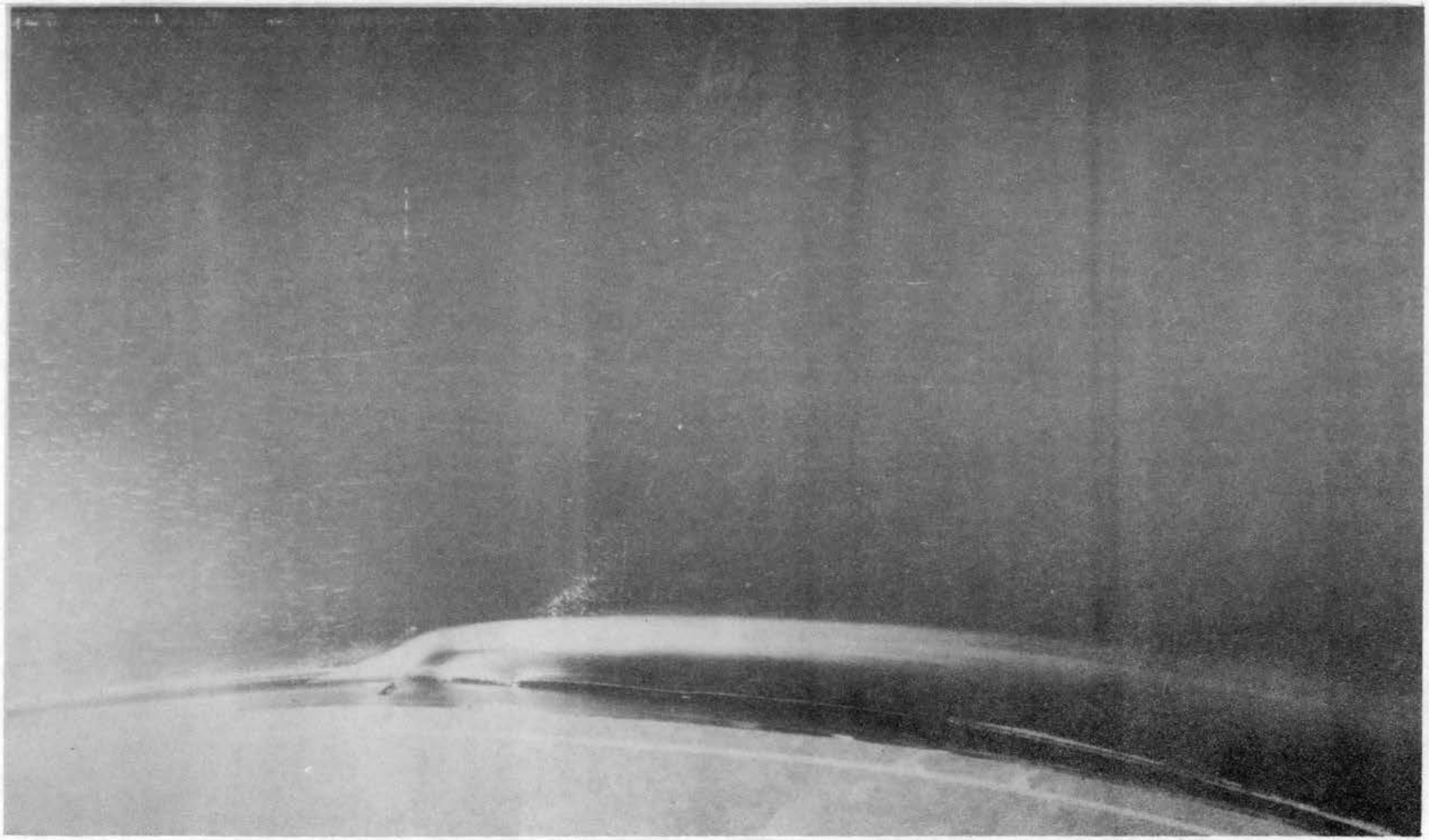

Figure 7. Aluminum Particles Being Recirculated by Pump.

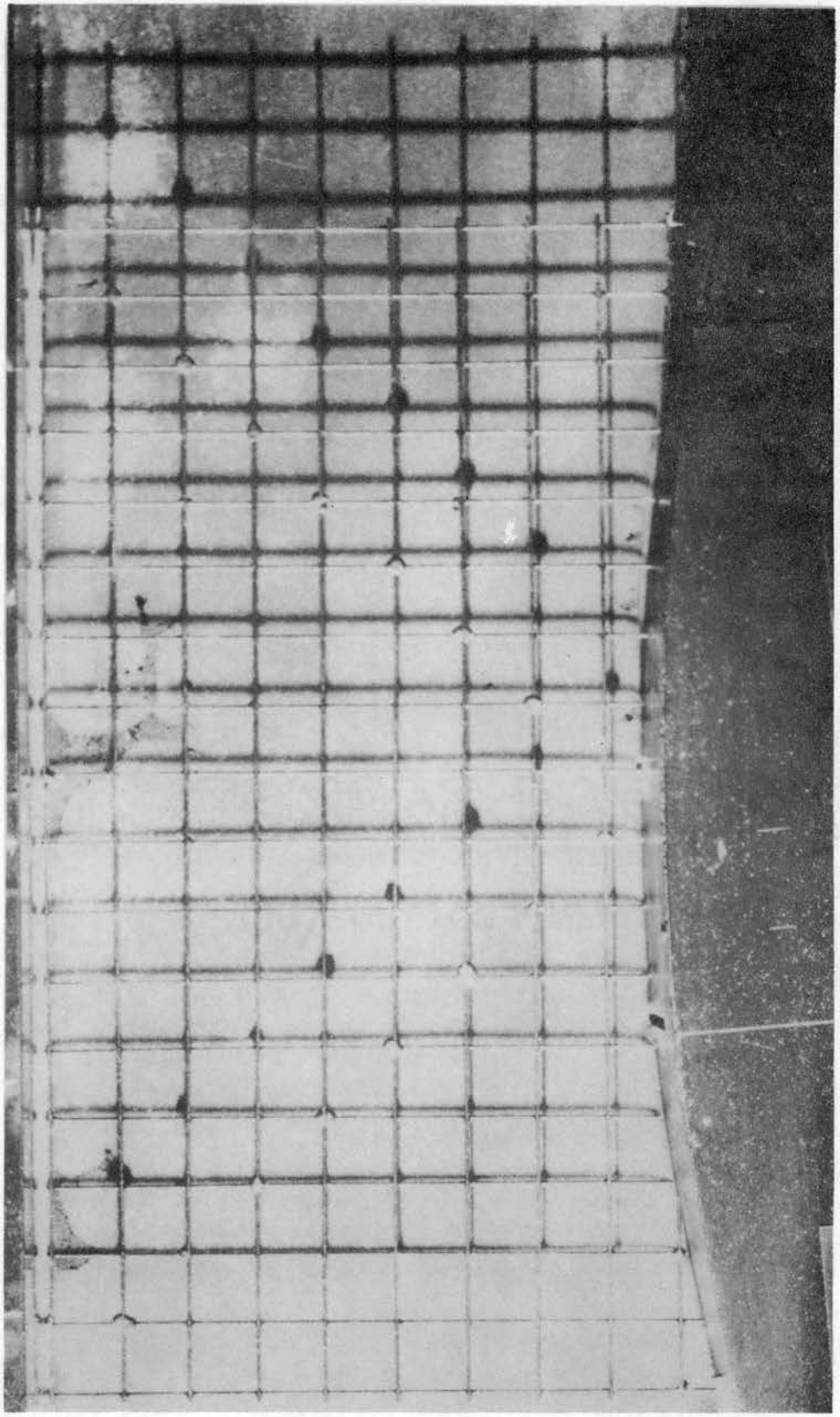

Figure 8. Calibration of Grid by Water Method.

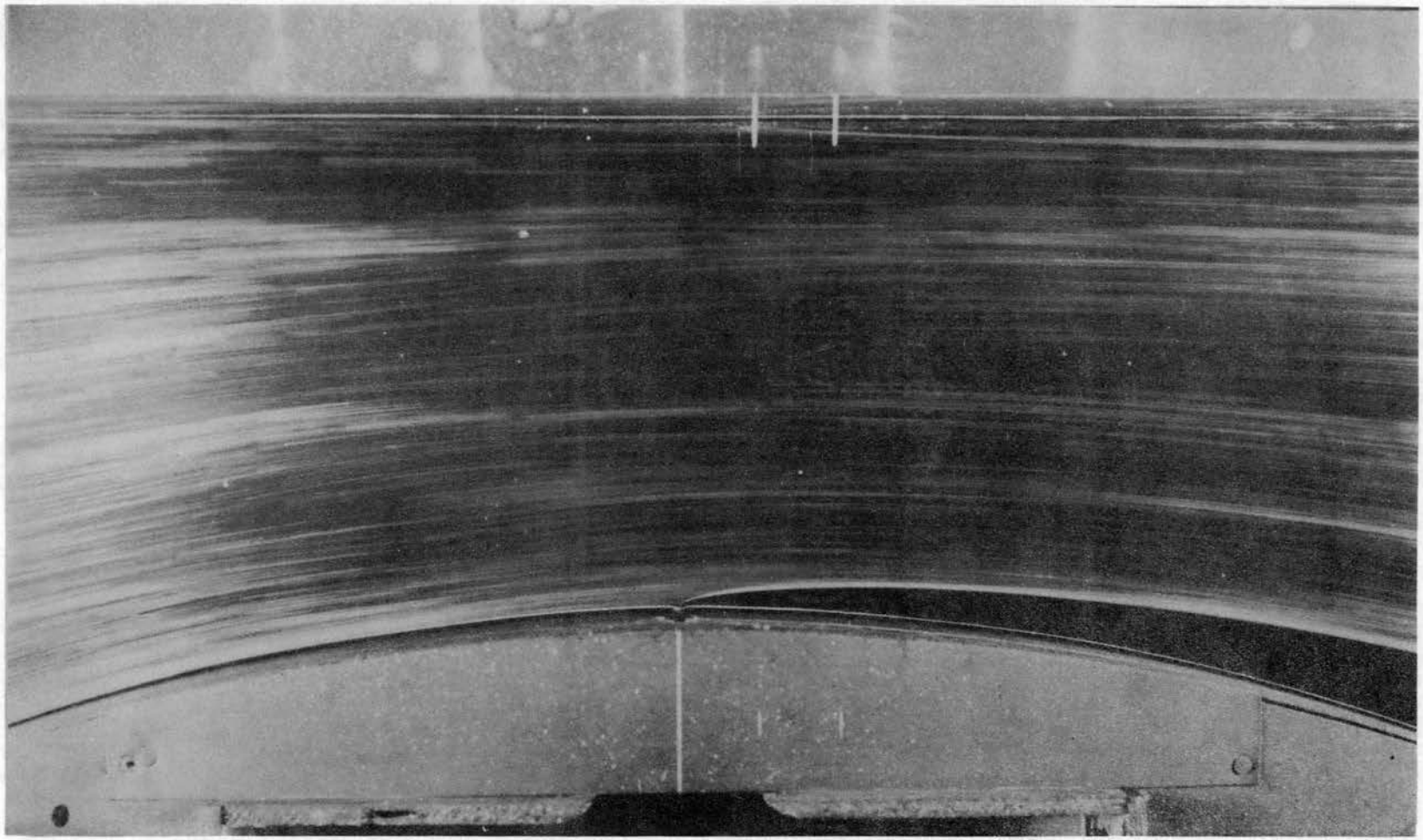

Figure 9. Typical Streak Lines for Open Slot; No Secondary Flow.

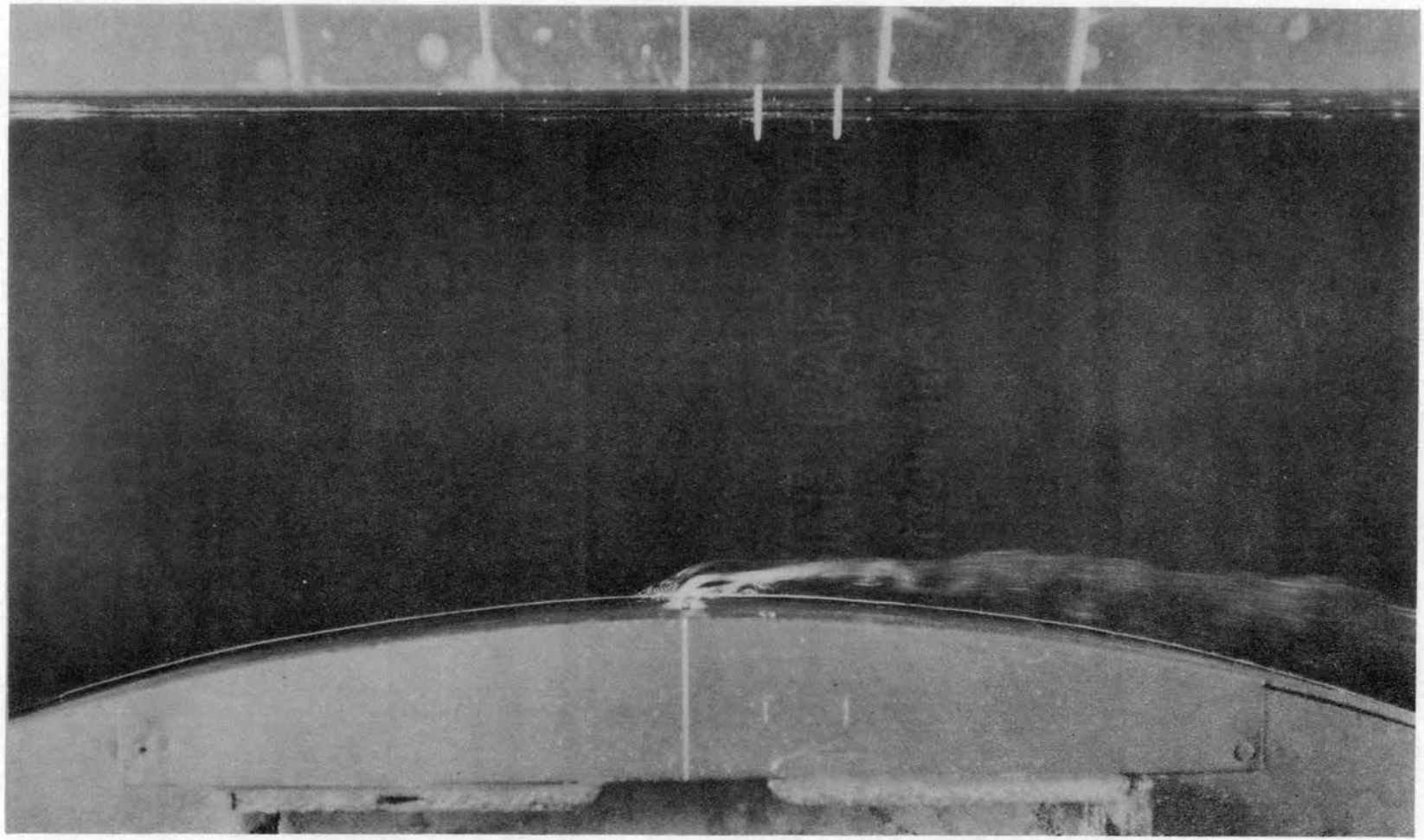

Figure 10. Typical Streak Lines for Particles Issuing from Slot; Secondary to Main Stream Head Approximately 1.00.

were, of course, illuminated only by the slide projector which was upstream at an angle of about 30 degrees to the bottom. The use of the aluminum powder to obtain the shadow photographs proved to be less than satisfactory and was modified in the second series of experiments (see figures 11 and 12).

The second series of experiments was necessitated by failure to calibrate the shrinkage of each roll of film and by the problems encountered in the data reduction as discussed above. Since it had been observed, during the first series, that the water analogy had probably failed to conform to the gas flow, the mass flow rates and the streak photographs were not repeated for the second series, however, the same flow conditions were recorded on new grid photographs. Thus the purposes of the second series were to confirm the theory of the shadow-photogrammetric method, to develop the techniques of practical application, and to obtain data for the isogrametric depths of the flow field, so only factors important to the shadow method were considered. The time required for a pair of exposures for each flow condition was less than two minutes.

After a confirmation series was run using the glass plate, leveled at different heights above the bottom, as the surface for the shadow projections (see figures 13, 14 and 15), the procedure for the second series was as follows: The water was recirculated by the pump (because of the shorter time required steady state could be maintained); one quart of white, together with 1 ounce of chrome yellow, Sherwood-Williams water soluble show card paint was added to the water to render it opaque; the flow rates were adjusted and allowed to stabilize to give the proper heads (measured by two micrometer probes); and the

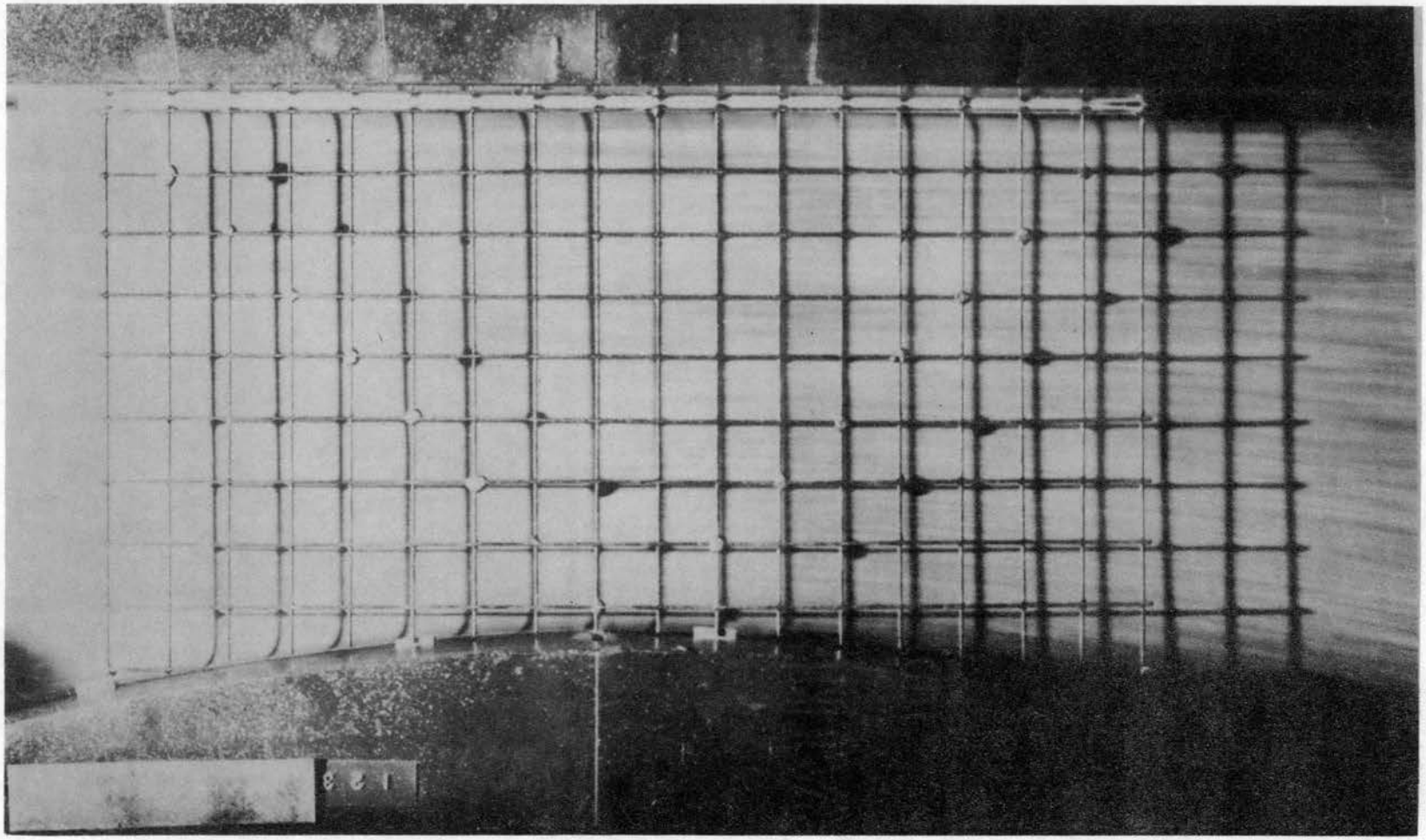

Figure 11. Typical Shadow Pattern with Aluminum Powder for Plugged Slot.

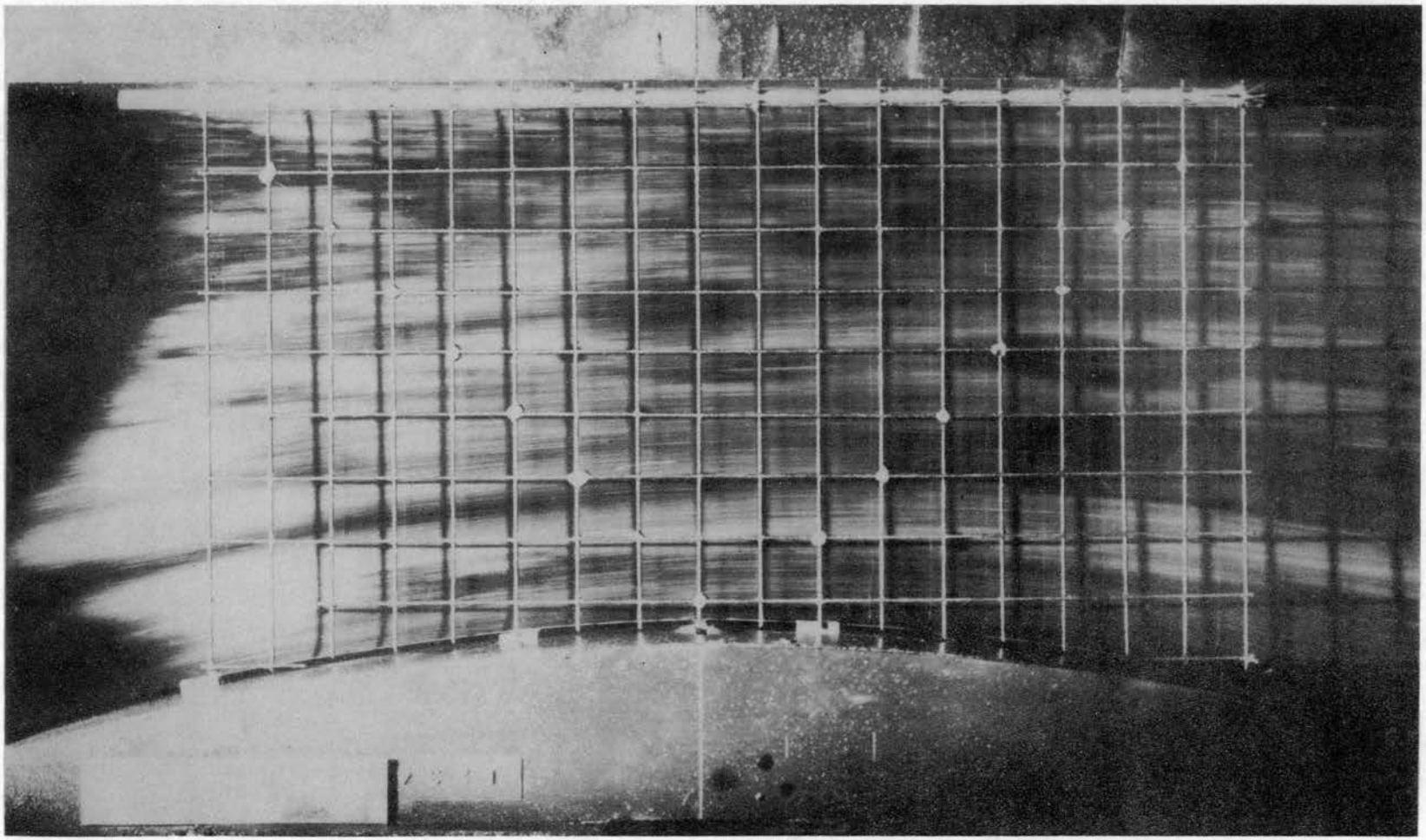

Figure 12. Typical Weak Shadow Pattern with Aluminum Powder for Plugged Slot.

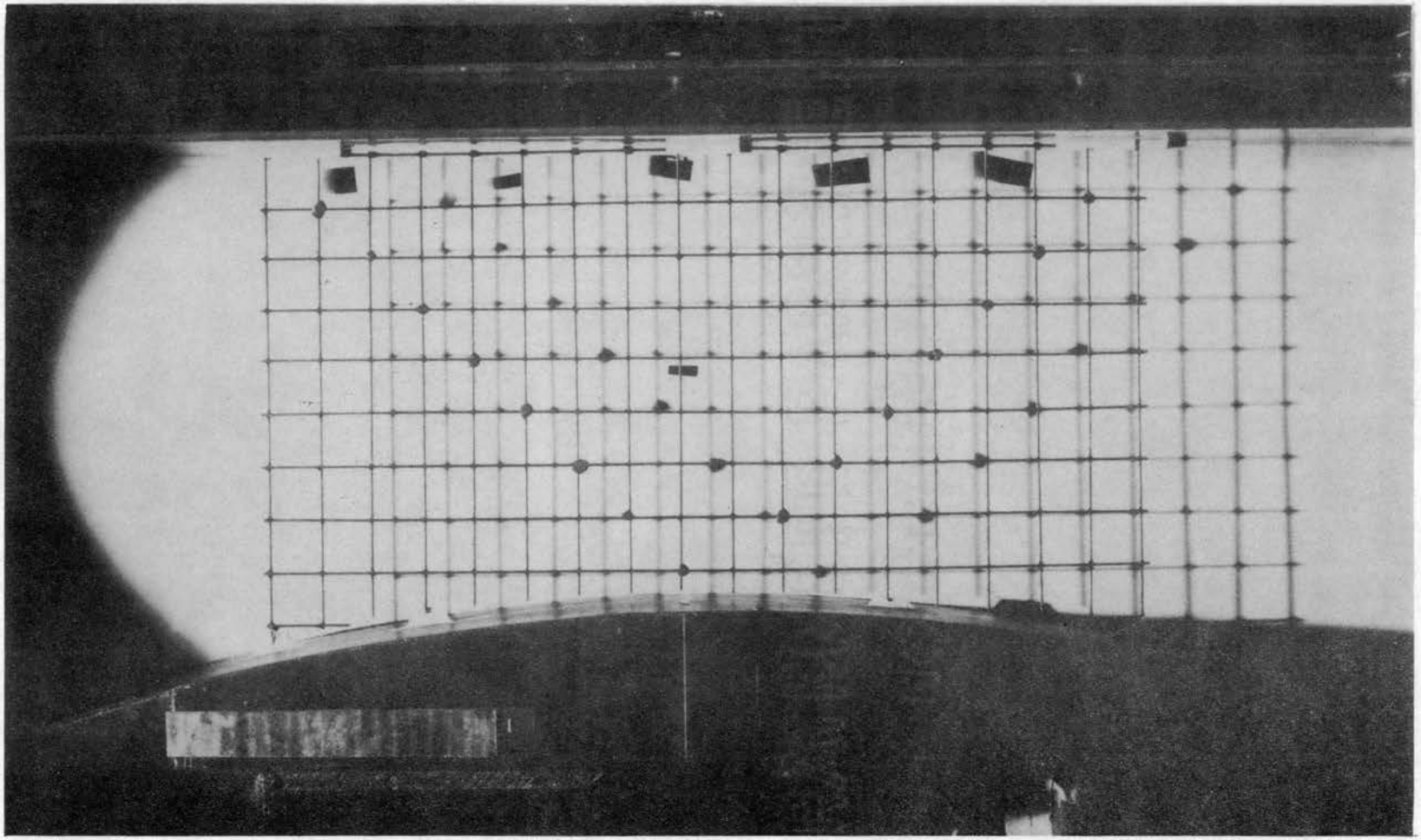

Figure 13. Shadow Pattern for Zero Depth Calibration Positions; White Painted Bottom.

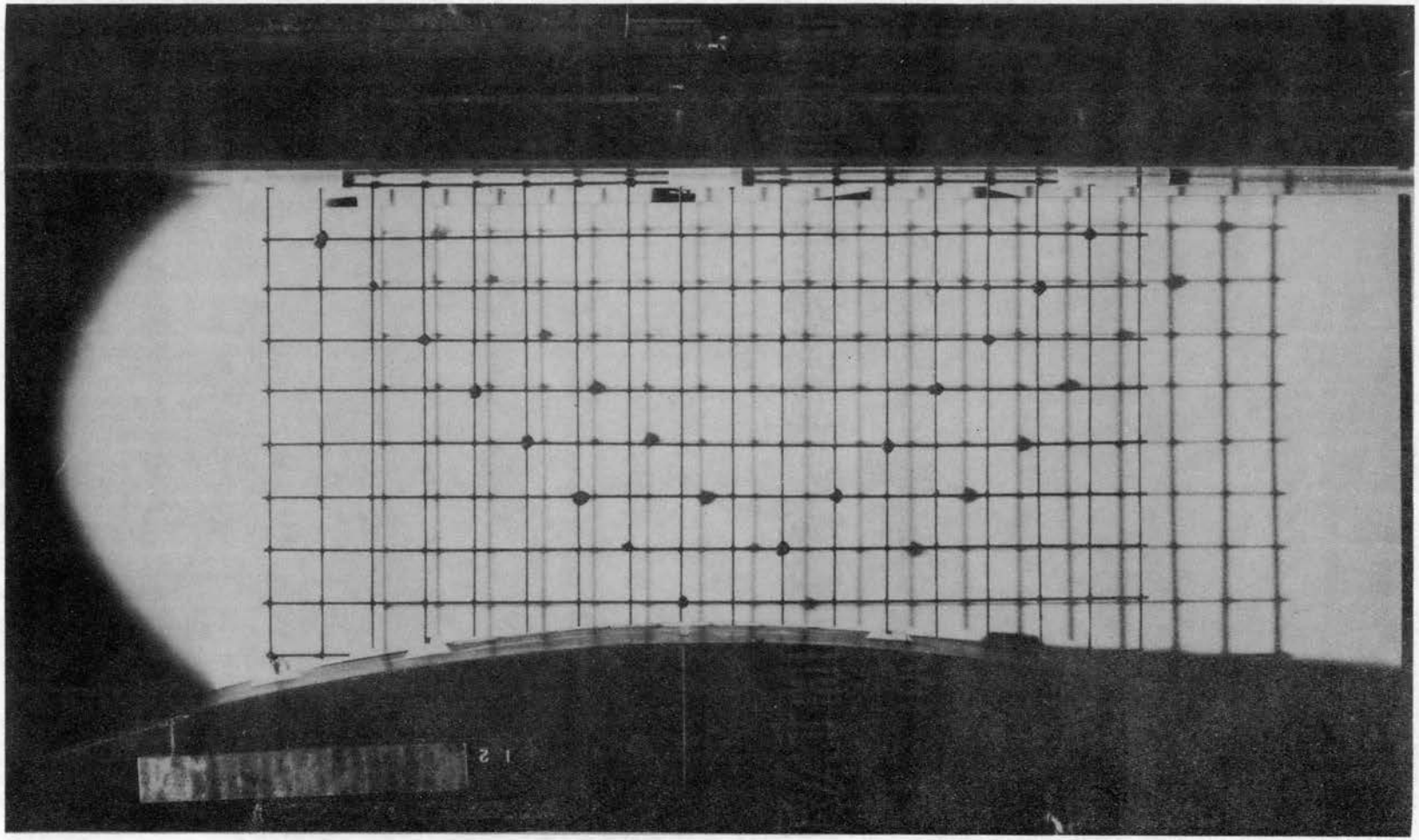

Figure 14. Shadow Pattern for .090 Inch Depth Calibration Position; Glass Plate.

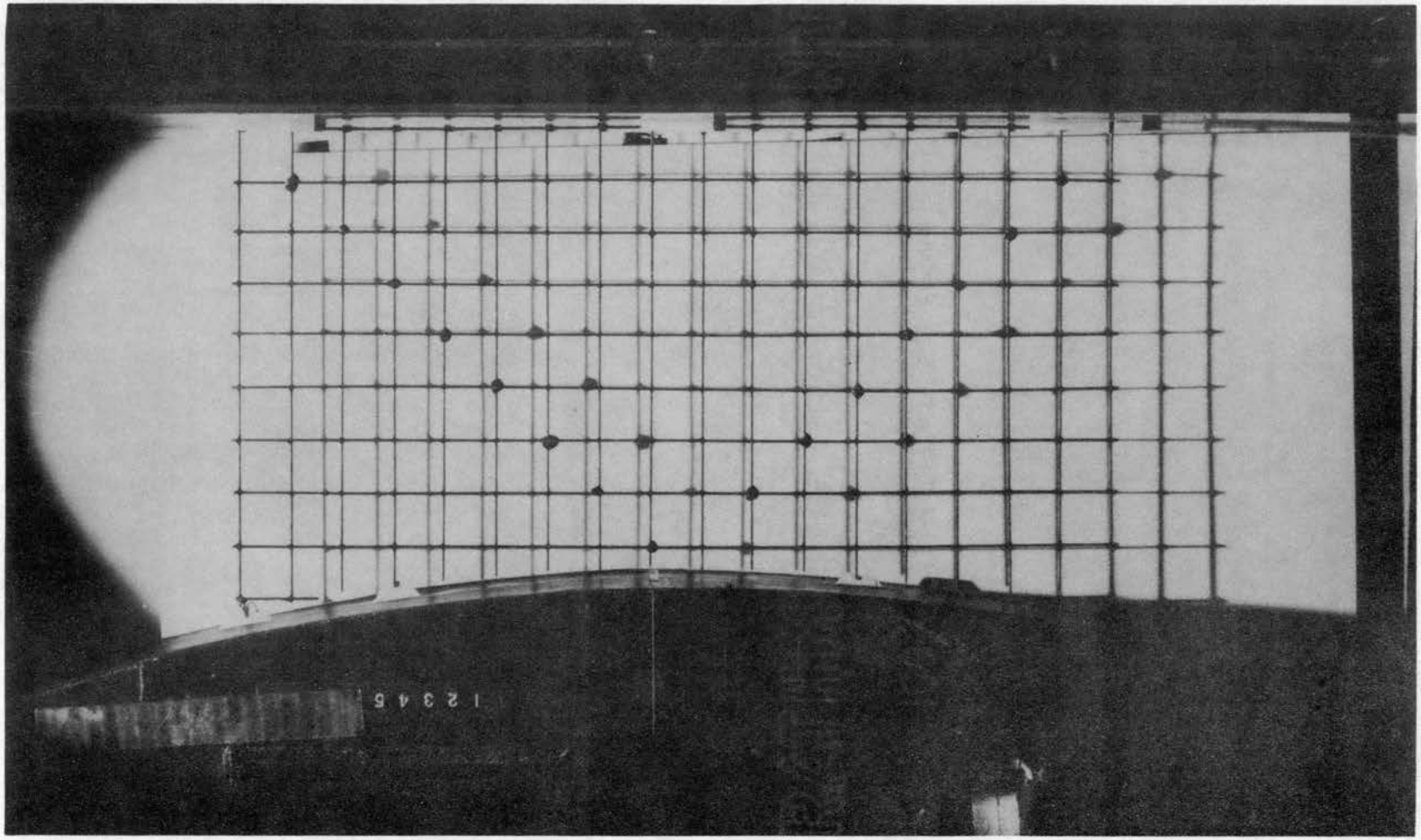

Figure 15. Shadow Pattern for .369 Inch Depth Calibration Position; Glass Plate.

exposures made. Calibration photographs were made at the beginning and the end of each roll of film using the bottom and the glass plate at 0.560 inch height.

The films and prints were carefully processed according to the manufacturers instructions, and the prints seasoned and measured as described above.

CHAPTER V

RESULTS AND DISCUSSION OF THE INVESTIGATION

Shadow-photogrammetric Method

The shadow-photogrammetric method of determining the topography of surfaces developed here seems to have wide application to a large variety of problems, such as the hydraulic analogy, panel flutter and distortion, fluid oscillators and amplifiers, strain in solids, and etc., especially where an optical method is desired so as not to alter the quantity to be measured by the measuring device. Although the limited application to which the method was put does not show its usefulness for time dependent fields, it could easily be extended to this class of problems by employing a motion picture camera. The method is simple, employs commercially available inexpensive equipment and supplies, and can be put to use by relatively inexperienced personnel, because no special skills are needed to obtain the raw data from the photographs, compared to Mann's stereophotogrammetric method which is complicated, requires special expensive equipment and supplies, and requires highly skilled personnel to obtain the raw data. This method also appears to be less laborious than Mann's. As far as could be determined from an extensive literature survey, this is the first time a single lens camera has been used with a shadow pattern obliquely projected on a surface to obtain the topography. The oblique projection permits magnifi-

cation of the vertical displacements. If the surface has extreme peaks that intercept the shadows, magnification may have to be limited in order to project the shadows onto the field.

The major faults of the method are common to all photogrammetric methods, however, it has been shown that some of them may be handled in a straight-forward manner without resorting to expensive, highly specialized equipment. Improved equipment will not alleviate the problems completely, but would probably reduce the anxiety in reaching the required correction equations. The advantages of an optical system, even with poor optical components as used in this study, of obtaining the topography of a surface seem to far outweigh the disadvantages of data reduction.

The expected overall precision of computed depth, using the technique described earlier, (see Appendix) is $\pm 1.3\ \%$ compared to Mann's (2) accuracy of $\pm 5\ \%$. For a comparable nominal depth of 0.310 inch, this gives the depth to ± 0.004 inch compared to Mann's ± 0.016 inch. It was possible to compute the longitudinal location of a particular point to $\pm 0.6\ \%$ for a nominal distance of 3.02 inches or ± 0.018 inch, which was considered adequate for the water analogy. The lateral location is known to good precision because the reference lines are not subject to foreshortening. Although Mann (2) does not discuss the problem of location of the point at which the depth was determined, the problem for the stereophotogrammetric method is even more complicated than for the present method if more than an approximate location is required. In cases such as plate strain, where the accurate location of the point is required, further improvements in the optical error correction equations by the use of shorter intervals would probably improve the

results.

Table I shows the values of the longitudinal locations and the depths computed by the three methods of computation that were discussed in Chapter III. In each group, the top figures are the actual values obtained from the physical measurements, and the others (in vertical order) are for Mark I, Mark II, and Mark III. The error terms, e, are given in inches, while the others are given in units of 1/50 inch. This comparison is a confirmation study using the glass plate at 0.090 inch height (4.50 units) for the projection plane. Figures 13, 14, and 15 show the corresponding shadow patterns. The average errors for the Mark I computation are 0.030 inch for location and 0.004 inch for depth. Thus, the average depth error is 2 % and the location error average is 0.6 % of the nozzle throat. For the Mark II and Mark III computations the average values are 0.060 and 0.023 inch for location errors, and 0.005 and 0.004 inch for depth errors; these are 0.75, 0.6, 4, and 2 % respectively. A detailed examination of the table reveals some points which are grossly in error which on rechecking could not be improved unless individual correction equations were developed point-by-point. If a procedure such as this were necessary, the usefulness of the method is seriously questioned. Thus, the table represents the results one can expect from a practical utilization of the method. The comparison of the actual with the computed value of S_o gives an indication of the accuracy of the optical error correction equations at the various points. As stated above, the Mark II series was based on three equations for each reference line. However, the S_o values were allowed to float away from the true S_o value in order to get the proper separation of the shadows for a given calibration

TABLE I

COMPARISON OF ACTUAL WITH COMPUTED VALUES BY THE DIFFERENT METHODS FOR CALIBRATION RUN 1802

Wire No.	Reference Line A					B					C					Reference Line D				
	e_s	S	S_o	h	e_h	e_s	S	S_o	h	e_h	e_s	S	S_o	h	e_h	e_s	S	S_o	h	e_h
1*		224.50	217.25	4.50			224.75	217.25	4.50			225.00	217.50	4.50			223.25	216.00	4.50	
	.016	225.32	217.77	4.89	.009	.008	225.17	218.14	4.59	.001	.023	226.13	218.53	4.94	.009	.038	225.16	217.58	4.94	.009
	.016	225.32	217.77	4.97	.009	.008	225.17	218.14	4.63	.003	.004	225.19	217.64	4.98	.010	.038	225.16	217.59	4.99	.010
	-.005	224.25	216.67	4.86	.007	-.015	223.98	216.94	4.57	.001	-.015	224.25	216.67	4.91	.008	.020	224.25	216.67	4.91	.008
2		184.00	176.50	4.50			184.00	176.50	4.50			184.00	176.50	4.50			183.00	175.50	4.50	
	.006	184.28	176.63	4.76	.005	.014	184.68	177.82	4.39	-.002	.038	185.92	178.23	4.94	.010	.031	184.54	177.13	4.76	.005
	.006	184.27	176.63	4.91	.008	.014	184.68	177.82	4.40	-.002	.024	185.21	177.56	4.91	.008	.031	184.54	177.14	4.76	.005
	-.015	183.23	175.56	4.73	.005	-.010	183.51	176.67	4.36	-.003	.007	184.34	176.67	4.91	.008	.016	183.79	176.39	4.74	.005
3		143.50	136.25	4.50			144.00	136.25	4.50			144.50	137.00	4.50			143.91	136.25	4.50	
	.017	144.34	136.59	4.72	.004	.020	144.98	137.51	4.60	.002	.025	145.73	138.20	4.62	.002	.027	145.28	137.25	4.93	.009
	.017	144.33	136.59	4.85	.007	.020	144.98	137.51	4.68	.004	.015	145.24	137.76	4.69	.004	.027	145.28	137.25	5.03	.011
	-.004	143.31	135.56	4.69	.004	-.003	143.87	136.39	4.57	.001	.002	144.42	136.94	4.61	.002	.016	144.70	136.67	4.90	.008
4		104.75	97.25	4.50			104.75	97.00	4.50			104.00	96.50	4.50			103.25	95.75	4.50	
	.021	105.79	98.51	4.56	.001	.022	105.85	98.02	4.77	.005	.041	106.05	97.90	4.97	.009	.034	104.93	97.07	4.81	.006
	.021	105.79	98.51	4.46	-.001	.022	105.85	98.02	4.79	.006	.036	105.79	97.68	4.96	.009	.034	104.93	97.08	4.81	.006
	.001	104.78	97.50	4.53	.001	.001	104.78	96.94	4.74	.005	.021	105.06	96.94	4.94	.009	.025	104.50	96.67	4.77	.005
5		65.75	58.00	4.50			65.50	57.75	4.50			65.75	58.00	4.50			65.25	57.50	4.50	
	.007	66.11	58.47	4.56	.001	.025	66.74	59.09	4.56	.001	.024	66.96	58.71	4.84	.007	.020	66.24	58.02	4.84	.007
	.007	66.12	58.47	4.57	.001	.025	66.74	59.09	4.57	.001	.023	66.91	58.72	4.90	.008	.020	66.24	58.02	4.91	.008
	-.012	65.14	57.50	4.53	.001	.004	65.69	58.06	4.53	.001	.010	66.25	58.06	4.81	.006	.014	65.97	57.78	4.81	.006
6		24.75	17.00	4.50			25.75	18.00	4.50			24.75	17.00	4.50			24.25	16.50	4.50	
	.039	26.72	18.72	4.72	.004	.021	26.78	18.78	4.68	.004	.023	25.91	17.85	4.68	.004	.033	25.88	17.29	5.00	.010
	.039	26.72	18.72	4.68	.002	.021	26.78	18.78	4.68	.004	.027	26.09	18.08	4.68	.004	.033	25.88	17.30	5.01	.010
	.021	25.78	17.78	4.69	.004	.001	25.78	17.78	4.65	.003	.015	25.51	17.50	4.66	.003	.031	25.78	17.22	4.97	.009
7		-14.00	-22.00	4.50			-13.50	-21.50	4.50			-13.50	-21.50	4.50			-14.00	-22.00	4.50	
	-.016	-13.21	-22.27	4.93	.004	.001	-13.54	-22.03	4.61	.002	.010	-12.96	-21.14	4.69	.003	-.014	-13.31	-21.95	4.91	.008
	-.029	-12.55	-21.82	5.29	.002	-.008	-13.08	-21.78	4.97	.009	.000	-13.50	-21.92	4.81	.006	.000	-14.00	-22.79	5.01	.010
	-.031	-12.47	-21.67	5.21	.004	-.015	-12.75	-21.39	4.89	.008	-.009	-13.03	-21.39	4.77	.005	-.014	-13.30	-21.94	4.89	.008
8		-55.00	-63.00	4.50			-54.25	-62.25	4.50			-54.25	-62.25	4.50			-54.75	-62.75	4.50	
	-.011	-54.44	-63.05	4.84	.007	.005	-54.49	-63.09	4.88	.008	-.003	-54.09	-62.26	4.60	.002	-.019	-53.80	-62.53	4.84	.007
	-.006	-54.70	-63.49	4.91	.008	.014	-54.94	-63.73	4.91	.008	.017	-55.08	-63.31	4.59	.002	.008	-55.14	-64.02	4.95	.009
	-.013	-54.33	-63.06	4.81	.006	.002	-54.33	-63.06	4.81	.007	.002	-54.33	-62.50	4.58	.002	-.019	-53.78	-62.50	4.80	.006
9		-94.50	-102.50	4.50			-94.00	-102.00	4.50			-94.25	-102.25	4.50			-94.25	-102.25	4.50	
	-.007	-94.15	-103.00	4.88	.008	.009	-94.44	-102.42	4.45	-.001	-.010	-93.71	-102.25	4.72	.004	-.010	-93.73	-102.28	4.72	.004
	-.007	-95.16	-104.05	4.85	.007	.034	-95.70	-103.73	4.38	-.002	.015	-94.99	-103.59	4.70	.004	.029	-95.71	-104.39	4.74	.005
	.000	-94.52	-103.33	4.81	.006	.016	-94.80	-103.78	4.38	-.002	-.005	-93.98	-102.50	4.69	.004	-.011	-93.70	-102.22	4.69	.004

*The results of the Mark I, Mark II, and Mark III computations are listed vertically in that order under the actual values in each group.

TABLE I (Continued)

Wire No.	Reference Line E					Reference Line F					Reference Line G					Reference Line H				
	e_s	S	S_o	h	e_h	e_s	S	S_o	h	e_h	e_s	S	S_o	h	e_h	e_s	S	S_o	h	e_h
1		223.50	216.00	4.50			223.25	216.00	4.50			223.25	216.00	4.50			222.00	214.75	4.50	
	.031	225.03	217.39	4.45	.001	.028	224.63	217.58	4.69	.004	.034	224.94	217.89	4.73	.003	.043	224.13	217.09	4.73	.003
	.029	224.97	217.39	4.99	.010	.061	226.30	219.19	4.69	.004	.077	227.08	219.94	4.71	.004	.096	226.80	219.66	4.71	.004
	.015	224.25	216.67	4.91	.008	.014	223.97	216.94	4.65	.003	.014	223.96	216.94	4.70	.004	.034	223.71	216.67	4.70	.004
2		182.50	175.00	4.50			182.50	175.00	4.50			181.75	174.50	4.50			181.25	174.00	4.50	
	.039	184.29	176.34	5.06	.011	.035	184.23	176.55	4.89	.008	.044	183.95	176.81	4.69	.004	.045	183.50	176.10	4.81	.006
	.039	184.28	176.34	5.10	.012	.061	185.53	177.79	4.97	.009	.077	185.61	178.38	4.65	.003	.087	185.60	178.10	4.82	.006
	.026	183.79	175.83	5.04	.010	.026	183.79	176.11	4.87	.007	.030	183.23	176.11	4.66	.003	.040	183.23	175.83	4.78	.006
3		143.50	136.00	4.50			143.50	136.00	4.50			142.75	135.25	4.50			143.00	135.50	4.50	
	.030	145.01	136.96	4.97	.009	.024	144.69	137.19	4.68	.004	.049	145.19	137.68	4.73	.005	.036	144.82	137.33	4.73	.005
	.030	145.00	136.96	5.04	.010	.043	145.65	138.08	4.74	.005	.071	146.31	138.80	4.76	.005	.068	146.39	138.80	4.76	.005
	.024	144.70	136.67	4.94	.009	.018	144.42	136.94	4.65	.003	.039	144.70	137.22	4.70	.004	.034	144.70	137.22	4.70	.004
4		102.25	94.50	4.50			102.00	94.50	4.50			101.75	94.25	4.50			101.50	94.00	4.50	
	.042	104.33	96.19	4.92	.008	.035	103.75	96.15	4.62	.002	.038	103.63	95.76	4.85	.007	.037	103.37	96.06	4.56	.001
	.042	104.33	96.19	4.97	.009	.047	104.34	96.68	4.68	.004	.052	104.35	96.39	4.87	.007	.057	104.37	96.95	4.53	.001
	.039	104.22	96.11	4.90	.008	.033	103.67	96.11	4.61	.002	.033	103.40	95.56	4.82	.006	.038	103.40	96.11	4.53	.001
5		63.75	56.00	4.50			63.75	56.00	4.50			64.25	56.50	4.50			63.50	56.00	4.50	
	.043	65.88	57.65	4.89	.008	.037	65.58	57.91	4.60	.002	.035	65.99	58.03	4.77	.005	.046	65.80	58.13	4.64	.003
	.043	65.88	57.65	4.92	.008	.042	65.84	58.10	4.63	.003	.040	66.27	58.22	4.81	.006	.056	66.28	58.50	4.65	.003
	.044	65.97	57.78	4.85	.007	.039	65.69	58.06	4.57	.001	.034	65.97	58.06	4.73	.005	.049	65.97	58.33	4.61	.002
6		23.75	16.00	4.50			23.75	16.00	4.50			24.25	16.50	4.50			23.75	16.00	4.50	
	.035	25.48	16.87	4.72	.004	.029	25.19	17.50	4.76	.005	.026	25.55	17.51	4.77	.005	.028	25.17	17.69	4.48	.000
	.035	25.48	16.88	5.02	.010	.027	25.09	16.98	4.74	.005	.022	25.37	17.22	4.75	.005	.027	25.09	17.51	4.43	-.001
	.041	25.78	17.22	4.97	.009	.035	25.51	17.50	4.70	.004	.030	25.77	17.78	4.73	.005	.035	25.51	18.06	4.45	-.001
7		-15.25	-23.00	4.50			-15.25	-23.00	4.50			-15.25	-23.00	4.50			-16.25	-24.00	4.50	
	-.047	-12.88	-21.36	5.06	.009	.036	-13.43	-21.09	4.61	.002	.036	-13.47	-21.39	4.76	.003	-.062	-13.17	-21.39	4.95	.009
	-.017	-14.40	-23.18	5.01	.010	.006	-14.97	-22.90	4.53	.001	-.006	-14.97	-23.18	4.69	.004	-.031	-14.68	-23.18	4.85	.007
	-.033	-13.58	-22.22	4.93	.009	.022	-14.14	-21.94	4.49	.000	-.022	-14.14	-22.22	4.65	.003	-.048	-13.86	-22.22	4.81	.006
8		-54.75	-62.75	4.50			-55.00	-62.75	4.50			-55.50	-63.25	4.50			-56.50	-64.25	4.50	
	-.050	-52.27	-61.03	4.96	.009	-.044	-52.80	-60.42	4.36	-.003	-.044	-53.32	-61.24	4.52	.000	-.085	-52.27	-61.21	4.56	.001
	.004	-54.96	-63.84	4.94	.009	.011	-55.54	-63.28	4.32	-.004	.012	-56.10	-64.12	4.48	.000	-.008	-56.10	-64.12	4.48	.000
	-.025	-53.50	-62.22	4.89	.008	-.019	-54.06	-61.67	4.29	-.004	-.018	-54.61	-62.50	4.45	-.001	-.038	-54.61	-62.50	4.49	.000
9		-95.00	-103.00	4.50			-95.25	-103.00	4.50			-94.75	-102.50	4.50			-94.75	-102.75	4.50	
	.042	-92.89	-101.17	4.60	.001	-.050	-92.77	-100.46	4.32	-.004	-.051	-92.18	-100.16	4.52	.000	-.052	-92.14	-100.39	4.64	.003
	.022	-96.11	-104.50	4.58	.001	.017	-96.12	-103.93	4.27	-.005	.016	-95.55	-103.65	4.42	-.002	.016	-95.54	-103.93	4.58	.002
	-.020	-93.98	-102.22	4.57	.001	-.025	-93.98	-101.67	4.29	-.004	-.027	-93.42	-101.39	4.49	.000	-.027	-93.42	-101.67	4.61	.002

TABLE I (Continued)

Wire No.	Reference Line I					Reference Line J					Reference Line K					Reference Line L				
	e_s	S	S_o	h	e_h	e_s	S	S_o	h	e_h	e_s	S	S_o	h	e_h	e_s	S	S_o	h	e_h
1		222.00	214.75	4.50			221.75	214.50	4.50			221.75	214.50	4.50			221.75	214.50	4.50	
	.055	224.73	217.41	4.86	.007	.051	224.30	217.48	4.55	.001	.053	224.38	217.54	4.55	.001	.054	224.43	217.82	4.34	-.003
	.055	224.73	217.41	4.83	.006	.051	224.31	217.48	4.50	.000	.070	225.27	218.39	4.54	.001	.054	224.42	217.82	4.35	-.003
	.040	223.98	216.67	4.82	.006	.034	223.43	216.67	4.52	.000	.028	223.15	216.39	4.52	.000	.022	222.86	216.39	4.31	-.004
2		181.50	174.00	4.50			181.75	174.50	4.50			182.00	174.50	4.50			182.00	174.50	4.50	
	.050	183.99	176.29	4.89	.009	.044	183.95	176.50	4.81	.006	.033	183.67	176.46	4.60	.002	.042	184.12	176.89	4.56	.001
	.050	183.98	176.29	4.94	.009	.044	183.96	176.51	4.78	.006	.046	184.32	177.07	4.65	.003	.042	184.12	176.89	4.64	.003
	.040	183.51	175.83	4.87	.007	.035	183.51	176.11	4.78	.006	.019	182.95	175.83	4.57	.001	.025	183.23	176.11	4.53	.001
3		143.00	135.50	4.50			142.50	135.00	4.50			142.50	135.00	4.50						
	.039	144.93	137.41	4.68	.004	.046	144.78	137.78	4.43	-.001	.043	144.65	137.36	4.56	.001					
	.039	144.93	137.41	4.71	.004	.046	144.78	137.78	4.39	-.002	.051	145.07	137.74	4.60	.002					
	.034	144.70	137.22	4.65	.003	.044	144.70	137.78	4.40	-.002	.038	144.42	137.22	4.53	.001					
4		101.50	94.00	4.50			101.00	93.50	4.50			101.00	93.50	4.50						
	.043	103.64	96.57	4.39	-.002	.052	103.61	96.24	4.52	.000	.048	103.39	96.28	4.31	-.004					
	.043	103.64	96.57	4.32	-.004	.052	103.61	96.24	4.50	.000	.051	103.56	96.42	4.37	-.003					
	.043	103.67	96.67	4.36	-.003	.059	103.95	96.67	4.49	.000	.053	103.67	96.67	4.28	-.004					
5		63.75	56.00	4.50			63.00	55.50	4.50			63.25	55.50	4.50						
	.044	65.94	57.97	4.72	.004	.045	65.24	58.08	4.31	-.004	.039	65.19	57.45	4.60	.002					
	.044	65.94	57.98	4.76	.005	.045	65.25	58.08	4.28	-.004	.038	65.14	57.36	4.65	.003					
	.050	66.25	58.33	4.70	.004	.059	65.97	58.89	4.28	-.004	.055	65.97	58.33	4.57	.001					
6		23.75	16.00	4.50			22.25	14.50	4.50			22.25	14.50	4.50						
	.034	25.47	17.42	4.72	.004	.048	24.63	16.82	4.56	.001	.045	24.48	16.65	4.60	.002					
	.034	25.47	17.42	4.70	.004	.048	24.63	16.82	4.56	.001	.039	24.20	16.32	4.59	.002					
	.046	26.06	18.06	4.69	.004	.071	25.78	18.06	4.53	.001	.071	25.78	18.06	4.57	.001					
7		-16.14	-24.00	4.50			-17.00	-24.75	4.50			-17.16	-24.75	4.50						
	-.067	-12.81	-20.72	4.83	.007	-.102	-11.89	-20.26	5.29	.016	-.098	-12.24	-19.22	4.61	.002					
	-.029	-14.68	-22.92	4.69	.004	-.057	-14.12	-22.62	4.85	.007	-.049	-14.69	-21.77	4.05	-.009					
	-.045	-13.86	-21.94	4.61	.002	-.074	-13.30	-21.67	4.82	.006	-.066	-13.86	-20.83	4.12	-.008					
8		-56.00	-64.25	4.50			-56.00	-63.75	4.50			-56.00	-63.75	4.50						
	-.075	-52.27	-61.58	5.04	.011	-.083	-51.83	-59.71	4.52	.000	-.081	-51.94	-59.27	4.20	-.006					
	-.021	-54.96	-64.41	5.27	.015	-.026	-54.69	-62.70	4.48	.000	-.020	-54.98	-62.43	4.16	-.007					
	-.050	-53.50	-62.78	5.03	.010	-.075	-53.22	-61.11	4.49	.000	-.050	-53.50	-60.83	4.17	-.007					
9		-94.75	-102.75	4.50			-94.75	-102.75	4.50			-95.75	-102.75	4.50						
	-.057	-91.90	-100.43	4.68	.004	-.065	-91.48	-99.45	4.44	-.001	-.088	-91.34	-99.32	4.41	-.002					
	.010	-95.25	-103.93	4.74	.005	.005	-94.98	-103.09	4.43	-.004	-.015	-94.98	-103.09	4.43	-.001					
	-.032	-93.14	-101.67	4.65	.003	-.038	-92.87	-100.87	4.41	-.002	-.058	-92.87	-100.83	4.37	-.003					

TABLE I (Continued)

Wire No.	Reference Line A					Reference Line B					Reference Line C					Reference Line D				
	e_s	S	S_o	h	e_h	e_s	S	S_o	h	e_h	e_s	S	S_o	h	e_h	e_s	S	S_o	h	e_h
10		-134.50	-142.50	4.50			-134.00	-142.00	4.50			-134.25	-142.25	4.50			-134.50	-142.50	4.50	
	-.006	-134.21	-142.57	4.56	.001	.008	-134.38	-142.73	4.53	.001	-.007	-133.89	-142.51	4.68	.004	-.011	-133.96	-142.30	4.53	.001
	.017	-135.37	-143.76	4.49	.000	.038	-135.89	-144.28	4.49	.000	.024	-135.46	-144.14	4.64	.003	.041	-136.57	-145.04	4.53	.001
	.001	-134.44	-142.78	4.54	.001	.014	-134.72	-143.06	4.50	.000	.002	-134.16	-142.78	4.65	.003	-.012	-133.89	-142.22	4.49	.000
11		-172.75	-181.00	4.50			-172.00	-180.25	4.50			-172.00	-180.00	4.50			-172.50	-180.50	4.50	
	-.003	-172.59	-181.02	4.49	.000	.002	-172.10	-180.81	4.64	.003	-.002	-171.88	-180.00	4.37	-.003	-.011	-171.96	-180.37	4.49	.000
	.023	-173.89	-182.36	4.44	-.001	.037	-173.84	-182.60	4.59	.002	.035	-173.73	-181.90	4.29	-.004	.054	-175.18	-183.72	4.48	.000
	.001	-172.70	-181.11	4.46	-.001	.008	-172.42	-181.11	4.61	.002	.003	-172.14	-180.28	4.34	-.003	-.013	-171.86	-180.28	4.46	-.001
12		-213.25	-221.50	4.50			-212.75	-221.00	4.50			-212.25	-220.50	4.50			-213.25	-221.50	4.50	
	-.002	-213.15	-222.54	4.83	.007	.003	-212.88	-221.67	4.60	.002	.012	-212.87	-221.65	4.57	.001	.001	-213.29	-221.78	4.38	-.002
	.025	-214.51	-223.25	4.49	.000	.033	-214.40	-223.36	4.60	.002	.027	-213.60	-222.65	4.65	.003	.061	-216.29	-225.34	4.64	.003
	-.002	-213.17	-222.50	4.80	.006	.008	-213.17	-221.94	4.57	.001	.018	-213.17	-221.94	4.54	.001	.002	-213.17	-221.67	4.35	-.003
13		-253.50	-261.75	4.50			-252.75	-261.25	4.50			-253.25	-261.50	4.50			-253.00	-261.25	4.50	
	.011	-254.06	-262.67	4.45	-.001	.018	-253.67	-262.54	4.49	.000	-.004	-253.03	-262.19	4.72	.004	.025	-254.25	-251.52	1.99	-.090
	.043	-255.64	-264.46	4.44	.001	.045	-254.98	-263.99	4.53	.001	.015	-254.02	-263.42	4.73	.005	.116	-258.79	-255.97	1.43	-.061
	.008	-253.91	-262.50	4.42	.002	.021	-253.91	-262.78	4.47	.001	.002	-253.36	-262.50	4.69	.004	.007	-253.36	-251.39	1.98	-.050
14		-292.00	-300.25	4.50			-290.25	-298.50	4.50			-290.25	-298.50	4.50			-290.00	-298.50	4.50	
	-.014	-291.32	-300.29	4.52	.000	.011	-290.82	-300.07	4.68	.004	.004	-290.46	-299.40	4.53	.001	.014	-290.68	-299.32	4.34	-.003
	.038	-293.90	-303.10	4.54	.001	.050	-292.74	-302.12	4.64	.003	.045	-292.50	-301.67	4.53	.001	.150	-297.51	-306.69	4.52	.000
	-.019	-291.07	-300.00	4.50	.000	.016	-291.06	-300.28	4.65	.003	.010	-290.77	-299.72	4.50	.000	.010	-290.51	-299.17	4.32	-.004
15		-331.50	-340.00	4.50			-331.50	-340.00	4.50			-331.00	-339.50	4.50			-330.50	-339.00	4.50	
	.013	-332.16	-341.80	4.75	.005	.002	-331.58	-341.21	4.75	.005	.004	-331.21	-340.22	4.46	-.001	.019	-331.44	-340.46	4.46	-.001
	.087	-335.84	-345.74	4.79	.006	.053	-334.16	-343.93	4.73	.005	.067	-334.37	-343.63	4.48	.000	.215	-340.75	-350.33	4.62	.002
	.006	-331.81	-341.39	4.72	.004	.006	-331.81	-341.39	4.72	.004	.011	-331.53	-340.56	4.43	-.002	.015	-331.25	-340.28	4.43	-.001
16		-370.00	-378.50	4.50			-369.75	-378.25	4.50			-369.75	-378.25	4.50			-370.00	-378.75	4.50	
	-.006	-369.72	-379.14	4.61	.002	-.008	-369.33	-378.74	4.61	.002	.018	-368.85	-378.54	4.72	.004	.018	-370.91	-379.09	3.92	-.012
	.088	-374.42	-384.09	4.60	.002	.055	-372.52	-382.06	4.54	.001	.066	-373.07	-383.02	4.73	.005	.252	-382.62	-391.31	4.12	-.008
	-.005	-369.23	-378.61	4.58	.002	.005	-369.51	-379.89	4.58	.002	.010	-369.23	-378.89	4.69	.004	.012	-370.62	-378.89	3.89	-.012
17		-411.00	-419.50	4.50			-409.50	-418.25	4.50			-410.25	-418.75	4.50			-409.75	-418.50	4.50	
	-.002	-410.02	-419.82	4.68	.004	.002	-409.58	-419.04	4.50	.000	-.024	-409.03	-418.81	4.72	.004	.009	-410.20	-419.67	4.46	-.001
	.096	-415.82	-425.88	4.69	.004	.078	-413.40	-423.02	4.49	-.001	.082	-414.37	-424.40	4.68	.004	.291	-424.31	-434.37	4.67	.003
	-.031	-409.43	-419.17	4.65	.003	.004	-409.71	-419.17	4.47	-.001	.016	-409.43	-419.17	4.69	.004	.005	-409.98	-419.44	4.43	-.001
18		-450.50	-459.00	4.50			-447.75	-456.50	4.50			-448.50	-457.00	4.50			-447.25	-456.00	4.50	
	-.016	-449.72	-460.23	4.97	.009	.002	-447.83	-457.68	4.64	.003	-.035	-446.77	-456.01	4.42	-.001	.016	-446.46	-456.91	4.86	.007
	.122	-456.60	-467.37	4.93	.009	.091	-452.28	-462.28	4.59	.002	.093	-453.17	-462.65	4.34	-.003	.310	-462.77	-473.88	5.07	.011
	-.028	-449.07	-459.44	4.94	.009	.004	-447.96	-457.78	4.61	.002	-.027	-447.13	-456.39	4.39	-.002	-.019	-446.29	-456.67	4.83	.007

TABLE I (Continued)

Wire No.	Reference Line E					Reference Line F					Reference Line G					Reference Line H				
	e_s	S	S_o	h	e_h	e_s	S	S_o	h	e_h	e_s	S	S_o	h	e_h	e_s	S	S_o	h	e_h
10		-133.75	-142.00	4.50			-134.00	-142.00	4.50			-135.25	-143.00	4.50			-134.00	-142.00	4.50	
	.010	-133.23	-141.59	4.45	-.001	-.037	-132.14	-141.05	4.84	.007	-.057	-132.39	-141.02	4.72	.004	-.033	-132.34	-140.68	4.56	.001
	.064	-136.96	-145.44	4.53	.001	.042	-136.10	-145.15	4.84	.007	.023	-136.40	-145.15	4.68	.004	.048	-136.40	-144.87	4.53	.000
	.008	-134.16	-142.50	4.42	-.002	-.013	-133.33	-142.22	4.81	.006	-.032	-133.61	-142.22	4.69	.004	-.008	-133.61	-141.94	4.53	.000
11		-172.00	-180.00	4.50			-172.00	-180.00	4.50			-172.25	-180.25	4.50			-173.00	-181.00	4.50	
	-.013	-171.35	-179.50	4.33	-.004	-.020	-171.02	-179.15	4.33	-.004	-.031	-170.68	-179.10	4.56	.001	.048	-170.61	-179.02	4.49	.000
	.072	-175.58	-183.83	4.32	-.004	.072	-175.58	-183.83	4.32	-.004	.061	-175.28	-183.83	4.48	.000	.046	-175.28	-183.83	4.48	.000
	.003	-172.14	-180.28	4.31	-.004	.003	-172.14	-180.28	4.31	-.004	-.008	-171.86	-180.28	4.54	.001	-.023	-171.86	-180.28	4.46	-.001
12		-213.00	-221.25	4.50			-213.00	-221.25	4.50			-213.00	-221.25	4.50			-213.00	-221.25	4.50	
	.010	-212.51	-221.32	4.53	.001	-.024	-211.78	-220.57	4.60	.002	-.025	-211.73	-220.53	4.60	.002	-.039	-211.06	-220.43	4.83	.007
	.075	-216.74	-225.94	4.72	.004	.058	-215.88	-225.06	4.71	.004	.065	-216.27	-225.35	4.66	.003	.039	-214.93	-224.59	4.96	.009
	.003	-213.17	-221.94	4.50	.000	.002	-212.89	-221.67	4.58	.002	-.002	-212.89	-221.67	4.58	.002	-.013	-212.34	-221.67	4.80	.006
13		-253.50	-261.75	4.50			-253.75	-261.75	4.50			-254.00	-262.00	4.50			-253.75	-262.00	4.50	
	.007	-253.14	-261.74	4.41	.002	-.035	-252.00	-260.89	4.68	.004	-.041	-251.95	-260.83	4.68	.003	-.038	-251.85	-260.72	4.60	.002
	.092	-258.09	-267.02	4.49	.000	.062	-256.87	-266.10	4.64	.003	.056	-256.82	-265.95	4.59	.002	.044	-255.97	-265.08	4.58	.002
	.003	-253.64	-262.22	4.38	-.002	-.013	-253.08	-261.94	4.65	.003	-.018	-253.08	-261.94	4.65	.003	.013	-253.08	-261.94	4.57	.001
14		-291.50	-299.75	4.50			-291.50	-299.75	4.50			-291.00	-299.25	4.50			-291.25	-299.75	4.50	
	-.027	-290.13	-298.81	4.45	-.001	-.040	-289.49	-298.15	4.41	-.002	-.026	-289.72	-298.08	4.33	-.003	-.023	-290.11	-299.34	4.61	.002
	.101	-296.53	-305.55	4.44	-.001	.087	-295.87	-304.86	4.44	-.001	.094	-295.71	-304.30	4.24	-.005	.080	-295.27	-304.75	4.68	.004
	-.020	-290.51	-299.17	4.42	-.002	-.020	-290.51	-299.17	4.39	-.002	-.004	-290.79	-299.17	4.31	-.004	.002	-291.34	-300.56	4.58	.002
15		-330.25	-338.75	4.50			-330.50	-338.75	4.50			-330.25	-338.50	4.50			-330.75	-339.25	4.50	
	.022	-331.33	-340.07	4.31	-.004	-.016	-329.71	-338.74	4.57	.001	-.006	-329.93	-338.67	4.41	-.002	-.020	-329.74	-339.35	4.72	.004
	.181	-339.32	-348.41	4.39	-.002	.144	-337.71	-347.10	4.54	.001	.137	-337.11	-346.09	4.34	-.003	.105	-335.98	-345.86	4.78	.006
	.026	-331.53	-340.28	4.28	-.004	.004	-330.70	-339.72	4.53	.001	.015	-330.98	-339.72	4.38	-.002	.005	-330.98	-340.56	4.69	.004
16		-370.00	-378.50	4.50			-370.00	-378.50	4.50			-370.50	-379.00	4.50			-371.00	-379.50	4.50	
	-.006	-369.70	-378.82	4.42	-.002	-.050	-368.52	-378.23	4.75	.003	-.030	-369.01	-378.42	4.64	.003	-.038	-369.12	-378.81	4.68	.004
	.184	-379.19	-388.67	4.79	.006	.162	-378.08	-388.18	4.61	.002	.137	-377.34	-387.01	4.59	.002	.109	-376.43	-380.64	4.73	.005
	.004	-369.79	-378.89	4.39	-.002	.010	-369.51	-379.17	4.72	.004	.009	-370.06	-379.44	4.61	.002	.013	-370.34	-380.00	4.65	.003
17		-410.25	-419.00	4.50			-410.50	-419.00	4.50			-410.75	-419.25	4.50			-410.75	-419.50	4.50	
	.007	-410.61	-419.80	4.35	-.003	-.035	-408.76	-418.54	4.68	.003	-.042	-408.64	-418.73	4.82	.006	-.039	-408.80	-418.27	4.50	.000
	.029	-421.69	-431.25	4.44	-.001	.189	-419.95	-430.12	4.74	.005	.148	-418.13	-428.51	4.83	.007	.129	-417.20	-426.92	4.53	.001
	.006	-410.54	-419.72	4.32	-.004	.015	-409.71	-419.44	4.65	.003	-.020	-409.71	-419.72	4.79	.006	.015	-410.83	-419.44	4.47	-.001
18		-448.25	-457.00	4.50			-448.25	-457.00	4.50			-449.25	-458.00	4.50			-450.00	-458.75	4.50	
	.025	-447.01	-456.87	4.57	.001	-.046	-445.93	-456.08	4.71	.004	-.063	-446.09	-456.25	4.82	.006	-.060	-447.02	-457.17	4.71	.004
	.225	-459.51	-469.77	4.69	.004	.208	-458.60	-469.18	4.83	.007	.147	-456.59	-467.15	4.78	.006	.129	-456.45	-466.88	4.77	.005
	.028	-446.85	-456.67	4.54	.001	-.028	-446.85	-456.91	4.68	.007	.042	-447.13	-457.22	4.79	.006	-.035	-448.24	-458.33	4.68	.004

TABLE I (Continued)

Wire No.	Reference Line I					Reference Line J					Reference Line K					Reference Line L				
	e_s	S	S_o	h	e_h	e_s	S	S_o	h	e_h	e_s	S	S_o	h	e_h	e_s	S	S_o	h	e_h
10		-134.00	-142.00	4.50			-134.50	-142.50	4.50			-134.50	-142.50	4.50						
	-.027	-132.69	-140.69	4.37	-.003	-.045	-132.24	-140.57	4.56	.001	-.034	-132.71	-140.48	4.25	-.005					
	.054	-136.69	-144.87	4.37	-.003	.038	-136.40	-144.87	4.53	.001	.050	-136.98	-144.87	4.22	-.006					
	.002	-133.89	-141.94	4.34	-.003	-.018	-133.61	-141.94	4.53	.001	-.007	-134.16	-141.94	4.22	-.006					
11		-173.50	-181.00	4.50			-173.25	-181.50	4.50			-173.44	-181.50	4.50						
	-.032	-170.88	-179.85	4.64	.003	-.064	-170.06	-179.47	4.45	-.001	-.044	-171.26	-179.69	4.53	.001					
	.061	-175.54	-184.68	4.79	.006	.052	-175.85	-184.40	4.48	.000	.054	-176.13	-184.68	4.48	.000					
	-.007	-172.14	-181.11	4.61	.002	-.017	-172.42	-180.83	4.42	-.002	-.015	-172.70	-181.11	4.49	.000					
12		-213.00	-221.25	4.50			-213.00	-221.25	4.50			-213.25	-221.25	4.50						
	-.028	-211.62	-220.39	4.53	.001	-.024	-211.80	-220.88	4.68	.004	-.029	-211.77	-220.57	4.68	.004					
	.050	-215.51	-224.62	4.67	.003	.046	-215.33	-224.63	4.78	.006	.045	-215.48	-224.62	4.69	.004					
	.002	-212.89	-221.67	4.50	.000	.003	-213.17	-222.22	4.65	.003	.002	-213.17	-221.94	4.65	.003					
13		-253.50	-262.00	4.50			-254.00	-262.25	4.50			-254.25	-262.25	4.50						
	-.023	-252.36	-261.21	4.49	.000	-.028	-252.58	-261.44	4.53	.001	-.022	-253.15	-261.45	4.40	-.002					
	.065	-256.74	-265.90	4.60	.002	.042	-256.12	-265.17	4.55	.001	.064	-257.44	-266.01	4.31	-.004					
	.003	-253.64	-262.50	4.46	-.001	.002	-253.91	-262.78	4.50	.000	.004	-254.47	-262.78	4.34	-.003					
14		-291.50	-299.75	4.50			-292.50	-300.75	4.50			-292.50	-300.75	4.50			-292.50	-300.75	4.50	
	-.018	-290.62	-299.26	4.34	-.003	-.021	-291.43	-299.79	4.26	-.005	.015	-291.74	-300.11	4.33	-.003	.013	-293.13	-301.51	4.23	-.005
	.096	-296.29	-305.22	4.40	-.002	.066	-295.80	-304.32	4.20	-.006	.097	-297.36	-306.00	4.26	-.005	.111	-298.06	-306.68	4.25	-.005
	.008	-291.89	-300.56	4.32	-.004	.004	-292.72	-301.11	4.24	-.005	.010	-293.00	-301.37	4.31	-.004	.032	-294.11	-302.50	4.20	-.006
15		-330.75	-339.25	4.50			-331.50	-339.75	4.50			-331.50	-339.75	4.50			-331.50	-339.75	4.50	
	-.016	-329.95	-338.96	4.46	-.003	-.026	-330.22	-339.24	4.49	.000	-.007	-331.17	-339.60	4.23	-.005	.006	-331.78	-340.53	4.38	-.002
	.123	-336.94	-346.25	4.50	.000	.078	-335.41	-344.62	4.46	-.001	.133	-338.15	-346.86	4.22	-.006	.127	-337.86	-346.86	4.35	-.003
	.010	-331.25	-340.28	4.43	-.001	.001	-331.53	-340.56	4.47	-.001	.017	-332.37	-340.83	4.20	-.006	.023	-332.64	-341.39	4.35	-.003
16		-371.00	-379.50	4.50			-372.50	-381.00	4.50			-372.50	-381.00	4.50			-372.50	-381.00	4.50	
	-.023	-369.87	-378.95	4.39	.002	-.042	-370.42	-379.81	4.57	.001	-.016	-371.70	-380.20	4.19	-.006	-.002	-372.38	-381.51	4.49	.000
	.144	-378.18	-387.57	4.46	-.001	.079	-376.45	-386.04	4.55	.001	.152	-380.08	-388.87	4.17	-.007	.143	-379.66	-389.05	4.45	-.001
	.003	-371.17	-380.28	4.36	-.003	.015	-371.73	-381.11	4.54	.001	.012	-372.84	-381.39	4.17	-.007	.012	-373.12	-382.22	4.46	-.001
17		-410.75	-419.50	4.50			-411.75	-419.75	4.50			-411.50	-419.75	4.50			-411.00	-419.75	4.50	
	-.036	-408.96	-418.10	4.32	-.004	-.046	-408.96	-418.38	4.55	.001	.041	-409.45	-418.03	4.19	-.006	.011	-410.46	-420.26	4.64	.003
	.156	-418.57	-428.03	4.41	-.007	.092	-419.83	-429.43	4.48	.000	.153	-419.15	-428.00	4.12	-.008	.157	-418.85	-428.94	4.70	.004
	.010	-410.26	-419.44	4.29	-.004	-.020	-410.36	-419.72	4.54	.001	.019	-410.54	-419.17	4.17	-.007	.002	-411.09	-420.83	4.61	.002
18		-450.00	-458.75	4.50			-451.00	-459.50	4.50			-451.00	-459.50	4.50			-451.00	-459.50	4.50	
	-.045	-447.73	-457.28	4.43	-.001	-.060	-448.00	-458.17	4.82	.006	-.032	-449.41	-458.07	4.19	-.006	-.020	-449.99	-459.28	4.46	-.001
	.173	-458.64	-468.50	4.51	.000	.094	-456.69	-466.06	4.74	.005	.190	-460.51	-469.43	4.08	-.008	.171	-459.57	-469.12	4.36	-.003
	.001	-449.07	-458.61	4.40	-.001	-.033	-449.36	-459.44	4.79	.006	.011	-450.44	-459.19	4.17	-.007	.011	-450.46	-459.72	4.43	-.001

depth; note group 17-D where the depth is given to 0.003 inch while the location is in error by 0.291 inch. It should also be noted that one can not judge the accuracy of the depth by the accuracy of the location, or conversely, in any of the methods. This can be seen by comparing 9-E where the depth is 0.001 inch in error with 2-A where the depth is 0.008 inch in error.

Table II gives a comparison of the locations and depths of the nozzle flow field, with the secondary slot plugged, computed by the three methods (run 1904). There is actually little choice between the methods so far as the results that are shown. The preparation time for each is the same, i.e., for obtaining the raw data, and if a computer is used to reduce the data there is no time saved except for method III which does not require the tedious determination of the optical error correction equations. Thus, method III requires about 25 % less time than I and II.

Figure 16 is the plot of the results, given in Table II, for run 1904 which was a nozzle without injection, and shows the isogrametric lines to be comparable to those of Preiswerk's shown as figure 78f in his second paper (8). The field is typical of those shown in various other publications that were obtained by other methods of measuring the depths. The Froude one ($h/h_o = 0.67$) line is in the typical location beginning at the nozzle wall just downstream of the physical throat. The hash lines at each end of the plot represent the reference lines, designated by letters in the tables. Position E is the center of the field of view. The size may be judged by the 1 inch scale in the upper left corner. Figure 17 is the shadow pattern from which the data for Table II and Figure 16 were obtained, and Figure 18 is the streak line

TABLE II

COMPARISON OF VALUES COMPUTED BY DIFFERENT METHODS
FOR RUN 1904

Wire No.	Reference Line A		B		C		D		E		F	
	S	h	S	h	S	h	S	h	S	h	S	h
1*	248.99	20.86	248.80	20.94	249.13	20.86	247.56	20.65	247.39	20.77	247.25	21.15
	248.96	21.09	248.80	20.93	248.04	21.11	247.54	20.82	247.39	20.84	249.14	21.03
	247.87	20.99	247.60	20.88	247.07	20.79	246.55	20.57	246.53	20.71	246.48	21.09
2	208.56	20.41	208.39	20.29	208.73	20.17	207.27	20.15	207.04	20.48	206.67	20.56
	208.55	20.50	208.37	20.50	207.86	20.52	207.28	20.06	207.05	20.41	208.20	20.42
	207.49	20.33	207.22	20.22	206.97	20.10	206.41	20.07	206.37	20.41	206.10	20.49
3	168.66	20.00	168.74	20.00	169.11	19.77	167.78	19.74	167.53	19.91	167.75	19.68
	168.65	20.08	168.74	20.09	168.47	20.10	167.79	19.65	167.53	19.84	168.89	20.01
	167.63	19.93	167.63	19.93	167.65	19.70	167.09	19.67	166.56	19.50	167.37	19.60
4	129.85	19.61	129.38	19.51	129.18	19.61	127.73	19.24	126.88	19.40	126.27	19.46
	129.84	19.68	129.39	19.36	128.79	19.70	127.73	19.25	126.88	19.43	127.07	19.43
	128.83	19.54	128.29	19.43	128.01	19.54	127.20	19.16	126.64	19.32	126.09	19.38
5	90.47	19.23	90.54	19.18	90.10	19.12	88.50	18.53	88.16	18.80	88.11	19.18
	90.47	19.29	90.54	19.13	89.91	19.31	88.50	18.54	88.16	18.72	88.57	19.04
	89.49	19.15	89.49	19.10	89.22	19.04	88.13	18.45	88.12	19.04	88.12	19.11
6	51.35	19.01	50.58	18.91	49.06	18.38	48.13	18.27	47.47	18.43	47.45	18.64
	51.35	19.06	50.59	18.75	49.11	18.44	48.13	18.16	47.47	18.34	47.55	18.49
	50.39	18.93	49.57	18.83	48.48	18.30	47.93	18.18	47.66	18.35	47.65	18.56
7	11.67	18.64	11.45	18.60	9.65	17.88	8.58	17.69	7.60	17.56	7.32	17.60
	10.56	18.34	10.53	18.45	9.59	18.15	8.80	18.04	8.37	18.33	8.10	18.17
	10.74	18.24	10.47	18.20	9.36	17.82	8.54	17.60	8.00	17.76	7.72	17.80
8	-31.71	17.66	-32.03	17.55	-31.86	17.29	-31.83	17.43	-30.76	17.74	-31.59	17.29
	-31.35	17.79	-31.87	17.48	-32.57	17.16	-32.70	17.32	-32.80	17.64	-33.65	17.01
	-27.81	19.44	-31.42	17.46	-31.97	17.15	-31.68	17.34	-31.68	17.56	-32.52	17.12
9	-71.24	17.31	-71.83	17.02	-71.98	16.82	-72.81	16.79	-71.62	17.08	-70.98	17.27
	-71.59	17.28	-72.39	16.81	-72.82	16.66	-74.18	16.50	-74.27	16.96	-73.71	16.96
	-71.10	17.17	-71.66	16.90	-71.94	16.74	-72.50	16.70	-72.50	16.99	-71.93	17.18
10	-111.49	16.89	-112.00	16.64	-112.10	16.64	-112.98	16.36	-112.19	16.51	-112.86	16.04
	-112.13	16.62	-112.93	16.47	-113.07	16.47	-114.82	16.16	-115.20	16.31	-116.07	15.84
	-111.36	16.80	-111.81	16.55	-111.81	16.55	-112.48	16.27	-112.76	16.43	-113.60	15.96
11	-150.09	16.55	-150.23	16.52	-150.60	16.00	-150.65	16.29	-151.12	15.80	-151.12	15.63
	-150.72	16.44	-151.24	16.44	-151.70	15.84	-152.94	15.98	-154.49	15.52	-154.77	15.52
	-149.70	16.43	-149.98	16.44	-150.28	15.91	-149.99	16.18	-151.40	15.63	-151.70	15.54
12	-191.77	16.13	-191.54	16.05	-192.13	15.70	-192.79	15.66	-192.83	15.33	-192.42	15.54
	-191.66	16.39	-191.86	16.18	-191.45	15.74	-193.73	15.77	-195.47	15.33	-194.88	15.78
	-191.08	16.04	-191.10	15.96	-191.67	15.61	-191.96	15.57	-192.81	15.24	-192.22	15.76
13	-231.96	16.02	-231.62	16.07	-231.61	15.87	-232.91	15.35	-232.45	15.65	-232.26	15.40
	-233.00	15.69	-232.63	15.79	-232.07	15.50	-236.31	15.22	-236.66	15.41	-236.37	15.24
	-231.93	15.67	-231.93	15.72	-231.95	15.52	-234.05	13.87	-233.08	15.30	-233.38	15.07
14	-270.52	15.14	-269.22	15.50	-268.61	15.35	-270.22	14.86	-270.17	14.99	-270.15	14.84
	-272.57	15.08	-270.80	15.48	-270.04	15.49	-275.88	14.90	-275.81	15.09	-275.74	15.07
	-270.84	15.05	-269.46	15.41	-268.80	16.30	-270.09	14.77	-270.65	14.90	-271.20	14.74
15	-312.11	14.54	-311.01	14.68	-310.61	14.69	-311.40	14.54	-311.50	14.47	-311.08	14.39
	-315.31	14.32	-313.28	14.57	-313.25	14.58	-319.54	14.73	-318.75	14.47	-318.37	14.31
	-311.82	14.45	-311.23	14.59	-310.96	14.60	-311.26	14.45	-311.85	14.37	-312.13	14.30
16	-350.12	13.94	-349.21	14.09	-349.65	13.79	-351.03	13.56	-351.20	13.79	-351.29	13.42
	-354.36	13.73	-352.12	13.85	-353.39	13.55	-361.62	13.52	-360.05	13.59	-360.21	13.28
	-349.72	13.86	-349.42	14.00	-350.00	13.71	-350.87	13.47	-351.38	13.70	-352.28	13.33
17	-390.20	13.44	-390.20	13.44	-390.56	13.36	-391.70	13.19	-392.00	13.35	-391.69	13.13
	-393.76	13.27	-393.76	13.27	-395.42	13.26	-404.78	13.07	-402.44	13.14	-402.24	12.98
	-390.66	13.33	-390.38	13.35	-390.93	13.27	-391.53	13.10	-392.03	13.26	-392.63	13.03
18	-428.99	12.87	-428.99	12.87	-428.79	12.63	-429.74	12.22	-429.54	12.68	-429.42	12.39
	-433.17	12.71	-433.17	12.71	-434.74	12.41	-445.15	12.05	-441.45	12.43	-441.52	12.12
	-430.86	12.46	-429.17	12.78	-429.21	12.54	-429.56	12.13	-429.43	12.60	-430.36	12.29

*The results of the Mark I, Mark II, and Mark III computations are listed vertically in that order.

TABLE II (Continued)

Wire No.	Reference Line G		H		I		J		K		L	
	S	h	S	h	S	h	S	h	S	h	S	h
1	246.28	20.51	245.68	20.64	245.59	20.16	245.47	20.27	245.86	20.51	245.17	20.00
	248.66	20.60	248.66	20.60	245.57	20.36	245.45	20.42	246.87	20.60	245.17	20.03
	245.17	20.44	245.09	21.04	244.67	20.07	244.38	20.20	244.35	20.44	243.33	19.93
2	205.62	20.10	204.59	19.93	205.16	19.91	204.68	19.47	205.21	20.12	205.20	19.81
	207.53	20.16	206.99	19.99	205.14	20.10	204.68	19.50	206.02	19.84	205.19	19.95
	204.77	20.03	204.23	19.86	204.51	19.83	204.00	19.40	204.21	20.05	203.96	19.74
3	166.90	19.53	166.21	19.59	166.11	19.46	166.03	19.36	165.69	19.36		
	168.36	19.59	168.09	19.42	166.11	19.53	166.04	19.27	166.23	19.43		
	166.29	19.45	165.99	19.51	165.75	19.28	165.75	19.28	165.20	19.28		
4	125.10	19.30	124.51	19.03	124.84	18.97	124.08	18.58	123.90	18.64		
	126.07	19.33	125.82	18.84	124.85	18.80	124.09	18.37	124.22	18.36		
	124.72	19.22	124.47	18.95	124.74	18.89	124.22	18.50	123.94	18.55		
5	87.18	18.53	86.67	18.31	86.33	18.26	85.43	17.93	84.89	17.71		
	87.72	18.46	87.45	18.14	86.34	18.10	85.43	17.83	84.96	17.66		
	87.03	18.45	86.77	18.23	86.50	18.17	86.16	17.97	85.41	17.62		
6	46.46	18.10	46.30	18.10	45.30	17.46	44.53	17.30	44.43	17.61		
	46.52	17.92	46.52	17.92	45.30	17.40	44.53	17.30	44.27	17.44		
	46.55	18.01	46.55	18.20	45.74	17.38	45.47	17.22	45.46	17.52		
7	5.72	17.01	5.65	17.01	5.35	16.72	4.72	16.51	4.80	16.76		
	6.50	17.73	6.50	17.73	6.50	17.73	6.50	17.73	6.76	17.88		
	6.06	17.21	6.06	17.22	6.06	17.12	6.06	17.12	6.34	17.48		
8	-32.97	16.92	-33.81	16.70	-33.11	16.68	-33.76	16.07	-33.86	15.77		
	-35.06	16.53	-35.90	16.53	-35.62	16.37	-36.19	16.06	-36.47	15.58		
	-33.91	16.73	-34.73	16.55	-34.46	16.39	-35.02	15.98	-35.30	15.68		
9	-72.66	16.32	-74.32	15.43	-74.66	15.12	-75.34	14.79	-74.91	14.80		
	-75.42	16.03	-77.13	15.25	-77.42	14.94	-78.27	14.78	-77.99	14.62		
	-73.62	16.22	-75.30	15.35	-75.58	15.03	-76.42	14.71	-76.16	14.71		
10	-113.11	16.04	-114.48	15.33	-114.51	15.33	-114.94	15.18	-115.11	15.02		
	-116.35	15.84	-117.78	15.22	-117.78	15.22	-118.35	15.07	-118.64	14.91		
	-113.88	15.96	-115.30	15.24	-115.30	15.24	-115.86	15.09	-115.91	15.06		
11	-151.64	15.71	-153.00	15.08	-153.00	15.24	-153.74	14.85	-154.24	14.40		
	-155.33	15.52	-156.76	15.06	-156.75	15.21	-157.62	14.90	-158.21	14.45		
	-152.23	15.63	-153.65	14.99	-153.65	15.15	-154.50	14.76	-155.10	14.30		
12	-193.56	14.78	-193.75	14.78	-194.87	14.39	-195.93	14.00	-196.47	13.61		
	-196.72	14.67	-196.32	14.63	-197.39	14.25	-198.28	13.93	-198.82	13.51		
	-193.95	14.91	-194.23	14.91	-195.35	14.53	-196.49	14.15	-197.08	13.77		
13	-233.06	15.17	-234.10	14.78	-234.93	14.40	-235.73	14.01	-236.87	13.64		
	-237.40	14.92	-237.78	14.58	-238.79	14.20	-238.97	13.60	-240.60	13.63		
	-234.23	14.84	-235.38	14.45	-236.26	14.07	-237.11	13.70	-238.26	13.33		
14	-270.94	14.69	-272.84	14.02	-273.62	13.79	-275.02	13.35	-276.21	12.89		
	-276.36	14.76	-277.55	13.98	-278.74	13.90	-279.03	13.45	-281.30	12.88		
	-272.05	14.60	-274.06	13.93	-274.93	13.70	-276.36	13.26	-277.52	12.79		
15	-311.62	14.02	-312.92	13.65	-313.69	13.36	-315.15	12.76	-316.13	12.15	-316.70	12.30
	-318.26	14.01	-318.71	13.68	-320.13	13.60	-320.03	12.72	-322.60	12.15	-322.35	12.26
	-312.71	13.93	-314.15	13.56	-315.01	13.27	-316.48	12.67	-317.41	12.06	-317.65	12.21
16	-352.04	13.42	-353.03	13.21	-354.37	12.68	-355.83	12.32	-357.39	11.79	-358.71	11.41
	-359.90	13.27	-359.94	13.09	-362.22	12.57	-361.59	12.15	-365.30	11.72	-365.62	11.25
	-353.11	13.33	-354.25	13.11	-355.70	12.59	-357.16	12.23	-358.65	11.70	-359.51	11.32
17	-392.19	12.91	-393.21	12.48	-393.65	12.26	-394.86	11.88	-395.93	11.29	-396.77	11.02
	-401.25	12.70	-401.24	12.23	-402.81	12.15	-401.48	11.59	-405.19	11.16	-404.78	10.99
	-393.23	12.82	-394.41	12.38	-395.04	12.06	-396.18	11.79	-397.13	11.20	-392.47	10.94
18	-430.41	12.49	-432.29	11.84	-433.54	11.61	-434.79	11.20	-435.84	10.93	-436.41	11.11
	-440.60	12.28	-441.37	11.68	-444.04	11.45	-442.23	11.04	-446.49	10.75	-445.61	11.01
	-431.42	12.40	-433.48	11.75	-434.90	11.52	-436.09	11.11	-436.97	10.85	-436.97	11.03

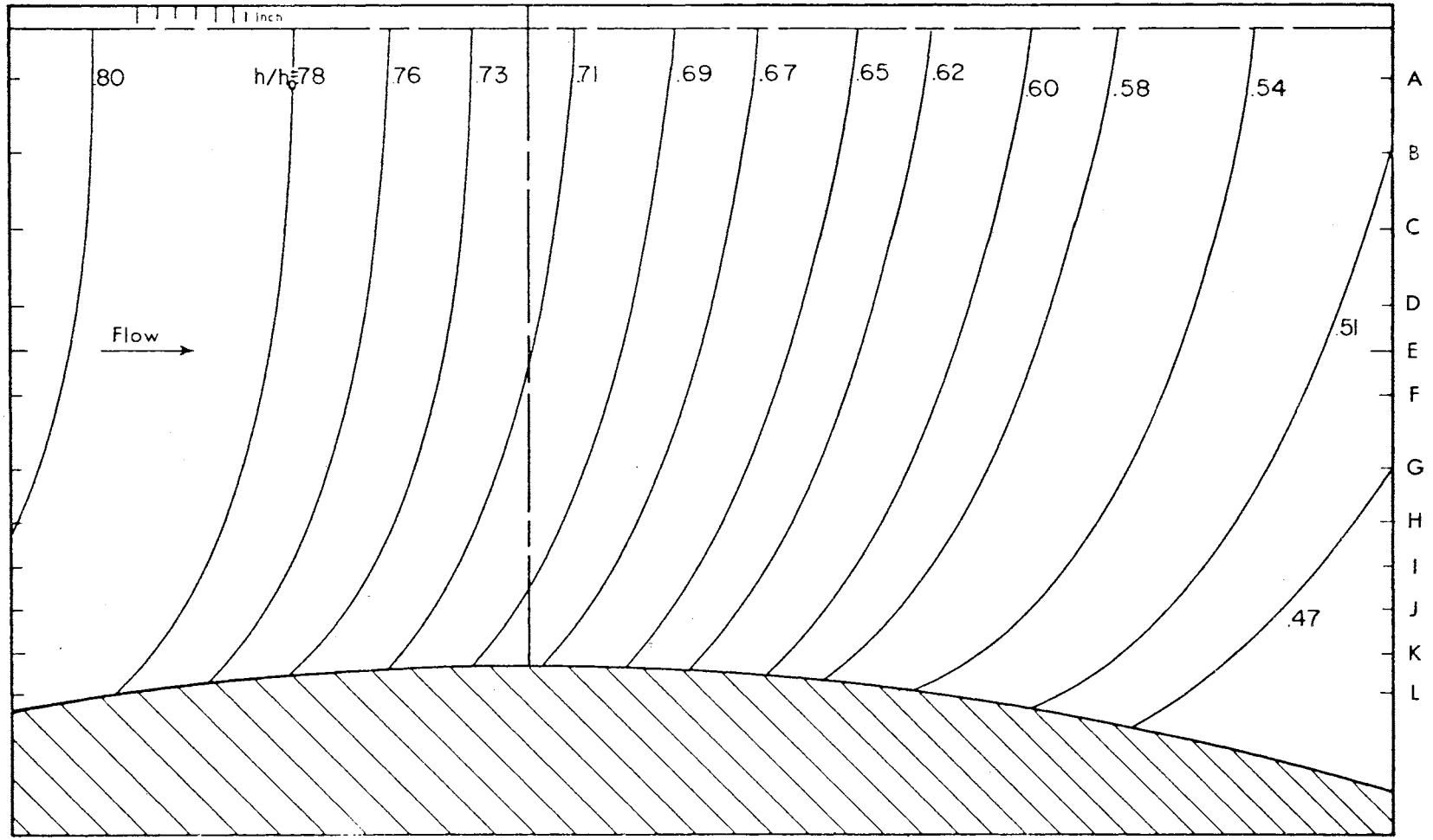

Figure 16. Isogrametric Depth Lines for Plugged Slot; No Secondary Flow.

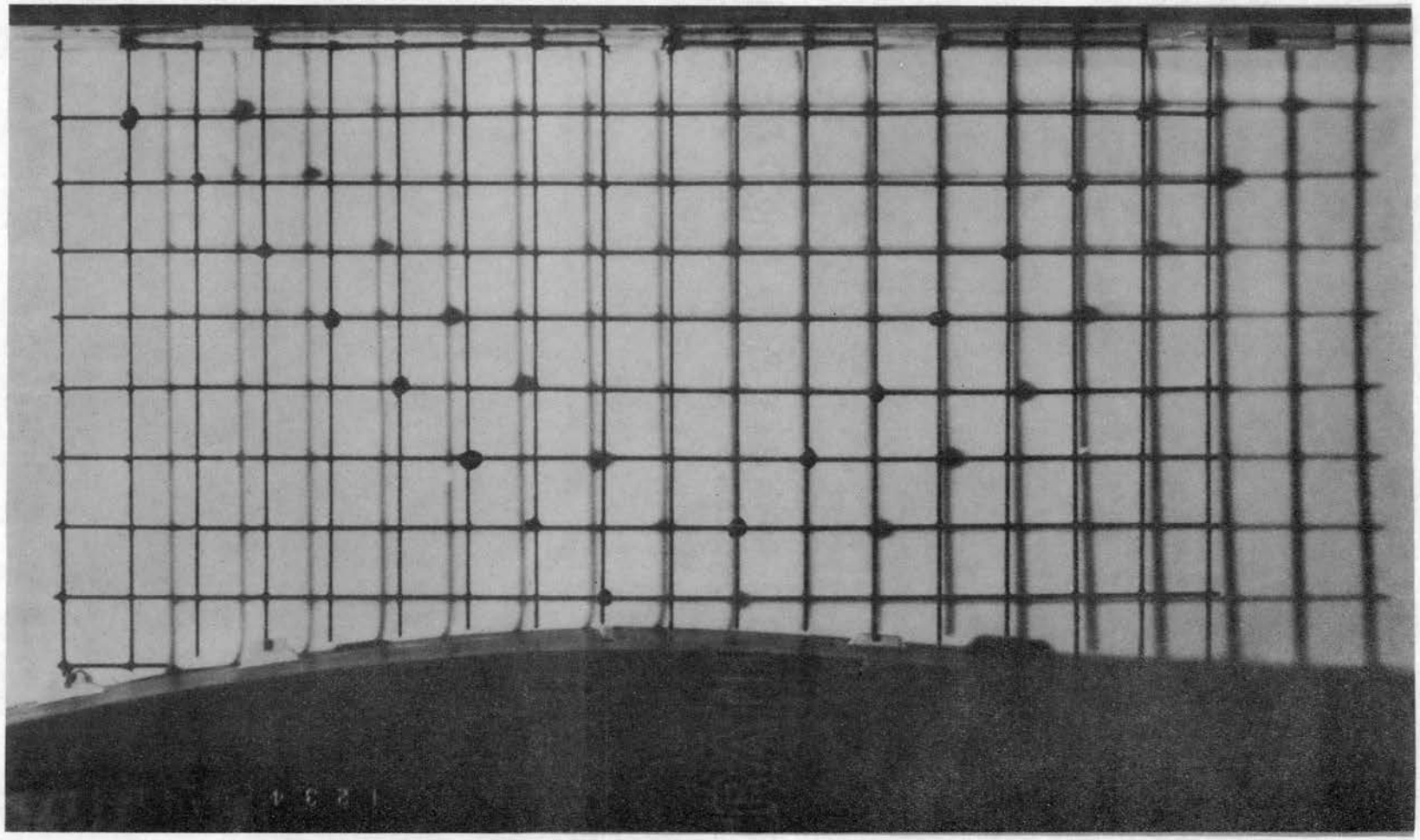

Figure 17. Shadow Pattern for Plugged Slot; No Secondary Flow; Slot at Geometric Throat. (Flow is from left to right.)

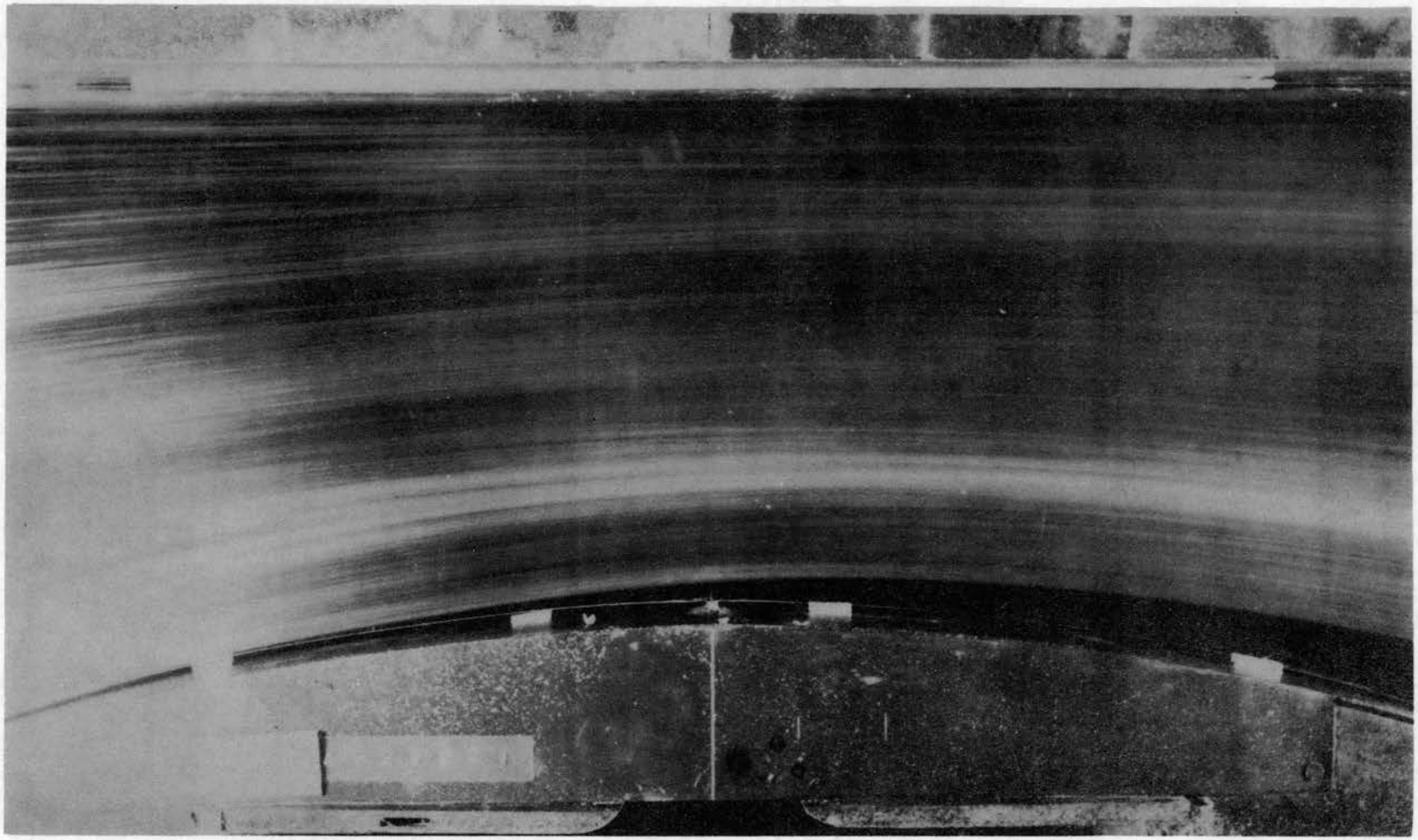

Figure 18. Typical Streak Lines for Plugged Slot;
Slot at Geometric Throat.

pattern for the same test.

Discussion of the Field Plots

Interpretation of the isogrametric depth plots will be facilitated if one refers to the corresponding shadow pattern photograph; a downstream displacement of the shadow (to the right) indicates a decrease in depth. The illumination source is to the left of the field.

Figures 19 to 69 inclusive show the isogrametric depths of some selected runs which are representative of the results that may be obtained by the shadow-photogrammetric method. The figures are arranged so that streak line photographs follow the corresponding field plot. The relative size of the secondary nozzle is indicated by two short lines intersecting the nozzle wall and the direction of injection is shown by a short heavy center line. The dashed lines labeled "outside" and "inside" represent the stream separation as shown by the aluminum particles supplied on the surface of the main stream or the secondary stream, respectively. The flow is from left to right in all figures. The capillary rise near the nozzle wall was neglected and here the shadow position was obtained by extrapolation.

Figure 19 indicates the slight disturbance of the isogrametric lines by an open slot; they become attenuated near the end of the field. The inflow to the secondary nozzle water box was so small that it was not possible to obtain a significant (photographable) particle flow from the secondary nozzle, however, the water level in the secondary water box was stabilized at the time the photographs were exposed so inflow and outflow were occurring. The streak line photographs confirm this. Compare figure 18, where the aluminum particles on the main

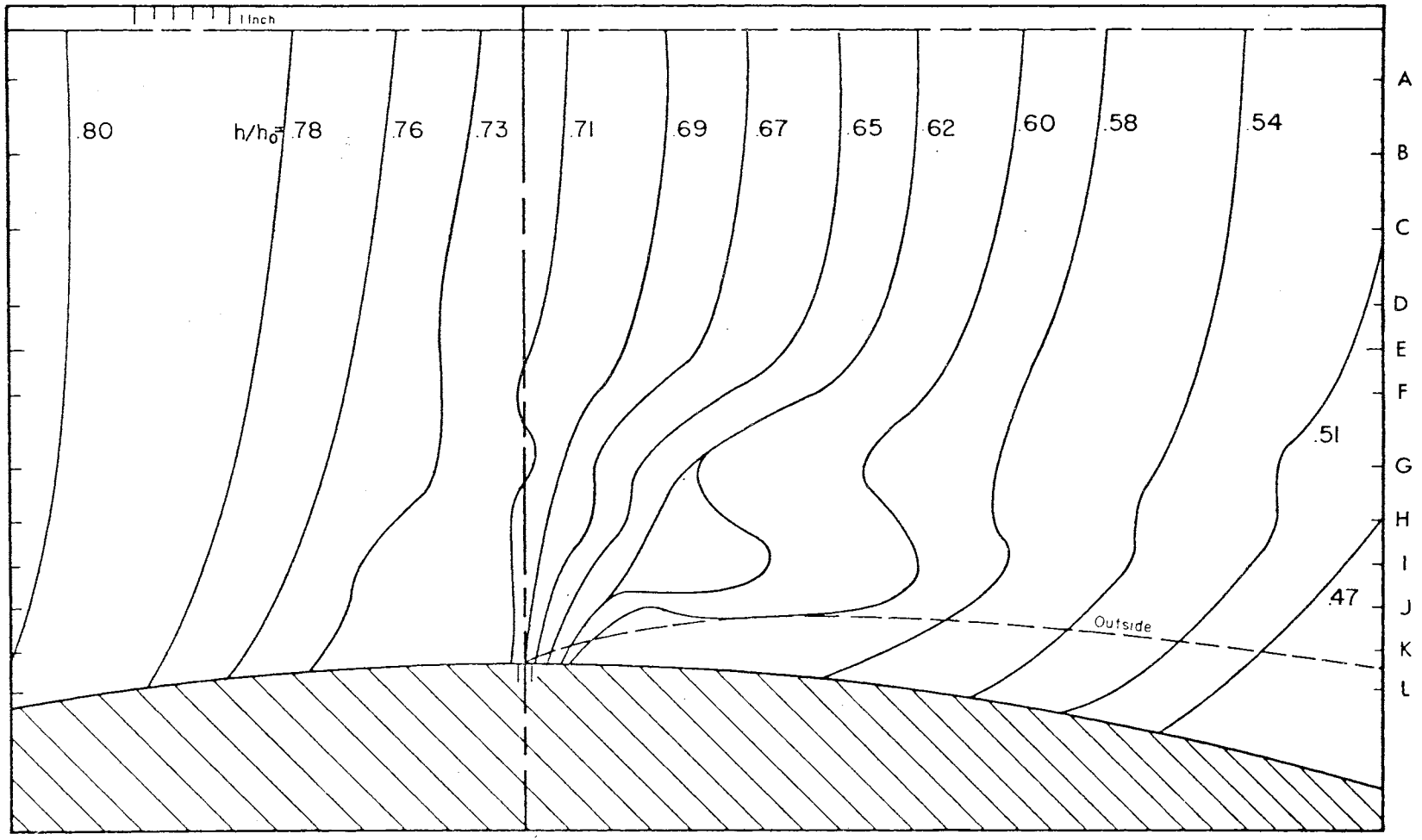

Figure 19. Isogrametric Depth Lines for Open Slot; No Secondary Flow; Slot at Geometric Throat.

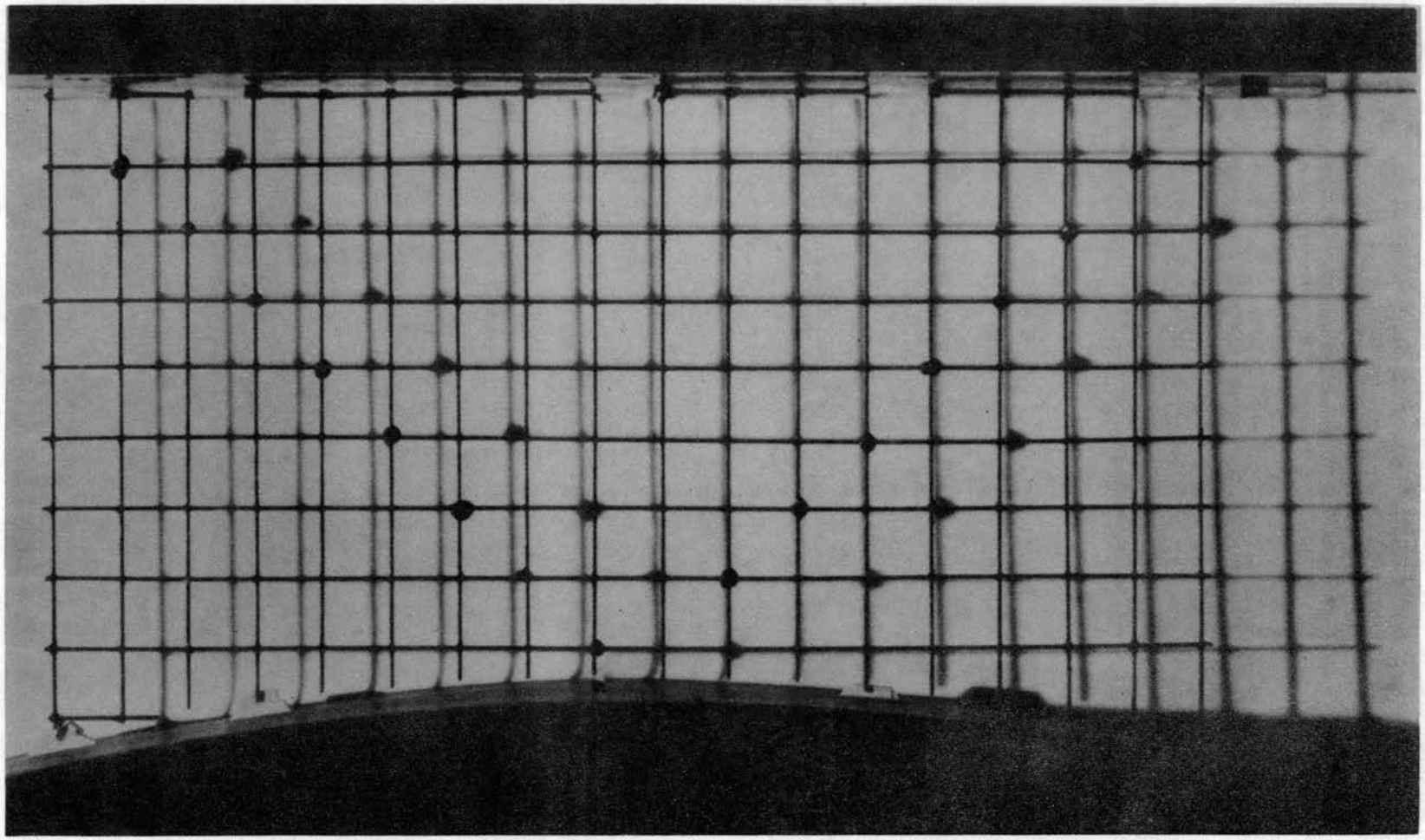

Figure 20. Shadow Pattern for Open Slot; No Secondary Flow; Slot at Geometric Throat.

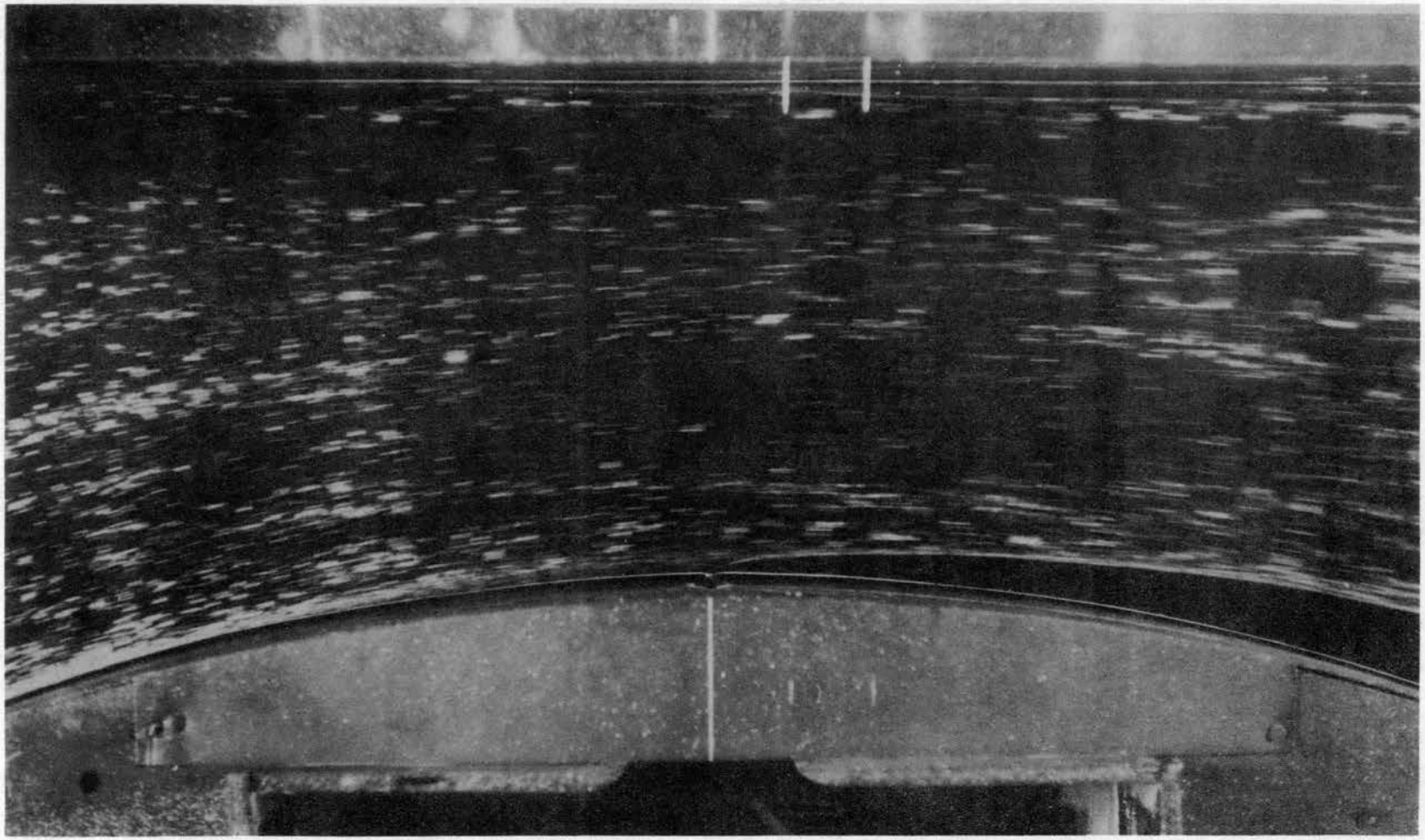

Figure 21. Typical Streak Lines for Open Slot;
Slot at Geometric Throat.

stream were forced away from the nozzle wall by the capillary "hill", to figure 21, where the particles remain next to the wall until given a lateral motion by the outflow of the secondary stream. It was observed during the first series of experiments that if the aluminum powder was dusted very heavily next to the nozzle wall the separation from the wall in the plugged slot case could be prevented, see figure 11, however, this seemed to be due to thinning out or spreading of the powder over the surface.

Figures 22, 26, 30, and 40 are additional plots for secondary injection at the geometric throat for secondary-to-main stream head ratios of 1, 1.50, 1.75, and 2.00. In general, the plots represent the topography of the surface and show the gradients very well. The penetration of the secondary stream as the head ratio increased is shown qualitatively, and the separation of the stream, the low pressure region below injection, is indicated. The head build-up due to partial blockage of the main stream and the low head feed-back along the nozzle wall from the exit side are shown. The three-dimensional character of the flow is seen as isolated bumps or hills in the main stream flow. The small waves eminating from the injection effect seen on the shadow pattern photographs are not discernible in the plots because of the wide spacing of the reference lines in this area. A close examination of the shadow pattern photographs for high head ratios reveals that the apparent capillary rise next to the nozzle wall just below and just above the point of injection is higher than that farther removed from the injection point. This indicates that the secondary flow at high head ratios is not flowing directly into the main stream, but is clinging to the nozzle wall and flowing downward on top of the stream. This

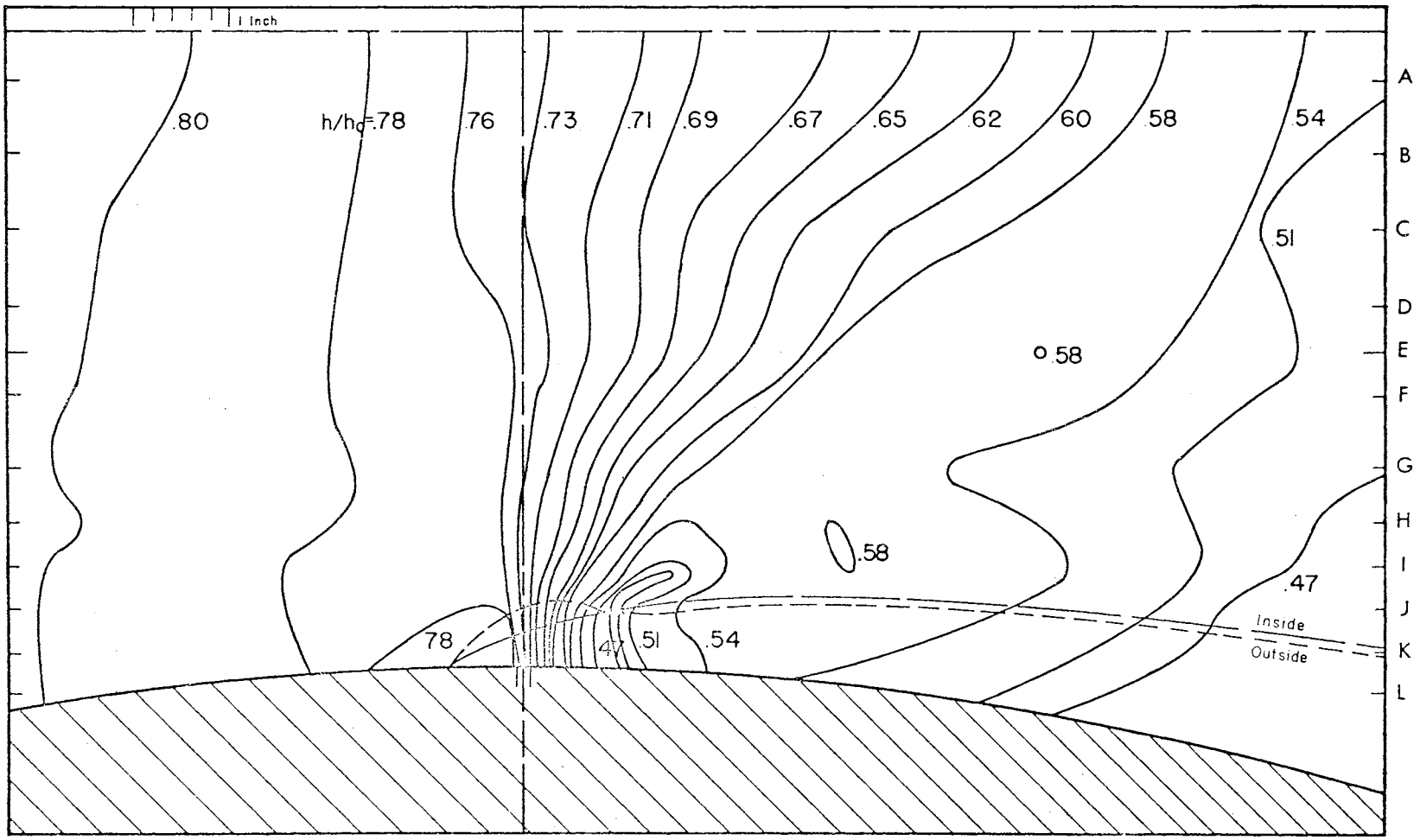

Figure 22. Isogrametric Depth Lines for Secondary to Main Stream Head Ratio of 1.00; Injection at Geometric Throat.

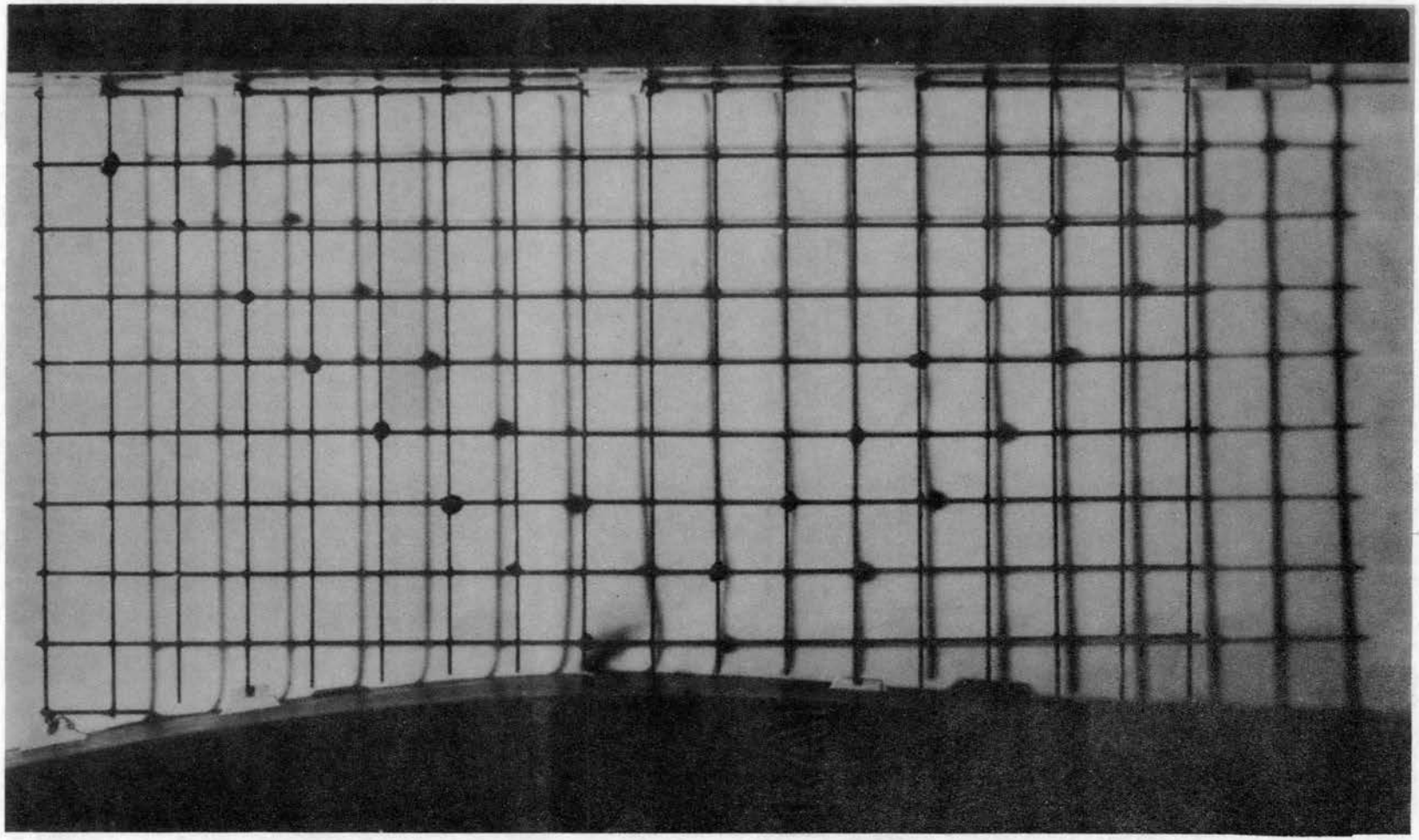

Figure 23. Shadow Pattern for Secondary to Main Stream Head Ratio of 1.00; Injection at Geometric Throat.

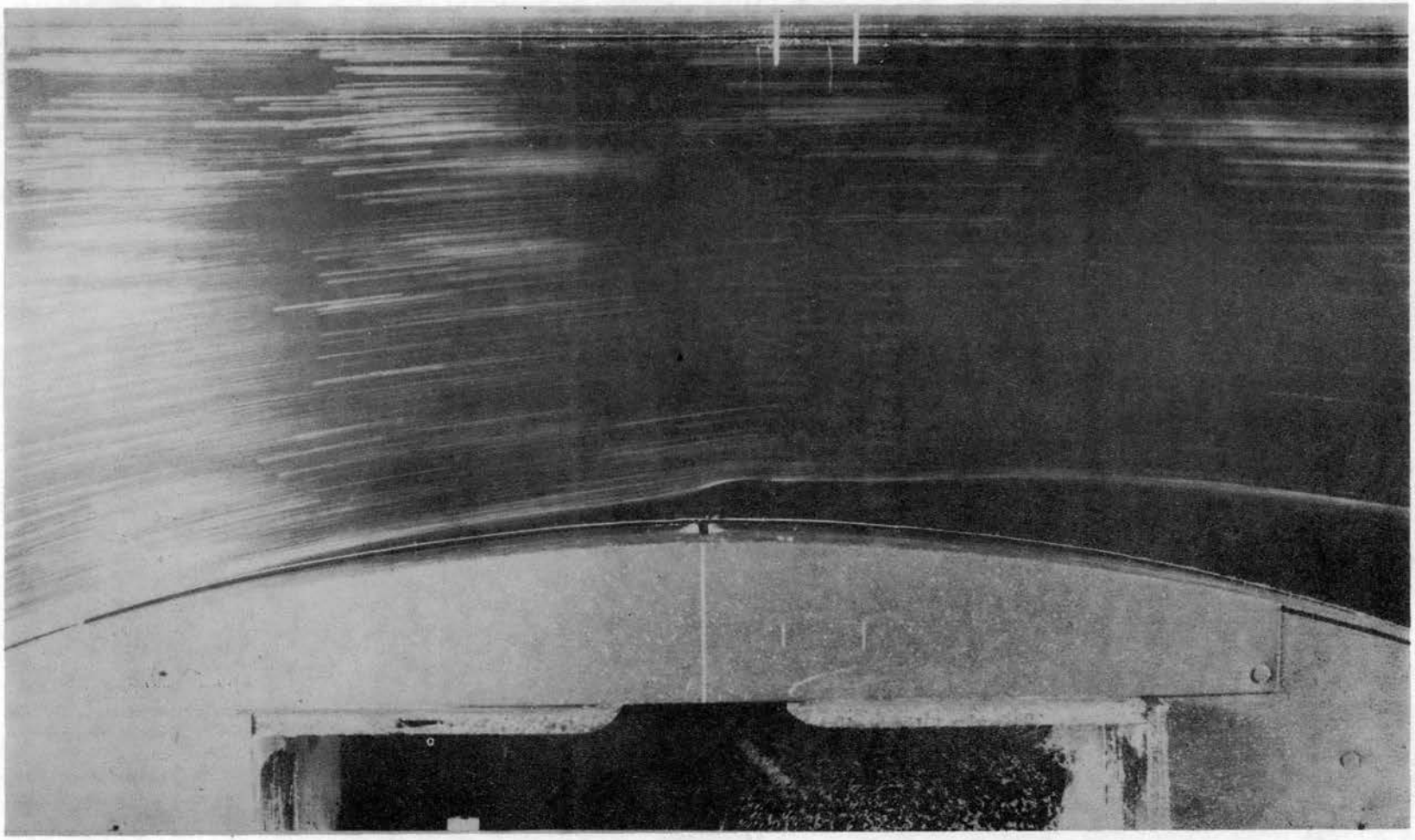

Figure 24. Typical Streak Lines for Secondary to Main Stream Head Ratio of 1.00; Injection at Geometric Throat.

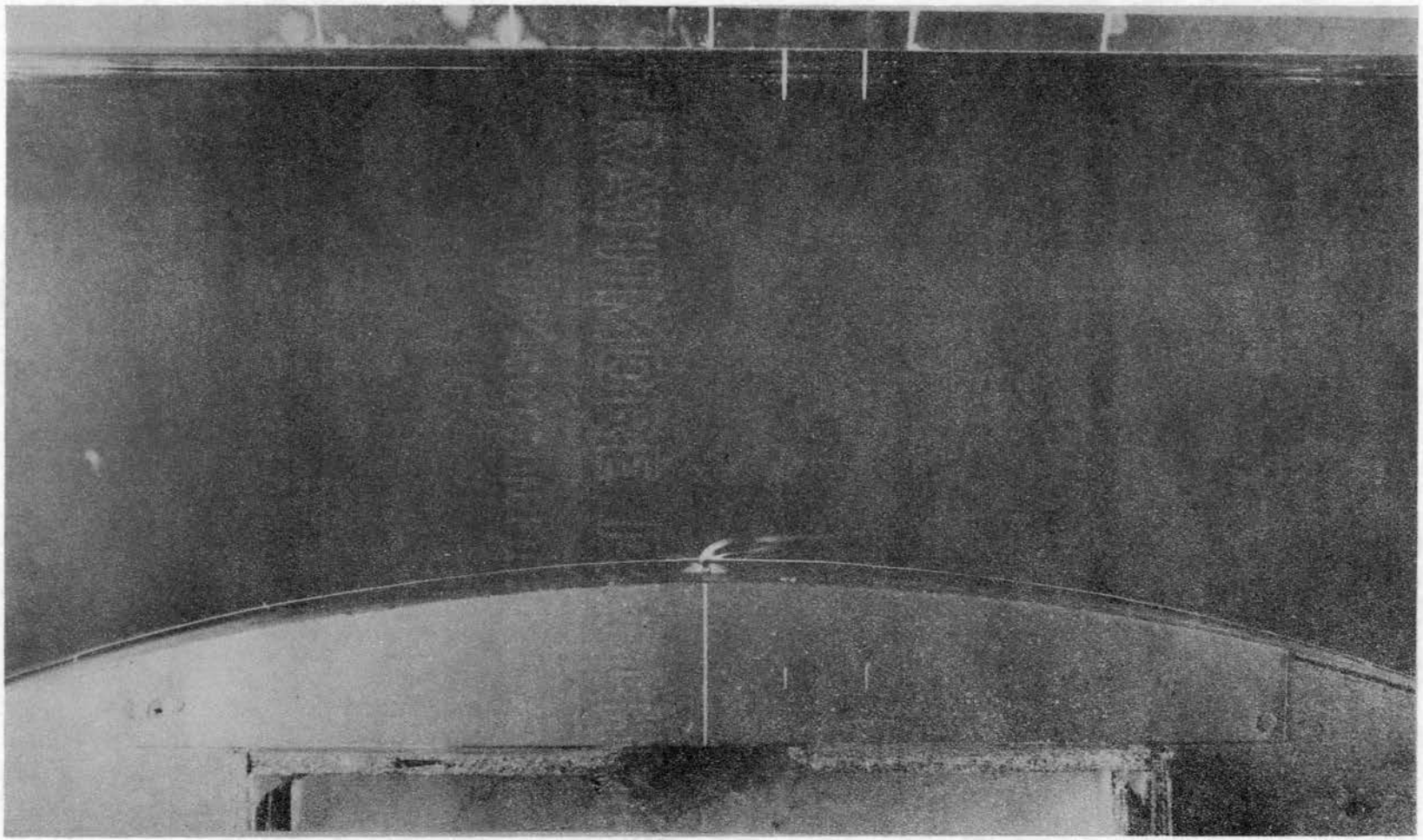

Figure 25. Typical Streak Lines for Secondary to Main Stream Head Ratio of 1.00; Injection at Geometric Throat.

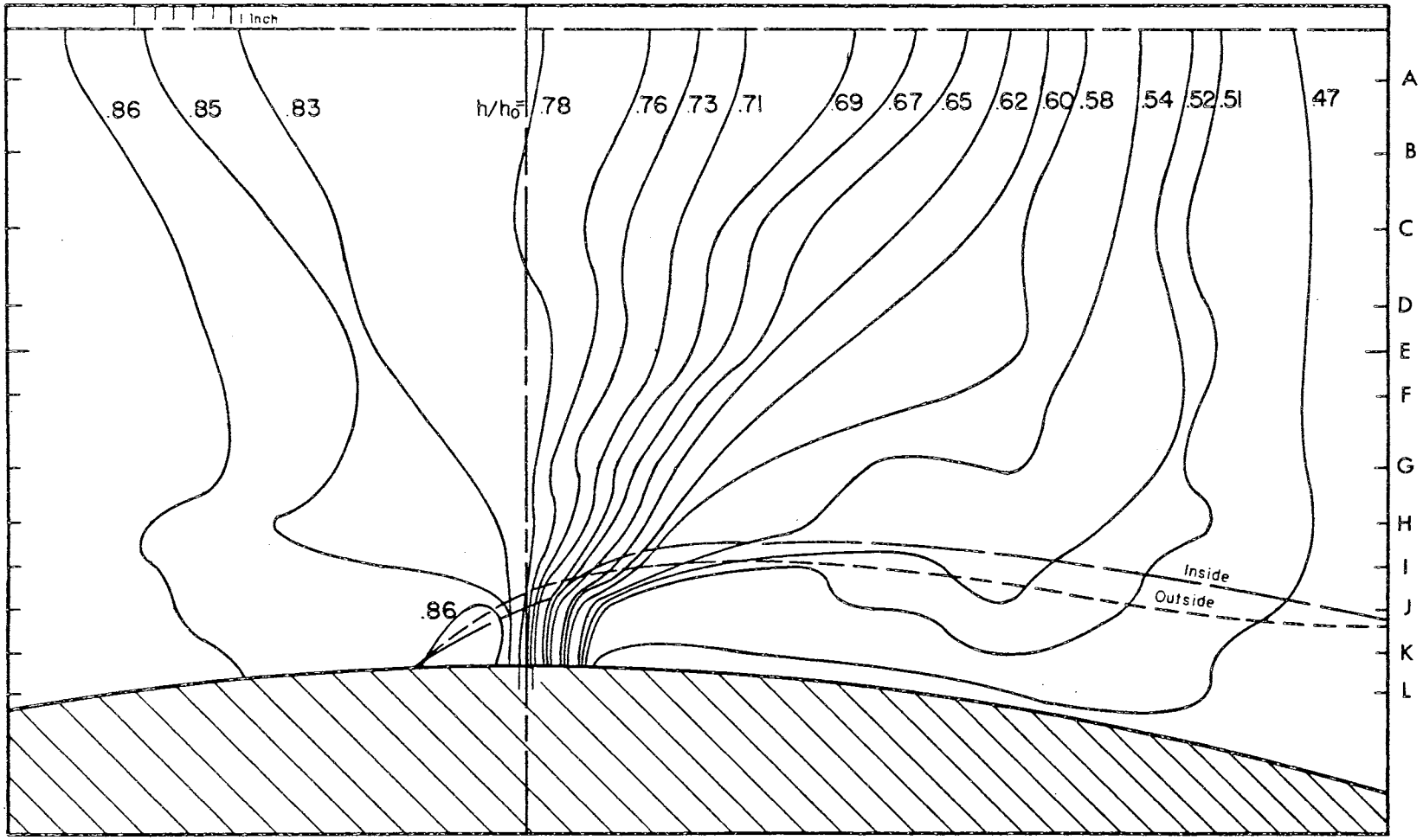

Figure 26. Isogrametric Depth Lines for Secondary to Main Stream Head Ratio of 1.50; Injection at Geometric Throat.

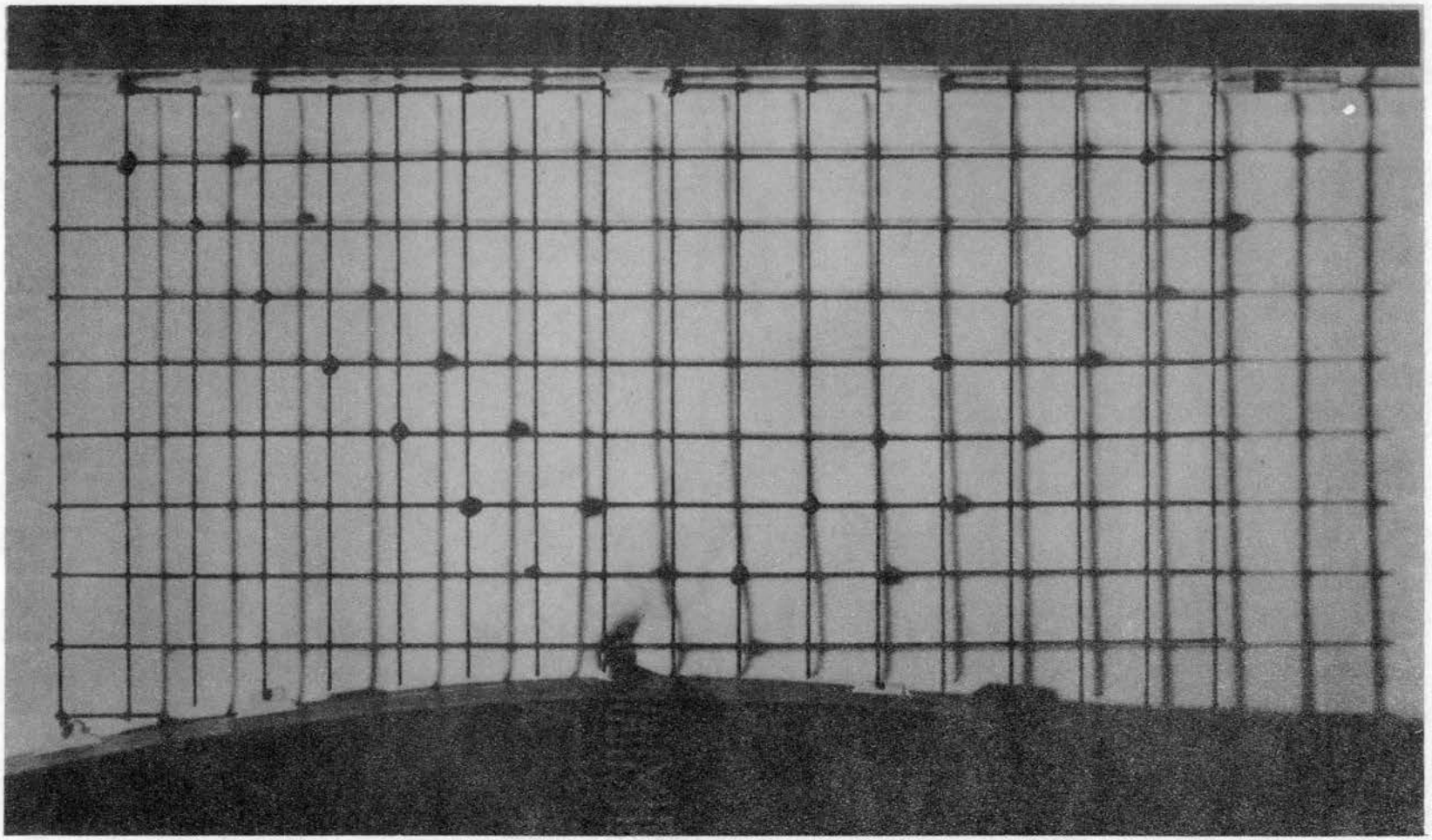

Figure 27. Shadow Pattern for Secondary to Main Stream Head Ratio of 1.50; Injection at Geometric Throat.

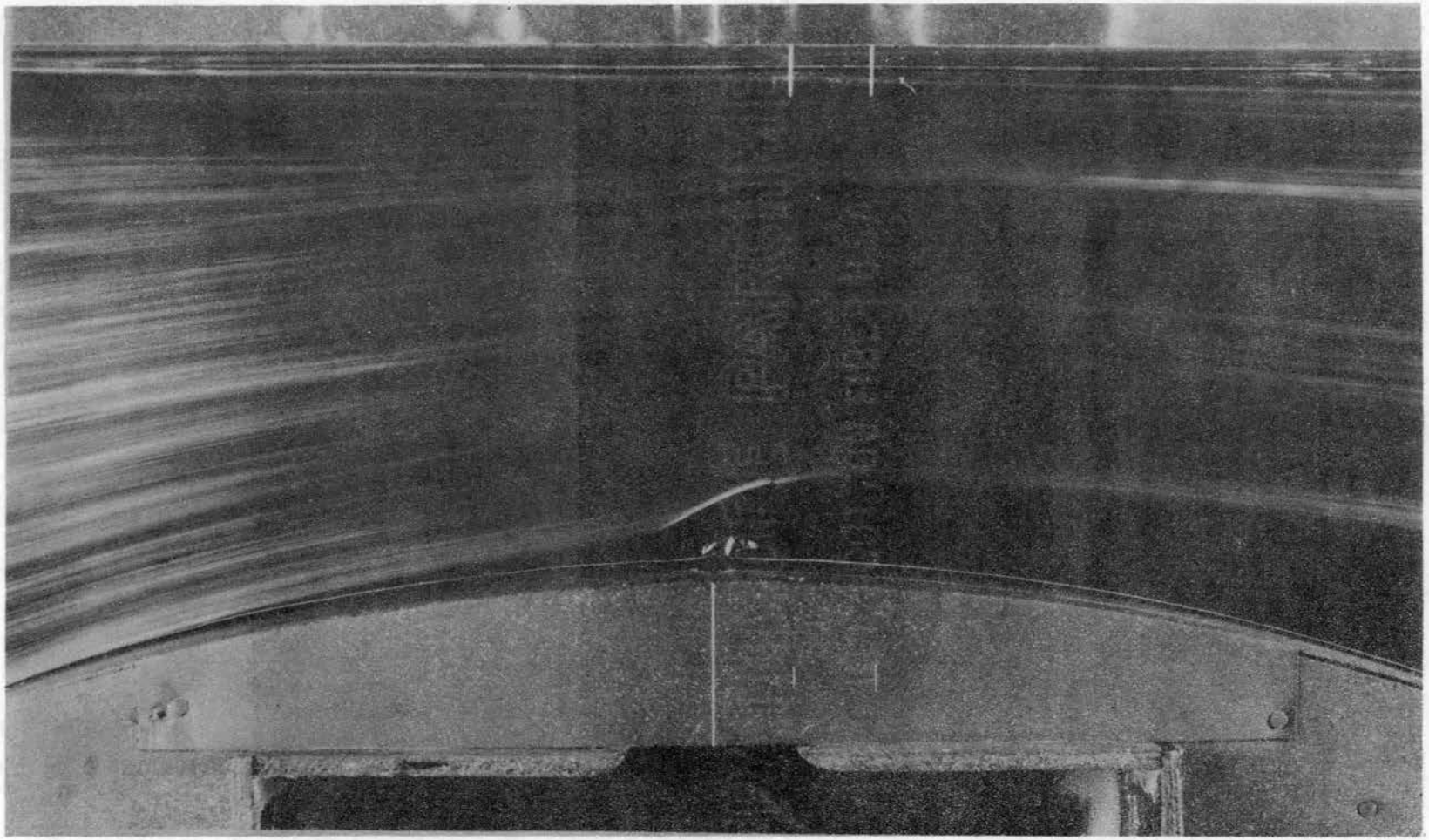

Figure 28. Typical Streak Lines for Secondary to Main Stream Head Ratio of 1.50; Injection at Geometric Throat.

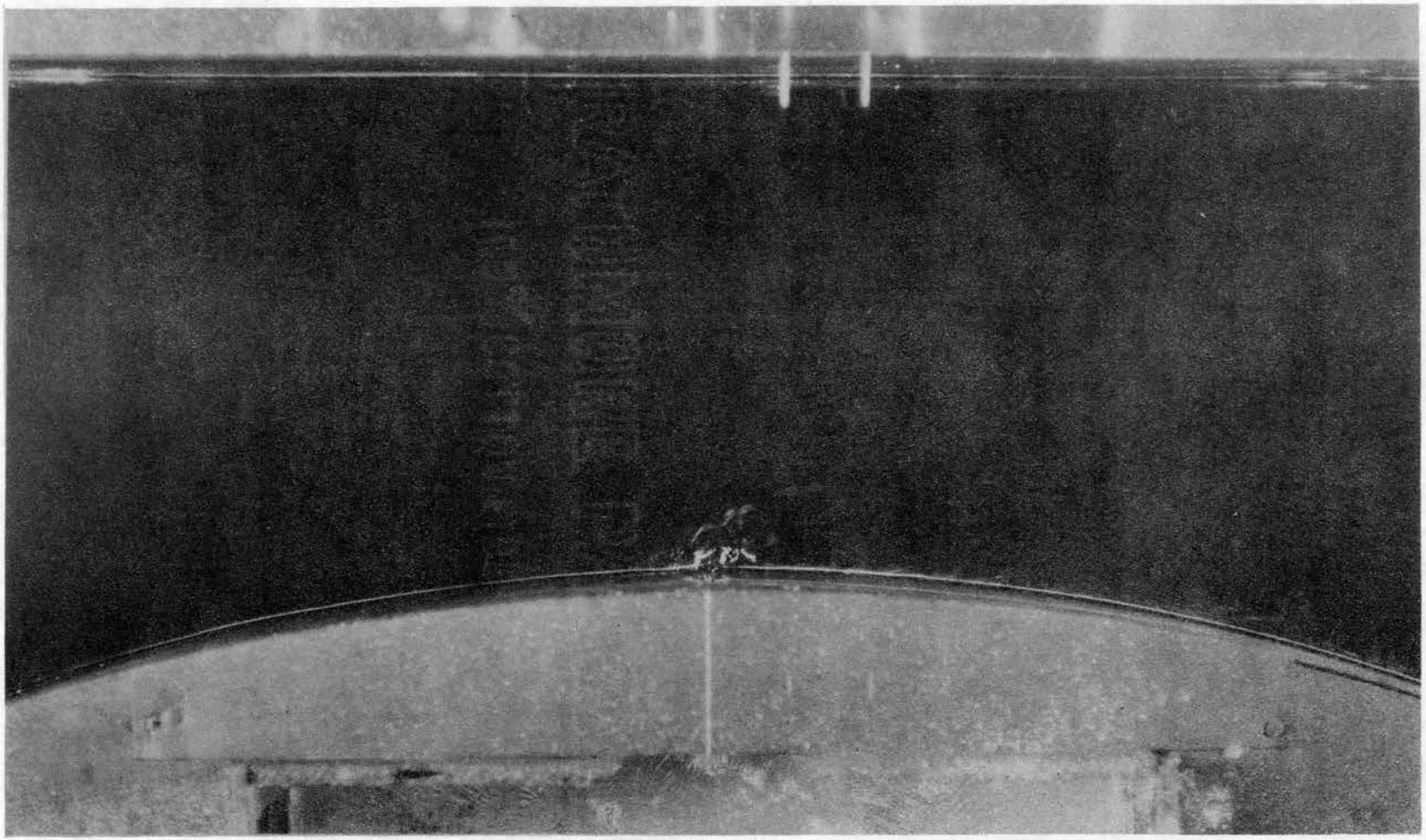

Figure 29. Typical Streak Lines for Secondary to Main Stream Head Ratio of 1.50; Injection at Geometric Throat.

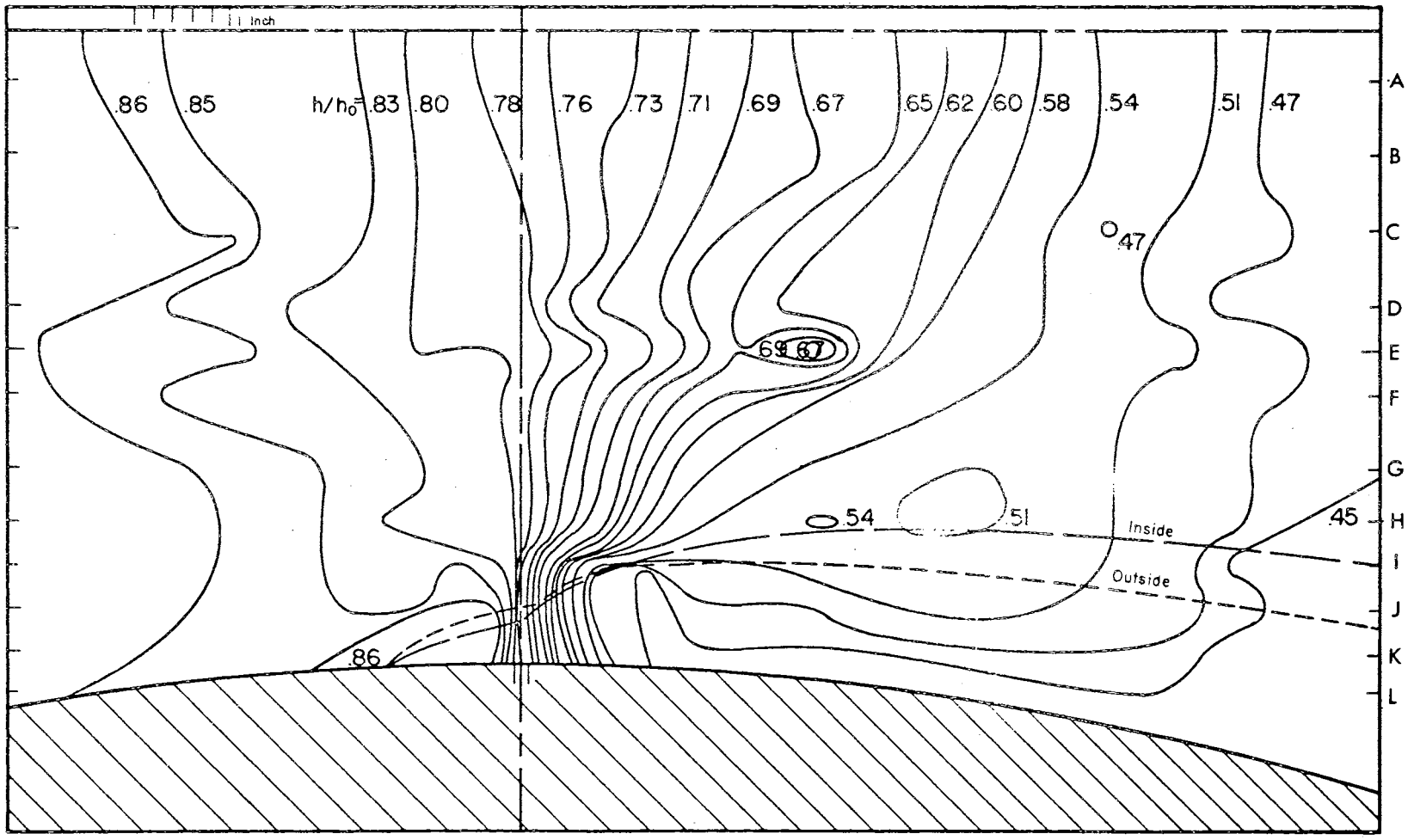

Figure 30. Isogrametric Depth Lines for Secondary to Main Stream Head Ratio of 1.75; Injection at Geometric Throat.

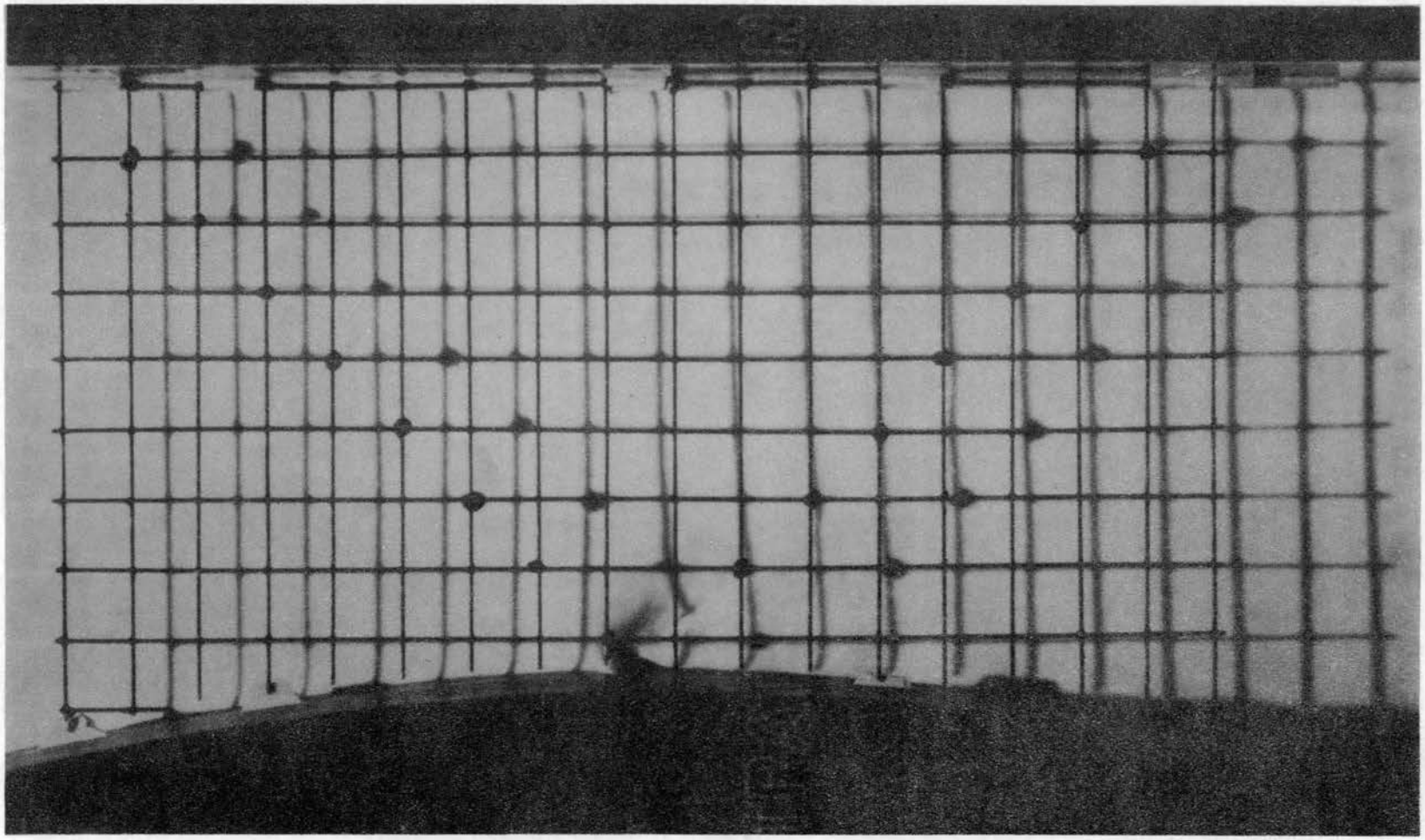

Figure 31. Shadow Pattern for Secondary to Main Stream Head Ratio of 1.75; Injection at Geometric Throat.

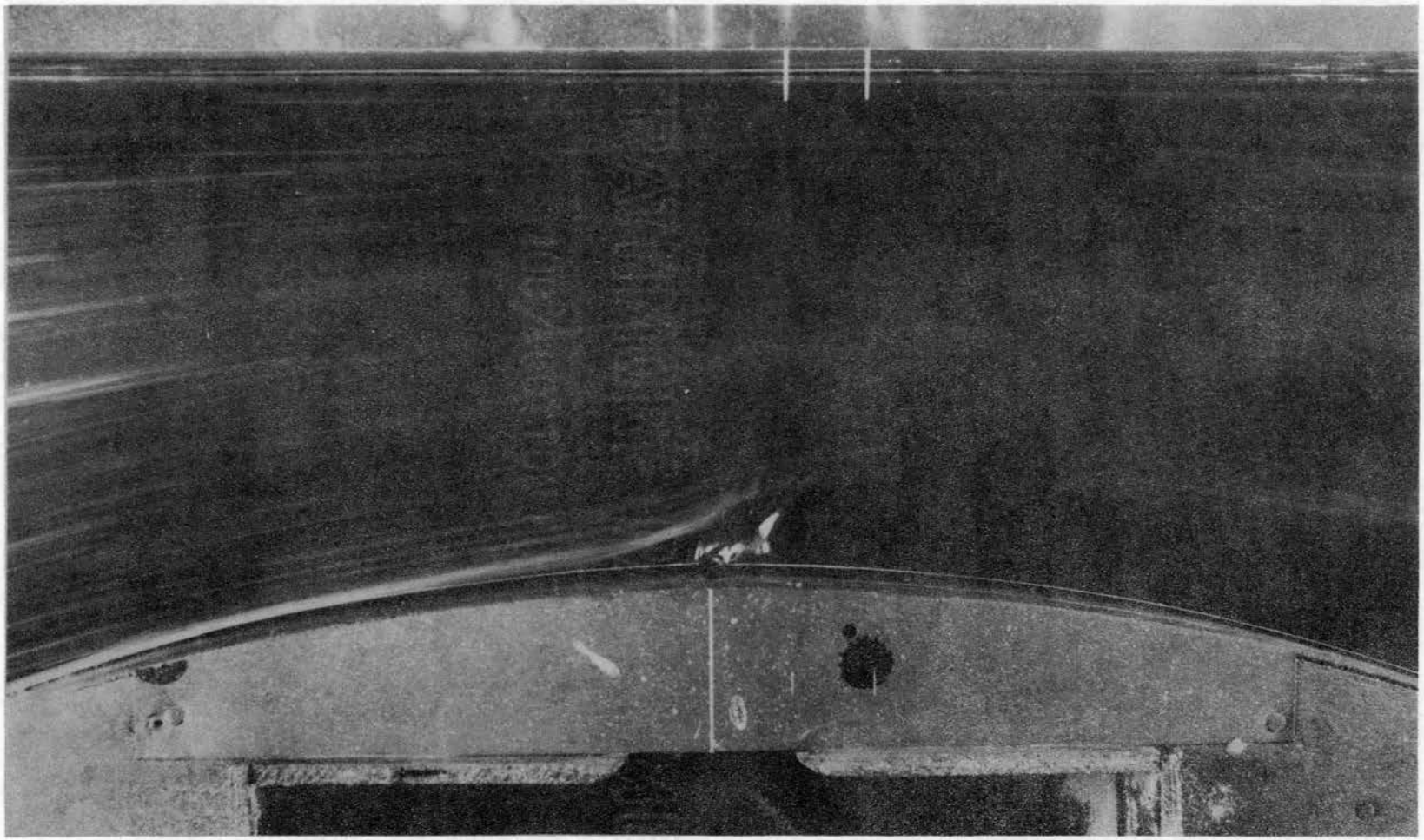

Figure 32. Typical Streak Lines for Secondary to Main Stream Head Ratio of 1.75; Injection at Geometric Throat.

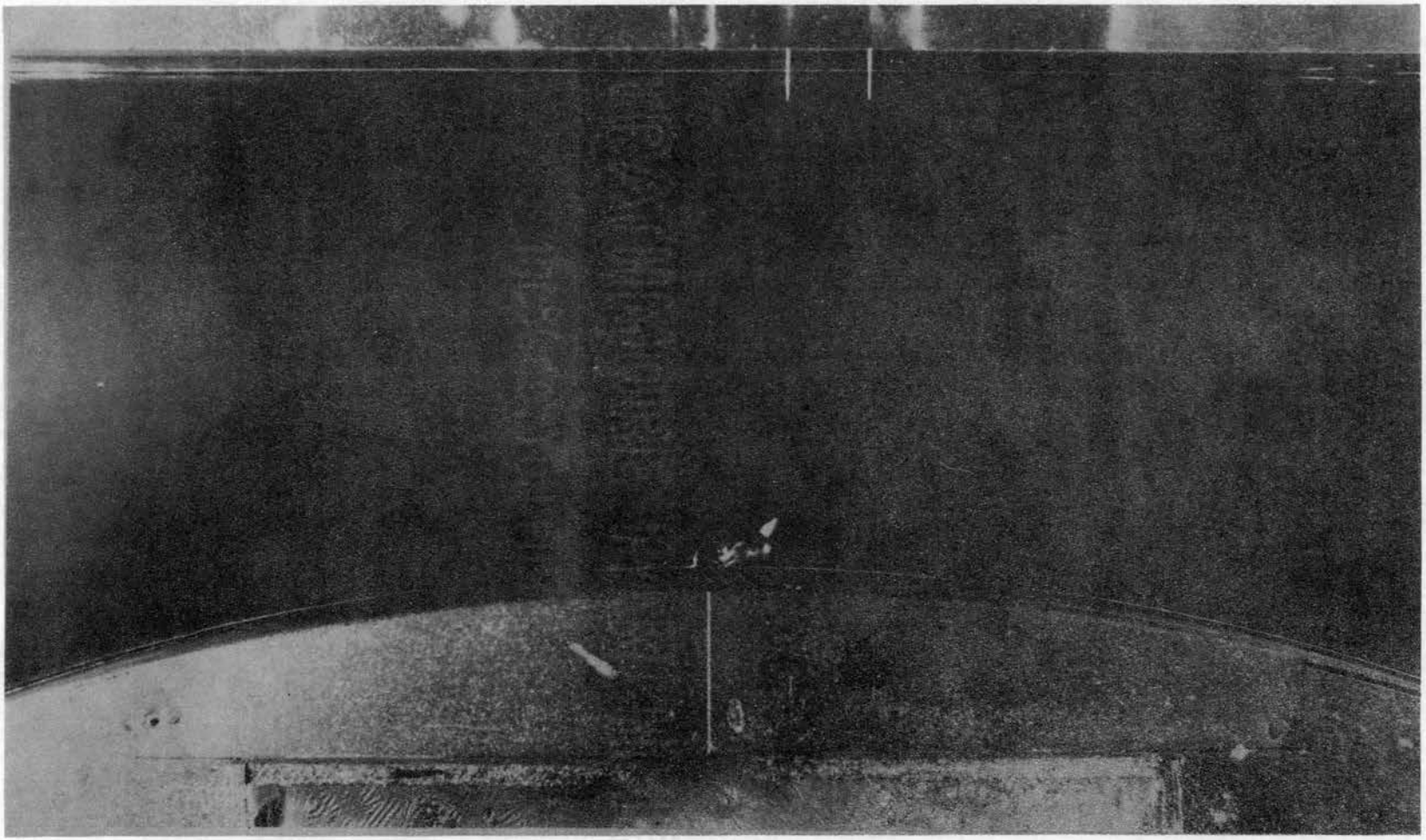

Figure 33. Typical Streak Lines for Secondary to Main Stream Head Ratio of 1.75; Injection at Geometric Throat.

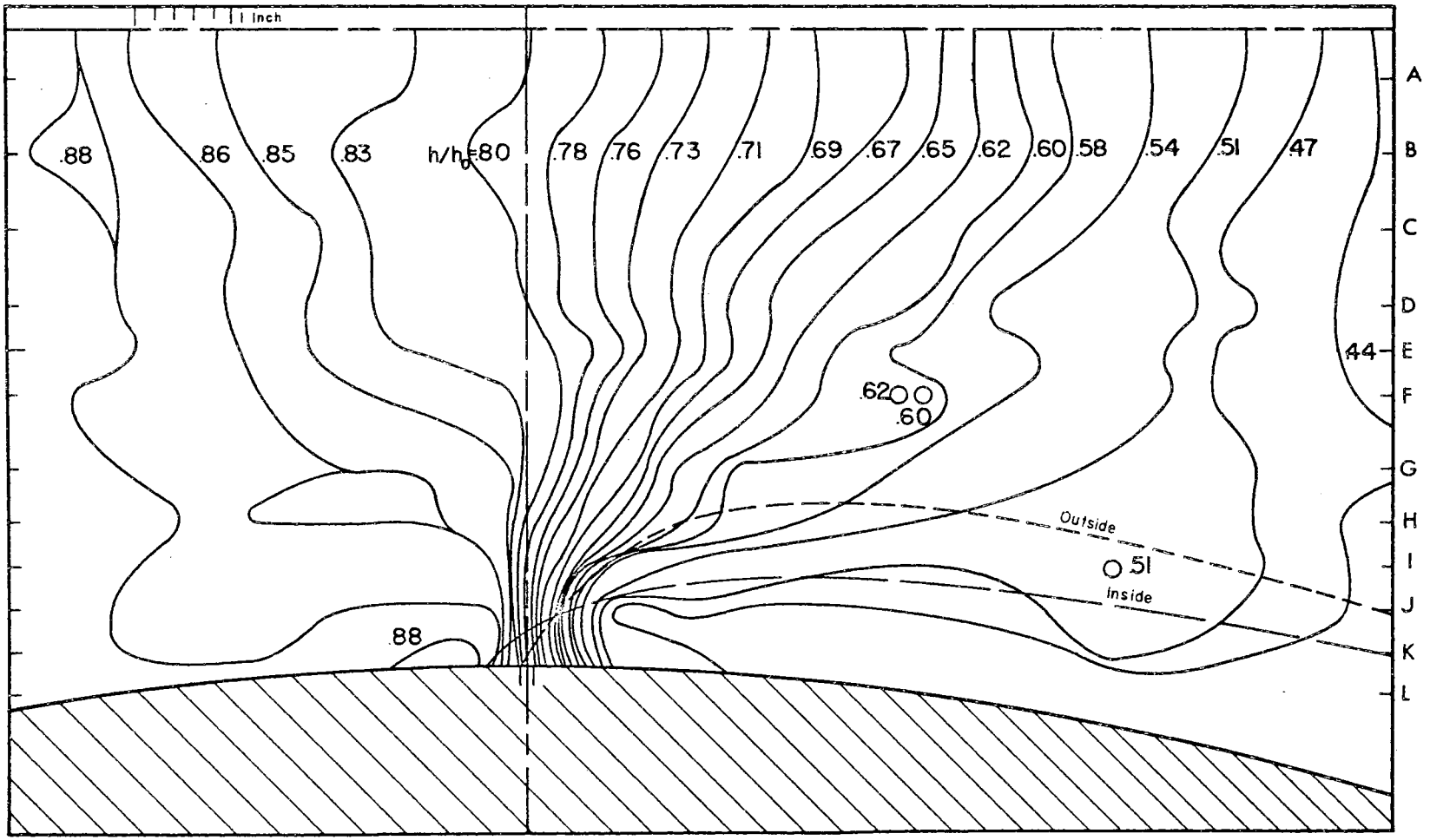

Figure 34. Isogrametric Depth Lines for Secondary to Main Stream Head Ratio of 2.00; Injection at Geometric Throat.

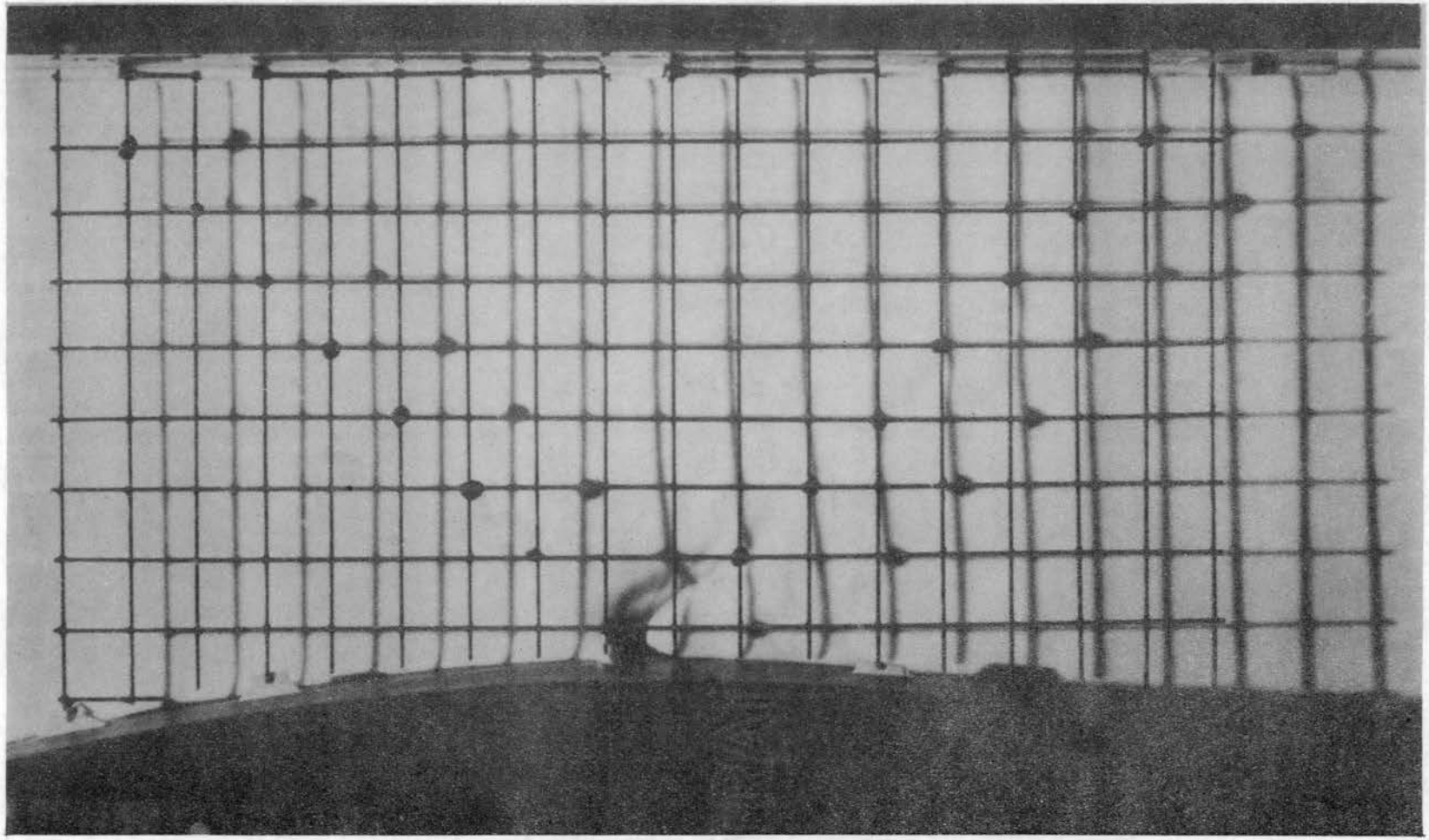

Figure 35. Shadow Pattern for Secondary to Main Stream Head Ratio of 2.00; Injection at Geometric Throat.

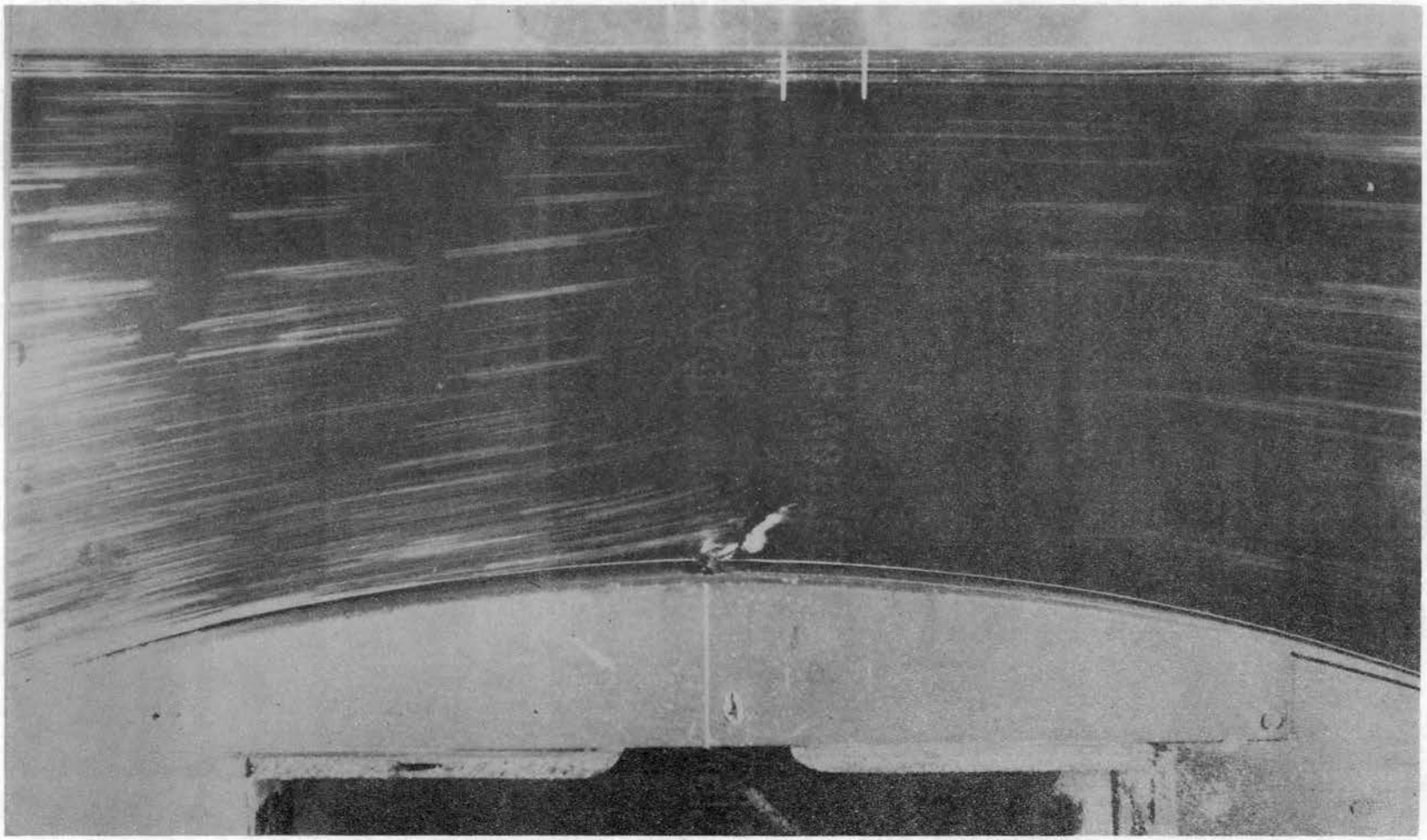

Figure 36. Typical Streak Lines for Secondary to Main Stream Head Ratio of 2.00; Injection at Geometric Throat.

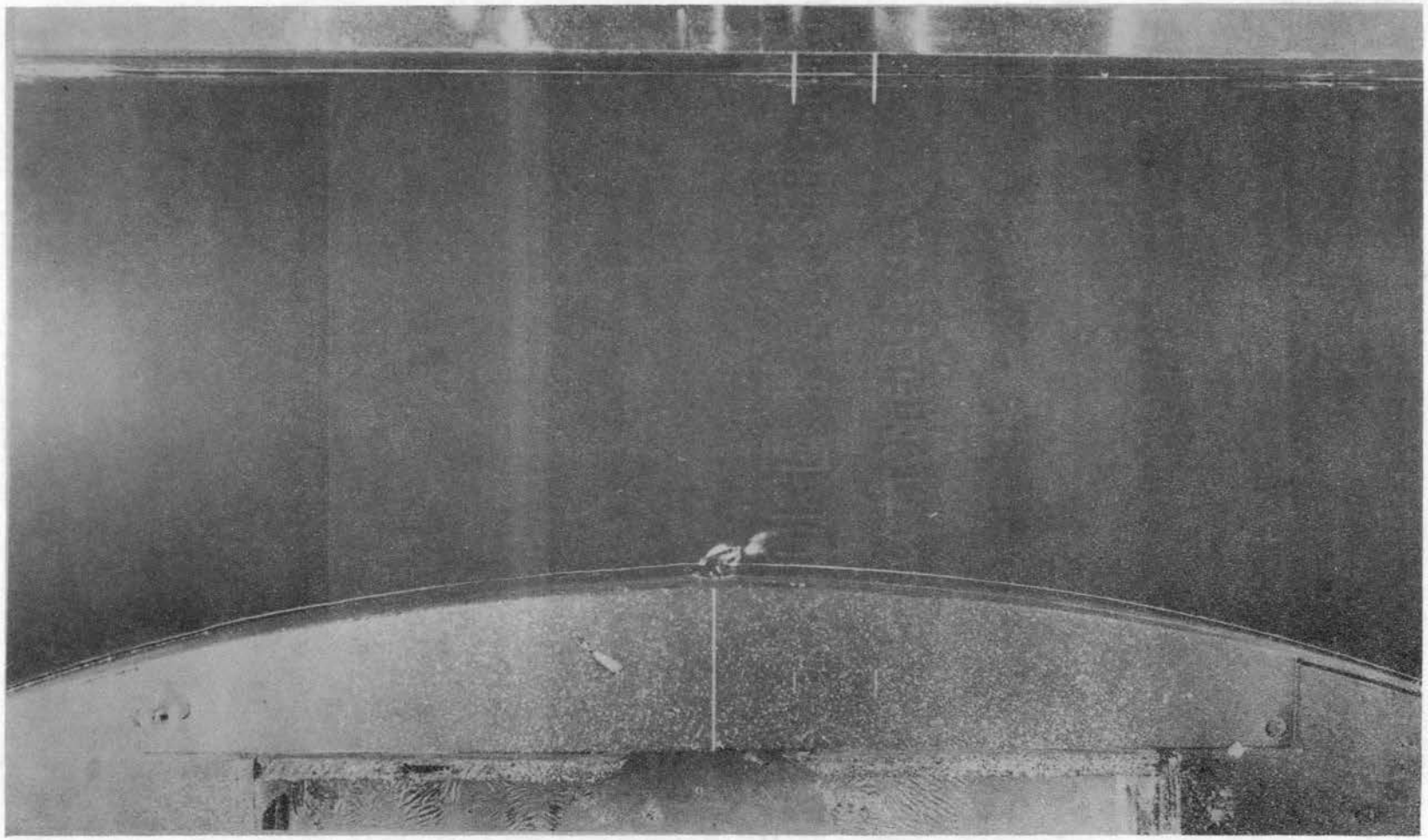

Figure 37. Typical Streak Lines for Secondary to Main Stream Head Ratio of 2.00; Injection at Geometric Throat.

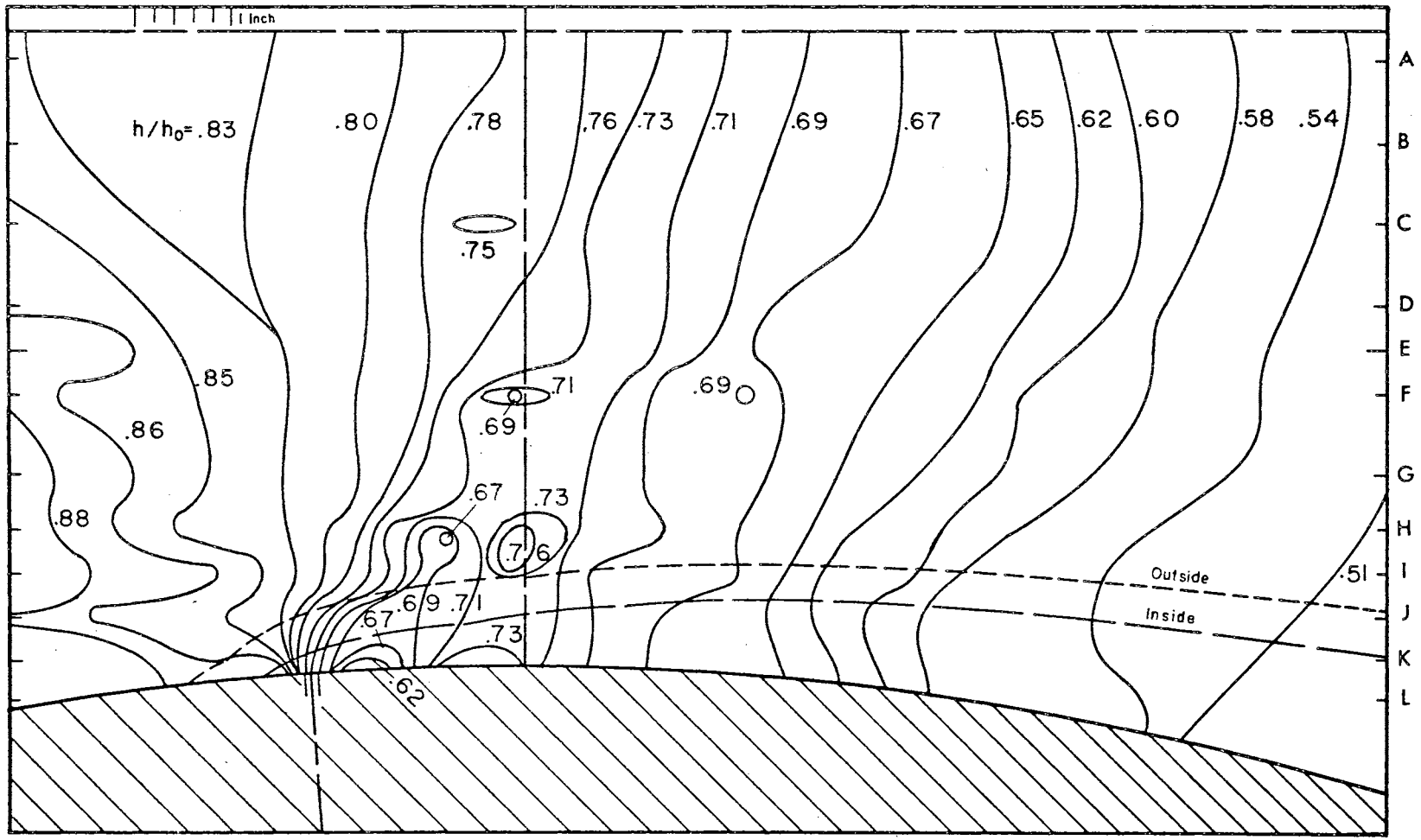

Figure 38. Isogrametric Depth Lines for Secondary to Main Stream Head Ratio of 1.00; Injection at 4° Upstream of Geometric Throat.

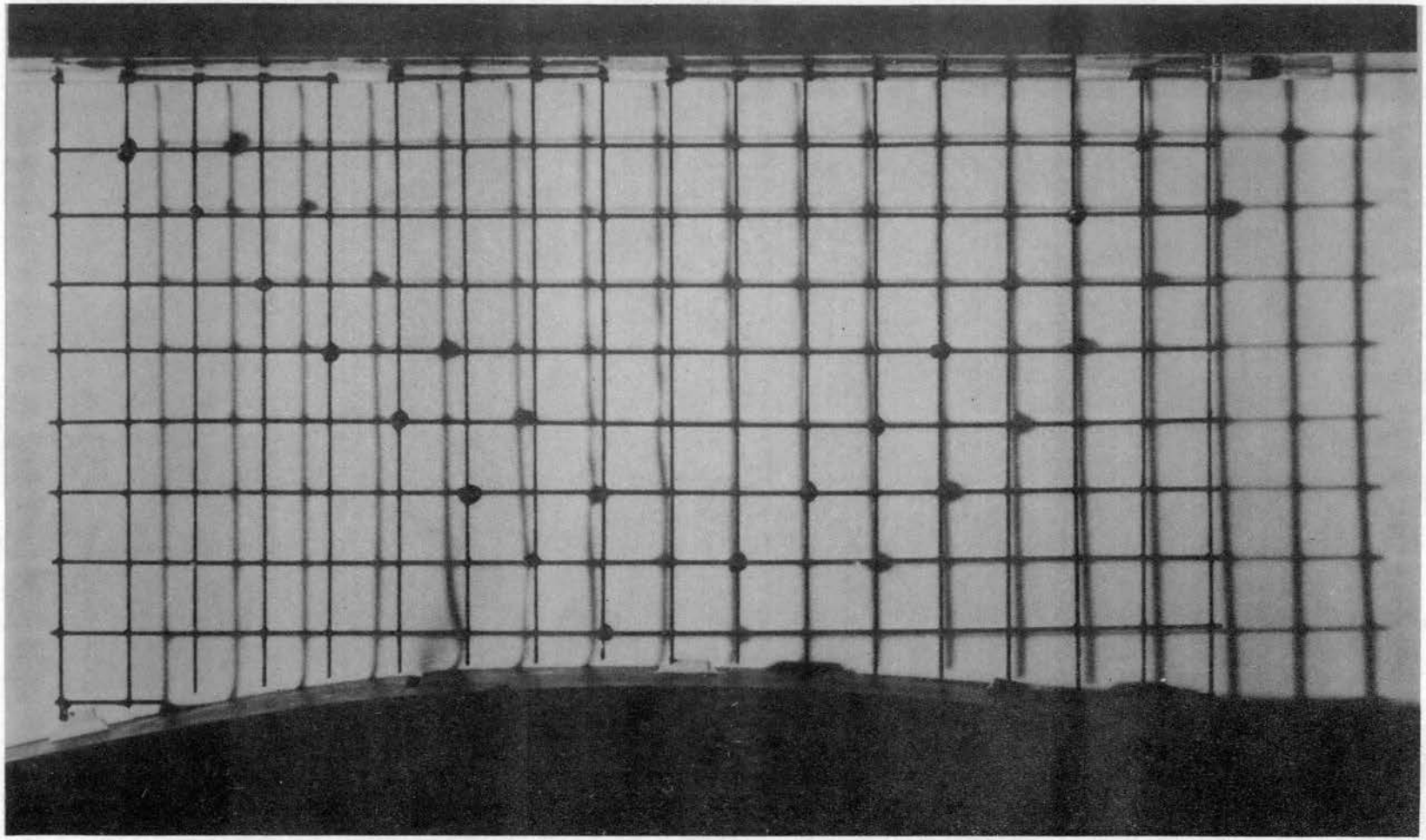

Figure 39. Shadow Pattern for Secondary to Main Stream Head Ratio of 1.00; Injection at 4^{0} Upstream of Geometric Throat.

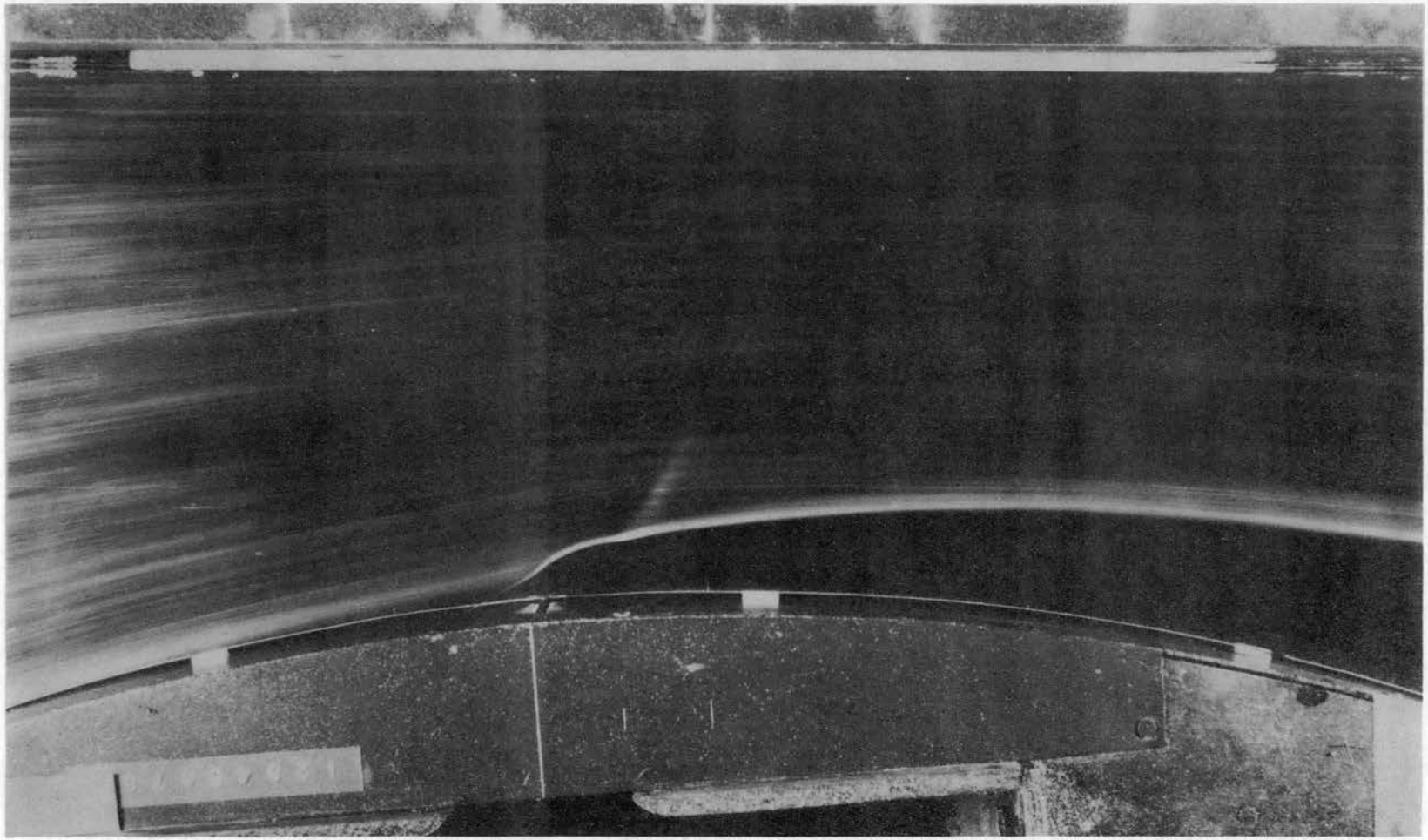

Figure 40. Typical Streak Lines for Secondary to Main Stream Head Ratio of 1.00; Injection at 4° Upstream of Geometric Throat.

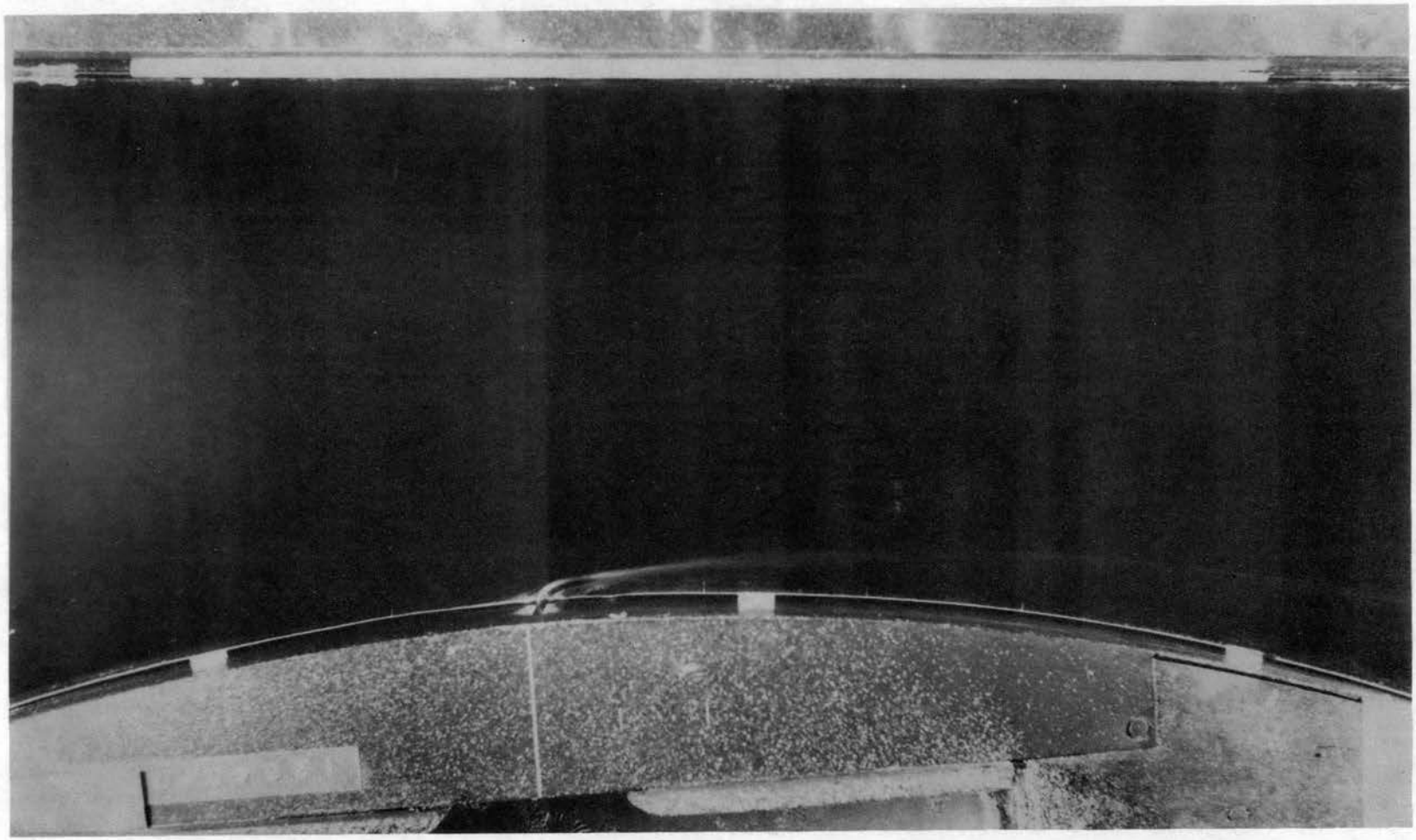

Figure 41. Typical Streak Lines for Secondary to Main Stream Head Ratio of 1.00; Injection at 4° Upstream of Geometric Throat.

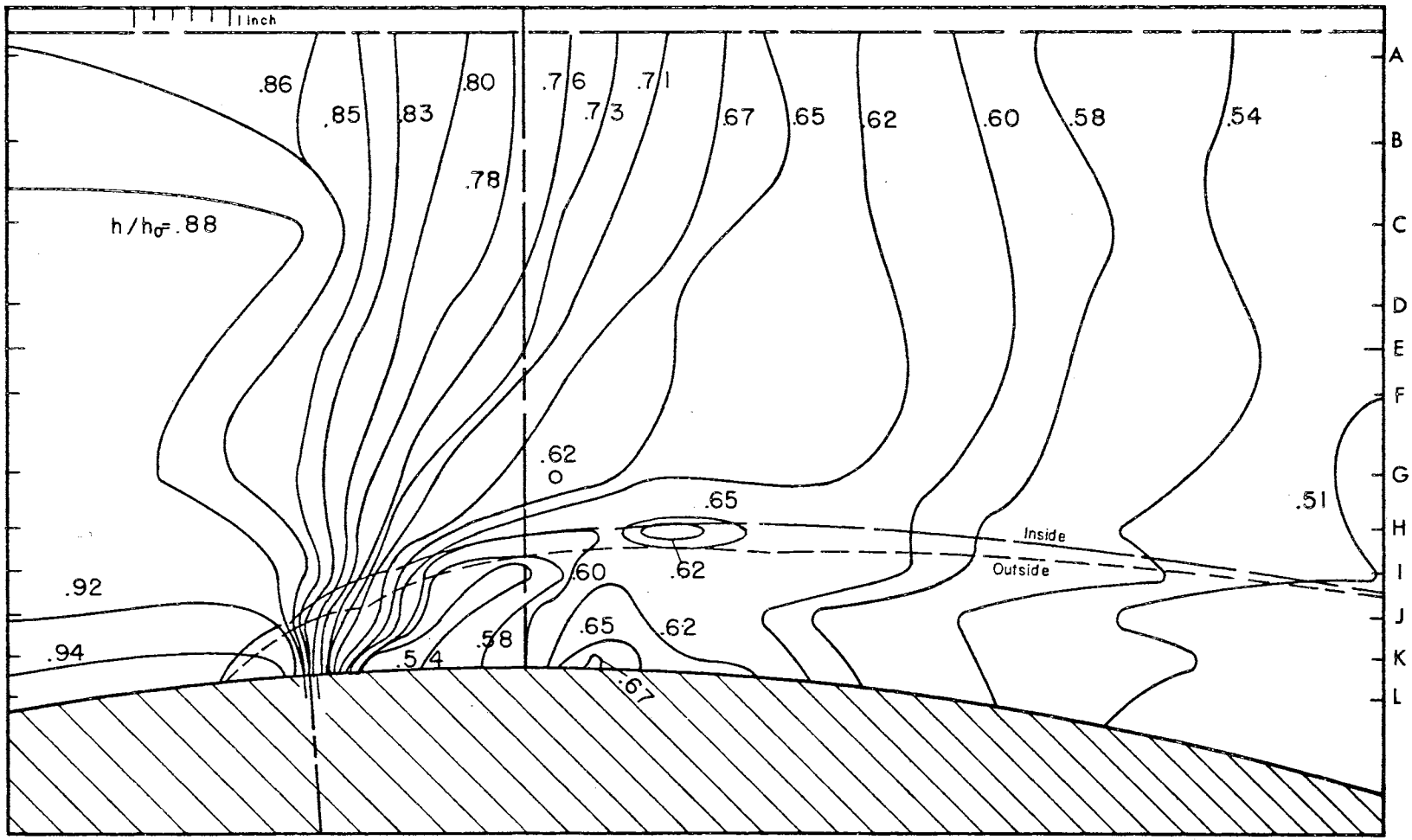

Figure 42. Isogrametric Depth Lines for Secondary to Main Stream Head Ratio of 1.50; Injection at 4° Upstream of Geometric Throat.

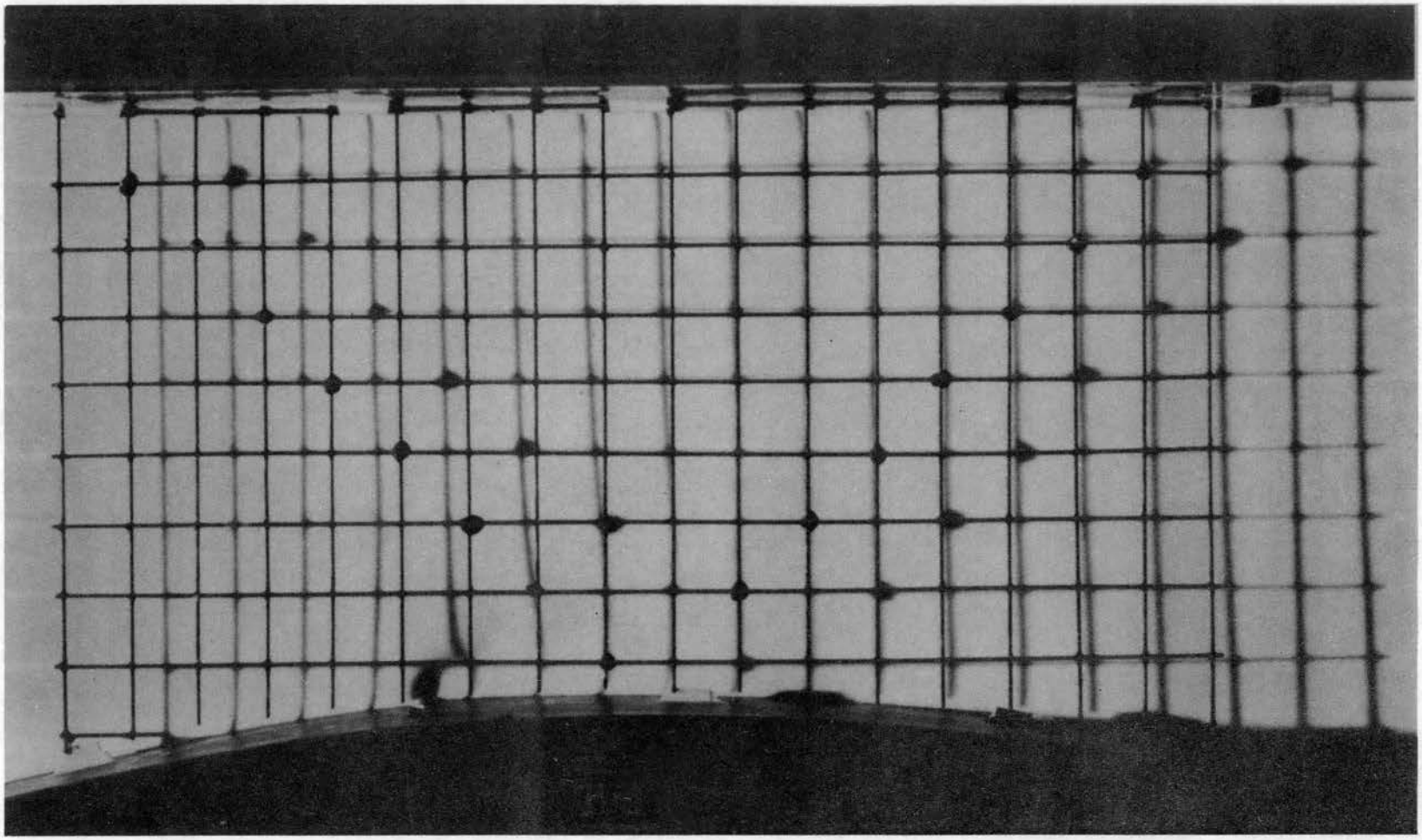

Figure 43. Shadow Pattern for Secondary to Main Stream Head Ratio of 1.50; Injection at 4° Upstream of Geometric Throat.

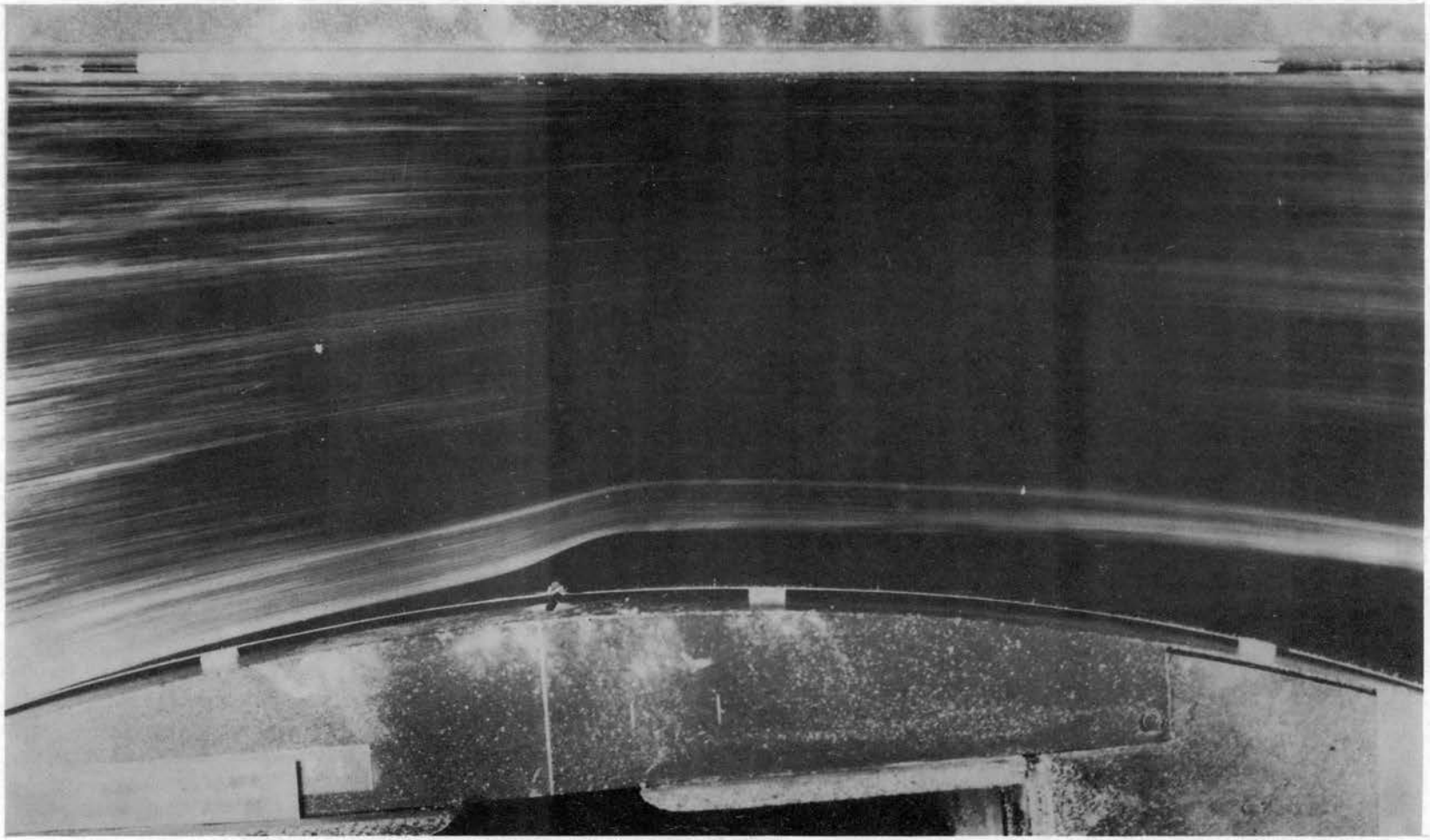

Figure 44. Typical Streak Lines for Secondary to Main Stream Head Ratio of 1.50; Injection at 4° Upstream of Geometric Throat.

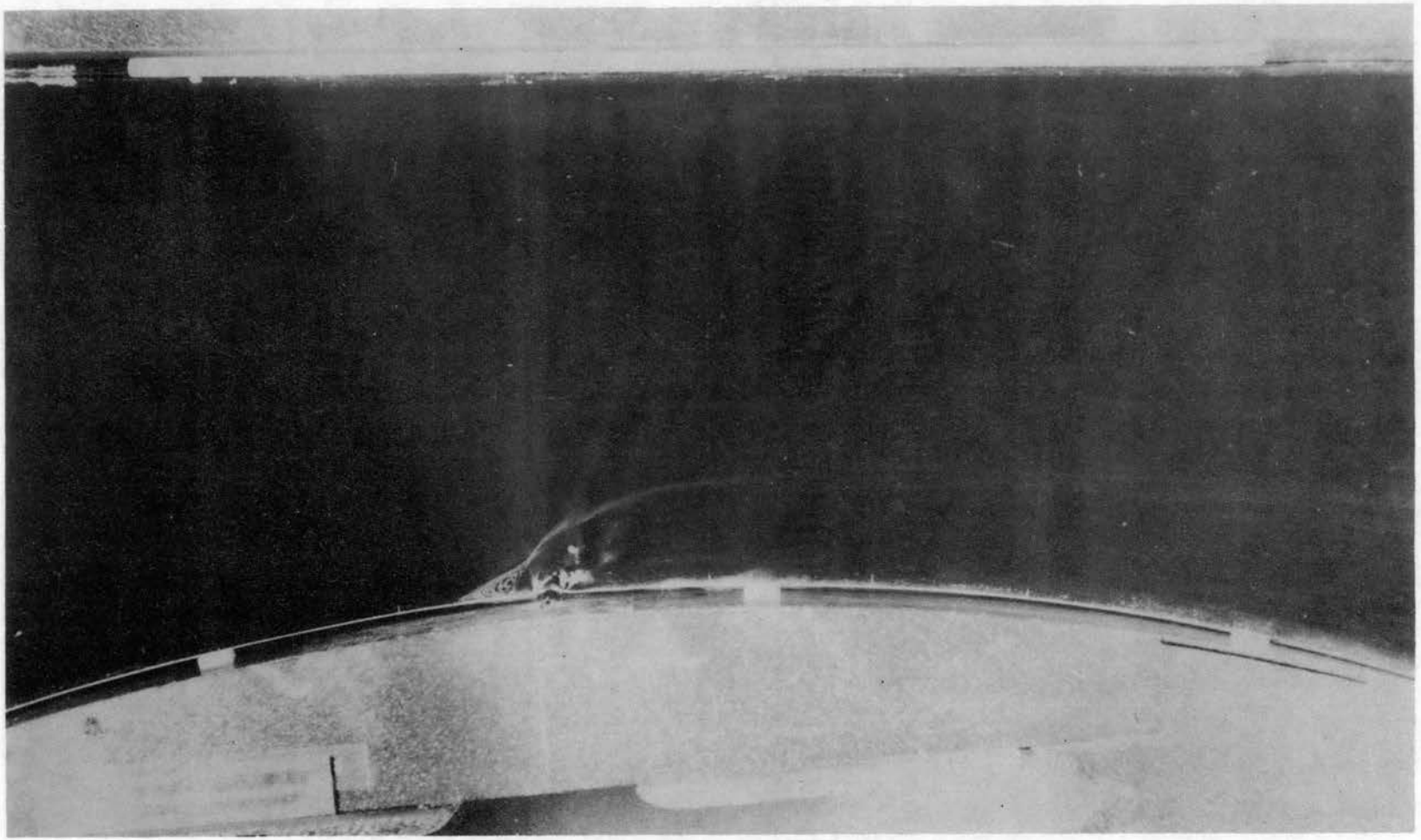

Figure 45. Typical Streak Lines for Secondary to Main Stream Head Ratio of 1.50; Injection at 4^{0} Upstream of Geometric Throat.

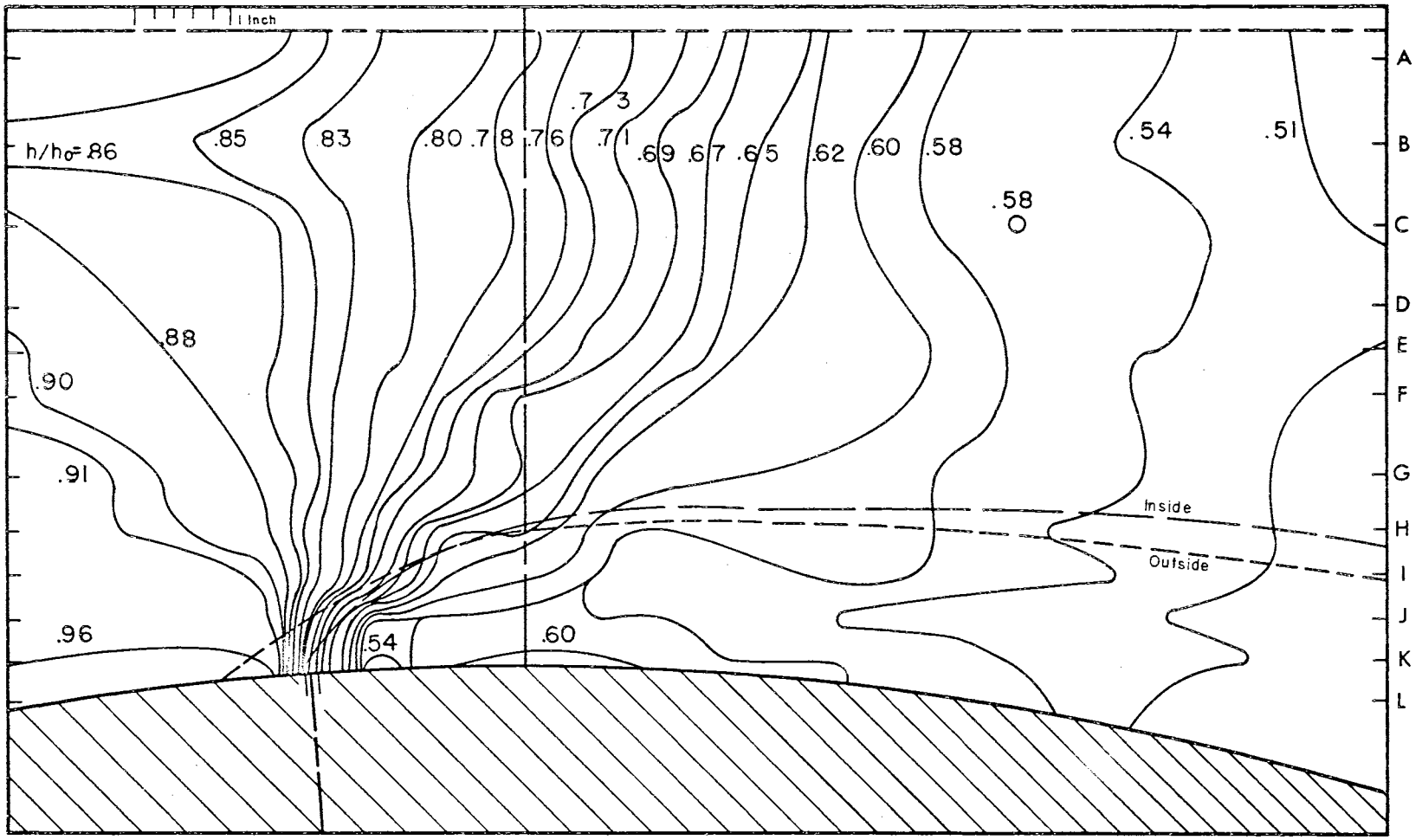

Figure 46. Isogrametric Depth Lines for Secondary to Main Stream Head Ratio of 1.75; Injection at 4° Upstream of Geometric Throat.

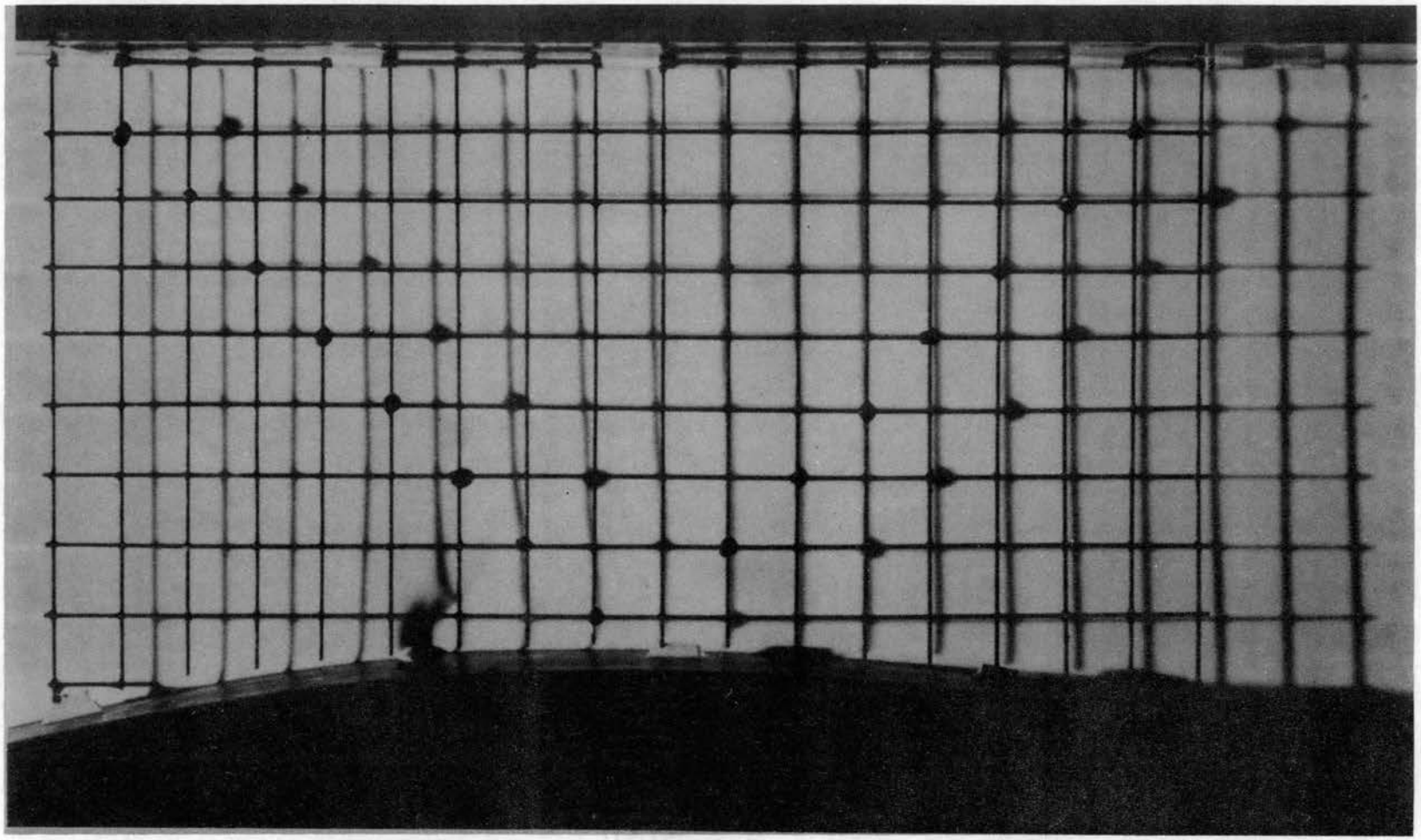

Figure 47. Shadow Pattern for Secondary to Main Stream Head Ratio of 1.75; Injection at 4° Upstream of Geometric Throat.

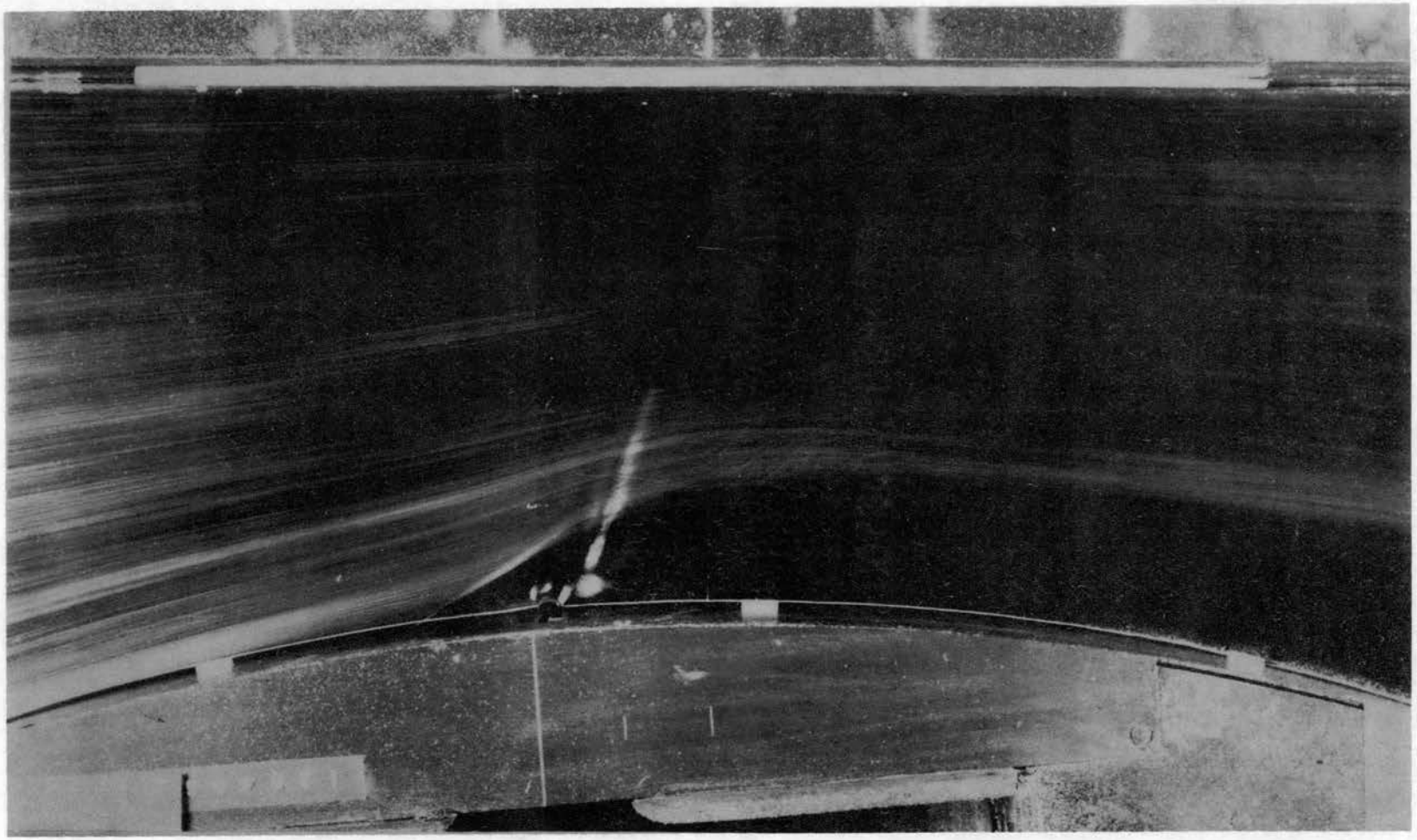

Figure 48. Typical Streak Lines for Secondary to Main Stream Head Ratio of 1.75; Injection at 4° Upstream of Geometric Throat.

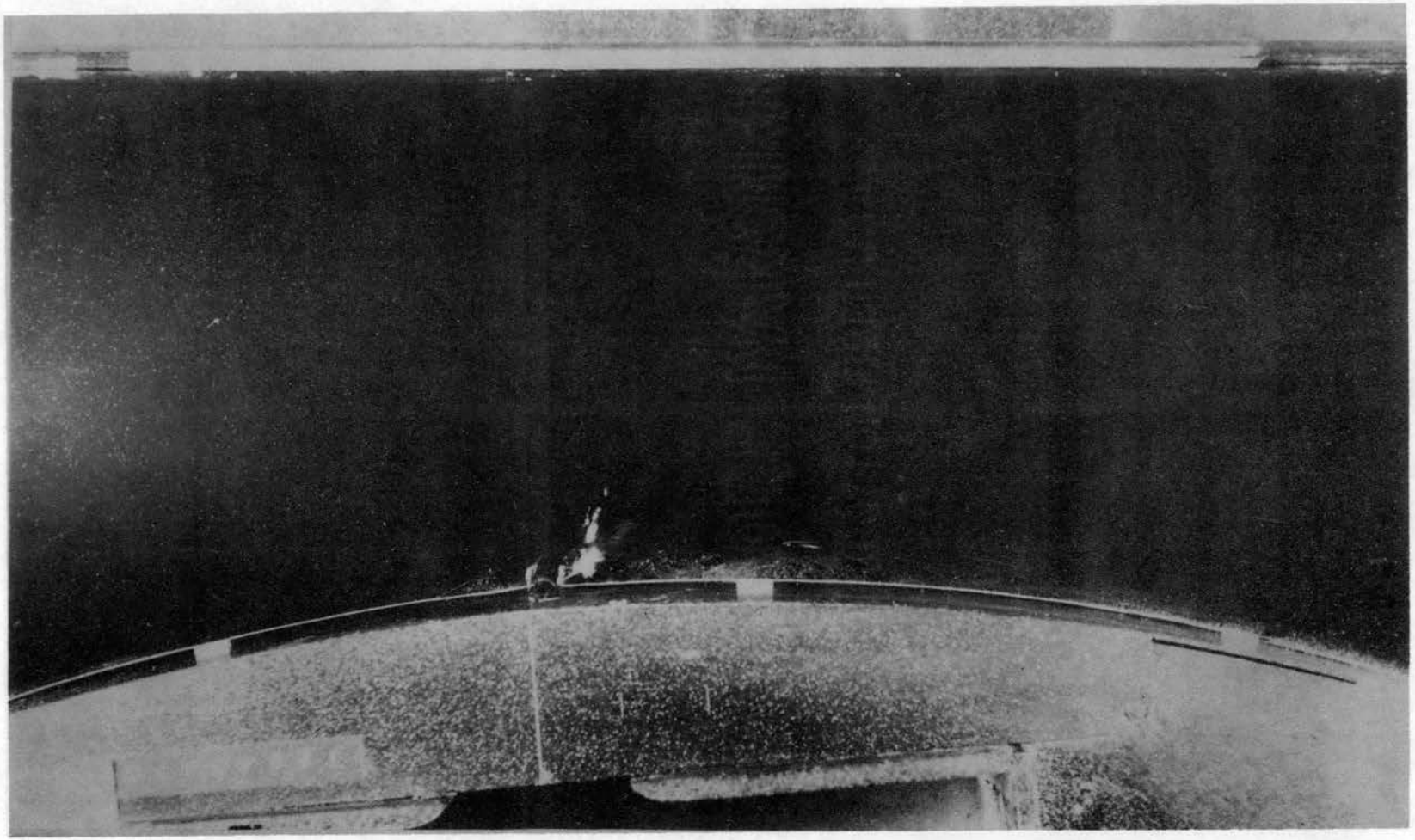

Figure 49. Typical Streak Lines for Secondary to Main Stream Head Ratio of 1.75; Injection at 4^{0} Upstream of Geometric Throat.

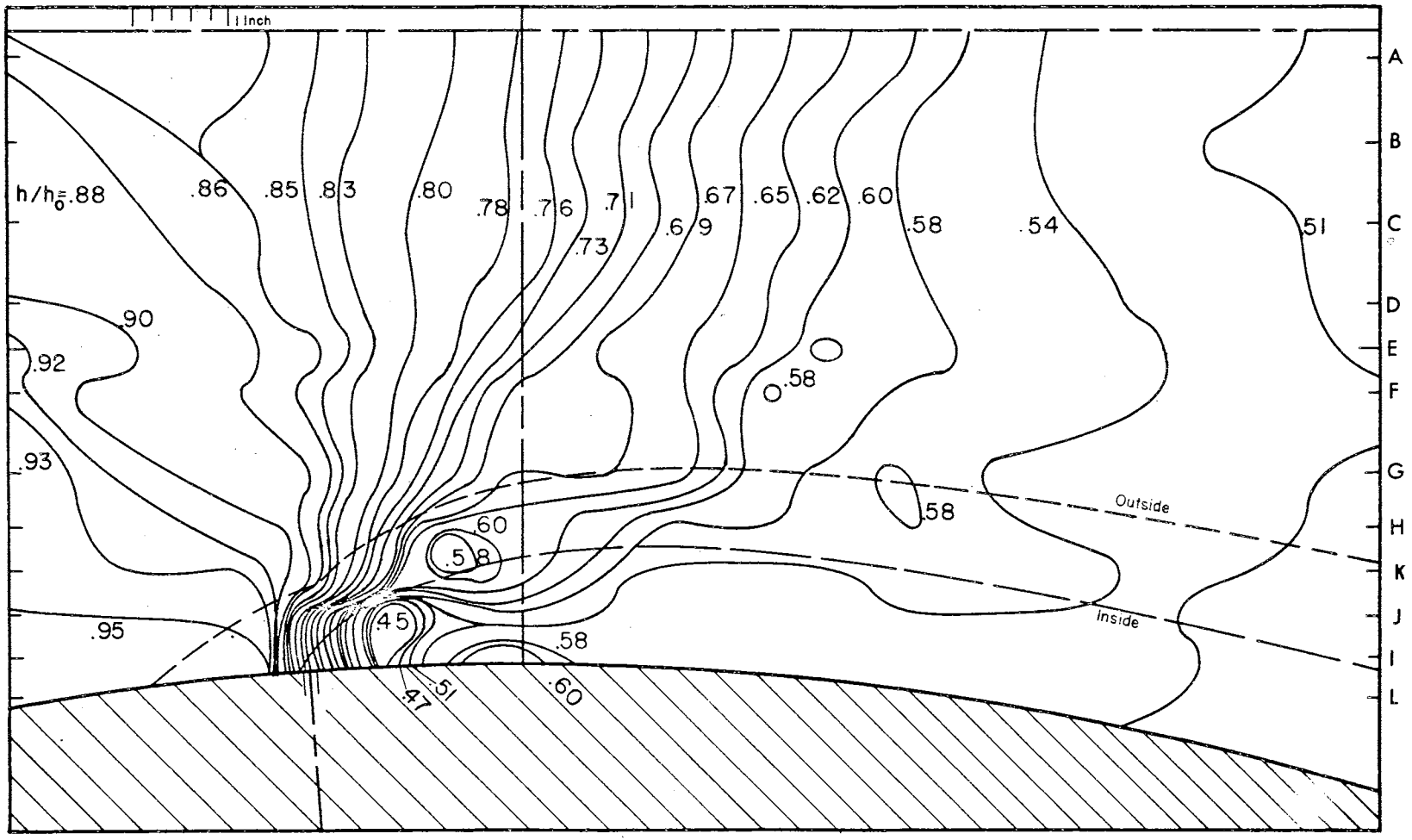

Figure 50. Isogrametric Depth Lines for Secondary to Main Stream Head Ratio of 2.00; Injection at 4° Upstream of Geometric Throat.

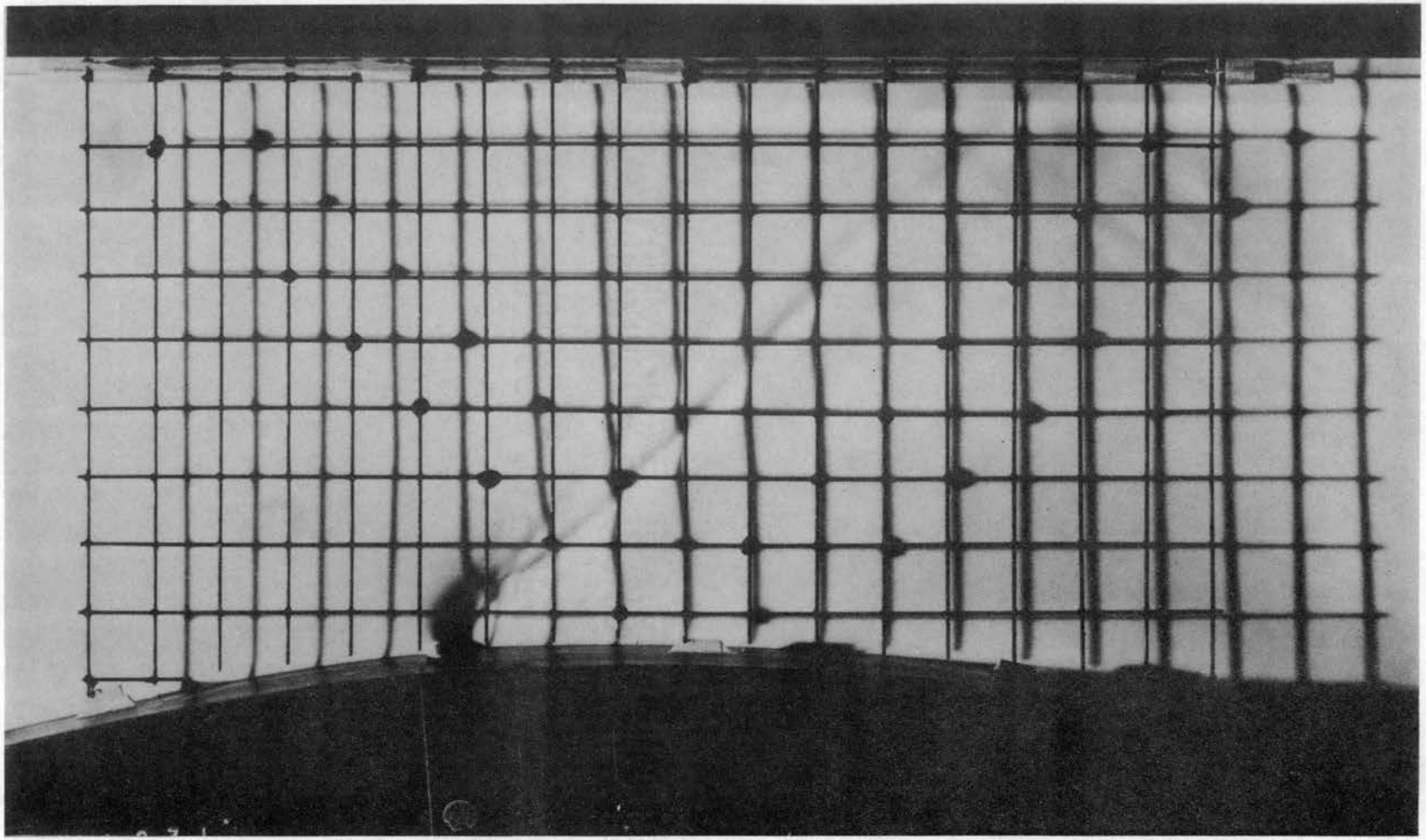

Figure 51. Shadow Pattern for Secondary to Main Stream Head Ratio of 2.00; Injection at 4° Upstream of Geometric Throat.

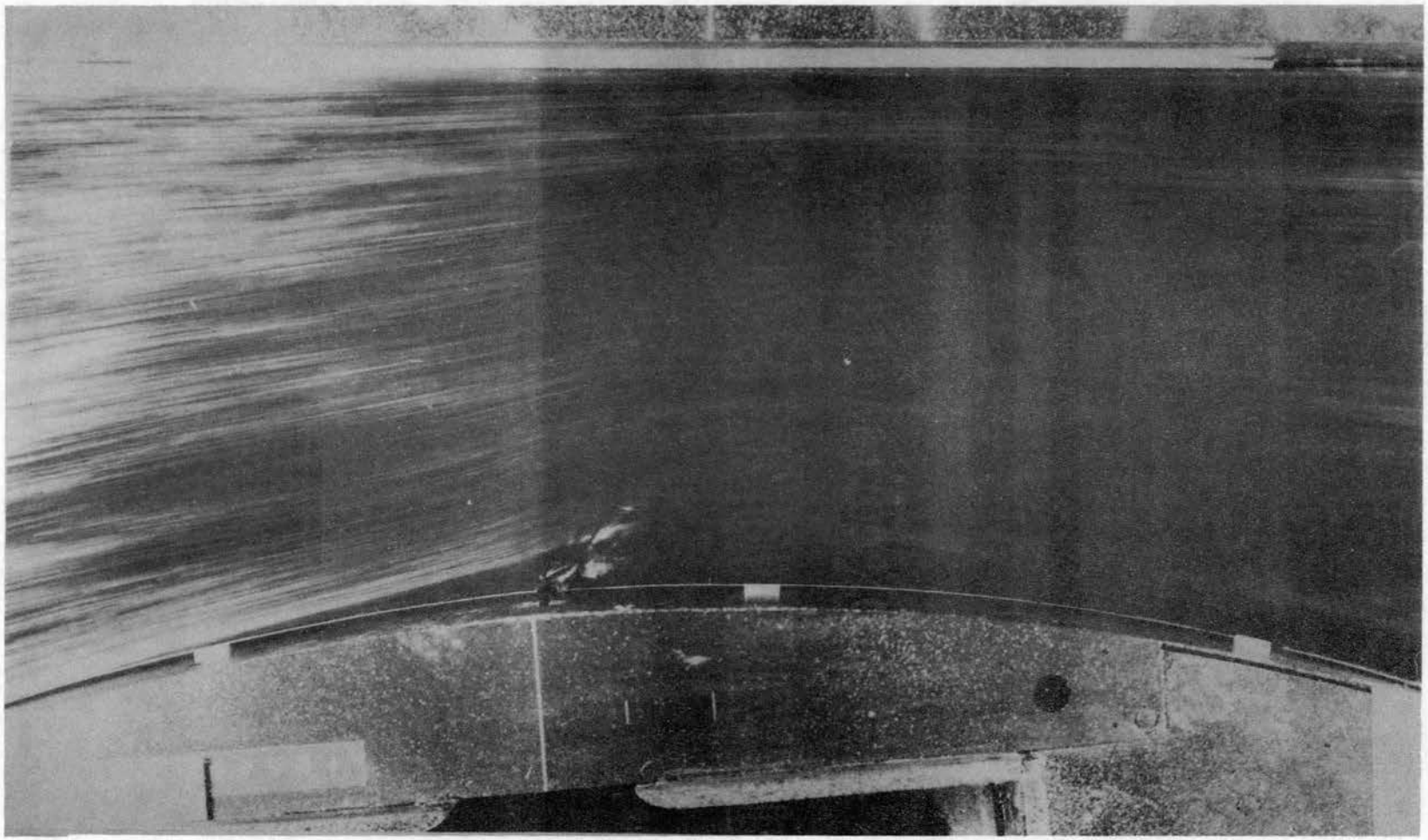

Figure 52. Typical Streak Lines for Secondary to Main Stream Head Ratio of 2.00; Injection at 4° Upstream of Geometric Throat.

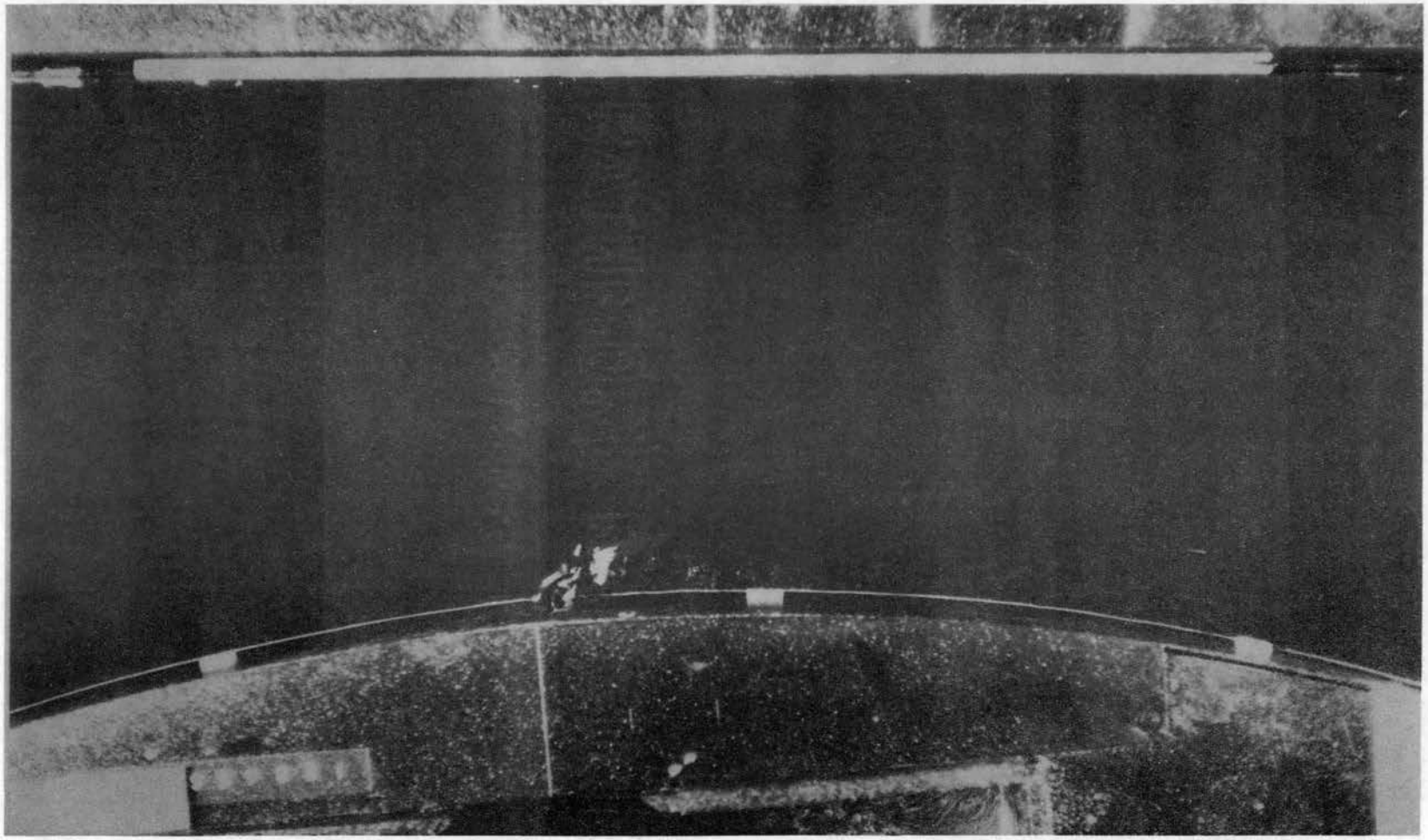

Figure 53. Typical Streak Lines for Secondary to Main Stream Head Ratio of 2.00; Injection at 4^{0} Upstream of Geometric Throat.

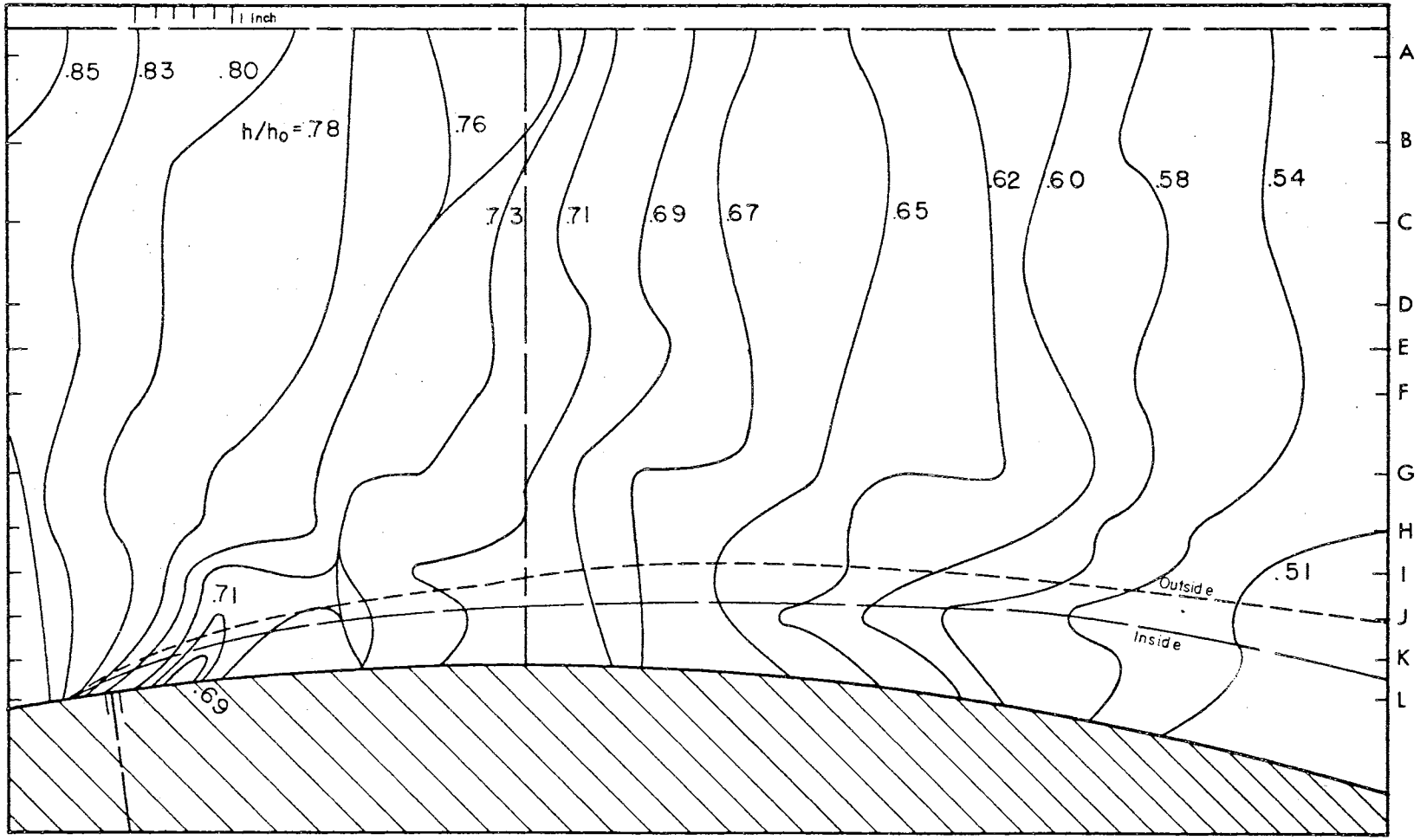

Figure 54. Isogrametric Depth Lines for Secondary to Main Stream Head Ratio of 1.00; Injection at 8° Upstream of Geometric Throat.

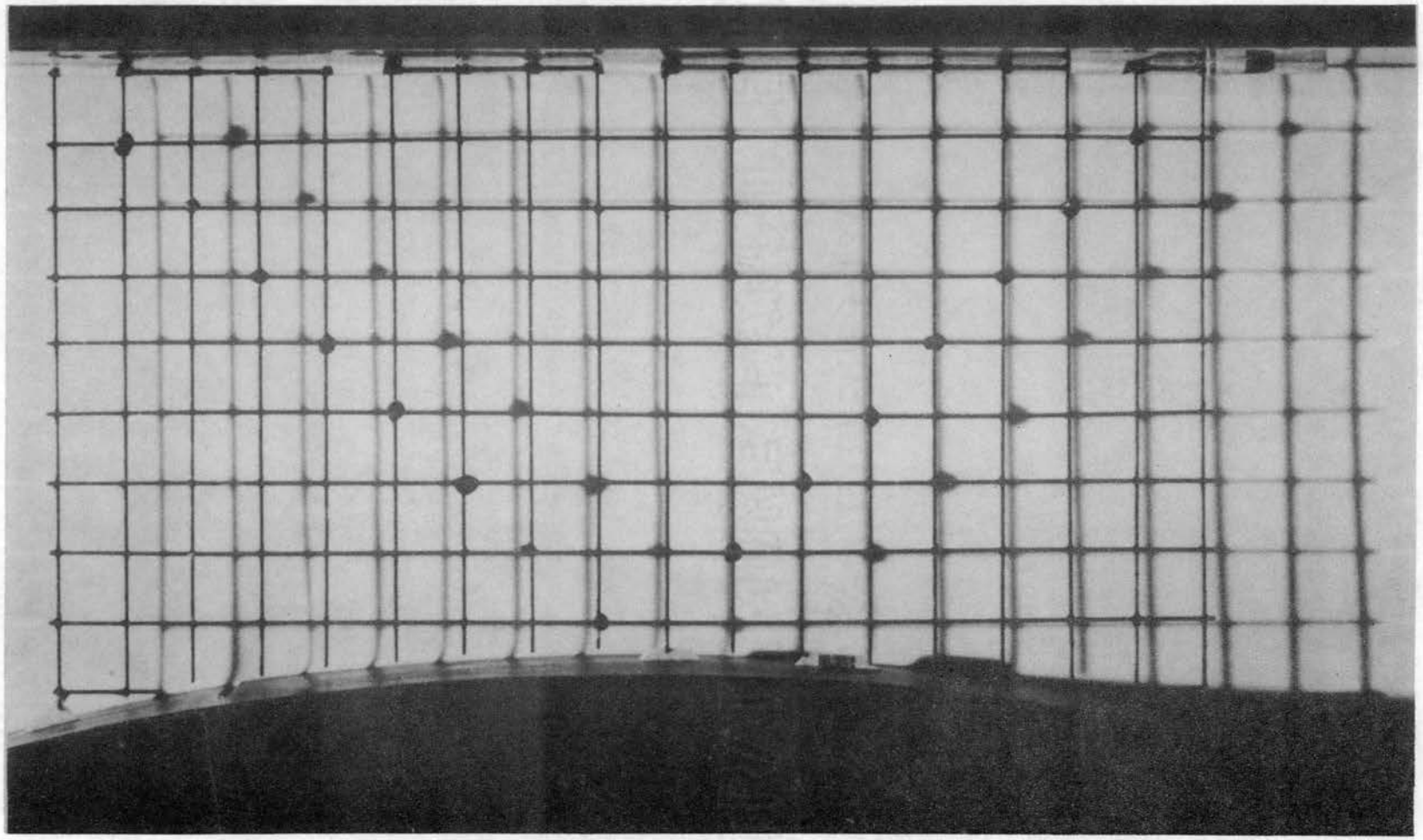

Figure 55. Shadow Pattern for Secondary to Main Stream Head Ratio of 1.00; Injection at 8° Upstream of Geometric Throat.

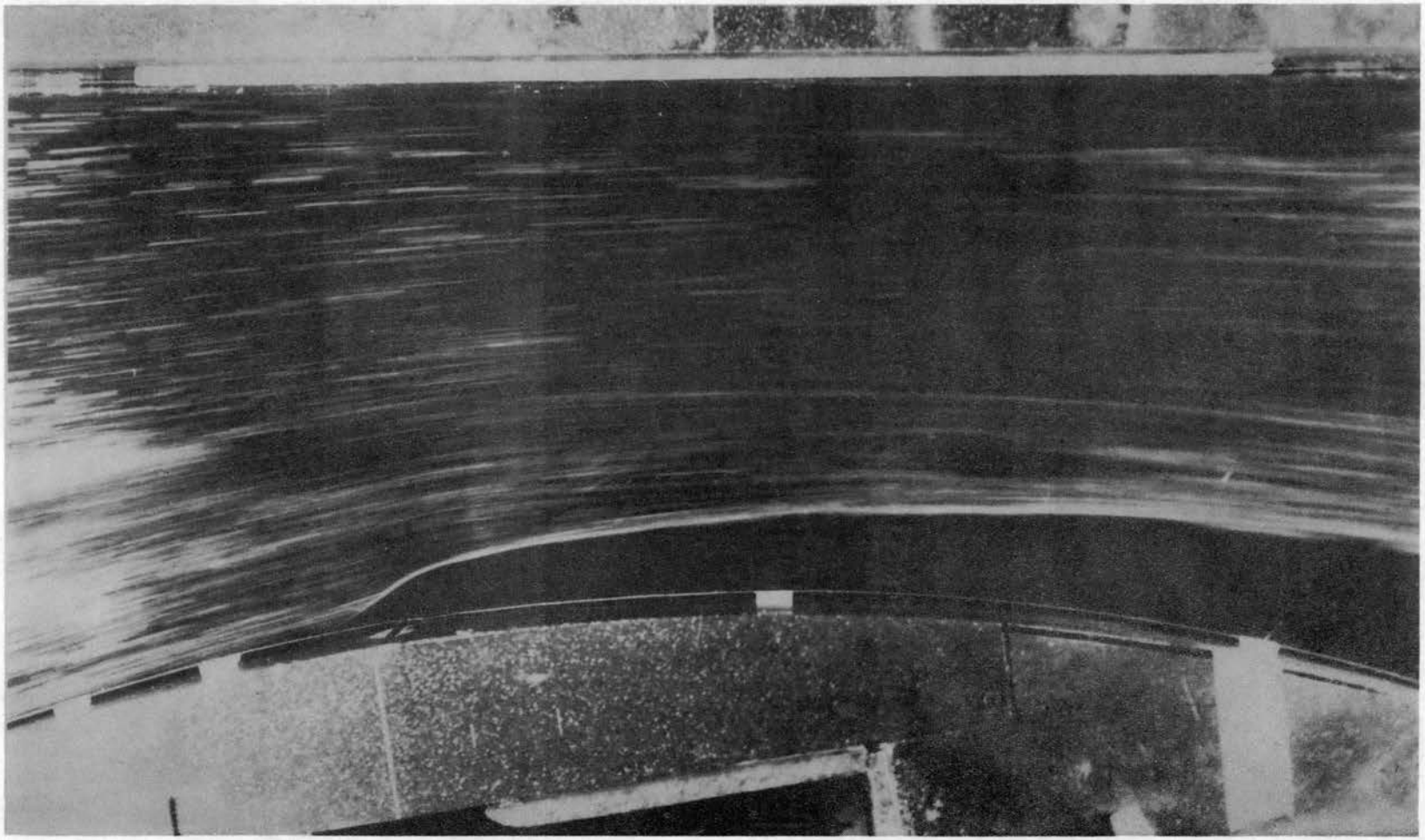

Figure 56. Typical Streak Lines for Secondary to Main Stream Head Ratio of 1.00; Injection at 8° Upstream of Geometric Throat.

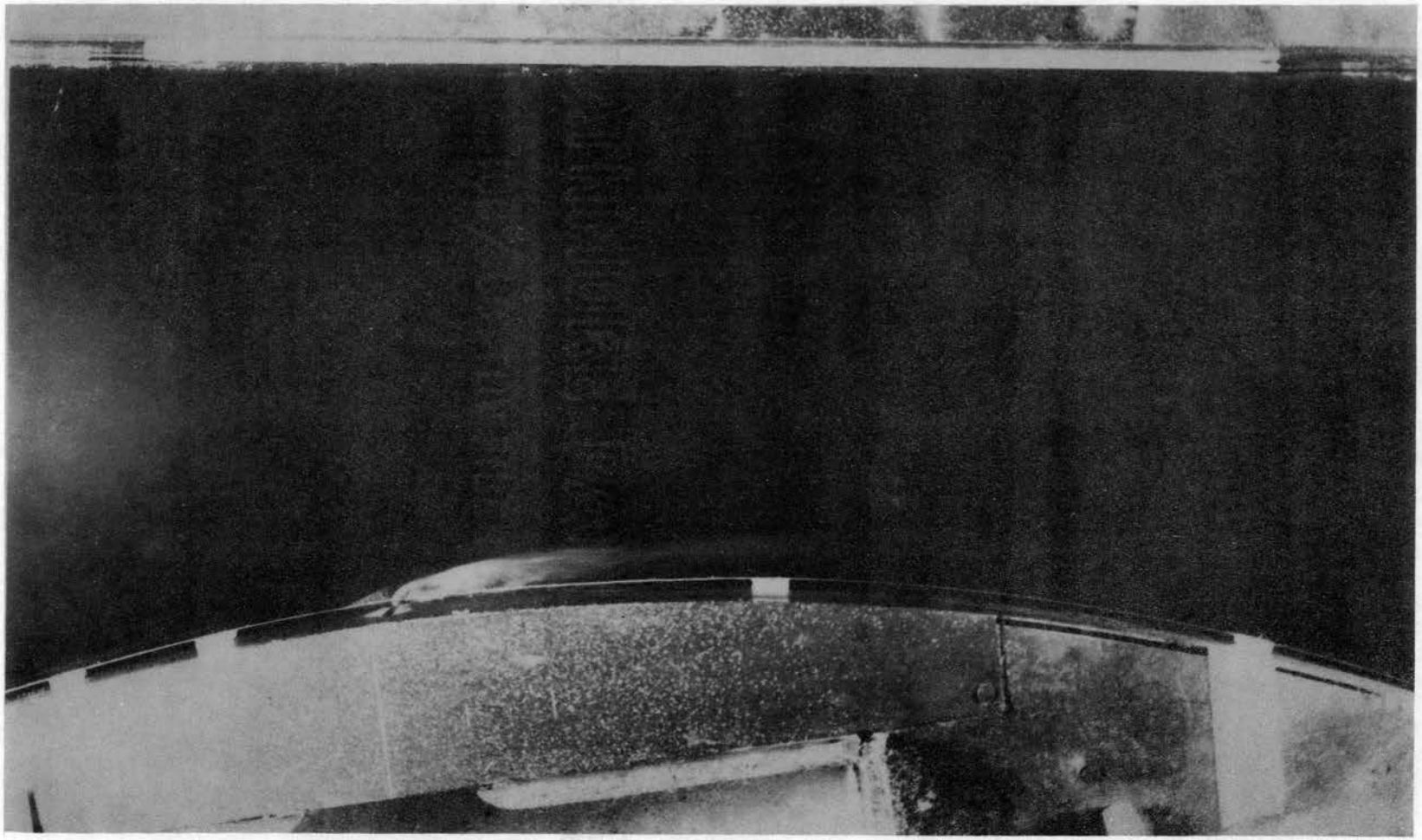

Figure 57. Typical Streak Lines for Secondary to Main Stream Head Ratio of 1.00; Injection at 8^{0} Upstream of Geometric Throat.

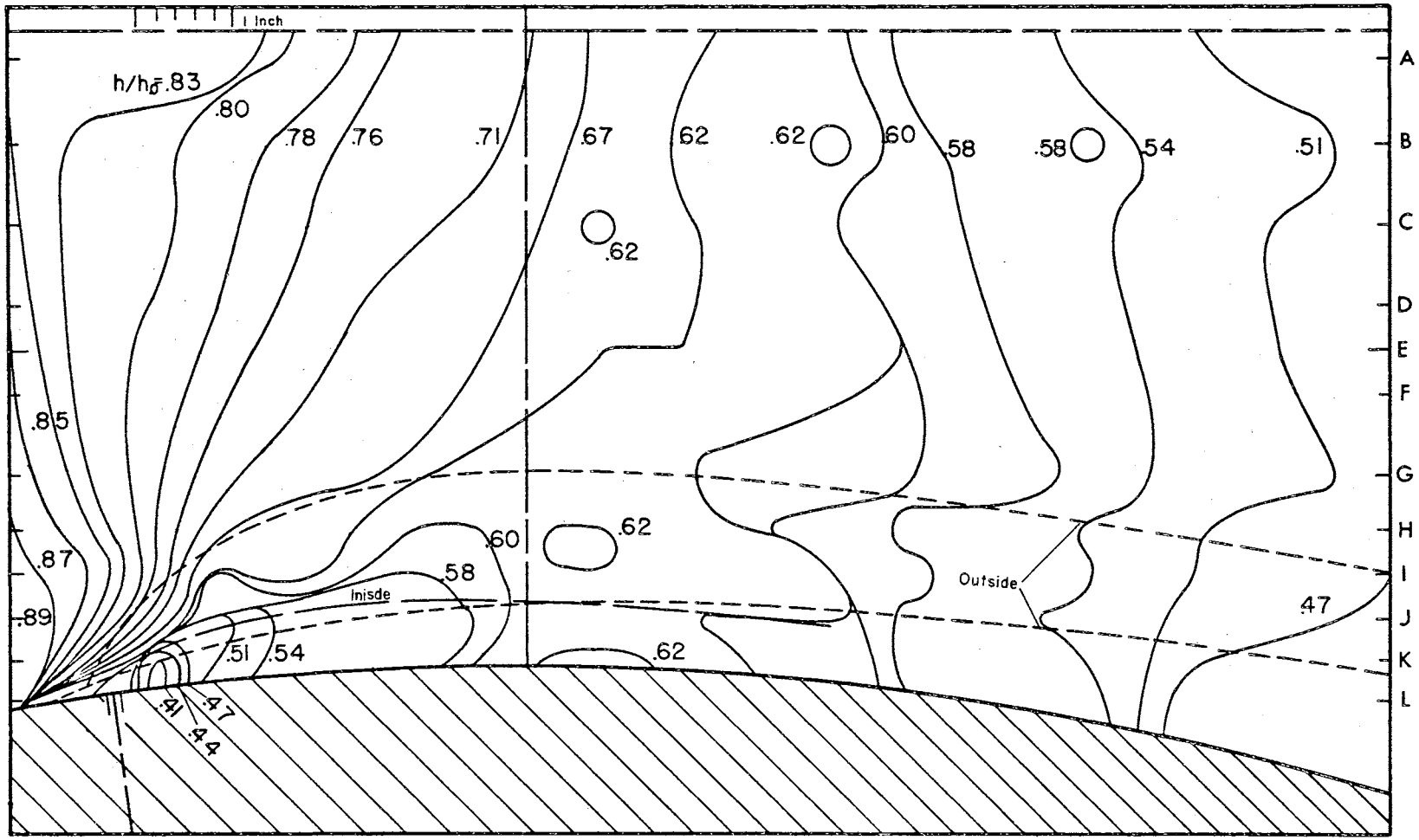

Figure 58. Isogrametric Depth Lines for Secondary to Main Stream Head Ratio of 2.00; Injection at 8^0 Upstream of Geometric Throat.

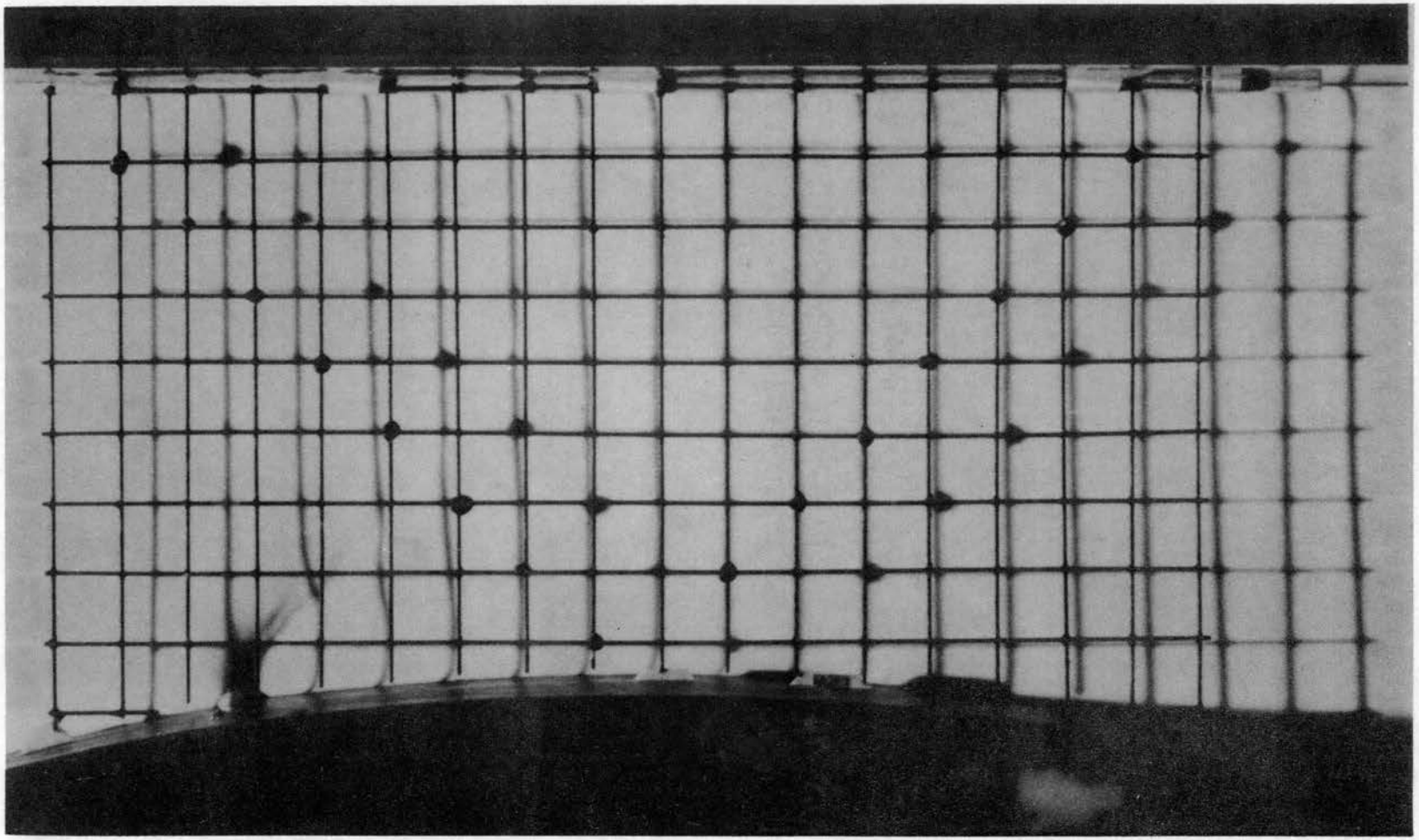

Figure 59. Shadow Pattern for Secondary to Main Stream Head Ratio of 2.00; Injection at 8° Upstream of Geometric Throat.

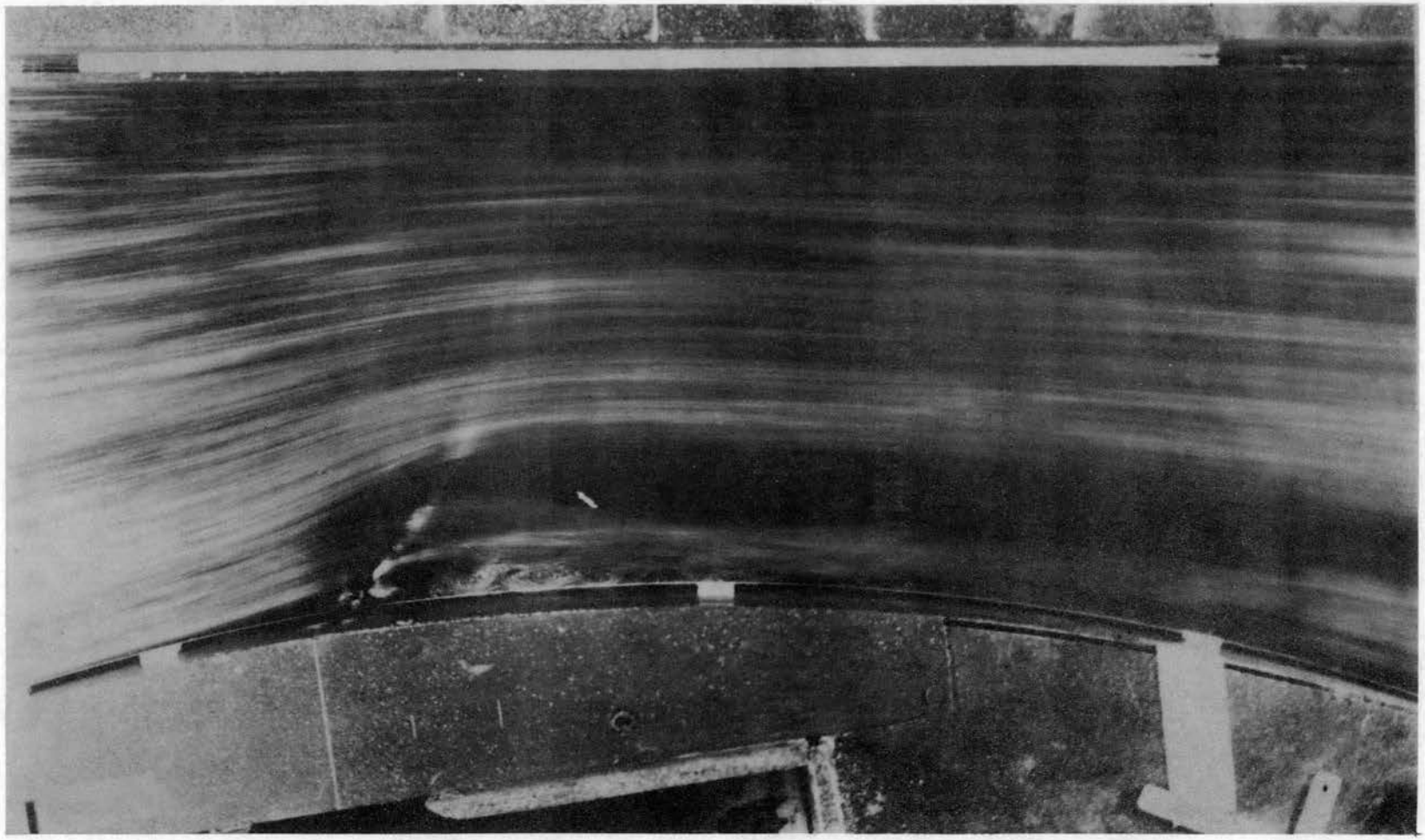

Figure 60. Typical Streak Lines for Secondary to Main Stream Head Ratio of 2.00; Injection at 8° Upstream of Geometric Throat.

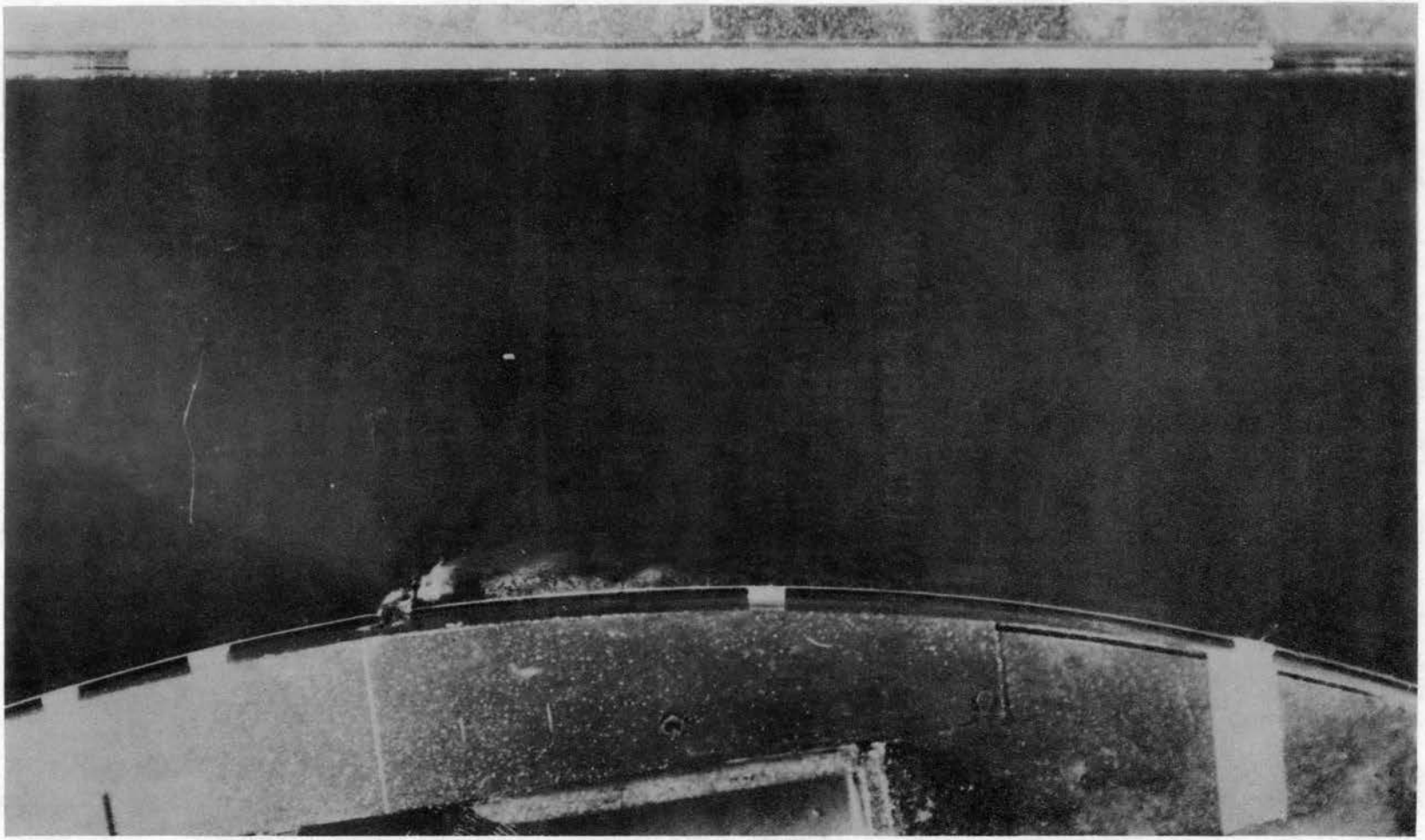

Figure 61. Typical Streak Lines for Secondary to Main Stream Head Ratio of 2.00; Injection at 8° Upstream of Geometric Throat.

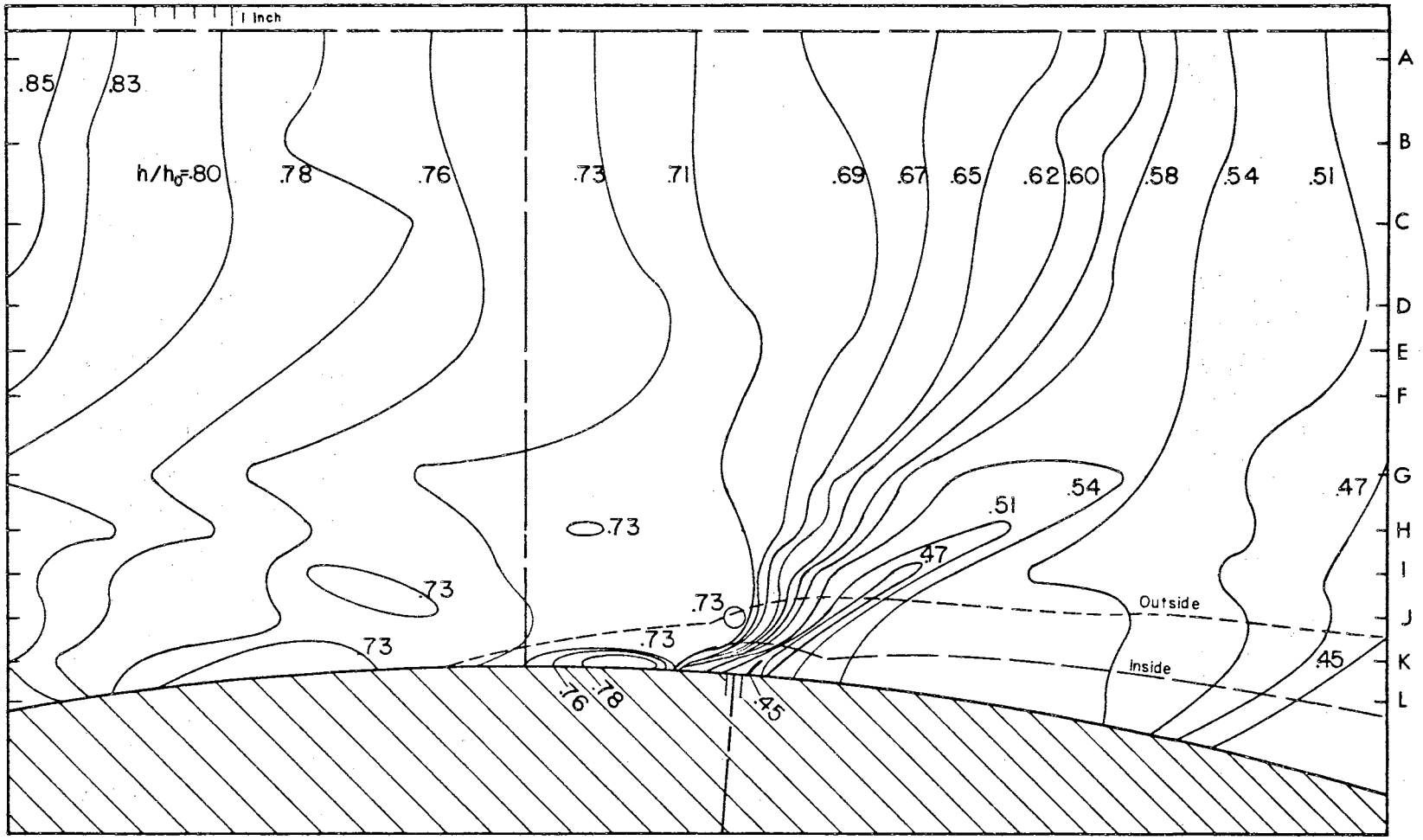

Figure 62. Isogrametric Depth Lines for Secondary to Main Stream Head Ratio of 1.00; Injection at 4° Downstream of Geometric Throat.

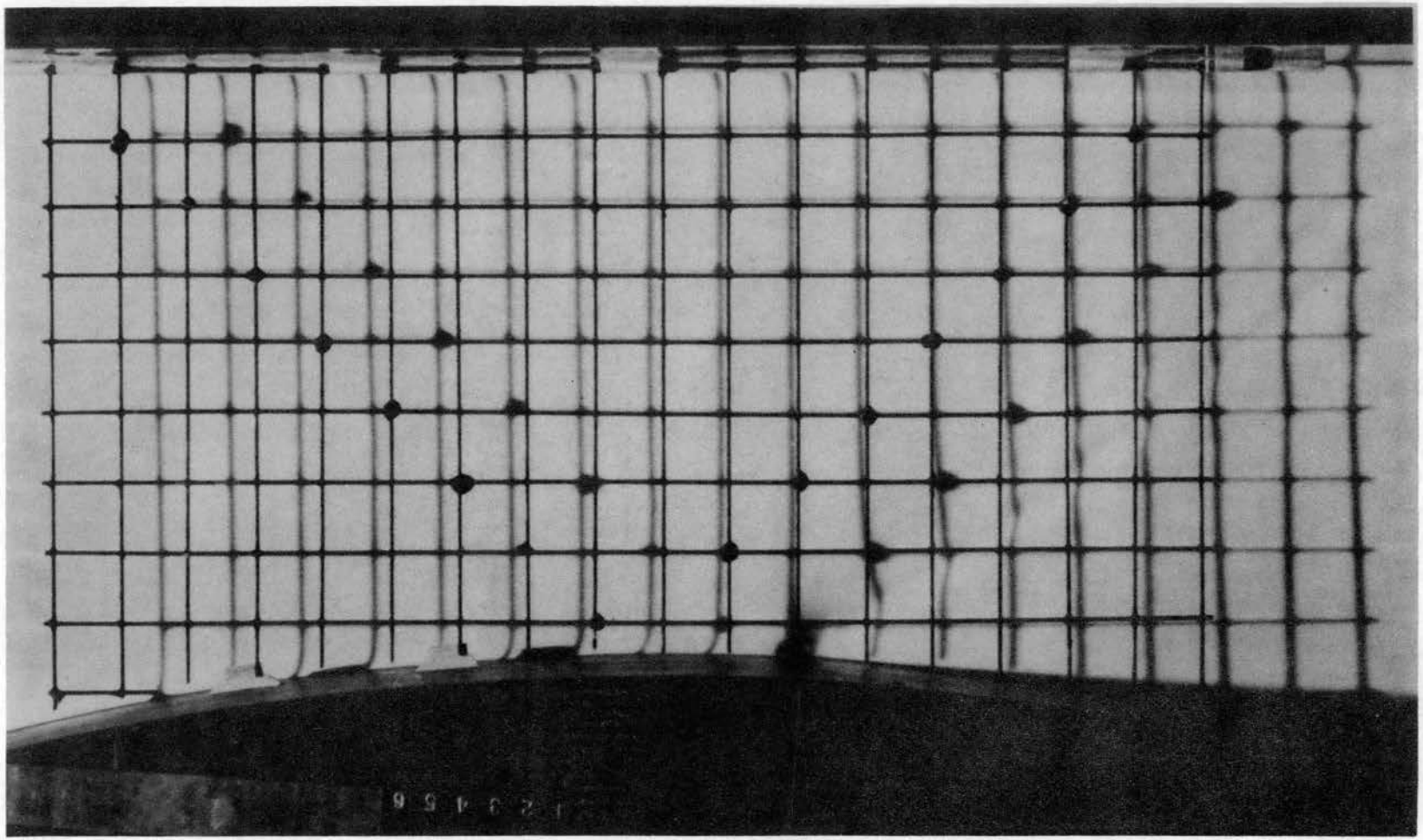

Figure 63. Shadow Pattern for Secondary to Main Stream Head Ratio of 1.00; Injection at 4° Downstream of Geometric Throat.

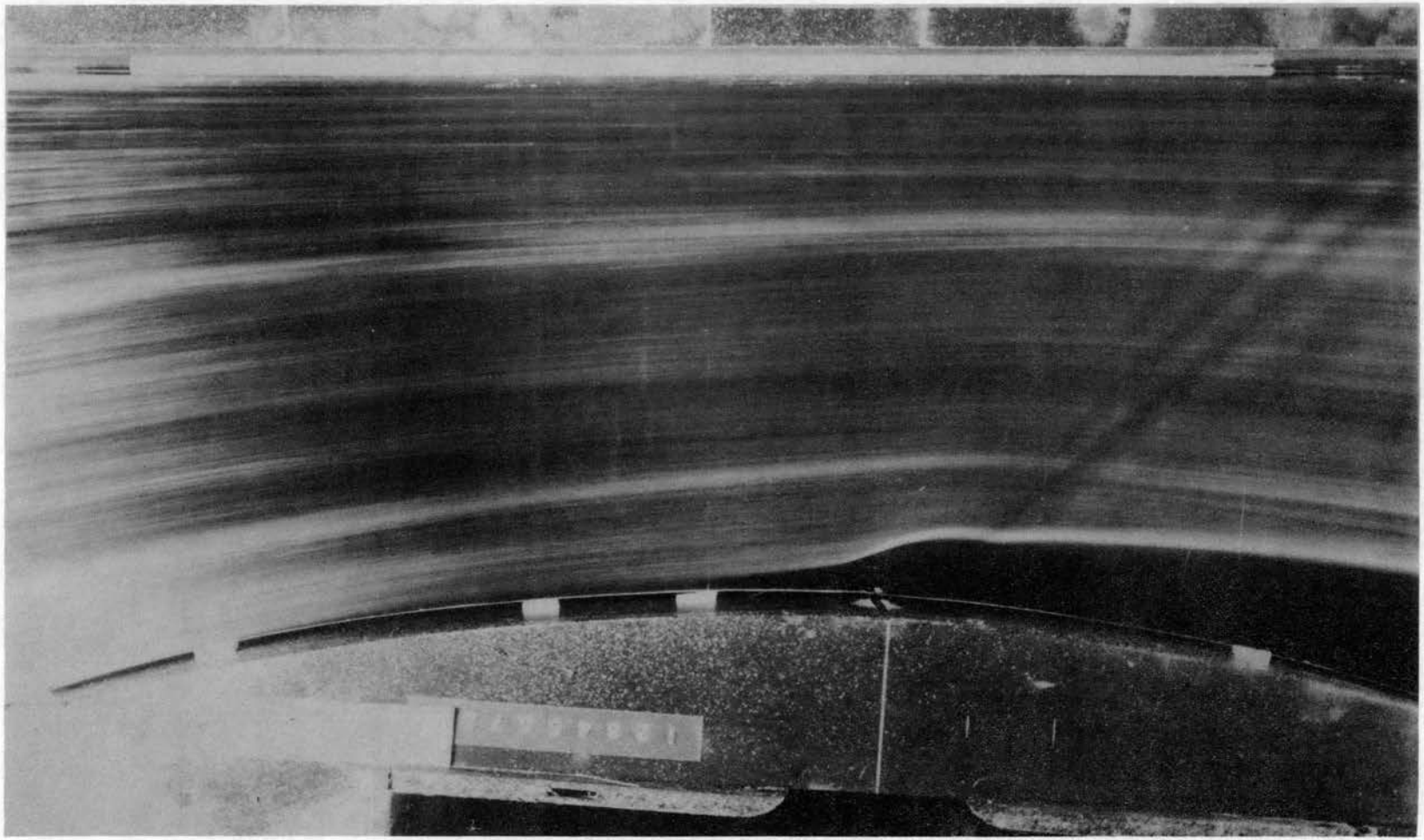

Figure 64. Typical Streak Lines for Secondary to Main Stream Head Ratio of 1.00; Injection at 4° Downstream of Geometric Throat.

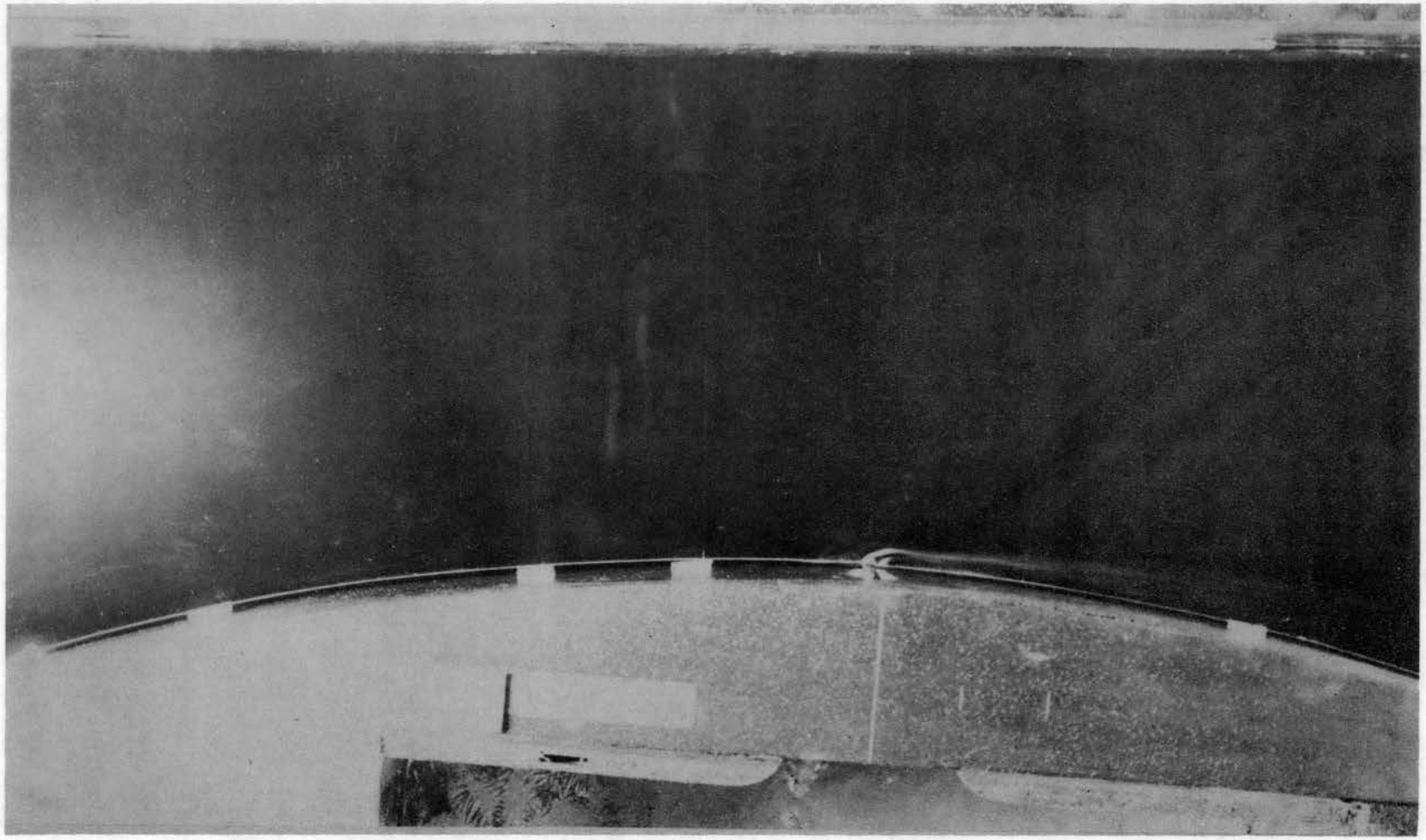

Figure 65. Typical Streak Lines for Secondary to Main Stream Head Ratio of 1.00; Injection at 4^{0} Downstream of Geometric Throat.

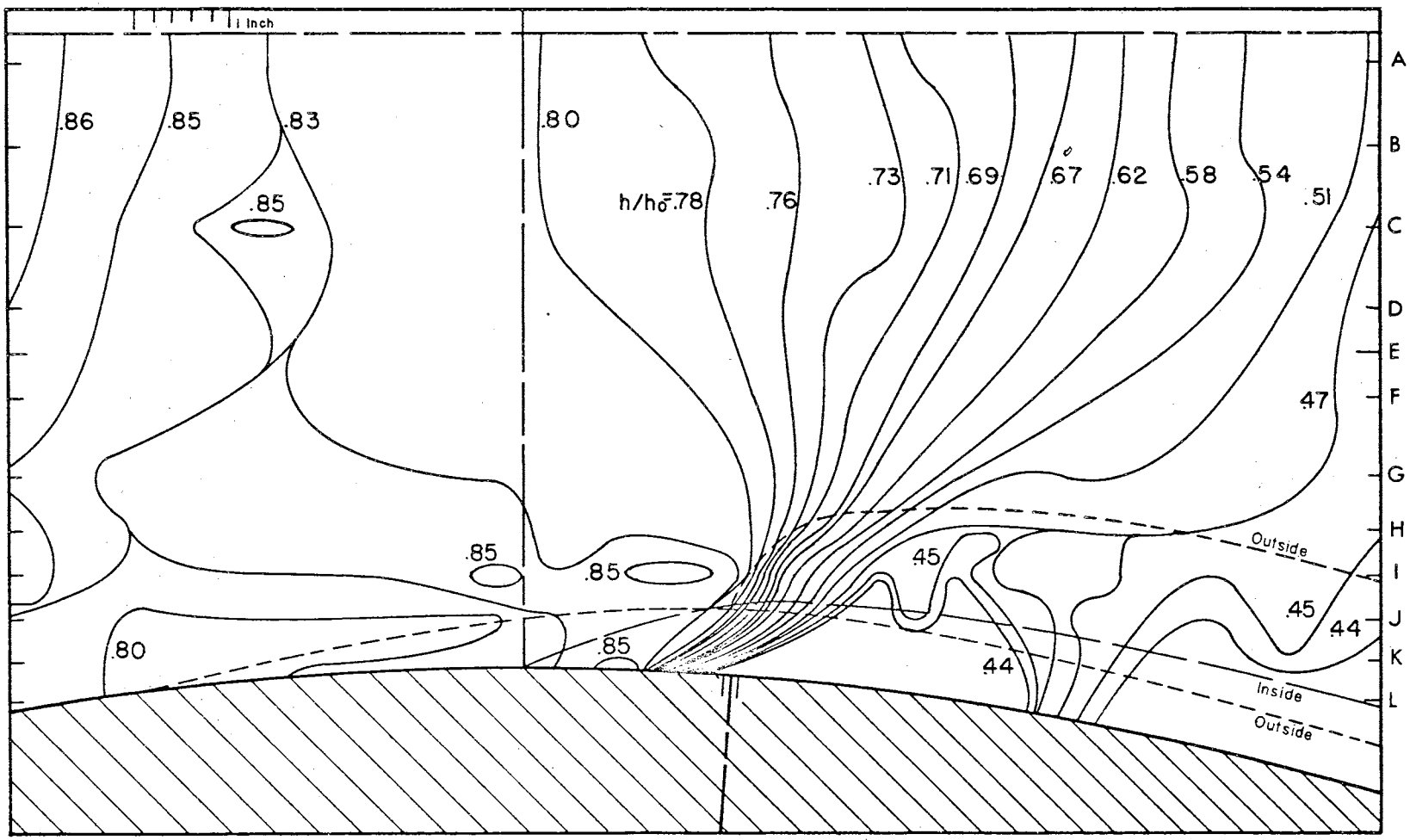

Figure 66. Isogrametric Depth Lines for Secondary to Main Stream Head Ratio of 2.00; Injection at 4° Downstream of Geometric Throat.

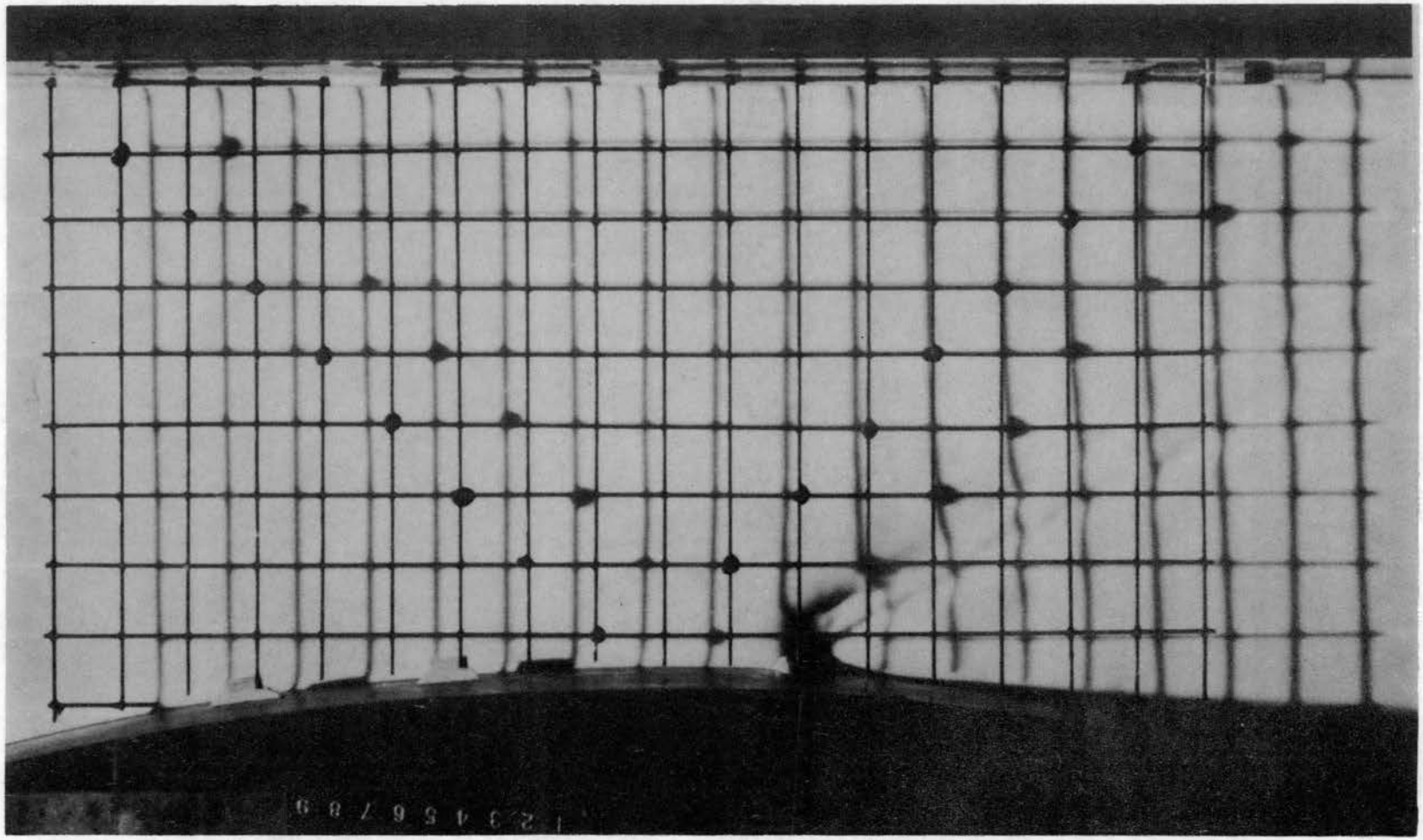

Figure 67. Shadow Pattern for Secondary to Main Stream Head Ratio of 2.00; Injection at 4° Downstream of Geometric Throat.

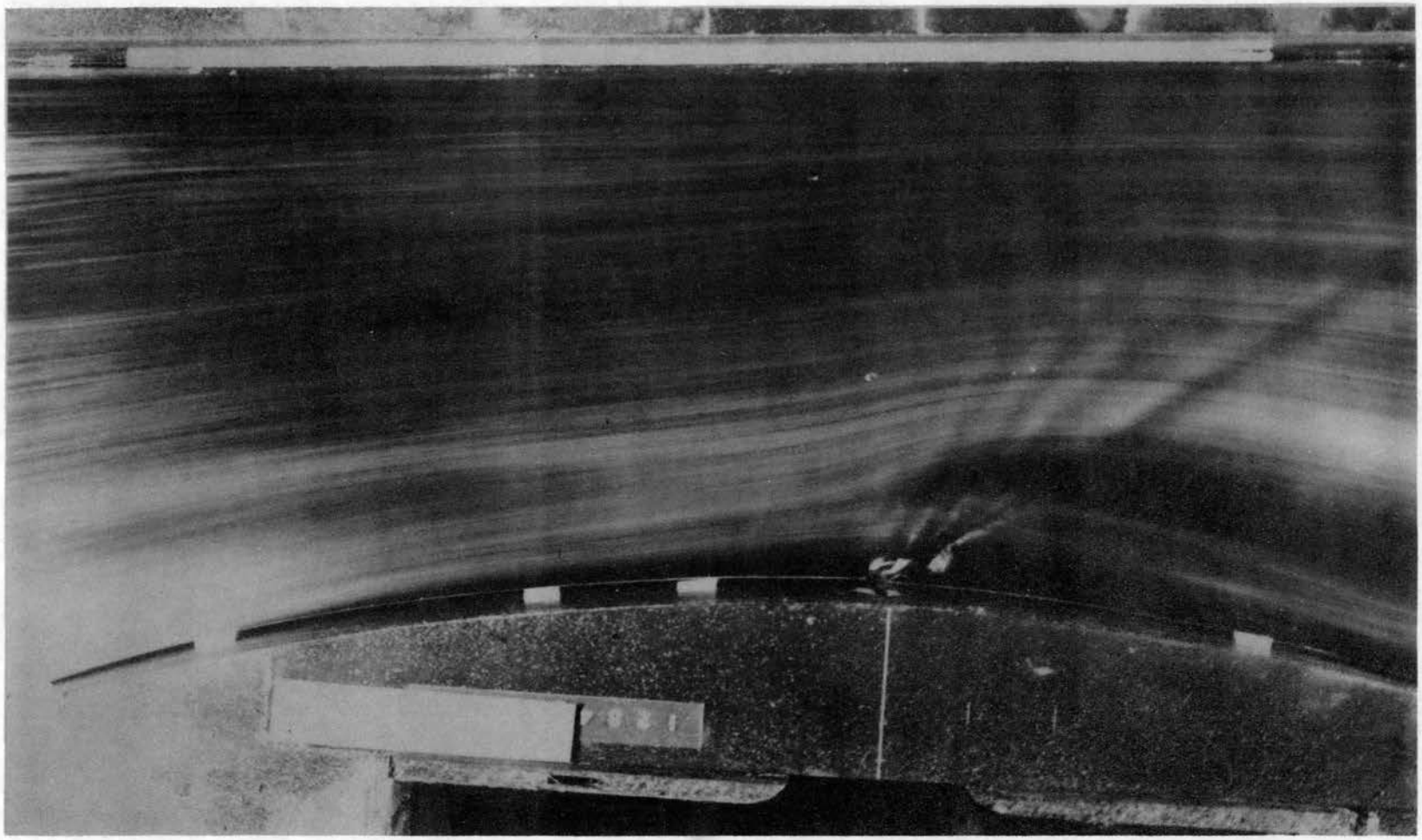

Figure 68. Typical Streak Lines for Secondary to Main Stream Head Ratio of 2.00; Injection at 4° Downstream of Geometric Throat.

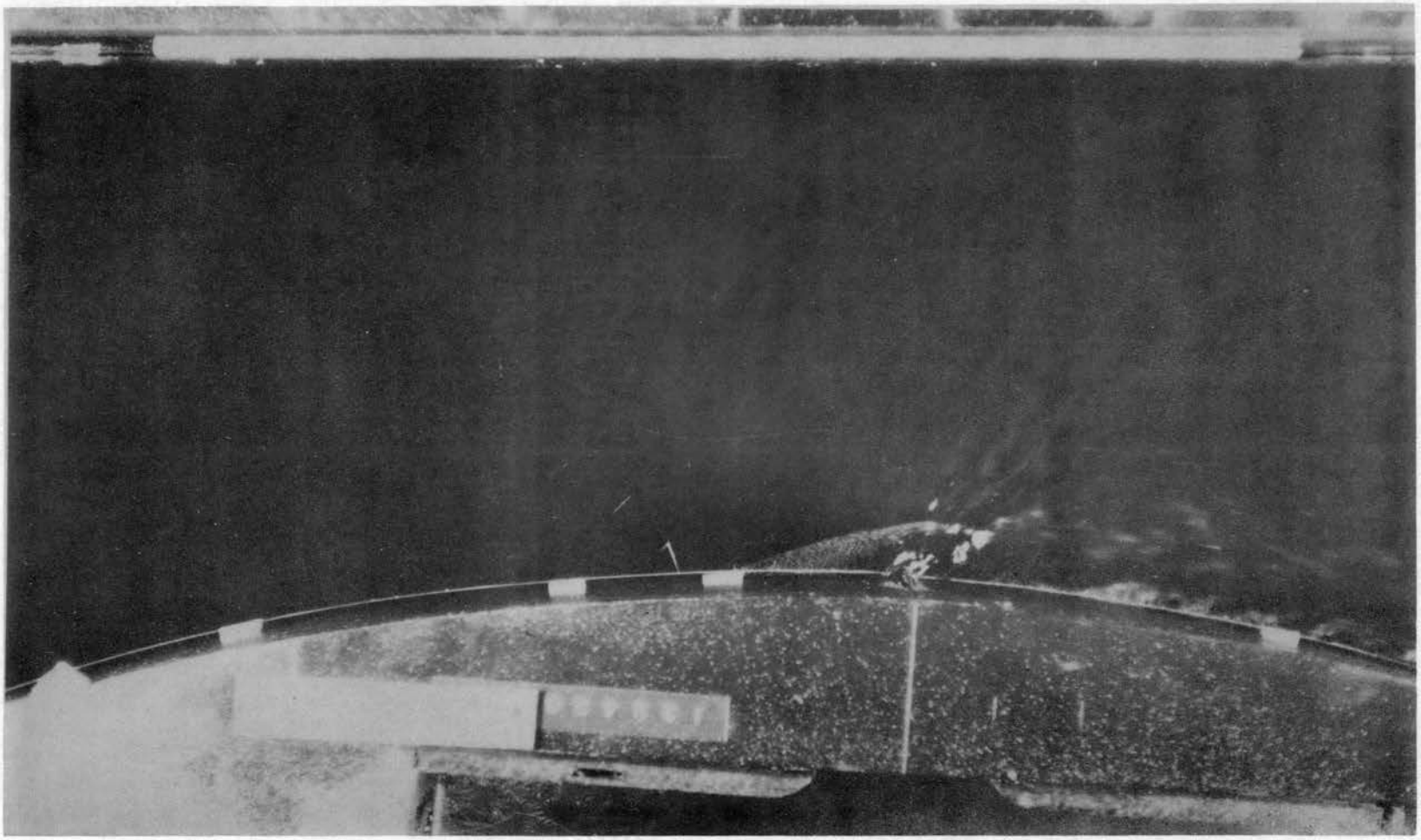

Figure 69. Typical Streak Lines for Secondary to Main Stream Head Ratio of 2.00; Injection at 4° Downstream of Geometric Throat.

observation is confirmed in figure 37 where the secondary stream is seen to be spreading over the nozzle face and flowing downward.

Figures 38, 42, 46, and 50 illustrate the surface topography for secondary injection at 4^0 upstream of the geometric throat for head ratios of 1.00, 1.50, 1.75, and 2.00. Compared to injection at the throat, the effect of the injection on the main stream is more drastic and all the fields show the main stream flow to be somewhat three-dimensional.

Figures 54 and 58 are the topographic plots for injection at 8^0 upstream from the geometric throat. The main stream flow is disturbed less than in the case of 4^0 upstream injection and the field is almost two-dimensional in character.

Figures 62 and 66 illustrate the topography of the surface for injection 4^0 downstream of the geometric throat at head ratios corresponding to those given above. The character of the main stream flow is changed considerably and apparently the effective throat of the nozzle has moved downstream.

Critique of the Shadow-photogrammetric Method

The shadow-photogrammetric method is apparently capable of yielding excellent results in the determination of the topography of a surface, however, the techniques of application to a particular problem may have to be developed further if more accuracy is required. Since the photographs may be enlarged up to the point of grain interference, the magnification factor for an actual measurement is very large and thus minute measurements can be made. As after thoughts, many things come to mind that would have eliminated much of the development work

described in this thesis; a critique of the experimental techniques and equipment is given below.

A critical alinement problem is encountered in setting up the camera and the shadow grid. Much of the set-up time could have been saved if a micromatic adjustable camera mount had been used. A more accurate grid would have proven extremely useful in checking the data reduction methods--it is suggested that the grid be made with a heavy framework so that the wires can be placed under tension and index marks can be scribed along the edges of the frame.

The use of the glass plate for calibration was by far the most convenient method, however, the plate varied in thickness by ± 0.001 inch and had to be supported in several places to eliminate the sag. A liquid surface such as mercury, or water, would give far better results because the still surface would be plane.

The optical system used was poorly corrected even though it was reported to be of excellent quality in the photographic literature. Much time would have been saved if the camera lens had been calibrated before the development of the shadow-photogrammetric method was undertaken. Lenses of reproduction quality that are designed to operate at close range should be considered. A problem associated with the optical errors is of course the print; elimination of the print by direct projection on a screen would be desirable, however, without automatic reading equipment, heating of the film would initiate more problems due to the time required to obtain the data for a large field. The basic design of an automatic reader with digital output has been conceived and the development of it is in progress.

Hydraulic Analogy Check

The hydraulic analogy provides an excellent tool for the study of gas flow because the flow patterns can be observed directly, the wave speed is about 1/1000 of that in the corresponding gas, and instrumentation is simple compared to that needed for gas flow studies. The conditions of an actual experiment violate the assumptions of the theoretical analogy; "--friction is present in both gas and water cases but frictional similitude and therefore frictional effects, i.e., boundary layer buildup, can not be satisfied and shock and rarefaction waves and interaction of these with each other and with the boundary layer are inevitable" (2). Despite the limitations, the water analogy can be applied to flow conditions where the gradients are small. In this study the injection of a secondary stream into the main stream does not meet this requirement; the head of the secondary was much greater than the main stream head at the point of injection, the secondary flow was not two-dimensional, and the secondary stream appeared to flow over the top of the main stream. Figures 70 and 71 illustrate the two characteristic flow patterns for the secondary stream. The first shows the secondary stream over-riding the main stream with little or no disturbance of the main flow, and the powder is fed from the downward flowing secondary stream over the region just upstream. Thence the powder flows around the "bump" to be dissipated shortly. In the second case, the counter clockwise vortex has been formed in the approach region by the penetrating secondary stream and a more complete disturbance of the main stream is shown. The other vortex of the pair can not be seen in the photograph, however, it was observed to be a very small clockwise

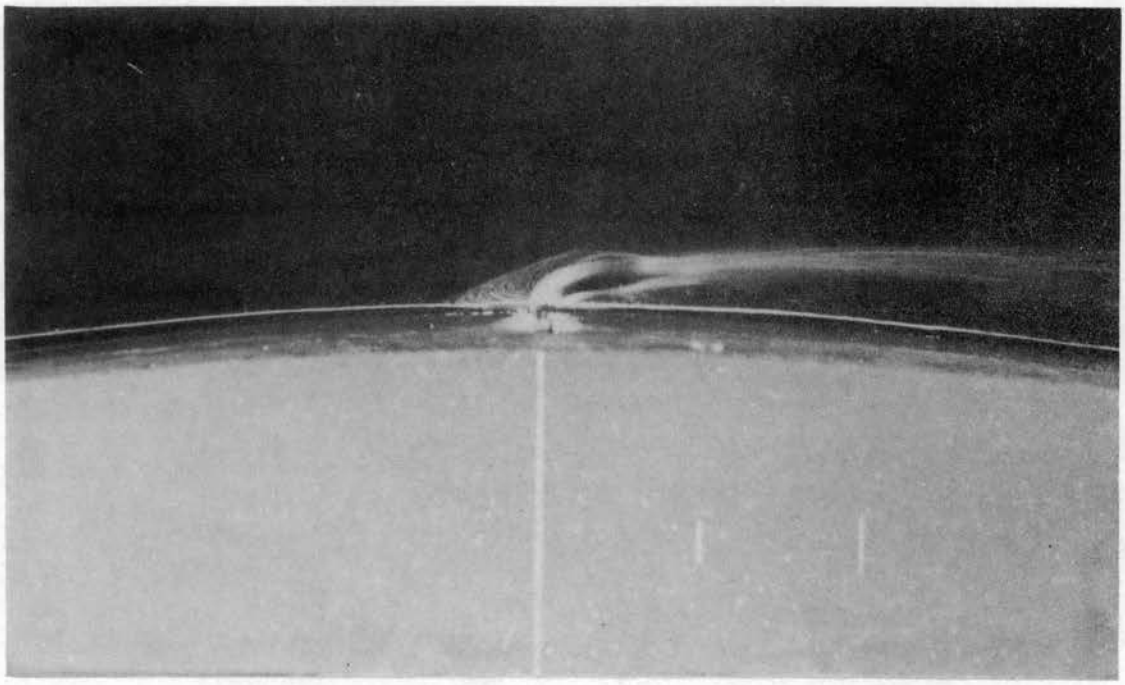

Figure 70. Characteristic Particle Flow Pattern.

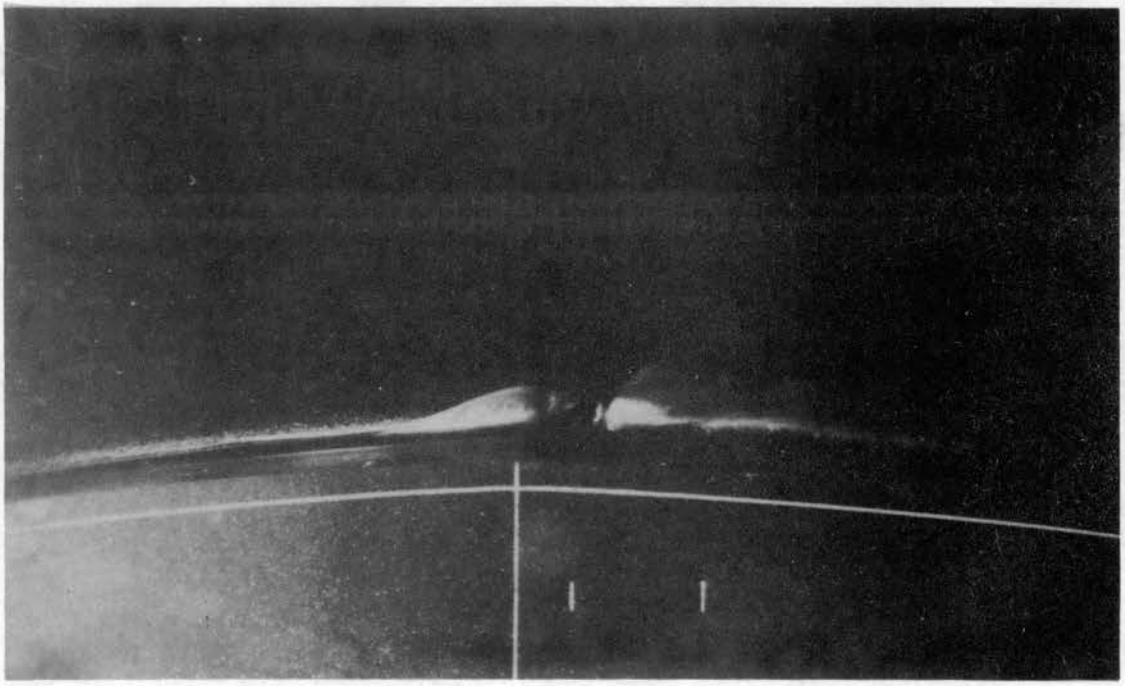

Figure 71. Characteristic Particle Flow Pattern.

motion next to the secondary nozzle opening. No control was found that would maintain either of the patterns for any length of time. Thus the hydraulic analogy, as applied here, fails to correspond to gas flow for a throat injection nozzle.

The experimental set-up for the water analogy has been discussed above. There seems to be some disagreement among the various writers as to the optimum depth to use for the analogy. Laitone (9) shows that unless the wave length of the water surface waves is much much smaller than the depth that the surface tension and the density of the water must be taken into account, because of their effect on the wave propagation equation. On the other hand, the depth must be small compared to any significant width dimension. However, if the depth is too small then the surface tension becomes the predominate factor in the wave speed equation. So some optimum depth must be found. He has determined it to be 1/4 inch for pure water. Mann (2), on the other hand, states that depths of from 3 inches to 0.3 inch are perfectly suitable for unsteady flow while 0.9 inch may be used for steady flow. Since the object here was to maintain two-dimensional flow as far as possible, this was the main consideration in selecting 0.5 inch for the main stream stagnation head. A preliminary series of runs with 3/4 inch heads showed the flow field to be three-dimensional in the downstream region even for small injection rates. Figure 72 illustrates a 3/4 inch head run; the transition to shooting water is outlined as the upstream ends of the wavelets, and there is probably little over-shoot of the secondary flow. Figure 72 resembles very closely the photographs of Maegley (3) for gas flow.

Although secondary fluid over-ride had been observed during the

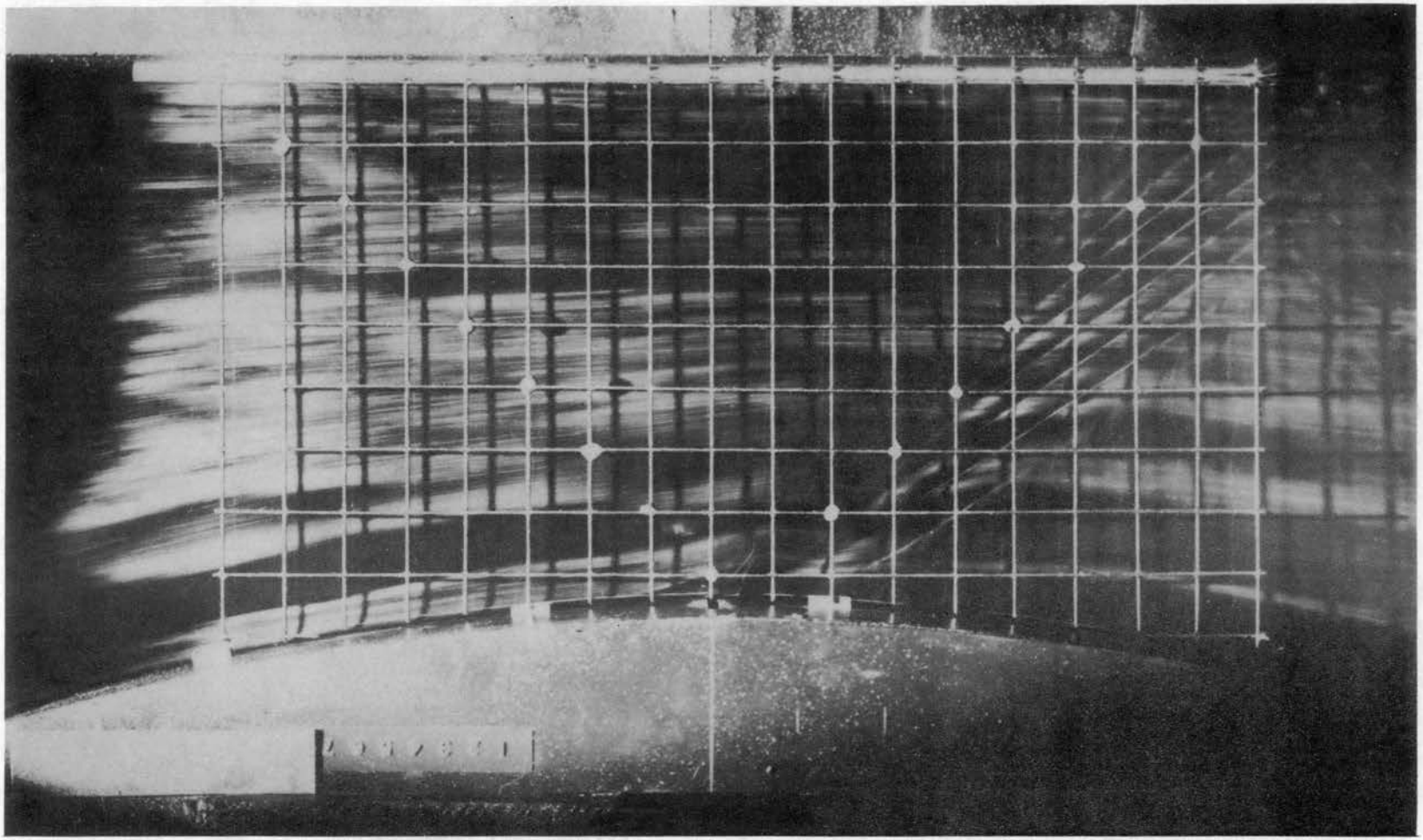

Figure 72. Shadow Pattern for Secondary to Main Stream Head Ratio of 1.00; 3/4 Inch Main Stream Head.

experiments and several other results indicated the water analogy was not valid for this flow field, a further check was made by comparing the indicated blockage with that found by Warloe (29) for air flow. Figure 73 shows the comparison using both the metered flow rate ratios and the corresponding pressure analog. It is seen that the blockage approaches Warloe's for low secondary heads, but quickly becomes grossly in error as the secondary head and flow rate increase. Thus the analogy, as applied here, again failed to conform to the gas flow results.

Shown on the field plots are traces of the limit of the aluminum powder, as determined from the streak photographs, as it appeared when dusted on the main stream (outside) and when it was dusted in the secondary water box (inside). The photographs were exposed within one or two minutes of one another. If the true separation of the streams is indicated, or short time steady state has been achieved, one would expect the lines to more nearly coincide, however, they have a random relative location. It appears that no conclusions can be reached to indicate the boundary between the two streams, if indeed there is a discernible boundary. Maegley's (30) efforts to obtain the stream separation by schlieren and shadowgraph photography also left this point in question as the optical blockage he found did not check with that of Warloe. Zukoski and Spaid (37) injected a heavy gas into an air flow field for the purpose of obtaining schlieren photographs of the boundary of a jet and found the apparent separation line was actually the line of maximum concentration of the injectant rather than the jet boundary. Thus the separation of the two streams is still in question and the analogy did not supply any additional information.

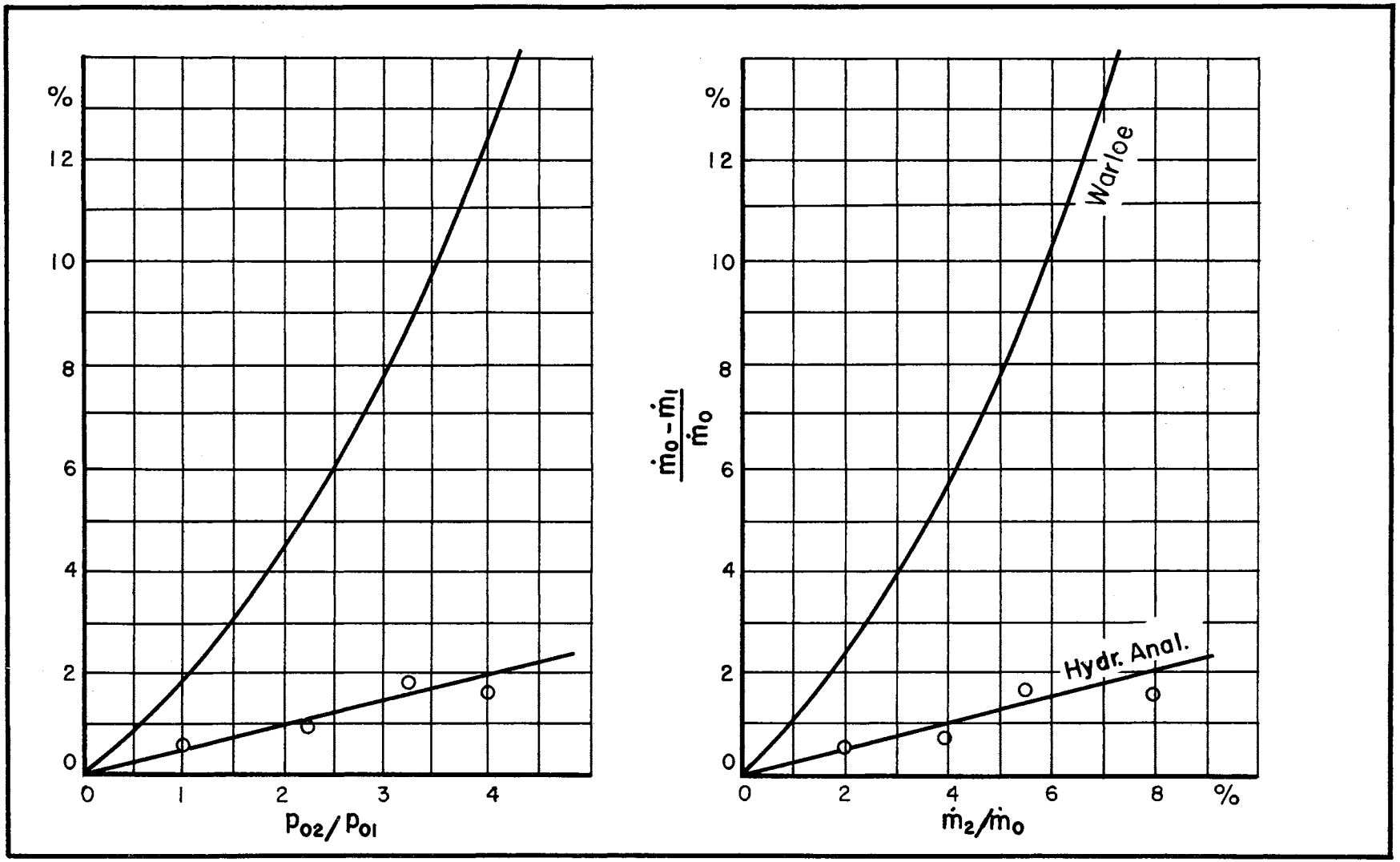

Figure 73. Comparison of Blockage for Injection at Geometric Throat.

Critique of the Water Analogy Application

If one hopes to improve the water analogy for throat injection of a nozzle to obtain quantitative data that may be used to help develop a theoretical analysis of such problems, then he should consider the following factors which were not accounted for in the present study. First, the table should be lower at the outlet end to account for the boundary layer growth; computations of the displacement thickness show it to approximately 1/3 of the depth at the throat, and mass flow rates computed by piecewise integration along an isogrametric depth line gave values 12 % too high at the throat when the bottom boundary layer was neglected (38). Second, large gradients must be avoided at secondary injection, and the jet must penetrate the main stream. One possible solution to the latter may be to design the secondary nozzle so that the contraction to obtain shooting water at the outlet is in the vertical plane rather than the horizontal plane as it was in this study, thus the top of the outlet of the secondary nozzle could be made even with the undisturbed main stream flow to eliminate the downward flow of the secondary stream.

CHAPTER VI

CONCLUSIONS AND RECOMMENDATIONS

A new method has been developed using a single lens camera to obtain the topography of an opaque surface by photographing the shadow pattern of a wire grid projected obliquely onto the surface. The method is superior to other methods of obtaining topographic maps of surfaces from the standpoints of equipment expense, time and the skill required of the operator. In addition, the accuracy obtainable is as good or better than that obtained by stereophotogrammetric methods. Since it is a photographic method, it can be applied to time dependent fields; such as panel flutter and distortion, fluid oscillators and amplifiers, strain in solids, thermal distortions; as well as to stationery fields. The writer believes that with this new method of obtaining depths on the water table, that this useful tool may come into more extensive use.

The application of the shadow-photogrammetric method to the hydraulic analogy study of throat injection of a nozzle provided a severe test of the method and illustrates a practical use. It was shown that not only a known flat field could be mapped, but also that the contours of the water surface could be found to within 2 % of the known depth.

The water analogy as applied here to the problem of throat injection into a nozzle failed to comply with the corresponding gas flow.

Large gradients due to injection of the secondary stream invalidate the analogy.

It is recommended that a more stable base film, such as "Eastman Estar", be used to help eliminate some of the shrinkage problems, and an automatic reader be developed so the print can be eliminated. Also the method should be applied to various other fields so that special techniques may be developed to make the method a practical, common tool for topographical studies.

SELECTED BIBLIOGRAPHY

1. Heen, Helge K. and Robert W. Mann, "The Hydraulic Analogy Applied to Nonsteady, Two-Dimensional Flow in the Partial-Admission Turbine [1]1, Paper No. 60--WA-168, Transactions of ASME

2. Mann, Robert W., "Stereophotogrammetry Applied to Hydraulic Analogue Studies of Unsteady Gas Flow," Report Number 8543-1, Department of Mechanical Engineering, Massachusetts Institute of Technology, March 30, 1962.

3. Preiswerk, Ernst, "Application of the Methods of Gas Dynamics to Water Flows with Free Surface, Part I., Flows with no Energy Dissipation," NACA TM-934, 1940.

4. Murphy, Glen, D. I. Shippy and H. L. Lau, Engineering Analogies, Iowa State University Press, Ames, Iowa, 1963, pp. 29-35.

5. Lamb, Sir Horace, Hydrodynamics, Dover Publications, New York, 1945, Sixth Edition, 738 pp.

6. Hoyt, J. W., "A Study of Supersonic Jet Deflection by the Hydraulic Analogy," Ph.D. Dissertation, University of California, Los Angeles, January 1962.

7. Loh, W. H. T., "Hydraulic Analogue For One Dimensional Unsteady Gas Dynamics," Journal of the Franklin Institute, Vol. 269, No. 1, January 1960, pp. 43-55.

8. Preiswerk, Ernst, "Application of the Methods of Gas Dynamics to Water Flows with Free Surface, Part II., Flows with Momentum Discontinuities (Hydraulic Jumps)," NACA TM-935, 1940.

9. Laitone, E. V., "A Study of Transonic Gas Dynamics by the Hydraulic Analogy," Journal of the Aeronautical Sciences, Vol. 19, No. 1, January 1952, pp. 265-272.

10. Gupta, O. P., "An Analytical Method of Evaluating the Optimum Depth in Hydraulic Analogy Experiments," AIAA Journal, Vol. 3, No. 10, October 1965, pp. 1953-1954.

11. Werlé, Henri, Le Laboratoire Des Analogies Hydrauliques De La Direction Aérodynamique De L'O.N.E.R.A., Office National D'Études Et De Recherches Aéronatiques, Publication No. 103, 1961, 36 pp.

12. Johnson, R. W., W. R. Nial and N. C. Witbeck, "Water Analogy to Two-Dimensional Air Flow," General Electric Co., Report No. 55218, August 1947.

13. Clutter, Darwin W., and A. M. O. Smith, "Flow Visualization by Electrolysis of Water," Aerospace Engineering, January 1961, pp. 24-28 and 75-76.

14. Poetzschke, Heinz G. and Donald F. Menne, "A Photogrammetric Method For Determining the Topography of Liquid Surfaces," Report No. 1196, Ballistic Research Laboratories, Aberdeen Proving Ground, Maryland, March 1963.

15. Moore, A. D., "Soap-Film and Sandbed-Mapper Techniques," Journal of Applied Mechanics, Vol. 17, No. 3, September 1950, pp. 291-298.

16. Tewinkel, G. C., Manual of Photogrammetry, Chapter VI, Basic Mathematics of Photogrammetry, American Society of Photogrammetry, Washington, D. C., 1952, Second Edition, 876 pp.

17. Bagley, James W., Aerophotography and Aerosurveying, McGraw-Hill Book Company, Inc., New York and London, 1941, 324 pp.

18. ----------"Physical Characteristics of Kodak Glass Base Plates," Kodak Pamphlet No. Q-35, 1960, Eastman Kodak Company, Rochester, N. Y.

19. ----------"Dimensional Stability of Kodak Acetate Films for the Graphic Arts," Kodak Pamphlet No. Q-33, 1960, Eastman Kodak Company, Rochester 4, N. Y.

20. Swann, W. F., Private Communication, Letter of August 24, 1964, Eastman Kodak Company, Rochester, N. Y.

21. ----------"Kodak Photographic Papers," Kodak Publication No. G-1, 32 pp., Seventh Edition, 1960, Eastman Kodak Company, Rochester 4, N. Y.

22. Kingslake, Rudolf, Lenses in Photography, Garden City Books, Garden City, New York, 1951, 246 pp.

23. Ask, Reynold E., Manual of Photogrammetry, Chapter II, Elements of Photogrammetric Optics, American Society of Photogrammetry, Washington, D. C., 1952, Second Edition, 876 pp.

24. Jacobs, Donald H., Fundamentals of Optical Engineering, McGraw-Hill Book Company, Inc. New York and London, 1943, 487 pp.

25. Moffitt, Francis H., Photogrammetry, International Textbook Company, Scranton, Pennsylvania, Second Printing, 1961, 455 pp.

26. Tyler, Lynn Dolan, "Numerical Solutions of the Flow Field Produced by a Plane Shock Wave Emerging into a Cross flow," Ph.D. Thesis, Oklahoma State University, Stillwater, Oklahoma, May 1965, 178 pp.

27. Welton, D. E., S. M. Bensky and J. R. Hiland, "Toward the Variable-Thrust Liquid-Rocket Engine," Astronautics and Aerospace Engineering, Vol. 1, No. 11, 1963, pp. 77-81.

28. Jackomis, W. N., "An Experimental Study of Aerodynamically Variable Throat Area (AVT) Nozzles," M.S. Thesis, Oklahoma State University, August 1962.

29. Warloe, R. O., "A Study of Secondary Air Injection into a Two-Dimensional Converging-Diverging Nozzle," M.S. Thesis, Oklahoma State University, August 1963.

30. Maegley, W. J., "An Optical Study of the Injection of a Gas into the Throat Region of an Air Nozzle," M.S. Thesis, Oklahoma State University, August 1963.

31. Stutzman, R. D., "Investigation of Secondary Injection Using Hydraulic Analogy," Unpublished Special Project Report, Oklahoma State University, May 1963.

32. McAulay, John E., "Cold-Air Investigation of Three Variable-Throat-Area Convergent-Divergent Nozzles," NASA, Technical Memorandum X-42, September 1959, 32 pp., Declassified 1962.

33. Rodriquez, C. J., "An Experimental Investigation of Jet-Induced Thrust Vector Control Methods," Bull. 17th Meeting, JANAF-ARPA-NASA Solid Propellent Group, Vol. III, May 1960.

34. Nesterov, Ye. D., "Aerodynamic Compression of a Gas Stream," FTD-TT-62-1555, Wright-Patterson Air Force Base, Ohio, January 1963, English Translation of Izvestiya Vysshikh Uchebnykh Zavendeniy, Aviatsionnaya Tekhnika, No. 1, 1962, pp. 82-91.

35. Zumwalt, G. W. and W. N. Jackomis, "Secondary Injection Nozzle for Solid Rocket Thrust Magnitude Control," ARS Reprint No. 2337-62, Solid Propellent Rocket Conference, Baylor University, Waco, Texas, 1962.

36. Samos, John, "Design of a Free Water Surface Table to Be Used as an Analogy to Two-Dimensional Compressible Gas Flow, M.S. Report, Oklahoma State University, May 1960.

37. Zukoski, E. E. and F. W. Spaid, "Secondary Injection of Gases into a Supersonic Flow," AIAA Journal, Vol. 2, No. 10, October 1964, pp. 1689-1696.

38. Schlichting, Hermann, Boundary Layer Theory, McGraw-Hill Book Company, Inc., New York, Fourth Edition, 1960, 647 pp.

APPENDIX A

COMPUTATION OF EXPECTED ERRORS IN RESULTS DUE TO ERRORS OF MEASUREMENTS

Measurements of the positions of the shadows relative to the perspective axis on the photographs were easily made to within ± 0.25 unit; accounting for a maximum of 3 % for print shrinkage this gave the probability of a maximum measurement error of ± 0.26 unit, or ± 0.0052 inch, in the corrected apparent location. Since this error is included in any subsequent calculations, the expected error in the results can be found by showing the effect of other possible errors relative to the initial measurement error. The center of the field of photograph 1904 was used to determine the total effect of all errors assuming the true apparent shadow location could be computed by the optical error equations for the Mark I computation. Thus if errors are found to be larger than those predicted below, they must be due to the optical error correction equation being incorrect. The complete computation showing all the possible combinations of errors is given below; it also serves as an example calculation for a point. The symbols $+\Delta$ and $-\Delta$ are used to designate a high and low value respectively, while the regular symbol is used for the mean value.

Location Error--

Data for intersection 11 E

$S_{oa} = -162.50$ $\quad B = 177.50$

$S_{ca} = -117.25$ $\quad h' = 1989.35$

$S_a = -137.25$ $\quad h_c = 28$

$S_o = -180.00$ (act.) $\quad K_1 = 1.020$

where K_1 is the shrinkage factor for this location.

Optical error equation--

$$|[S'_a]| = |S'_a| - 1.3 - (.00760)\, S'_a \qquad S'_a < -40.$$

Foreshortening correction--

$$S = [S'_a]\ (1 + B/h' - h/h'),$$

or for mean values of B and h'

$$S = [S'_a]\ (1.08922 - h/1989.35).$$

Depth equation--

$$h = \frac{[(h' + B)\ ([S'_a]/h')] - S_o}{[(S_c - S_o)/h_c] + ([S'_a]/h')}.$$

Data corrected for print shrinkage--

Note: Δ error applied to original data.

$S'_{oa} + \Delta = -166.00$

$S_{oa} = (1.020)\ (-162.50) = -165.75$

$S'_{oa} - \Delta = -165.49$

$S'_{ca} + \Delta = -119.85$ $\qquad S'_a + \Delta = -140.25$

$S'_{ca} = -119.60$ $\qquad S'_a = -140.00$

$S'_{ca} - \Delta = -119.34$ $\qquad S'_a - \Delta = -139.74$

Data corrected for optical error (true apparent location)--

$[S'_{oa} + \Delta] = 165.96$

$[S'_{oa}] = 165.75 - 1.3 - (.00760)(-165.75) = 165.71$

$[S'_{oa} - \Delta] = 165.44$

$[S'_{ca} + \Delta] = 119.46$ $\qquad$ $[S'_{a} + \Delta] = 140.02$

$[S'_{ca}] = 119.21$ $\qquad$ $[S'_{a}] = 139.76$

$[S'_{ca} - \Delta] = 118.95$ $\qquad$ $[S'_{a} - \Delta] = 139.50$

Calculated true shadow locations assuming h' and B are known to be mean values--

$S_o + \Delta = -180.77$

$S_o = -165.71\ (1.08922 - 0/1989.35) = -180.49$

$S_o - \Delta = -180.20$

$S_c + \Delta = -128.44$

$S_c = -128.17$

$S_c - \Delta = -127.89$

The calculation of S_o shows a maximum error of .77 unit (.015 inch) compared to the value from set-up measurements, however, they agree to within .4 % or less. An error in optical corrections is apparent here, however, it need not be considered for the present check on expected errors. Note that S is at an unknown depth so may not be caluclated at this point.

The precision of measurement of B was very good, since it was determined, from the water table set-up, using calipers,

however, assume it was in error by ± 1.0 unit. The foreshortening constant for zero position shadows is then:

$$1 + B + \Delta/h' = 1.08972$$

$$1 + B/h' = 1.08922$$

$$1 + B - \Delta/h' = 1.08872.$$

Also the measurements made for the computation of h' (page 34) were made from the camera and flow field, however, assume it was in error by ± 10 units, or 0.20 inch, then:

$$h' + \Delta = 1999.35$$

$$h' = 1989.35$$

$$h' - \Delta = 1979.35$$

Thus 9 values of the foreshortening constant are possible:

TABLE A-I

FORESHORTENING CONSTANT

	B+Δ	B	B-Δ
h' + Δ	1.08927	1.08877	1.08827
h'	1.08972	1.08922	1.08872
h' - Δ	1.09018	1.08967	1.08917

Further possible values of S_o and S_c because of errors in B and h' are given below:

TABLE A-II

B+Δ

	$S_o+\Delta$	S_o	$S_o-\Delta$	$S_c+\Delta$	S_c	$S_c-\Delta$
h' + Δ	-180.78	-180.50	-180.21	-128.45	-128.18	-127.90
h'	-180.85	-180.58	-180.28	-128.50	-128.23	-127.95
h' - Δ	-180.93	-180.65	-180.36	-128.54	-128.27	-127.99

B

	$S_o+\Delta$	S_o	$S_o-\Delta$	$S_c+\Delta$	S_c	$S_c-\Delta$
h' + Δ	-180.69	-180.42	-180.13	-128.39	-128.12	-127.84
h'	-180.77	-180.49	-180.20	-128.44	-128.17	-127.89
h' - Δ	-180.84	-180.57	-180.28	-128.48	-128.21	-127.93

B-Δ

	$S_o+\Delta$	S_o	$S_o-\Delta$	$S_c+\Delta$	S_c	$S_c-\Delta$
h' + Δ	-180.61	-180.34	-180.04	-128.33	-128.06	-127.78
h'	-180.68	-180.41	-180.12	-128.38	-128.11	-127.83
h' - Δ	-180.76	-180.49	-180.19	-128.42	-128.15	-127.87

It seems from the above table of computed values of S_o (= -180.00 act.), that the maximum error of 0.93 unit, or 0.018 inch, can be expected for errors in both h' and B. Thus errors of 0.5 % or less are possible in S_o and S_c.

Calculated true depth errors--

The cotangent θ is needed in the depth calculations and, of course, is dependent upon the values of S_o, S_c and h_c used in its calculation, however, note that the extreme conditions shown in the table above cannot occur together. The value of h_c is assumed correct compared to the other measurements since it was found to 0.001 inch or 0.05 unit. The cotangent θ may take on the values shown in Table A-III.

The two extreme values of the cotangent θ are 1.89071, when S_o is high, h' is low, and B is high; and 1,84678 when S_o is low, h' is high, and B is low. These values are within 2 % of 1.86857 which is obtained when all mean values are used.

TABLE A-III

COTANGENT θ

B+Δ

	$S_o+\Delta$ $S_c+\Delta$	$S_o+\Delta$ S_c	$S_o+\Delta$ $S_c-\Delta$	S_o $S_c+\Delta$	S_o S_c	S_o $S_c-\Delta$	$S_o-\Delta$ $S_c+\Delta$	$S_o-\Delta$ S_c	$S_o-\Delta$ $S_c-\Delta$
h'+Δ	1.86892	1.87857	1.88857	1.85892	1.86857	1.87857	1.84857	1.85821	1.86821
h'	1.86964	1.87928	1.88928	1.86000	1.86964	1.87964	1.84928	1.85892	1.86892
h'-Δ	1.87107	1.88071	1.89071	1.86107	1.87071	1.88071	1.85071	1.86035	1.87035

B

h'+Δ	1.86785	1.87750	1.88750	1.85821	1.86785	1.87785	1.84785	1.85750	1.86750
h'	1.86892	1.87857	1.88857	1.86785	1.86857	1.87857	1.84857	1.85821	1.86821
h'-Δ	1.87000	1.87964	1.88967	1.86035	1.87000	1.88000	1.85000	1.85964	1.86964

B-Δ

h'+Δ	1.86714	1.87678	1.88678	1.85750	1.86714	1.87715	1.84678	1.85642	1.86642
h'	1.86785	1.87750	1.88750	1.85821	1.86785	1.87785	1.84785	1.85750	1.86750
h'-Δ	1.86928	1.87892	1.88892	1.85964	1.86928	1.87928	1.84892	1.85857	1.86857

The possible values of the depth considering the extremes above are:

TABLE A-IV

	h (depth)		
	$S_o+\Delta$	S_o	$S_o-\Delta$
	$h'-\Delta$	h'	$h'+\Delta$
	$B+\Delta$	B	$B-\Delta$
$[S'_a+\Delta]$	15.56	15.72	15.57
$[S'_a]$	15.73	15.88	15.73
$[S'_a-\Delta]$	15.88	16.03	15.89

The maximum error between the extremes is 2.9 %, however, the error on either side of the mean value is 2 %; note that this gives the depth to within 0.006 inch or to the same uncertainty as the original measurement.

Location of intermediate points--

The location for unknown points depends on the depth calculations; for the point in question the following values are obtained:

TABLE A-V

	S (location)		
	$S_o+\Delta$	S_o	$S_o-\Delta$
	$h'-\Delta$	h'	$h'+\Delta$
	$B+\Delta$	B	$B-\Delta$
$[S'_a+\Delta]$	-151.54	-151.40	-151.29
$[S'_a]$	-151.25	-151.11	-151.00
$[S'_a-\Delta]$	-151.00	-150.82	-150.71

The difference in the location for extreme conditions is 0.010 inch or about the error in the original values; differences from the mean are less than 0.4 % of throat width.

The effect of the error in the cotangent θ on the depth calculations, assuming all values constant is 2.7 % between the extremes and 1.33 % between the mean and the extremes. If this is accounted for in the true location calculation it was found that an error of less than 1 % can be expected.

Thus, assuming the true apparent shadow location can be computed from the given optical error equation, the expected accuracy with photograph measurements of ± 0.25 units accuracy should give the depths to within ± 1.33 % or at most 2.7 % between extremes, and locations based on these depths to ± 0.6 %. Errors in the computation of the cotangent θ are the source of the greatest error and this depends upon the calculation of the true apparent locations of the zero and calibration shadow locations being correct, which in turn requires the optical error correction equation to be correct.

APPENDIX B

COMPUTER PROGRAMS

The following computer programs are written in Fortran II D for use on the IBM 1620. The input and output variables are defined as follows:

SOA = S_{oa}, the apparent shadow location for zero depth.

SCA = S_{ca}, the apparent shadow location for a calibration point.

SLA = S_{la}, the apparent lateral location on either side of the principal axis.

SA = S_a, the apparent location of a data point.

A, B, C, D, E, F = constants in optical error correction equations.

AKI, BKI, CKI = constants for shrinkage equations.

BB = depth of zero datum plane below projection plane.

HI = principal distance of photograph.

HO = stagnation head.

HC = calibration depth.

AL, BL, CL = format location for print out.

AK = range of shrink equations.

SO = true location of zero depth shadow.

SC = true location of calibration shadow.

Z2 = cotangent of illumination angle.

H = true depth at data point.

S = true location of data point.

SL = true lateral location of data point.

P = pressure (analog).

FR = Froude number based on main stream stagnation head.

Since some of the programs were developed before it was known the water analogy failed some of the output shown for the programs was not reported.

Program Listing for Mark I Method

```
    DIMENSION SOA(18,12),SCA(18,12),SLA(12),SA(12),A(12),B(12),C(12),D
   1(12),AL(12),SO(18,12),SC(18,12),Z2(12),H(12),S(12),SL(12),P(12),FR
   2(12),BL(18),CL(12)
    READ 500,BB
    READ 1,N,AK1,BK1,CK1,AK
    READ 3,(AL(J),J=1,12)
    READ 4,(A(J),J=1,12)
    READ 6,(B(J),J=1,12)
    READ 4,(C(J),J=1,12)
    READ 6,(D(J),J=1,12)
500 FORMAT(F6.2)
  5 FORMAT (12F6.2)
  1 FORMAT (14,3F5.3,F5.0)
  3 FORMAT (12F4.0)
  4 FORMAT (12F5.2)
  6 FORMAT (6F7.5)
    H1=1989.35
    HO=25.0
    HC=28.0
    IF(SENSE SWITCH 1) 600,620
600 DO 601 I=1,18
    READ 602,(SO(I,J),J=1,12)
601 READ 602,(SC(I,J),J=1,12)
602 FORMAT (6E13.7)
    GO TO 90
620 DO 10 I=1,18
 10 READ 5,(SOA(I,J),J=1,12)
    DO 20 I=1,18
 20 READ 5,(SCA(I,J),J=1,12)
    DO 120 I=1,18
    DO 120 J=1,12
    IF (SOA(I,J)-999.99) 110,105,105
110 IF(SOA(I,J)) 33,32,32
 32 SOA(I,J)=AK1*SOA(I,J)
    GO TO 37
 33 IF(SOA(I,J)-AK) 36,35,35
 35 SOA(I,J)=BK1*SOA(I,J)
    GO TO 37
 36 SOA(I,J)=CK1*SOA(I,J)
 37 IF(SCA(I,J)) 39,38,38
 38 SCA(I,J)=AK1*SCA(I,J)
    GO TO 50
 39 IF(SCA(I,J)-AK) 41,40,40
 40 SCA(I,J)=BK1*SCA(I,J)
    GO TO 50
 41 SCA(I,J)=CK1*SCA(I,J)
 50 IF(SOA(I,J)) 49,140,140
140 IF(SOA(I,J)-AL(J)) 143,142,142
142 SOA(I,J)=SOA(I,J)+A(J)+B(J)*SOA(I,J)
    GO TO 145
```

Program Listing for Mark I Method (Continued)

```
 49 IF(SOA(I,J)-AL(J)) 57,56,56
 56 SOA(I,J)=   -(ABSF(SOA(I,J))+A(J)+B(J)*SOA(I,J))
    GO TO 145
 57 SOA(I,J)=   -(ABSF(SOA(I,J))+C(J)+D(J)*SOA(I,J))
145 IF(SCA(I,J)) 58,150,150
150 IF(SCA(I,J)-AL(J)) 153,152,152
152 SCA(I,J)=SCA(I,J)+A(J)+B(J)*SCA(I,J)
    GO TO 62
153 SCA(I,J)=SCA(I,J)+C(J)+D(J)*SCA(I,J)
    GO TO 62
 58 IF(SCA(I,J)-AL(J)) 60,59,59
 59 SCA(I,J)=   -(ABSF(SCA(I,J))+A(J)+B(J)*SCA(I,J))
    GO TO 62
 60 SCA(I,J)=   -(ABSF(SCA(I,J))+C(J)+D(J)*SCA(I,J))
 62 SO(I,J)=SOA(I,J)*(1.+BB/H1)
 63 SC(I,J)=SCA(I,J)*(1.+(BB-HC)/H1)
    GO TO 120
105 SO(I,J)=999.99
    SC(I,J)=999.99
120 CONTINUE
    DO 590 I=1,18
    PUNCH 602,(SO(I,J),J=1,12)
590 PUNCH 602,(SC(I,J),J=1,12)
    PUNCH 102
 90 READ 92,KK
    PUNCH 2,N,KK
  2 FORMAT(14,3X,14//)
 92 FORMAT (14)
    READ 5,(SLA(J),J=1,12)
    NN=0
    DO 85 I=1,18
    BL(I)=I
    READ 5,(SA(J),J=1,12)
    DO 130 J=1,12
    CL(J)=J
    CL(J)=CL(J)/100.+BL(I)
    IF(SA(J)-999.99) 115,220,220
115 IF(SA(J))68,67,67
 67 SA(J)=AK1*SA(J)
    GO TO 160
 68 IF(SA(J)-AK) 70,69,69
 69 SA(J)=BK1*SA(J)
    GO TO 160
 70 SA(J)=CK1*SA(J)
160 IF(SA(J)) 75,165,165
165 IF(SA( J )-AL(J)) 173,170,170
170 SA(J)=SA(J)+A(J)+B(J)*SA(J)
    GO TO 80
173 SA(J)=SA(J)+C(J)+D(J)*SA( J )
    GO TO 80
```

Program Listing for Mark I Method (Continued)

```
 75 IF(SA(J)-AL(J))77,76,76
 76 SA(J)=   -(ABSF(SA(J))+A(J)+B(J)*SA(J))
    GO TO 80
 77 SA(J)=   -(ABSF(SA(J))+C(J)+D(J)*SA(J))
 80 Z2(J)=(SC(I,J)-SO(I,J))/HC
    H(J)=((H1+BB)*(SA( J )/H1)-SO(I,J))/(Z2(J)+(SA( J )/H1))
    S(J)=SA( J )*(1.+(BB-H(J))/H1)
    SL(J)=SLA(J)*(1.+(BB-H(J))/H1)
    P(J)=(H(J)/HO)*(H(J)/HO)
    X=2.*(HO/H(J)-1.)
    IF(X) 83,82,82
 83 X=-X
    FR(J)=90.+SQRTF(X)
    GO TO 130
 82 FR(J)=SQRTF(X)
    GO TO 130
220 Z2(J)=999.99
    SL(J)=999.99
    H(J)=999.99
    S(J)=999.99
    P(J)=999.99
    FR(J)=999.99
130 CONTINUE
    PUNCH 100,(CL(J),J=1,8)
    PUNCH 101,(CL(J),J=9,12)
    PUNCH 700
700 FORMAT(/)
    PUNCH 100,(SA(J),J=1,8)
    PUNCH 101,(SA(J),J=9,12)
100 FORMAT (8F10.5)
101 FORMAT (4F10.4,39X,1H-)
    PUNCH 100,(SO(I,J),J=1,8)
    PUNCH 101,(SO(I,J),J=9,12)
    PUNCH 100,(Z2(J),J=1,8)
    PUNCH 101,(Z2(J),J=9,12)
    PUNCH 100,(H(J),J=1,8)
    PUNCH 101,(H(J),J=9,12)
    PUNCH 100,(S(J),J=1,8)
    PUNCH 101,(S(J),J=9,12)
    PUNCH 100,(SL(J),J=1,8)
    PUNCH 101,(SL(J),J=9,12)
    PUNCH 100,(P(J),J=1,8)
    PUNCH 101,(P(J),J=9,12)
    PUNCH 100,(FR(J),J=1,8)
    PUNCH 101,(FR(J),J=9,12)
    PUNCH 701
    NN=NN+1
    IF(NN-4) 85,86,86
 86 PUNCH 102
    NN=0
```

Program Listing for Mark I Method

```
 85 CONTINUE
701 FORMAT(//)
    PUNCH 102
102 FORMAT (79X,1H+)
    GO TO 90
    END
```

Program Listing for Mark II Method

```
      DIMENSION SOA(18,12),SCA(18,12),SLA(12),SA(12),A(12),B(12),C(12),D
     1(12),SO(18,12),SC(18,12),Z2(12),H(12),S(12),SL(12),P(12),FR(12),BL
     2(18),CL(12),E(12),F(12)
      READ 500,BB
      READ 1,N,AK1,BK1,CK1,AK
      READ 5,(A(J),J=1,12)
      READ 6,(B(J),J=1,12)
      READ 5,(C(J),J=1,12)
      READ 6,(D(J),J=1,12)
      READ 5,(E(J),J=1,12)
      READ 6,(F(J),J=1,12)
  500 FORMAT(F6.2)
  602 FORMAT(6E13.7)
    5 FORMAT (12F6.2)
    1 FORMAT (14,3F5.3,F5.0)
    4 FORMAT (12F5.2)
    6 FORMAT (6F7.5)
      H1=1989.35
      HO=24.2
      HC=28.0
  620 DO 10 I=1,18
   10 READ 5,(SOA(I,J),J=1,12)
      DO 20 I=1,18
   20 READ 5,(SCA(I,J),J=1,12)
      NN=1
      DO 121 I=1,18
      IF(NN-6) 3,3,7
    3 LL=1
      GO TO 9
    7 IF(NN-11) 8,8,11
    8 LL=2
      GO TO 9
   11 LL-3
    9 DO 120 J=1,12
      IF (SOA(I,J)-999.99) 110,105,105
  110 IF(SOA(I,J)) 33,32,32
   32 SOA(I,J)=AK1*SOA(I,J)
      GO TO 37
   33 IF(SOA(I,J)-AK) 36,35,35
   35 SOA(I,J)=BK1*SOA(I,J)
      GO TO 37
   36 SOA(I,J)=CK1*SOA(I,J)
   37 IF(SCA(I,J)) 39,38,38
   38 SCA(I,J)=AK1*SCA(I,J)
      GO TO 50
   39 IF(SCA(I,J)-AK) 41,40,40
   40 SCA(I,J)=BK1*SCA(I,J)
      GO TO 50
   41 SCA(I,J)=CK1*SCA(I,J)
   50 IF(SOA(I,J)) 49,140,140
```

Program Listing for Mark II Method (Continued)

```
140 GO TO (142,143,144),LL
142 SOA(I,J)=SOA(I,J)+A(J)+B(J)*SOA(I,J)
    GO TO 145
143 SOA(I,J)=SOA(I,J)+C(J)+D(J)*SOA(I,J)
    GO TO 145
144 SOA(I,J)=SOA(I,J)+E(J)+F(J)*SOA(I,J)
    GO TO 145
 49 GO TO (56,57,58),LL
 56 SOA(I,J)=   -(ABSF(SOA(I,J))+A(J)+B(J)*SOA(I,J))
    GO TO 145
 57 SOA(I,J)=   -(ABSF(SOA(I,J))+C(J)+D(J)*SOA(I,J))
    GO TO 145
 58 SOA(I,J)=-(ABSF(SOA(I,J))+E(J)+F(J)*SOA(I,J))
145 IF(SCA(I,J)) 55,150,150
150 GO TO (152,153,154),LL
152 SCA(I,J)=SCA(I,J)+A(J)+B(J)*SCA(I,J)
    GO TO 62
153 SCA(I,J)=SCA(I,J)+C(J)+D(J)*SCA(I,J)
    GO TO 62
154 SCA(I,J)=SCA(I,J)+E(J)+F(J)*SCA(I,J)
    GO TO 62
 55 GO TO (59,60,61),LL
 59 SCA(I,J)=   -(ABSF(SCA(I,J))+A(J)+B(J)*SCA(I,J))
    GO TO 62
 60 SCA(I,J)=   -(ABSF(SCA(I,J))+C(J)+D(J)*SCA(I,J))
    GO TO 62
 61 SCA(I,J)=-(ABSF(SCA(I,J))+E(J)+F(J)*SCA(I,J))
 62 SO(I,J)=SOA(I,J)*(1.+BB/H1)
 63 SC(I,J)=SCA(I,J)*(1.+(BB-HC)/H1)
    GO TO 120
105 SO(I,J)=999.99
    SC(I,J)=999.99
120 CONTINUE
121 NN=NN+1
    DO 590 I=1,18
    PUNCH 602,(SO(I,J),J=1,12)
590 PUNCH 602,(SC(I,J),J=1,12)
    PUNCH 102
 90 READ 92,KK
    PUNCH 2,N,KK
  2 FORMAT(14,3X,14//)
 92 FORMAT (14)
    READ 5,(SLA(J),J=1,12)
    NB=0
    NN=1
    DO 85 I=1,18
    IF(NN-6) 13,13,17
 13 LL=1
    GO TO 19
 17 IF(NN-11) 18,18,21
```

Program Listing for Mark II Method (Continued)

```
 18 LL=2
    GO TO 19
 21 LL=3
 19 BL(I)=I
    READ 5,(SA(J),J=1,12)
    DO 130 J=1,12
    CL(J)=J
    CL(J)=CL(J)/100.+BL(I)
    IF(SA(J)-999.99) 115,220,220
115 IF(SA(J))68,67,67
 67 SA(J)=AK1*SA(J)
    GO TO 160
 68 IF(SA(J)-AK) 70,69,69
 69 SA(J)=BK1*SA(J)
    GO TO 160
 70 SA(J)=CK1*SA(J)
160 IF(SA(J)) 75,165,165
165 GO TO (170,173,174),LL
170 SA(J)=SA(J)+A(J)+B(J)*SA(J)
    GO TO 80
173 SA(J)=SA(J)+C(J)+D(J)*SA( J )
    GO TO 80
174 SA(J)=SA(J)+E(J)+F(J)*SA(J)
    GO TO 80
 75 GO TO (76,77,78),LL
 76 SA(J)=   -(ABSF(SA(J))+A(J)+B(J)*SA(J))
    GO TO 80
 77 SA(J)=   -(ABSF(SA(J))+C(J)+D(J)*SA(J))
    GO TO 80
 78 SA(J)=-(ABSF(SA(J))+E(J)+F(J)*SA(J))
 80 Z2(J)=(1775.-SO(I,J))/1026.25
    H(J)=((H1+BB)*SA( J )/H1)-SO(I,J))/Z2(J)+(SA( J )/H1))
    S(J)=SA( J )8(1.+(BB-H(J))/H1)
    SL(J)=SLA(J)*(1.+(BB-H(J))/H1)
    P(J)=(H(J)/HO)*(H(J)/HO)
    X=2.*(HO/H(J)-1.)
    IF(X) 83,82,82
 83 X=-X
    FR(J)=90.+SQRTF(X)
    GO TO 130
 82 FR(J)=SQRTF(X)
    GO TO 130
220 Z2(J)=999.99
    SL(J)=999.99
    H(J)=999.99
    S(J)=999.99
    P(J)=999.99
    FR(J)=999.99
130 CONTINUE
    PUNCH 100,(CL(J),J=1,8
```

Program Listing for Mark II Method (Continued)

```
      PUNCH 101,(CL(J),J=9,12)
      PUNCH 700
  700 FORMAT(/)
  100 FORMAT (8F10.5)
  101 FORMAT (4F10.4,39X,1H-)
      PUNCH 100,(SA(J),J=1,8)
      PUNCH 101,(SA(J),J=9,12)
      PUNCH 100,(SO(I,J),J=1,8)
      PUNCH 101,(SO(I,J),J=9,12)
      PUNCH 100,(Z2(J),J=1,8)
      PUNCH 101,(Z2(J),J=9,12)
      PUNCH 100,(H(J),J=1,8)
      PUNCH 101,(H(J),J=9,12)
      PUNCH 100,(S(J),J=1,8)
      PUNCH 101,(S(J),J=9,12)
      PUNCH 100,(SL(J),J=1,8)
      PUNCH 101,(SL(J),J=9,12)
      PUNCH 100,(P(J),J=1,8)
      PUNCH 101,(P(J),J=9,12)
      PUNCH 100,(FR(J),J=1,8)
      PUNCH 101,(FR(J),J=9,12)
      PUNCH 701
      NB=NB+1
      IF(NB-4) 85,86,86
   86 PUNCH 102
      NB=0
   85 NN=NN+1
  701 FORMAT(//)
      PUNCH 102
  102 FORMAT (79X,1H+)
      GO TO 90
      END
```

Program Listing for Numerical Interpolation

Note: The input variables are the output from the above programs, and are defined as A=S; B=Sl; C=Fr; D=position.

```
    DIMENSION A(18,12),B(18,12),C(18,12),D(18,12),A1(7),B1(7),D1(7),D2
   1(7)
 98 READ 1,I1,I2
    NN=0
    READ 2,N,KK
  2 FORMAT (I4,3X,I4//)
    DO 85 I=1,18
    READ 100,(D (I,J),J=1,8)
    READ 101,(D(I,J),J=9,12)
    READ 700
    READ 100,(A(I,J),J=1,8)
    READ 101,(A(I,J),J=9,12)
    READ 100,(B(I,J),J=1,8)
    READ 101,(B(I,J),J=9,12)
    READ 703
    READ 100,(C(I,J),J=1,8)
    READ 101,(C(I,J),J=9,12)
    READ 701
    NN=NN+1
    IF(NN-4) 85,86,86
 86 READ 705
    NN=0
 85 CONTINUE
    READ 705
100 FORMAT (8F10.5)
101 FORMAT (4F10.5)
700 FORMAT (/////////)
705 FORMAT(1H )
701 FORMAT (//)
  1 FORMAT (2I5)
    PUNCH 2,N,KK
    PUNCH 703
    DO 59 IX=I1,I2,2
    X=IX
    X=.01*X
    K=0
    DO 53 J=1,12
    DO 53 I=1,17
    IF(C(I,J)-X) 54,55,56
 54 IF(C(I+1,J)-X) 53,53,58
 56 IF(C(I+1,J)-X) 58,53,53
 58 IF(C(I,J)+C(I+1,J)-90.)63,53,53
 63 K=K+1
    D1(K)=D(I,J)
    D2(K)=-D(I+1,J)
    A1(K)=A(I,J)+(X-C(I,J))*(A(I+1,J)-A(I,J))/(C(I+1,J)-C(I,J))
    A1(K)= A1(K)+A1(K)/ABSF(A1(K)+1.E-08)*.005
```

Program Listing for Numerical Interpolation (Continued)

```
      B1(K)=B(I,J)+(X-C(I,J))*(B(I+1,J)-B(I,J))/(C(I+1,J)-C(I,J))
      B1(K)= B1(K)+B1(K)/ABSF(B1(K)+1.E-08)*.5
      GO TO 60
   55 D1(K)=D(I,J)
      D2(K)=-D(I,J)
      A1(K)=A(I,J)
      A1(K)= A1(K)+A1(K)/ABSF(A1(K)+1.E-08)*.005
      B1(K)=B(I,J)
      B1(K)= B1(K)+B1(K)/ABSF(B1(K)+1.E-08)*.5
   60 IF(K-6) 53,61,61
   61 PUNCH 90, X,(D1(K),D2(K),K=1,6)
      PUNCH 91,(A1(K),K=1,6)
      PUNCH 92,(B1(K),K=1,6)
      PUNCH 703
      K=0
   53 CONTINUE
  703 FORMAT (/)
   90 FORMAT (F8.2,12F6.2)
   91 FORMAT (8X,6F12.2)
   92 FORMAT(8X,F10.0,5F12.0)
      IF(K) 59,59,70
   70 MM=K
      PUNCH 90, X,(D1(K),D2(K),K=1,MM)
      PUNCH 91,(A1(K),K=1,MM)
      PUNCH 92,(B1(K),K=1,MM)
      PUNCH 703
   59 CONTINUE
      PUNCH 702
  702 FORMAT(79X,1H+)
      GO TO 98
      END
```

Program Listing for Mark III Method

```
    DIMENSION SOA(18,12),SCA(18,12),SLA(12),SA(18,12),Z2(12),H(12),SL(
   112),P(12),FR(12),BL(18),CL(12),S(12)
    READ 500,BB,N
500 FORMAT (F6.2,15)
    H1=1989.35
    HO=24.2
    HC=28.0
    DO 10 I=1,18
 10 READ 5,(SOA(I,J),J=1,12)
    DO 20 I=1,18
 20 READ 5,(SCA(I,J),J=1,12)
  5 FORMAT (12F6.2)
    DO 120 I=1,18
    DO 120 J=1,12
     IF(SOA(I,J)-999.99) 25,105,105
 25 SOA(I,J)=SOA(I,J)/.9
    SCA(I,J)=SCA(I,J)/.9
    GO TO 120
105 SOA(I,J)=999.99
    SCA(I,J)=999.99
120 CONTINUE
 90 READ 92,KK
 92 FORMAT (14)
    PUNCH 2,N,KK
  2 FORMAT (14,3X,14//)
    READ 5,(SLA(J),J=1,12)
    DO 30 I=1,18
 30 READ 5,(SA(I,J),J=1,12)
    NB=0
    DO 230 I=1,18
    BL(I)=I
    DO 130 J=1,12
    CL(J)=J
    CL(J)=CL(J)/100.+BL(I)
    IF(SA(I,J)-999.99) 115,220,220
115 SA(I,J)=SA(I,J)/.9
    Z2(J)=28./(SCA(I,J)-SOA(I,J))
    H(J)=(SA(I,J)-SOA(I,J))*Z2(J)
    SL(J)=SLA( J )*(1.+(BB-H(J))/H1)
    P(J)=(H(J)/HO)*(H(J)/HO)
    S(J)=SA(I,J)*(1.-H(J)/(BB+H1))
    X=2.*(HO/H(J)-1.)
    IF(X) 83,82,82
 83 X=-X
    FR(J)=90.+SQRTF(X)
    GO TO 130
 82 FR(J)=SQRTF(X)
    GO TO 130
220 Z2(J)=999.99
    SL(J)=999.99
```

Program Listing for Mark III Method (Continued)

```
      H(J)=999.99
      P(J)=999.99
      FR(J)=999.99
      S(J)=999.99
130   CONTINUE
      PUNCH 100,(CL(J),J=1,8)
      PUNCH 101,(CL(J),J=9,12)
      PUNCH 700
700   FORMAT (/)
100   FORMAT (8F10.5)
101   FORMAT (4F10.5,39X,1H-)
      PUNCH 100,(SA(I,J),J=1,8)
      PUNCH 101,(SA(I,J),J=9,12)
      PUNCH 100,(SOA(I,J),J=1,8)
      PUNCH 101,(SOA(I,J),J=9,12)
      PUNCH 100,(S(J),J=1,8)
      PUNCH 101,(S(J),J=9,12)
      PUNCH 100,(Z2(J),J=1,8)
      PUNCH 101,(Z2(J),J=9,12)
      PUNCH 100,(H(J),J=1,8)
      PUNCH 101,(H(J),J=9,12)
      PUNCH 100,(SL(J),J=1,8)
      PUNCH 101,(SL(J),J=9,12)
      PUNCH 100,(P(J),J=1,8)
      PUNCH 101,(P(J),J=9,12)
      PUNCH 100,(FR(J),J=1,8)
      PUNCH 101,(FR(J),J=9,12)
      PUNCH 701
701   FORMAT (//)
      NB=NB+1
      IF(NB-4) 230,85,85
 85   PUNCH 102
      NB=0
230   CONTINUE
      PUNCH 102
102   FORMAT (79X,1H+)
      GO TO 90
      END
```

APPENDIX C

FIGURE-FILM REFERENCE

The run identification and film number is stated as a two part number. The second two digits are the frame number on a particular roll of film, while the remainder is the roll number. Thus the second frame of roll 18 would be 1802.

Figure No.	Film	Figure No.	Film
7	807	39	2006
8	806	40	908
9	502	41	916
10	409	43	2014
11	1621	44	1002
12	1622	45	1010
13	1801	47	2016
14	1802	48	1016
15	1805	49	1027
17	1904	51	2108
18	1616	52	1033
20	1906	53	1106
21	504	55	2106
23	1908	56	1210
24	416	57	1215
25	401	59	2118
27	1916	60	1313
28	506	61	1321
29	515	63	2206
31	1918	64	1408
32	604	65	1415
33	609	67	2118
35	1919	68	1513
36	522	69	1524
37	516	71	1707

VITA

John Love, Jr.

Candidate for the Degree of

Doctor of Philosophy

Thesis: THE DEVELOPMENT AND EVALUATION OF A SHADOW-PHOTOGRAMMETRIC METHOD FOR DETERMINING THE TOPOGRAPHY OF AN OPAQUE SURFACE

Major Field: Mechanical Engineering (Aerospace)

Biographical:

Personal Data: Born in Paris, Texas, January 26, 1916, a son of John and Stella Maude Love.

Education: Attended grade school and graduated from Boonville High School, Boonville, Missouri in 1934; received Bachelor of Arts, 1939; Bachelor of Science in Mechanical Engineering, 1951; Master of Science in Mechanical Engineering 1953 all from the University of Missouri, Columbia, Missouri; completed the requirements for the Doctor of Philosophy degree in May, 1966.

Experience: Transportation Department, Missouri, Kansas, Texas Railroad Company, St. Louis, Missouri from 1939 to 1949; Instructor in Mechanical Engineering from 1949 to 1953; Assistant Professor in Mechanical Engineering from 1953 to 1954, both at the University of Missouri, Columbia, Missouri; Supervisor of Requisition Engineering, General Electric Company, Distribution Assemblies Department, Norwood, Ohio, from 1954 to 1958; Associate Professor of Mechanical Engineering from 1958 to present, University of Missouri, Columbia.

Publications: "Increase of Impact Strength of Threaded Fastenings", John Love and O. A. Pringle; Transactions ASME, Vol. 78, No. 7, 1956. Republished in Product Engineering, Oct. 1956, and Fasteners, Vol. 11, No. 1, Spring 1956. "Performance Calculations for Steam Condensation", M.S. Thesis, University of Missouri, 1953.

Organizations and Honors: The author is a member of the following: American Society for Engineering Education; American Institute of Aeronautics and Astronautics; Sigma Xi; Tau Beta Pi; Pi Tau Sigma; Alpha Chi Sigma; and Honors convocation, University of Missouri, 1950, 51, 53. He was a National Science Fellow in 1962-63. He is also listed in American Men of Science and Who's Who in Education.